U.PORTO

FEUP FACULDADE DE ENGENHARIA
UNIVERSIDADE DO PORTO

Experimental and numerical study of cohesive and adhesive failure of aged and contaminated adhesive joints

Author:

Catarina da Silva Pereira Borges

Supervisors:

Lucas Filipe Martins da Silva

Co-supervisors:

Eduardo André de Sousa Marques

Philipp Weißgraeber

Thesis submitted for the degree of Doctor of Philosophy

Doctoral Program of Mechanical Engineering (PRODEM)

Faculty of Engineering of the University of Porto

DEMec, Faculdade de Engenharia da Universidade do Porto, Rua Dr. Roberto Frias, 4200-465 Porto, Portugal

Porto, 2021

© **Catarina da Silva Pereira Borges**
Departamento de Engenharia Mecânica
Faculdade de Engenharia da Universidade do Porto

Rua Dr. Roberto Frias, s/n
4200-465 Porto
Portugal

Abstract

Adhesives are steadily being presented as an interesting alternative to conventional joining methods, such as riveting, bolting or welding, because they do not require the local heating of the materials or the introduction of holes. However, this method has important setbacks to its use, being two of them addressed in this work, the need for a careful surface preparation to avoid a decrease in bond strength, or even adhesive failure of the joint, and the sensitivity of adhesive joints to humid environments, that can harm the adhesive, substrate, or the adhesive/substrate interface.

The adhesive joints under analysis in this work belong to a housing for electronic components, manufactured from polybutylene terephthalate with 30% of short glass fiber (PBT-GF30). This housing is manufactured in two parts, using injection molding, and those two parts are joined using a silicone adhesive, which also acts as a sealant. The housing is then bonded to an aluminum heat sink and, in this bond, the adhesive also serves heat insulating purposes. In this assembly the adhesive needs to ensure the electronic components are not exposed to the exterior environment and contamination so that they are not damaged during service. Therefore, it is important to understand under which conditions this joint fails in the adhesive, substrate or adhesive/substrate interface.

In this project, the influence of humidity on PBT-GF30/silicone and aluminum/silicone joints was analyzed, to understand the effect a humid environment would have on the bond, particularly at high temperatures. For that, first, the bulk PBT-GF30 and silicone were analyzed. The water uptake behavior of PBT-GF30 and silicone was studied at different temperatures, combined with the evaluation of its effect on the mechanical properties of the materials. Single lap joints (SLJ) and double cantilever beam (DCB) joints were also analyzed at different temperatures when dried, aged and dried after aging. Finally, the water uptake behavior of PBT-GF30/silicone and aluminum/silicone joints was evaluated using rectangular joints (RJ) with different adhesive thicknesses and similar SLJs were tested to understand

if there is a change in joint strength and failure path after water immersion, using different substrate materials.

In the manufacturing of the aluminum heat sink, fluids, for example milling fluids, are used to cool and lubricate the process. Since these fluids can damage the adhesive joint if the adhesive is applied directly on the contaminated substrate, the surfaces are cleaned using a detergent that contains surfactants. However, these surfactants can also harm the joint quality. To evalute the surfactant contamination influence on the joints, first, adhesive with different amounts of surfactant mixed prior to curing was analyzed and, afterwards, SLJs and DCBs with different contamination levels applied to their surfaces were tested.

Finally, a method was created to implement industrially and swiftly evaluate if a given adhesive/substrate combination under environmental or surface contamination conditions has enough strength and fracture toughness for a given application.

Regarding the water aging studies, it was concluded that the silicone adhesive and PBT-GF30 have Fickian water diffusion behaviors, with a diffusion rate that can be described by the Arrhenius law as a function of temperature. The silicone does not significantly change its mechanical properties when aged and the PBT-GF30 decreases its mechanical properties. However, the increase of immersion temperature damages both materials decreasing their strength and stiffness. In the temperature range analyzed, silicone does not establish chemical bonds with water. However, the PBT-GF30 exhibits changes in its chemical profile at temperatures above a minimum of 80 to 85 °C. In PBT-GF30/silicone joints, for low immersion temperatures, water aging does not decrease the failure load. However, as immersion temperature increases, the damage in the substrate becomes progressively clear, changing the failure path to the substrate, particularly in the DCB joints that have a more severe loading on the substrate. Comparing joints with aluminum and PBT-GF30 substrates, it is clear that in aluminum/silicone joints the interphase has a more preponderant role, with a portion of the water gain being through this region. In PBT-GF30/silicone joints, knowing the behavior of the bulk materials it is possible to trace an estimation of the water mass gain of the joint, since water is only significantly absorbed by the bulk materials. This translates into failure of PBT-GF30/silicone joints being always cohesive through the adhesive and for water aged aluminum/silicone joints being adhesive, with a very significant decrease in joint strength.

Regarding the effect of contamination, as the amount of surfactant mixed to the silicone adhesive prior to curing increases, the strength and stiffness of the material

significantly decrease, paired with changes to the chemical profile and morphology of the adhesive. In a joint, as the amount of surface contamination increases, failure load decreases and the failure path changes from the middle of the adhesive to the adhesive close to the interface and, ultimately, adhesive failure. This is attributed to, for low amounts of surface contamination, the adhesive at the interphase absorbing surfactant during curing, decreasing its strength and shifting the failure path to this region. For higher levels of surface contamination, the surfactant acts as a physical separation between adhesive and substrate, promoting adhesive failure.

Finally, a method was developed and validated to analyze the tensile strength and mode I toughness of adhesive joints. In this method it is intended to evaluate if strength and toughness are above a given admissible value, assuming that the failure path can be through the middle of the adhesive, close to the interface or even interfacial.

Keywords: Adhesives; adhesive joints; adhesive bonding; moisture; contamination; interface; diffusion.

Resumo

Os adesivos são apresentados como uma alternativa interessante aos métodos de ligação convencionais, tais como rebitagem, aparafusamento ou soldadura, porque não requerem o aquecimento local dos materiais ou a introdução de furos. No entanto, este método tem importantes obstáculos à sua utilização, sendo dois deles abordados neste trabalho, a necessidade de uma preparação cuidadosa da superfície para evitar uma diminuição da força de ligação, ou mesmo a falha adesiva na junta, e a sensibilidade das juntas adesivas a ambientes húmidos, que podem prejudicar o adesivo, o substrato, ou a interface adesivo/substrato.

As juntas adesivas em análise neste trabalho pertencem a uma caixa para componentes eletrónicos, fabricada a partir de polibutileno tereftalato com 30% de fibra de vidro curta (PBT-GF30). Esta caixa é fabricada em duas partes, usando moldação por injecção, e essas duas partes são unidas usando um adesivo baseado em silicone, que também atua como selante. A carcaça é então colada a um dissipador de calor de alumínio e, nesta colagem, o adesivo serve também para fins de isolamento térmico. Nesta montagem, o adesivo precisa de assegurar que os componentes eletrónicos não sejam expostos ao ambiente exterior e à contaminação, para que não sejam danificados durante o serviço. Portanto, é importante compreender em que condições esta junta falha no adesivo, substrato ou interface adesivo/substrato.

Neste projecto, a influência da humidade em juntas PBT-GF30/silicone e alumínio/silicone foi analisada, para compreender o efeito que um ambiente húmido teria na ligação, particularmente a altas temperaturas. Para isso, primeiro, foram analisados provetes maciços de PBT-GF30 e silicone. O comportamento de absorção de água do PBT-GF30 e do silicone foi estudado a diferentes temperaturas, combinado com a avaliação do seu efeito sobre as propriedades mecânicas dos materiais. Juntas de simples sobreposição (SLJ) e *double cantilever beam* (DCB) também foram analisadas a diferentes temperaturas quando secas, envelhecidas e secas após o envelhecimento. Finalmente, o comportamento de absorção de água das juntas PBT-GF30/silicone e alumínio/silicone foi avaliado utilizando juntas rectangulares (RJ) com diferentes

espessuras de adesivo. SLJs fabricadas com os mesmos materiais, e com as mesmas espessuras de adesivo, foram testadas secas e após envelhecimento por absorção de água, para compreender se existe uma alteração na resistência das juntas e no percurso da falha após imersão em água, utilizando diferentes materiais de substrato.

No fabrico do dissipador de calor de alumínio são utilizados fluidos, como fluidos de fresagem, para arrefecer e lubrificar o processo. Uma vez que estes fluidos podem danificar a junta adesiva se o adesivo for aplicado directamente sobre o substrato contaminado, as superfícies são limpas utilizando um detergente que contém tensioativos. No entanto, estes tensioativos também podem prejudicar a qualidade das juntas. Para avaliar a influência da contaminação do tensioativo nas juntas, primeiro analisou-se o adesivo com diferentes quantidades de tensioativo misturado antes da cura e, posteriormente, foram testados SLJs e DCBs com diferentes níveis de contaminação aplicados às suas superfícies.

Finalmente, foi criado um método, adequado para implementação na indústria, que permite avaliar rapidamente se uma dada combinação adesivo/substrato em condições de contaminação ambiental ou superficial tem resistência e resistência à fractura suficientes para uma dada aplicação.

Relativamente aos estudos de envelhecimento da água, concluiu-se que o silicone e o PBT-GF30 têm comportamentos de difusão da água que seguem a lei de Fick, com uma taxa de difusão que pode ser descrita pela lei de Arrhenius em função da temperatura. As propriedades do silicone não são significativamente afetadas pelo envelhecimento em água, contudo, as properiedades mecâncias do PBT-GF30 diminuem. No entanto, o aumento da temperatura de imersão danifica ambos os materiais, diminuindo a sua resistência e rigidez. No intervalo de temperaturas analisado, o silicone não estabelece ligações químicas com a água. Porém, o PBT-GF30 apresenta alterações químicas a temperaturas superiores a um mínimo de 80 a 85 °C. Nas juntas PBT-GF30/silicone, para baixas temperaturas de imersão, o envelhecimento em água não dimiminui a carga de rotura. Contudo, à medida que a temperatura de imersão aumenta, os danos no substrato tornam-se progressivamente mais claros, alterando o percurso de falha para este material, particularmente nas juntas DCB que têm uma carga mais severa sobre o substrato. Comparando as juntas com os substratos de alumínio e PBT-GF30, é evidente que nas juntas de alumínio/silicone a interfase tem um papel mais preponderante, sendo que uma parte do ganho de água é através desta região. Nas juntas PBT-GF30/silicone, conhecendo o comportamento dos materiais maciços é possível traçar uma estimativa do ganho de massa de água da junta, uma vez que a água só é significativamente absorvida pelos

materiais maciços. Isto traduz-se nas roturas das juntas PBT-GF30/silicone, que são sempre coesivas através do adesivo e para as juntas envelhecidas de alumínio/silicone sendo adesivas, com uma diminuição muito significativa da resistência das juntas.

Quanto ao efeito da contaminação, à medida que a quantidade de tensioactivo misturado ao adesivo de silicone antes da cura aumenta, a resistência e rigidez do material diminui significativamente, juntamente com alterações do perfil químico e da morfologia do adesivo. Numa junta, à medida que a quantidade de contaminação da superfície aumenta, a carga de rotura diminui e a localização da fenda altera-se do meio do adesivo para o adesivo próximo da interface. Isto é atribuído, para quantidades baixas de contaminação superficial, ao adesivo na interfase que absorve o tensoativo durante a cura, diminuindo a sua resistência e deslocando a trajetória da fenda para esta região. Para níveis mais elevados de contaminação superficial, o tensioativo actua como uma separação física entre o adesivo e o substrato, promovendo a falha adesiva.

Finalmente, foi desenvolvido e validado um método para analisar a resistência à tração e a tenacidade em modo I das juntas adesivas. Neste método pretende-se avaliar se a resistência e a tenacidade estão acima de um determinado valor admissível, assumindo que a rotura ocorre através do meio do adesivo, próximo da interface ou mesmo de forma interfacial.

Keywords: Adesivos; juntas adesivas; ligação adesiva; humidade; contaminação; interface; difusão.

Acknowledgments

First, I would like to express my sincere gratitude to Professor Lucas da Silva, for the opportunity to participate in this project and the technical and academic insights, as well as support throughout this work.

I would also like to express my gratitude to Eduardo Marques and Ricardo Carbas for the help and availability to discuss the problems faced along the way and find solutions.

I would like to extend my gratitude to Philipp Weißgraeber for the constant desire to improve the work developed and to formulate different and creative solutions.

To Christoph Üffing for sharing his technical knowledge and advice along the development of this work, as well for welcoming and working with me in his laboratory at Renningen. I also must highlight Florian Schmid for always pushing me to think outside of the box during our meetings. My acknowledgement also to the other members of this workgroup at Robert Bosch GmbH, Corporate Research and Advance Engineering, for the warm welcome and the interesting exchange and discussions about our projects during my time at Renningen.

To Ricardo Brandão, who worked very closely with me during his Master thesis, making important contributions to this work. Thank you also for the friendship and positivism.

I also want to point out those who work in laboratories at FEUP that helped during my work. Among them are Emília Soares and José Ramiro Soares.

This research would also not have been possible without the financial support provided by Robert Bosch GmbH, Corporate Research and Advance Engineering and by Fundação para a Ciência e a Tecnologia through the 2020.06055.BD Ph.D. Grant.

To all the members of the Advanced Joining Processes Unit for constant support, group work and exchange that allows us to achieve better results in our individual projects. Thank you for your friendship, encouragement and for the time we shared in and out of this working group. I will forever be grateful.

To my friends for the moments I did not think about my thesis, and particularly Daniel for the infinite patience and support.

To my family, my mother for the inspiration, my father, my aunts, my grandmother and my cousin for always supporting my decisions and always helping me surpass the challenges I face. I could never have done it without you.

Contents

Abstract i

Resumo v

Acknowledgments ix

List of Figures xvi

List of Tables xvii

List of Acronyms xix

List of Symbols xxi

List of Publications xxiii

1 Introduction 1

1.1 Background and motivation 1

1.2 Objectives 3

1.3 Research methodology 3

1.4 Outline of the thesis 6

2 Literature review 13

2.1 Moisture aging of adhesive joints 13

2.1.1 Mechanisms of moisture aging 13

2.1.2 Effects of moisture aging on adhesive joints 17

2.2 Contamination of adhesive joints 19

2.2.1 Mechanisms of contamination 19

2.2.2 Effects of contamination on adhesive joints 20

3 Materials and experimental methods **23**
3.1 Materials . . . 23
3.1.1 Substrates . . . 23
3.1.2 Adhesive . . . 24
3.1.3 Contaminants . . . 25
3.2 Gravimetric tests . . . 25
3.2.1 Bulk materials . . . 25
3.2.2 Adhesive joints . . . 27
3.3 Mechanical tests . . . 29
3.3.1 Bulk tensile tests . . . 29
3.3.2 Single lap joint (SLJ) tests . . . 32
3.3.3 Double cantilever beam (DCB) tests . . . 33
3.3.4 Joints for the patent proposed . . . 36
3.4 Complementary tests . . . 39
3.4.1 Dynamic mechanical analysis (DMA) . . . 39
3.4.2 Glass transition temperature measurement using an in-house developed apparatus . . . 40
3.4.3 Differential Scanning Calorimetry (DSC) . . . 40
3.4.4 Fourier Transform Infrared Spectroscopy (FTIR) . . . 40
3.4.5 Scanning electron microscopy (SEM) . . . 41

4 Numerical methods **43**
4.1 Gravimetric simulation . . . 43
4.1.1 Bulk materials . . . 44
4.1.2 Adhesive joints . . . 44
4.2 Mechanical simulation . . . 46
4.2.1 Double cantilever beam (DCB) and single lap joints (SLJ) . . . 46
4.2.2 Patent tests . . . 48

5 Conclusions **51**

6 Future work **55**

References **57**

A Paper A **67**

B Paper B **93**

C Paper C **119**

D Paper D **147**

E Paper E **165**

F Paper F **191**

G Patent G **209**

H Paper H **235**

List of Figures

1.1 Schematic representation of the workflow of the tasks performed in this work. 4
1.2 Correspondence between tasks proposed and papers published. 6

2.1 Paths of water diffusion in adhesive joints. 13
2.2 Diffusion front near the metal/adhesive transition. 15
2.3 Mechanisms of water damage on the adhesive/substrate interface in an adhesive joint. 16
2.4 Swelling of the adhesive after being exposed to a humid environment in bulk and in a joint. 18
2.5 Oil accommodating adhesives. 20
2.6 Effect of contamination on adhesive joints. 21

3.1 Specimens used for the gravimetric study of the bulk materials following the ISO 294-3 standard. 26
3.2 Reduced scale specimens used for the gravimetric study of the bulk materials. 26
3.3 Interphase on thinner and thicker adhesive joints. 28
3.4 Rectangular joints manufactured for the gravimetric study of adhesive joints. 28
3.5 Trim RJs to make sure the adhesive is in the same plane of the end of the substrate for every side. 29
3.6 Standard “dogbone” specimens for bulk tensile tests. 30
3.7 Reduced scale “dogbone” specimens for bulk tensile tests. 31
3.8 Single lap joints manufactured. 33
3.9 Schematic representation of the of the geometry of the standard DCBs with high strength steel substrates. 34

3.10 Schematic representation of the geometry of the DCB specimens with aluminum substrates 35
3.11 Schematic representation of the geometry of the DCBs with PBT-GF30 substrates. 35
3.12 Schematic representation of the joint tested a) and of the testing method b). 36
3.13 Schematic representation of the different parts of the joint used for the test. 37
3.14 Assembly used to assist joint manufacturing a), cut view, considering the cut by plane 1 b) and the mask used to ensure the overlap area c). 38
3.15 Schematic representation of the joints and assemblies used to assist joint manufacturing in a mold. 39
3.16 Test setup attached to the universal testing machine to test the specimens. 39

4.1 Three-dimensional model used to simulate the water uptake behavior of bulk plates. 44
4.2 Two-dimensional approximation used to simulate the water uptake behavior of bulk plates. 45
4.3 Numerical model developed for the gravimetric study of RJs with aluminum substrates. 45
4.4 Numerical model developed for the gravimetric study of RJs with PBT-GF30 substrates. 46
4.5 Boundary conditions of the numerical model developed for the DCBs with metallic a) and PBT-GF30 b) substrates. 47
4.6 Boundary conditions of the numerical model developed for the SLJs. . 47
4.7 Numerical model developed for contaminated adhesive joints. 48
4.8 Numerical model used to simulate pull-off tests. 49
4.9 Numerical model used to simulate peel tests. 49

List of Tables

3.1 Properties of the adhesive used, provided by the manufacturer. 24

List of Acronyms

2D	Two-dimensional
3D	Three-dimensional
ASTM	American Society for Testing and Materials
BS	British Standard
C3D10	10-node quadratic tetrahedron element
C3D8R	8-node linear brick, reduced integration, hourglass control element
COH2D4	4-node two-dimensional cohesive element
COH3D8	8-node three-dimensional cohesive element
CPE4R	4-node bilinear plane strain quadrilateral, reduced integration, hourglass control element
DC2D4	4-node linear heat transfer quadrilateral element
DC3D20	20-node quadratic heat transfer brick element
DCB	Double cantilever beam
DIN	Deutsches Institut für Normung
DMA	Dynamic mechanical analysis
DSC	Differential scanning calorimetry
FEA	Finite element analysis
FEM	Finite element method
FTIR	Fourier-transform infrared spectroscopy
ISO	International Organization for Standardization
PBT	Polybutylene terephthalate
PBT-GF30	Polybutylene terephthalate with 30% of short glass fiber, in mass
PC	Polycarbonate
RJ	Rectangular joints
SEM	Scanning electron microscopy
SLJ	Single lap joint

List of Symbols

h	Thickness
t	Time
m_0	Initial mass
m_t	Mass at time t
m_∞	Mass at saturation
M_t	Water uptake at time t
M_∞	Water uptake at saturation
D	Coefficient of diffusion
σ	Tensile stress
τ	Shear stress
E	Young's modulus
G	Shear modulus
G_{Ic}	Mode I fracture energy
G_{IIc}	Mode II fracture energy
T_g	Glass transition temperature

List of Publications

In the scope of this thesis

- **Borges, C. S. P.**, Marques, E. A. S., Carbas, R. J. C., Ueffing, C., Weißgraeber, P., & da Silva, L. F. M. (2021). Review on the effect of moisture and contamination on the interfacial properties of adhesive joints. *Proceedings of the Institution of Mechanical Engineers, Part C: Journal of Mechanical Engineering Science*, 235(3), 527-549. DOI: 10.1177/0954406220944208.

- **Borges, C. S. P.**, Akhavan-Safar, A., Marques, E. A. S., Carbas, R. J. C., Ueffing, C., Weißgraeber, P., & da Silva, L. F. M. (2021). Effect of water ingress on the mechanical and chemical properties of polybutylene terephthalate reinforced with glass fibers. *Materials*, 14(5), 1261. DOI: 10.3390/ma14051261.

- **Borges, C. S. P.**, Brandão, R., Akhavan-Safar, A., Marques, E. A. S., Carbas, R. J. C., Ueffing, C., Weißgraeber, P., Schmid, F., & da Silva, L. F. M. (2021). Influence of water and surfactant contamination on the mechanical and chemical properties of a silicone adhesive before and after curing. *The Journal of Adhesion. Submitted.*

- Brandão, R., **Borges, C. S. P.**, Marques, E. A. S., Carbas, R. J. C., Akhavan-Safar, A., Schmid, F., Ueffing, C., Weißgraeber, P. & da Silva, L. F. M. (2022). The influence of humidity and immersion temperature on the properties and failure mode of PBT-GF30/silicone bonded joints. *Composite Structures*, 115421. DOI: 10.1016/j.compstruct.2022.115421.

- **Borges, C. S. P.**, Marques, E. A. S., Carbas, R. J. C., Akhavan-Safar, A., Ueffing, C., Weißgraeber, P. & da Silva, L. F. M. (2022). Effect of the interface/interphase on the water ingress properties of joints with PBT-GF30 and aluminum substrates using silicone adhesive. *Engineering Failure Analysis. Submitted.*

- Brandão, R., **Borges, C. S. P.**, Marques, E. A. S., Carbas, R. J. C., Akhavan-Safar, A., Nunes, P. D. P., Ueffing, C., Weißgraeber, P., Schmid, F. & da Silva, L. F. M. (2022) Effect of surfactant contamination on the properties of aluminum/silicone adhesive joints, *Mechanics of Advanced Materials and Structures*, DOI: 10.1080/15376494.2022.2046217.

- **Borges, C. S. P.**, Marques, E. A. S., Ueffing, C., Weißgraeber, P., & da Silva, L. F. M. (2022) *Prüfkörper, Prüfvorrichtung und Verfahren zur Überprüfung von stoffschlüssigen Verbindungen sowie Verwendung des Prüfkörpers* (German Patent and Trade Mark Office Application No. 102022202551.2).

- **Borges, C. S. P.**, Marques, E. A. S., Carbas, R. J. C., Akhavan-Safar, A., Ueffing, C., Weißgraeber, P. & da Silva, L. F. M. (2022). Testing method to determine the strength and fracture energy of adhesives in a single continuous test. *International Journal of Applied Mechanics. Submitted.*

Publications regarding adhesive joints research

- **Borges, C. S. P.**, Nunes, P. D. P., Akhavan-Safar, A., Marques, E. A. S., Carbas, R. J. C., Alfonso, L., & da Silva, L. F. M. (2020). A strain rate dependent cohesive zone element for mode I modeling of the fracture behavior of adhesives. *Proceedings of the Institution of Mechanical Engineers, Part L: Journal of Materials: Design and Applications*, 234(4), 610-621. DOI: 10.1177/1464420720904026.

- **Borges, C. S. P.**, Nunes, P. D. P., Akhavan, A., Marques, E. A. S., Carbas, R. J. C., Alfonso, L., & da Silva, L. F. M. (2020). Influence of mode mixity and loading rate on the fracture behaviour of crash resistant adhesives. *Theoretical and Applied Fracture Mechanics*, 107, 102508. DOI: 10.1016/j.tafmec.2020.102508.

- Nunes, P. D. P., **Borges, C. S. P.**, Marques, E. A. S., Carbas, R. J. C., Akhavan-Safar, A., Antunes, D. P., Lopes, A.M. & da Silva, L. F. M. (2020). Numerical assessment of strain rate in an adhesive layer throughout double cantilever beam and end notch flexure tests. *Proceedings of the Institution of Mechanical Engineers, Part E: Journal of Process Mechanical Engineering*, 234(5), 415-425. DOI: 10.1177/0954408920916007.

- Marques, E. A. S., Nunes, P. D. P., Akhavan-Safar, A., **Borges, C. S. P.**, Carbas, R. J. C., Machado, J. J. M., Parente, M. P. L. & da Silva, L. F.

M. (2021). Techniques for the Mechanical Characterization and Numerical Modelling of Bonded Automotive Structures Under Impact Loads. In *Industrial Applications of Adhesives* (pp. 79-106). Springer, Singapore. DOI: 10.1007/978-981-15-6767-4_5.

- **Borges, C. S. P.**, Marques, E. A. S., Carbas, R. J. C., Akhavan-Safar, A., Ueffing, C., Weißgraeber, P. & da Silva, L. F. M. (2022). Testing method to determine the strength and fracture energy of adhesives in a single continuous test *Submitted*.

Publications regarding educational research

- Reis, M., Duarte, T., Marques, E. A. S., **Borges, C. S. P.**, Castro Sousa, F., Carbas, R. J. C., & da Silva, L. F. M. (2021). The Increase of Brazilian Students in a Portuguese Engineering School: Motivations for International Mobility and the Key Educational Challenges. *U. Porto Journal of Engineering*, 7(1), 63-75.

- **Borges, C. S. P.**, Barbosa, A. Q., Duarte, T. M. G. P., Lopes, H. S., Najafabadi, A. J. & da Silva, L. F. M. (2022). Women in Mechanical Engineering: A case study of the Faculty of Engineering of the University of Porto in the last 20 years. *Journal on Teaching Engineering*. DOI: 10.24840/2795-4005_002.001_0005.

Books

- Marques, E. A. S., Carbas, R. J. C., **Borges, C. S. P.** & da Silva, L. F. M.(2022). *Introdução à ciência e engenharia dos materiais: Teoria* (1st ed.). Portugal: Engebook.

- Marques, E. A. S., Carbas, R. J. C., **Borges, C. S. P.**, Sousa, F. M. C. & da Silva, L. F. M.(2022). *Introdução à ciência e engenharia dos materiais: Prática* (1st ed.). Portugal: Engebook.

Chapter 1

Introduction

1.1 Background and motivation

Adhesives are progressively replacing more conventional joining methods, such as riveting, bolting and welding [1]. On one hand, bolting and riveting rely on the introduction of holes to the joined parts, which creates stress concentration sites, altering the damage mechanisms and causing premature failure of the joined assembly [2]. This is particularly relevant when joining composite materials, which are extremely notch sensitive. On the other hand, welding depends on the local heating of the components involved in the joining process, which can cause local degradation of the materials [1]. Adhesive bonding has been presented as an interesting alternative to address these issues, promoting a more uniform stress distribution, higher load transmission, good damping properties and also enabling more freedom of design and the use of composite materials in applications where they would otherwise be unsuitable.

This work focuses on a particular application of adhesive joints, a housing for electronic components used in the automotive industry. Adhesives often find suitability in the automotive industry in structural and non-structural applications, as the one studied in this work. In the transportation sector, in general, adhesives are advantageous due to their high strength-to-weight ratio, and their ability to bond dissimilar materials, including composites, which allows a more extensive weight reduction of the final assembly. The decrease in weight of the structure leads to a decrease in energy consumption of the vehicle and, consequently, a decrease in gas emissions. The housing for electronic components under analysis is manufactured from a composite material, polybutylene terephthalate with 30% of short glass fiber

reinforcement (PBT-GF30). This housing is manufactured in two parts, using injection molding, and then joined using a silicone adhesive. The silicone adhesive aims to not only join the two parts, but also seal the assembly, ensuring the electronic components within the housing are protected from environmental humidity and contamination. Additionally, the housing is connected to an aluminum heat sink and, in this connection, the adhesive is important to ensure joining, sealing and thermal insulation of the PBT-GF30 housing.

As for the main setbacks usually associated to the use of this joining method, one can highlight the need for tools to maintain the substrates in place when bonding and the time and/or temperature required to obtain the desired cure of the adhesive. The surface of the substrates also needs careful preparation cleaning and degreasing to ensure an appropriate bond strength, which can increase the complexity of the manufacturing process. Additionally, they are inadequate to use under peel and cleavage loading, and very sensitive to severe environmental conditions, particularly high temperature and humidity. This project focuses on two of these disadvantages: (i) the need for surface preparation, i.e., sensitivity to contaminated surfaces, and (ii) vulnerability to high temperature and humidity conditions.

The effect of humidity is particularly concerning in the housing under analysis since, if the joint fails to seal the assembly, the electronic components within the housing will be exposed to humidity and, therefore, compromised. And, in adhesive joints, although humidity can change the properties of the adhesive and substrate, it can also contribute to debonding of the adhesive from the substrate. Additionally, in the joint under analysis, as said, the PBT-GF30 is not only bonded to a similar material, but also to aluminum. In the manufacturing process of the aluminum heat sink, milling fluids that contain oils are used to ensure proper cooling and lubrication. Afterwards, to ensure these milling fluids do not damage the adhesive joint quality, by staying at the adhesive/substrate interface, they are cleaned using a detergent, that contains surfactants, and rinsed. However, after rinsing, the surfactant can also stay on the adhesive/substrate interface and act as a contamination layer.

Therefore, to ensure the adhesive joints follow their idealized behavior and accomplish their sealing purpose in this assembly, it is important to understand the effects of humidity, particularly at high temperature, and of surfactant contamination on the joint properties.

1.2 Objectives

This project had two main goals: the first was the careful and in-depth study of the effect of water and contamination on adhesive joints, and the second was the creation of a testing methodology, suitable for implementation in industrial environments, to easily assess the effects of a given environment or contaminant on an adhesive joint for any adhesive/substrate system used.

For the first goal, the specific objectives were:

- to study the effect of water on the bulk substrate and bulk adhesive;
- to evaluate the effect of water on the adhesive joint, including the interface;
- to analyze the effect of contamination on the adhesive;
- to determine the effect of contamination on the adhesive joint;
- to numerically simulate the phenomena described above.

The knowledge developed on the first part was, then, used to create a simple test, which can be used in industrial environments, to swiftly understand if a given adhesive/substrate system can resist a certain humidity, temperature and contamination condition without debonding.

1.3 Research methodology

In this work, the real joint under consideration was a two-part housing for electronic components. The two parts of the housing are composed of a composite (PBT-GF30) and bonded using a silicone adhesive. The housing is also bonded to an aluminum heat sink. Bulk specimens and standard joints were manufactured from those materials to conduct the analysis proposed in the project. The scheme of the work is represented in Figure 1.1.

Task 1: Review on the effect of aging and contamination on the interfacial properties of adhesive joints.

This task consists of a comprehensive review on the published results to illuminate the road of the research. In this part, the already published numerical and experimental results were analyzed. This task covered the already considered experimental efforts for characterizing the interfacial properties of adhesive joints and their variation with different levels of moisture and contamination exposure.

Task 2: Experimental study to investigate the effect of humidity on tensile and shear, adhesive and cohesive failure of adhesive joints.

Task 2.1: Effect of humidity on composite substrate. The aim of this sub-task was analyze the water uptake behavior of the substrate and understand how this behavior changes with: (i) the presence of fibers, comparing with fiber-free material; (ii) temperature, testing for three different immersion temperatures. The environmental temperature range for the humidity studies is between room temperature and 130 °C, since this is the peak temperature recorded in the manufacturing, packaging and transport processes.

Task 2.2: Effect of humidity on the silicone adhesive. The main purpose of this sub-task was analyzing the water uptake behavior of the adhesive for three different temperatures and its effect on the adhesive's properties.

Task 2.3: Effect of humidity on adhesive joints with silicone adhesives and composite and aluminum substrates. In this sub-task, the complete adhesive joint was analyzed. First, for PBT-GF30/silicone adhesive joints, tests were performed to

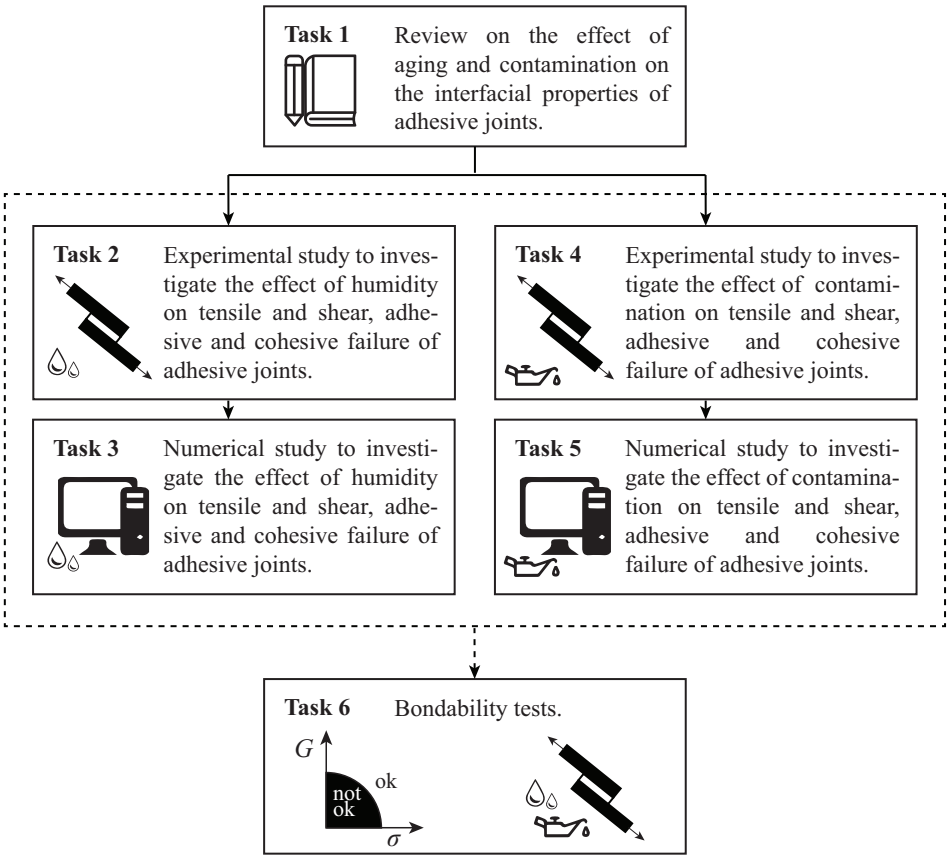


Figure 1.1: Schematic representation of the workflow of the tasks performed in this work.

assess the changes in joint strength and failure mode. The experimental tests performed were: (i) double cantilever beam (DCB), to study the effect of humidity on the crack propagation of adhesive joints; (ii) single lap joints (SLJ), to access shear strength of the joints. The results determined the influence of humidity on the adhesive and cohesive failure of the considered joints. The effect of substrate material on the water uptake of the joint was also studied by using two different materials as substrates (aluminum alloy and PBT-GF30). This experimental work provided insights on the time dependent competition of diffusion mechanisms under exposure to moisture and their effect on joint properties.

Task 3: Numerical study to investigate the effect of humidity on tensile and shear, adhesive and cohesive failure of adhesive joints.
Using the experimental results obtained in Task 2, a numerical procedure was developed to simulate the water uptake of the joints, as well as the adhesive and cohesive failure of the aged joint and validated with the experimental results. The main purpose of this task was creating a model, which is able to consider the conditions that lead to a significant decrease in joint strength and adhesive failure.

Task 4: Experimental study to investigate the effect of contamination on tensile and shear, adhesive and cohesive failure of adhesive joints.
In this task, first, the effect of surfactant on the bulk adhesive was studied. To study the effect of contamination on the failure mechanisms of adhesive joints, four different levels of contamination were experimentally replicated by using surfactant contamination. The same standard tests described in sub-task 2.2 were performed. The main challenge of this task was creating a method to contaminate the samples in a consistent and repeatable way, to obtain comparable results between samples with the same materials and the same levels of contamination.

Task 5: Numerical study to investigate the effect of contamination on tensile and shear, adhesive and cohesive failure of adhesive joints.
Using the experimental results obtained in Task 4, a numerical procedure was developed to simulate the interfacial failure of the contaminated joints in tensile and shear loading conditions. The numerical part takes into account the degradation of the interface properties as a function of different levels of contamination. The numerical model was validated through the experimental tests performed.

Task 6: Bondability tests.
The knowledge acquired in the previous Tasks 2-5 was used to develop a simple test that can be used to assess if substrates, adhesives and surface preparations perform within an acceptable range for a given environmental/contaminated condition.

The main purpose of this test is being easily reproduced in industrial applications, for a given environmental/contaminated, to quickly and accurately assess if the adhesive/substrate combination is suited to be used in a specific application. The geometrical configuration for this test, combines pull-off and peel testing.

1.4 Outline of the thesis

This thesis consists of seven peer reviewed papers, one patent and a summary. The correspondence between papers and tasks is presented in Figure 1.2

The summary is divided in seven main parts. This introductory chapter contains a brief description of the problem addressed, as well as the background and motivation of this work and its objectives. Additionally, it displays a brief summary of each paper presented. Chapter 2 presents a concise literature review on the mechanisms and effects of water absorption on adhesive joints. Chapter 3 clarifies the experimental procedures used throughout this work to assess the effect of humidity and surfactant contamination on adhesive joints. Chapter 4 presents a succinct description of the numerical models used in this work. Chapter 5 presents the main conclusions about the topics of research and Chapter 6 presents suggestions for further work on these topics. The appendices comprehend the publications developed in the scope of this thesis that represent the research developed, in detail.

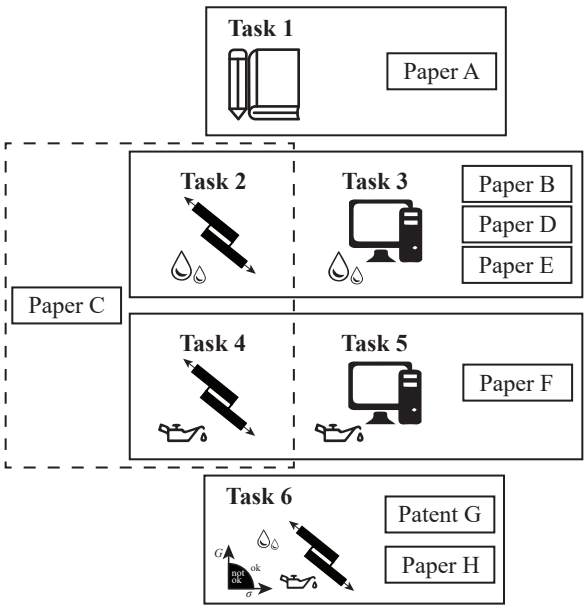


Figure 1.2: Correspondence between tasks proposed and papers published.

Paper A: Review on the effect of moisture and contamination on the interfacial properties of adhesive joints

Borges, C. S. P., Marques, E. A. S., Carbas, R. J. C., Ueffing, C., Weißgraeber, P., & da Silva, L. F. M. (2021). Review on the effect of moisture and contamination on the interfacial properties of adhesive joints. *Proceedings of the Institution of Mechanical Engineers, Part C: Journal of Mechanical Engineering Science*, 235(3), 527-549. DOI: 10.1177/0954406220944208. IF=1.762; Q2; ISI, Indexed in Scopus

Adhesives play an important role in many key industrial sectors, such as the automotive industry, enabling the construction of lightweight, multi-material structures, combining polymers, composites and metals. However, adhesives are usually polymeric materials, which can be affected by environmental and working conditions, such as moisture and contamination. Although moisture and contamination degrade the adhesive, the failure of a bonded joint is often ultimately interfacial. Therefore, a literature review on the influence of those factors on the interfacial properties of adhesive joints is performed to understand the phenomena that take part in the degradation on adhesive joints when subjected to humid and contaminated environments, which can oftentimes be the case in factory conditions, especially for parts from third-party suppliers. The mechanisms and effects of moisture aging and contamination are presented, as well as experimental testing methods and practical case studies. It is concluded that both moisture and other contaminants may lead to a reduction in joint strength and catastrophic adhesive failure. Moisture absorption can occur through the adhesive, but in an adhesive joint, it can additionally occur through the substrate, the interface between the adhesive and the substrate or in the cracks and pores of the adhesive. After water ingresses into the adhesive, it decreases its mechanical properties and plasticizes it. However, in an adhesive joint, water diffusion occurs much faster than in bulk adhesive due to the complementary diffusion paths, which typically leads to adhesive failure at the adhesive/substrate interface. Additionally, in an adhesive joint, water may induce the hydrolysis of the substrates or have other chemical interactions with them. Contaminants can diffuse through the joint or remain at the adhesive/ substrate interface. When they diffuse through the joint, they have consequences similar to those of water sorption. However, when they remain at the interface, they can produce locally debonded areas, which may lead to joint failure.

Paper B: Effect of water ingress on the mechanical and chemical properties of polybutylene terephthalate reinforced with glass fibers

Borges, C. S. P., Akhavan-Safar, A., Marques, E. A. S., Carbas, R. J. C., Ueffing, C., Weißgraeber, P., & da Silva, L. F. M. (2021). Effect of water ingress on the mechanical and chemical properties of polybutylene terephthalate reinforced with glass fibers. *Materials*, 14(5), 1261. DOI: 10.3390/ma14051261. IF=3.623; Q2; ISI, Indexed in Scopus

Short fiber reinforced polymers are widely used in the construction of electronic housings, where they are often exposed to harsh environmental conditions. The main purpose of this work is the in-depth study and characterization of the water uptake behavior of PBT-GF30 (polybutylene terephthalate with 30% of short glass fiber)as well as its consequent effect on the mechanical properties of the material. Further analysis was conducted to determine at which temperature range PBT-GF30 starts experiencing chemical changes. The influence of testing procedures and conditions on the evaluation of these effects was analyzed, also drawing comparisons with previous studies. The water absorption behavior was studied through gravimetric tests at 35, 70, and 130 °C. Fiber-free PBT was also studied at 35 °C for comparison purposes. The effect of water and temperature on the mechanical properties was analyzed through bulk tensile tests. The material was tested for the three temperatures in the as-supplied state (without drying or aging). Afterwards, PBT-GF30 was tested at room temperature following water immersion at the three temperatures. Chemical changes in the material were also analyzed through Fourier-transform infrared spectroscopy (FTIR). It was concluded that the water diffusion behavior is Fickian and that PBT absorbs more water than PBT-GF30 but at a slightly higher rate. However, temperature was found to have a more significant influence on the rate of water diffusion of PBT-GF30 than fiber content did. Temperature has a significant influence on the mechanical properties of the material. Humidity contributes to a slight drop in stiffness and strength, not showing a clear dependence on water uptake. This decrease in mechanical properties occurs due to the relaxation of the polymeric chain promoted by water ingress. Between 80 and 85 °C, after water immersion, the FTIR profile of the material changes, which suggests chemical changes in the PBT. The water absorption was simulated through heat transfer analogy with good results. From the developed numerical simulation, the minimum plate size to maintain the water ingress unidirectional was determined to be 30 mm, which was validated experimentally.

Paper C: Influence of water and surfactant contamination on the mechanical and chemical properties of a silicone adhesive before and after curing

Borges, C. S. P., Brandão, R., Akhavan-Safar, A., Marques, E. A. S., Carbas, R. J. C., Ueffing, C., Weißgraeber, P., Schmid, F., & da Silva, L. F. M. (2022). Influence of water and surfactant contamination on the mechanical and chemical properties of a silicone adhesive before and after curing. *The Journal of Adhesion. Submitted.* IF=2.917; Q1; ISI, Indexed in Scopus

This work aims to analyze the mechanical and chemical effects that contaminants can have prior to curing of the silicone adhesive, if they are in the substrate or surrounding environment at adhesive application, as well as after curing when they appear during the service life of the joint. In this case, the contaminants are water and a surfactant present in detergents used to clean oils from aluminum surfaces. For this, 2%, 5%, and 10% of contaminant was added to the adhesive prior to curing and neat adhesive after curing was immersed in contaminant at different temperatures. For all cases, the effect on the mechanical properties was evaluated through bulk tensile tests, the effect on the chemical profile was evaluated using Fourier-transform infrared spectroscopy (FTIR) and the morphology of the materials was studied with scanning electron microscopy (SEM). The water immersion increased slightly the mechanical properties of the adhesive, which returned to their initial value upon redrying. However, high immersion temperatures introduce irreversible damage in the material. Water added prior to curing introduces voids in the adhesive, decreasing its strength. The surfactant added prior to curing changes the adhesive morphology, showing a variation in the C-H bond. These changes translate into a lower strength and stiffness of the mixture.

Paper D: The influence of humidity and immersion temperature on the properties and failure mode of PBT-GF30/silicone bonded joints

Brandão, R., **Borges, C. S. P.**, Akhavan-Safar, A., Marques, E. A. S., Carbas, R. J. C., Ueffing, C., Weißgraeber, P., Schmid, F., & da Silva, L. F. M. (2021). The influence of humidity and immersion temperature on the properties and failure mode of PBT-GF30/silicone bonded joints. *Composite Structures*, 115421. DOI: 10.1016/j.compstruct.2022.115421. IF=5.407; Q1; ISI, Indexed in Scopus

The housing of automotive electrical components are commonly manufactured from polybutylene terephthalate with 30% of glass fiber (PBT-GF30). These housings can be subjected to severe conditions of temperature and humidity that can

catalyze the degradation of their properties. In order to connect the different parts of the housing, a silicone adhesive is used, which also serves as a sealant preventing moisture from entering the final component. Therefore, to understand if the joint serves its purpose correctly, the effects of temperature and water uptake in joints with PBT-GF30 substrates and silicone adhesive were studied. Single lap joints (SLJ) and double cantilever beam (DCB) joints were tested at three different temperatures (70, 90 and 130 °C) and in three different conditions (dried, aged in water and dried after aging). To understand if water immersion introduced irreversible damage to the joints, the re-dried condition was also analyzed. The tensile properties of the bulk substrate and adhesive for all conditions were also determined. It has been seen that, generally, since the adhesive has a higher strength when aged, this leads to a better joint performance at this condition. However, at 90 °C and 130 °C there was chemical degradation of the PBT-GF30 after aging, which led to failure approaching the substrate in those conditions for the SLJ. This was attributed to the release of chemical compounds that stay at the adhesive/substrate interface. In the DCB, since the loading of the substrate is even more severe, there was substrate failure. Finally, a numerical model was created for all conditions tested, which showed that the joints can be simulated by the properties of the bulk adhesive and substrate, showing that the effect of the interface is not preponderant.

Paper E: Effect of the interface/interphase on the water ingress properties of joints with PBT-GF30 and aluminum substrates using silicone adhesive

Borges, C. S. P., Marques, E. A. S., Carbas, R. J. C., Akhavan-Safar, A., Ueffing, C., Weißgraeber, P. & da Silva, L. F. M. (2022). Effect of the interface/interphase on the water ingress properties of joints with PBT-GF30 and aluminum substrates using silicone adhesive. *Engineering Failure Analysis. Submitted.* IF=3.114; Q1; ISI, Indexed in Scopus

One of the main setbacks of adhesive joints is their sensitivity to humid environments, particularly at high temperature. Although the adhesive and substrate (if polymeric in its matrix) can absorb water, failure of water aged joints has been seen to be ultimately interfacial. The aim of this work is to analyze the difference between adhesive/composite and adhesive/metal interphases, both in terms of water diffusion and failure of the aged joints, understanding if there is a difference in the failure of the adhesive joint, depending on the substrate material. For that, silicone joints with two different substrates were prepared. The substrates were polybutylene terephthalate with 30% of short glass fiber (PBT-GF30) and 6082-T6 aluminum. To

study the water diffusion behavior, rectangular joints were prepared. The water immersion was conducted at 70 °C. These joints were prepared with three different adhesive thicknesses (0.5, 1 and 2 mm) so that the effect of the interphase could be isolated. It was concluded that the aluminum/silicone joints absorbed more water through the interphase region than the PBT-GF30/silicone joints, since the difference between the expected water uptake and the experimentally measured mass gain is significantly higher, causing adhesive failure of the joint. The same was not observed in the PBT-GF30/silicone, with a more stable interphase, that does not absorb measurable quantities of water and always exhibits cohesive failure.

Paper F: Effect of surfactant contamination on the properties of aluminum/silicone adhesive joints

Brandão, R., **Borges, C. S. P.**, Marques, E. A. S., Carbas, R. J. C., Akhavan-Safar, A., Nunes, P. D. P., Ueffing, C., Weißgraeber, P., Schmid, F. & da Silva, L. F. M. (2022) Effect of surfactant contamination on the properties of aluminum/silicone adhesive joints, *Mechanics of Advanced Materials and Structures*, DOI: 10.1080/15376494.2022.2046217. IF=4.030; Q1; ISI, Indexed in Scopus

Adhesives are used to join and seal electronic packaging. In these applications, they are often used to bond aluminum components and, during the process of machining aluminum, oils and lubricants are used to facilitate the process. To remove these fluids, detergents such as surfactants are often used. However, if the surfactant itself is not removed completely and remains on the aluminum part, it can affect the bond properties of the joint, leading to abrupt joint failure. In this work, adhesive joint properties as a function of the amount of surfactant at the surface were studied. The joint substrates are Al6082-T6 aluminum, the adhesive a two-part silicone and the surfactant a cocosalkylaminethoxylate. For this, double cantilever beam (DCB) and single lap joints (SLJ) were used. An additional scanning electron microscopy (SEM) analysis was conducted to clarify the results. It was found that the adhesive bond strength continuously decreases with increasing amount of contaminant. Similarly, with increasing amounts of contaminant applied to the surface, the failure mode progressively changed from cohesive to adhesive, which was attributed to the adhesive at the interphase absorbing the contaminant during curing, moving the failure to this region, until the absorption limit of the adhesive is surpassed and the surfactant remains at the interface, leading to interfacial failure. A numerical model was created to simulate the behavior of the experimental joints and obtain the prop-

erties of the interphase by applying the inverse method, and a numerical study was done on the sensitivity of the model to variations in cohesive peel properties for the DCB and shear properties for the SLJ.

Patent G: Test specimen, test device and method for the inspection of material connections and use of the test specimen

Borges, C. S. P., Marques, E. A. S., Ueffing, C., Weißgraeber, P., & da Silva, L. F. M. (2022) *Prüfkörper, Prüfvorrichtung und Verfahren zur Überprüfung von stoffschlüssigen Verbindungen sowie Verwendung des Prüfkörpers* (German Patent and Trade Mark Office Application No. 102022202551.2).

A specimen, device and methodology to characterize an adhesive/substrate combination through one or more pull-off tests, to evaluate strength and one or more peel test, to evaluate fracture energy. This method allows the assessment of strength and fracture toughness under tensile loading to be performed through one continuous test. It also enables the evaluation of the specific adhesive/substrate combination that is going to be used in the productive process, regardless of the substrate geometry, as long as it has enough flat area to bond the specimen. The specimen comprises a pull-off test part, a steel strip, an adhesive and a substrate.

Paper H: Testing method to determine the strength and fracture energy of adhesives in a single continuous test

Borges, C. S. P., Marques, E. A. S., Carbas, R. J. C., Akhavan-Safar, A., Ueffing, C., Weißgraeber, P. & da Silva, L. F. M. (2022). Testing method to determine the strength and fracture energy of adhesives in a single continuous test. *International Journal of Applied Mechanics. Submitted.* IF=3.224; Q1; ISI, Indexed in Scopus

In this work, a new testing method for adhesive joints under tensile loading is presented. This method comprised three pull-off tests and one peel test in one single loading step, which enables the determination of the strength and fracture toughness of the material. The properties determined can be of the adhesive, if cohesive failure occurs, or of the interface, in the event of adhesive failure. To validate the testing method, the adhesive used was a commercially available silicone, for which strength and fracture toughness had already been determined using standard methods. It was concluded that this method accurately enables the determination of strength and toughness, using one single joint and loading.

Chapter 2

Literature review

In this chapter, a brief description of the main points of the review are presented, comprehending the mechanisms and effects of moisture aging and contamination. More information and details can be found in the appended review paper, **Paper A**.

2.1 Moisture aging of adhesive joints

2.1.1 Mechanisms of moisture aging

Moisture aging refers to the degradation of the adhesive joint due to the ingress of water. In the joint moisture can ingress in four different ways [3], Figure 2.1:

1. Diffusion into the adhesive;
2. Diffusion into the interface between the adhesive and the substrates;
3. Diffusion by capillarity into the pores and cracks of the adhesive;
4. Diffusion into the substrate.

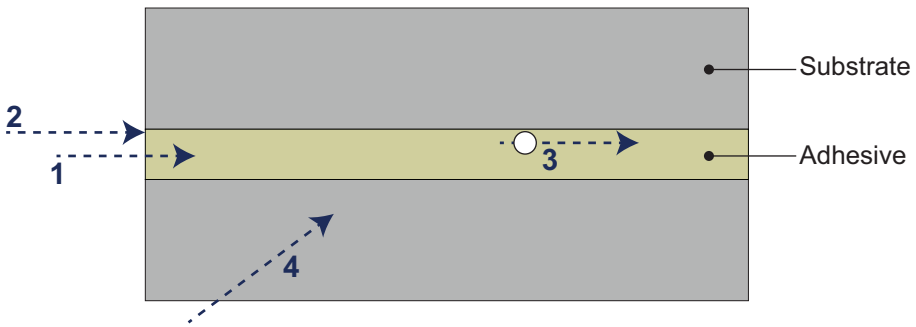


Figure 2.1: Paths of water diffusion in adhesive joints.

Diffusion into the adhesive

Water can be absorbed by adhesives in two different forms [4; 5]: free water and bound water. Free water fills the micro cavities of the polymeric chain of the material. Therefore, as it only occupies free volume, it does not cause volumetric changes. Bound water creates chemical connections with the molecules of the polymeric chain of the adhesive, therefore causing the material to swell. Bound water can be divided into type I and type II according to if it establishes single or multiple hydrogen bonds with the chain of the adhesive, respectively [6; 7].

Bound water interacts with specific sites of the adhesive backbone i.e., it has a discrete array of possible positions, rather than behaving like a gas in an inert matrix [8], these positions have been related to the polar centers of the polymer [6; 9]. To associate with the adhesive, water is able to break the bonds of the polymeric chain, causing the material to swell. Once the material swells, and due to the new openings in the polymeric chain, more water absorption centers are available, further increasing water uptake.

Diffusion of water into the adhesive is often modeled through the variation of mass as a function of time. However, it is not governed by a universal law, for all materials and service conditions. The more commonly used model is the Fick's law [10–14]:

$$M_t = \left[1 - \frac{8}{\pi^2} \sum_{n=0}^{\infty} \frac{1}{(2n+1)^2} \exp\left(\frac{-D(2n+1)^2\pi^2 t}{4h^2}\right)\right] M_\infty \tag{2.1}$$

where t represents the time, starting from immersion and h represents the thickness of the specimen. The coefficients that need to be defined for this model are: the coefficient of diffusion, D, which is related to the rate of water diffusion and M_∞ the water uptake at saturation. However, it is also common to employ the Langmuir model [15–19] or variations of the Fick's law, such as the dual Fick's law [20–22], which consists on two consecutive applications of the Fick's law.

Diffusion into the interface between the adhesive and the substrates

In an adhesive joint, diffusion through the interface is oftentimes the key factor for joint failure, since it may lead to the complete separation between the substrate and the adhesive [23].

Zanni-Deffarges and Shanahan [24] reported that the coefficient of diffusion, D, of an adhesive joint was almost one order of magnitude higher than the D for

the adhesive in bulk form. Therefore, it was concluded that water was folowing different paths, not only entering the joint through the adhesive, and that those paths contributed for a very significant increase in the coefficient of diffusion. In this work, it was suggested that the diffusion was due to capillarity: the energy of the dry adhesive/substrate interface is very high, pulling the water diffusion front into the system. It is also noted that the process by which the water diffuses through the interface is more significant than the diffusion through the bulk adhesive, causing premature failure along the bondline, Figure 2.2.

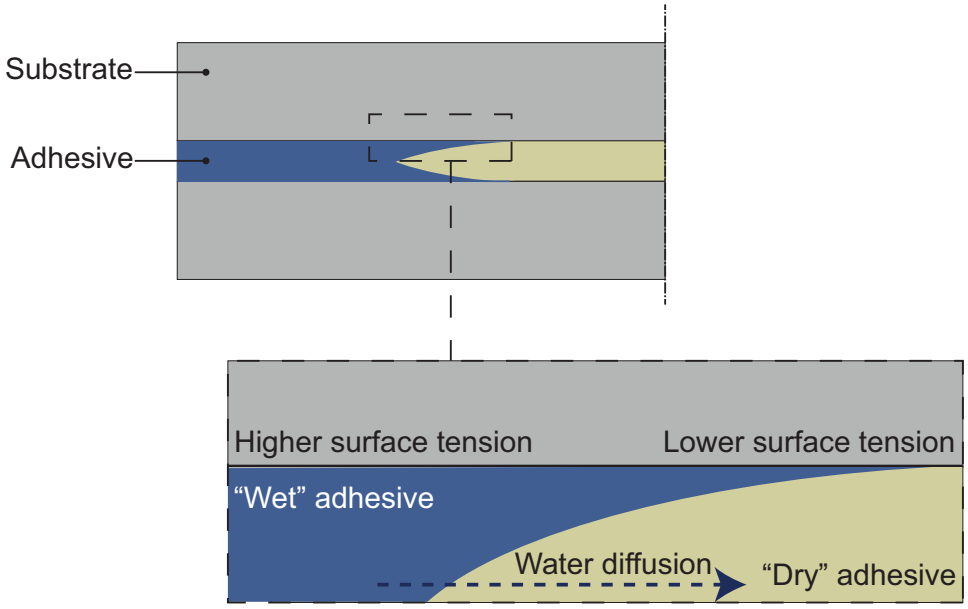


Figure 2.2: Diffusion front near the metal/adhesive transition. The model suggested by Zanni-Deffarges and Shanahan [24].

Diffusion through the interface may also occur due to the structure or polymeric orientation of the adhesive in the regions close to the interface [5].

Drain *et al.* [25], to understand the role that the interface plays in the water absorption process for different substrate materials, analyzed steel-steel and polycarbonate-polycarbonate joints, bonded using a cyanoacrylate adhesive. When bonding polycarbonate substrates, no interface was clearly identified due to the dissolution of the composite in the ethylcyano-acrylate monomer, present in the adhesive, although there is an interphase region of dissolution. Therefore, in the polycarbonate-polycarbonate joints, despite the fact that both the substrate and the adhesive are able to absorb water, there is a higher water resistance since no interfacial diffusion was occurring. In the steel-steel joints, where the interface plane is noticeable, there is interfacial failure of the joint after exposure to water, which

reveals the interface plays a key role in the water diffusion process and must be studied.

Diffusion by capillarity in the pores and cracks of the adhesive

Kinloch *et al.* [26] and Cognard *et al.* [27] discussed the relevance of capillary diffusion in the water ingress in adhesive joints. When water is adsorbed by porous solid materials, it will condensate when its chemical potential matches that of the liquid [27]. Capillary diffusion can cause interfacial failure, through the process of, after condensing, creating an osmotic pressure on the interface, which causes the adhesive to debond, Figure 2.3.

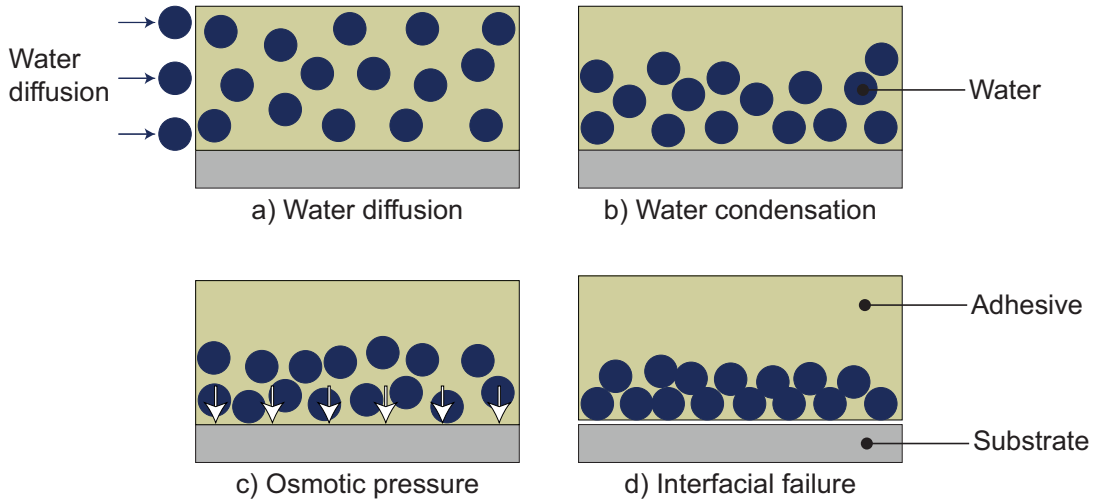


Figure 2.3: Mechanisms of water damage on the adhesive/substrate interface in an adhesive joint (adapted from [27; 28]).

Diffusion into the substrate

Substrates also play an important role in the aging process since they may also interact with water. The behavior of the substrates is highly dependent on their nature. Steel substrates can create a corrosion layer or some migration of components of the substrate to the surface. These components or corroded areas will act as contaminants.

De'Nève *et al.* [29] studied steel joints bonded with an epoxy based adhesive cured with dicyandiamide (DDA) and concluded that prior to aging the failure was interfacial, due to an enrichment of hardener near the interface. For short aging times it was in the adhesive, near the interface, and for long immersion times it occurred at a layer of corrosion mixed with adhesive. If the substrates were zinc

coated, it was observed that zinc diffused into the adhesive during aging, which translated into a better performance of the joint.

Two of the main advantages of adhesive joints are the non-existence of holes in the materials being bonded (which avoids stress concentrations to which composite materials are very sensitive), as well as the ability to bond dissimilar materials, such as composites and metal. Therefore, it can be understood that composites are a very representative family of substrates when studying adhesive joints. In composite substrates, the matrix is usually much more hydrophilic than the fibers, or other inclusions. The matrix will absorb water as as previously described for the adhesive, since it is also a polymer. Additionally, a similar phenomenon as the one represented in Figure 2.2 was reported, where water diffusion occurs at the matrix/inclusion interface [24; 30]. Consequently, it is very relevant to study the effect of moisture in composite materials since if composite materials are used as substrates in an adhesive joint, water will diffuse through them, reaching the adhesive/substrate interface and, therefore, the adhesive. Additionally, as said, a parallelism may be done between the adhesive/substrate interface in adhesive joints and the matrix/inclusion interface in composite materials.

2.1.2 Effects of moisture aging on adhesive joints

The effects of moisture aging are analyzed in this subsection, considering first the effect of water on the bulk adhesive and, afterwards, the effect on the whole adhesive joint.

Effect on adhesives

Adhesives, after being exposed to humid environments generally show a significant decrease in their elastic modulus and strength [31–33] as well as their fracture toughness [24; 34–36]. However, this decrease in strength is pared with an increase in ductility [31–33] and creep strain [37]. The glass transition temperature, T_g, has been also shown to decrease with increasing water content in the majority of the cases [38–41]. However, in some cases water absorption may slightly increase T_g, since there is a creation of secondary cross-linking between the polymeric chain and type II bound water. The portion of type II bound water depends on the temperature and it is more difficult to remove than type I, since it establishes more hydrogen bonds with the adhesive [5].

As said in subsection 2.1.1, bound water absorbed by the adhesive creates chem-

ical bonds with the material, changing its volume which is referred to as swelling of the adhesive. This volumetric change is highly affected by temperature, increasing as temperature increases [42] and is dependent on the chemical affinity of the adhesive with water, since it only happens if chemical bonds are established.

Effect on adhesive joints

The properties of the adhesive may be degraded by the presence of water, however, it has been reported that the key factor for premature failure of an adhesive joint when exposed to water is the effect of moisture on the interface, or the interphase, rather than on the bulk materials themselves [43].

The first clear effect of water on a joint is the effect of the osmotic pressure, discussed previously and presented in Figure 2.3. There is also interfacial stress caused by the adhesive swelling, constricted by the substrates, Figure 2.4.

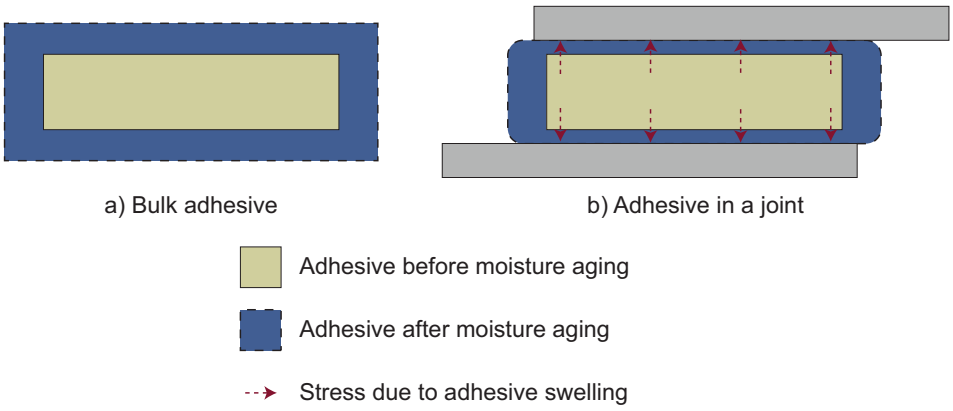


Figure 2.4: Swelling of the adhesive after being exposed to a humid environment in bulk and in a joint (adapted from [28]).

The substrates also play an important role in the variation of properties of the adhesive joint. In joints with steel substrates, and particularly at high temperatures, corrosion may occur, with the apearence of iron oxides at the adhesive/substrate interface [43–45]. In joints with composite substrates, as for the mechanisms of water diffusion explored in subsection 2.1.1, a parallelism between the adhesive/substrate and the matrix/inclusion may be done. That said, the matrix/inclusion interface often presents a preferential water ingress path, as well as a higher stress location (due to the swelling of the matrix or osmotic pressure), which can result in the separation between the matrix and the inclusions, reducing the stress transfer between them [4; 46; 47].

The damage caused by water in an adhesive, or adhesive joint, is oftentimes a combination of reversible and irreversible processes [9; 48; 49]. If the material fully restores its properties after being re-dried, the changes are said to be reversible [4; 50]. If this does not occur, there is some irreversible damage, which suggests the presence of some chemically attached water. If the specimens are re-dried at low temperatures, a difficulty in achieving complete water desorption can be observed, which may indicate that the bound water needs more energy to break the chemical bonds [42].

2.2 Contamination of adhesive joints

2.2.1 Mechanisms of contamination

Contamination can arise from multiple sources, both during the manufacturing process and service life. In this review, the external contaminants considered are oil, which can originate from the cutting of aluminum substrates, and tensides, which can be found on detergents. Contaminants can lead to an unpredictable behavior of the adhesive joint. Contaminants at the adhesive/substrate interface, typically, exhibit three types of behaviors [51]:

- Diffuse into the adhesive;
- Diffuse into the substrate;
- Remain at the adhesive/substrate interface imposing a physical separation between them.

The most concerning cases occur when the contaminant remains at the interface, composing a very thin-layer, which can be in the nanometric scale, that impedes the inter-molecular interactions between the adhesive and the substrate [52–54]. Therefore, these contaminated areas are regions where the adhesive and substrate are not in intimate contact and only weak adhesion bonds are formed, which in the most extreme cases can be what some authors call kissing bonds or zero volume debonds.

Oil accommodating adhesives

Adhesives can be tuned to improve their performance when contaminants, such as oils, arise at the adhesive/substrate interface. Generally, when in contact with an

oily surface, adhesives must be able to, first, displace the excess contaminant from the substrate surface and, second, absorb the remaining contaminant [51; 55], which may be trapped due to the roughness of the surface, Figure 2.5.

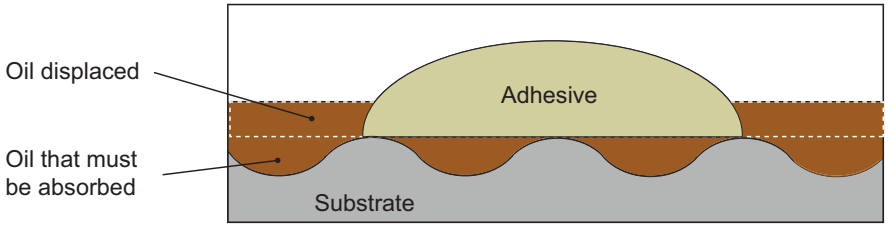


Figure 2.5: Oil accommodating adhesives (adapted from [55; 56]).

In an attempt to mimic and understand what happens if oil appears at the substrate during the cutting of the metallic substrates, Greiveldinger *et al.* [57] placed an oil contaminant on the surface of the substrate prior to the curing of the adhesive. The interface was then analyzed using Fourier-transform infrared spectroscopy (FTIR). Prior to curing, the profile of the interface was very close to that of the oil, suggesting that the oil was, as expected, accommodated between the adhesive and the substrate. However, at the end of the curing process it was similar to that of the uncontaminated adhesive, suggesting that the adhesive absorbed the oil without a significant change in its FTIR profile.

2.2.2 Effects of contamination on adhesive joints

Contaminants may have an influence at different stages of the adhesion process: prior to the application of the adhesive, the curing of the adhesive or the service life of the joint.

Prior to the adhesive application, tensides, as found in detergents, mold release agents and oils decrease the surface energy, leading to poorer wettability of the substrate by the adhesive, which leads to lower adhesion strength.

In adhesive joints with epoxy based adhesives, during the curing of the adhesive, a difference in T_g was observed when in the presence of contamination, being the T_g lower for higher contamination levels, which suggests contaminants change the kinetics of the cross-linking. Despite this difference in the cross-linking process, Debski *et al.* [55] reported that the final T_g is the same for all cases. Hong *et al.* [58], through a differential scanning calorimetry (DSC) analysis, concluded that there is a decrease of the cure exotherm in the presence of contamination, also reporting that the final T_g of the adhesive increased as the oil content increased.

An additional thermogravimetric analysis (TGA) showed a decrease in total weight loss percentage with increasing oil content, which suggests the presence of oil has an influence on the thermal degradation mechanisms. Comyn [3] stated that steel substrates interact with the amine component used as curing agent, which leaves the adhesive layer particularly rich in epoxy. Epoxy is incompatible with oil and acts as a barrier to the absorption of contaminant which, therefore, remains at the interface.

The effect of contamination on adhesive joints is a highly complex subject, since it will depend on the adhesive, the substrate, the contaminant and the interactions between them. However, two typical of behaviors can be established, Figure 2.6: (i) the contaminant disappears from the adhesive/substrate interface, diffusing into the adhesive or the substrate, (ii) the contaminant remains at the adhesive/substrate interface.

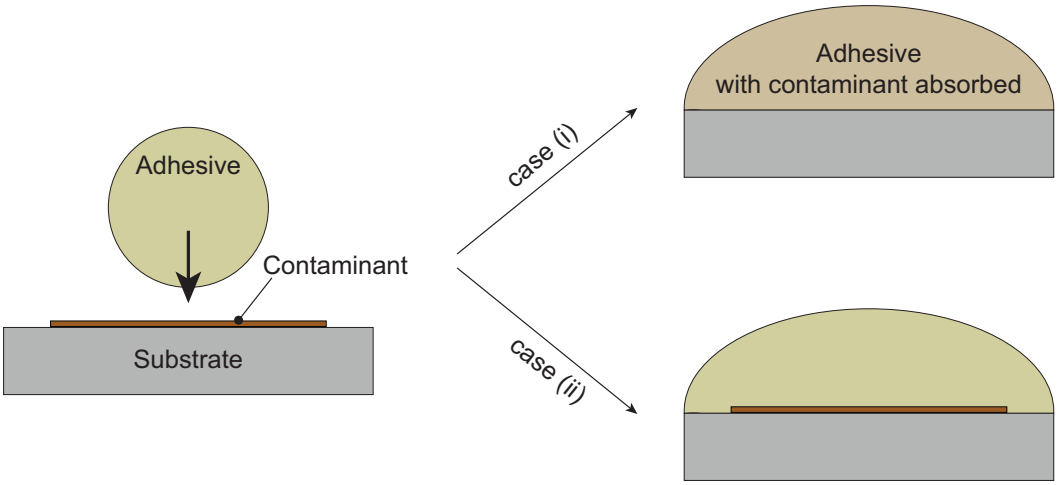


Figure 2.6: Effect of contamination on adhesive joints.

Moisture aging generally represents a particular situation of the first case, where the contaminant is absorbed. Other examples are the oil contaminants previously discussed in this subsection, which are absorbed by the adhesive during the curing process.

If a contaminant cannot be absorbed by the adhesive or the substrate, due to chemical or physical incompatibilities, zero volume debonds may appear. These debonds present preferential paths for crack propagation and contribute to unstable crack growth, through the interface, also decreasing significantly the strength of the joint, which may have catastrophic consequences if a sufficient area of the joint is affected [53; 59].

Chapter 3

Materials and experimental methods

In this chapter, the materials used, as well as the general characteristics of the tests performed are presented. The experimental tests are divided into three sections: gravimetric tests, mechanical tests and complementary tests. In the gravimetric tests, the fluid uptake of specimens is the object of study. In this humidity study, a temperature range between room temperature and 130 °C is analyzed, since this represents the peak temperature recorded in the manufacturing, packaging and transport process. Mechanical tests are performed to characterize bulk materials or joints. Complementary tests comprehend analysis performed to further characterize the materials or help results' interpretation.

3.1 Materials

3.1.1 Substrates

Two substrates were used in this work: polybutylene terephthalate with 30% of short glass fiber (PBT-GF30) and aluminum 6082-T6.

PBT-GF30

PBT is particularly interesting due to its rapid crystallization, good processing characteristics for short extrusion and injection molding, excellent mold flow, and improved flexibility when compared to other polyesters, since it has two additional methylene units in the main chain when compared to polyethylene terephthalate (PET) [60–62]. However, at low temperatures and high deformation rates, the material has limited toughness.

PBT-GF30 is widely used in applications such as the housing for electronic components due to its good properties and suitability for manufacture through injection molding. Its fast crystallization rate enhances moldability and, consequently, leads to parts with good surface quality [63; 64].

Aluminum

The aluminum substrates used in this study are 6082-T6. This structural alloy is from the 6XXX series, which comprehends aluminum-magnesium-silicon alloys [65]. 6082-T6 aluminum is a medium to high strength alloy with increased ductility and toughness [66]. The T6 indicates that this material was submitted to a temper, a solution heat treatment followed by quenching in water and precipitation hardening, which induces higher alloy strengthening [67; 68].

3.1.2 Adhesive

The silicone adhesive used was a flowable two-part addition curing silicone rubber, which is commercially available.

The main characteristics of this adhesive after curing are medium hardness, ability to bond a wide variety of substrates, heat resistance and long-term stability. The mechanical properties of the adhesive, given by the manufacturer, can be found in Table 3.1.

Table 3.1: Properties of the adhesive used, provided by the manufacturer.

Property	Silicone adhesive
Tensile strength [MPa]	2.2
Elongation at break [%]	200

However, the manufacturer suggests an adhesive/catalyst ratio of 10:1 and a cure at room temperature for two weeks.

In this project, these values were adjusted to mimic the ones used in the productive process at the company of interest. The adhesive/catalyst ratio used was 1:1 and the mixture was performed using a speed mixer and cured at 120 °C for 25 minutes.

3.1.3 Contaminants

The contaminants used in this study are distilled water, for the humidity studies, and surfactant for the surface contamination studies.

The surfactant is Cocosalkylaminethoxylate, manufactured by SysKem Chemie GmbH (Wuppertal, Germany). This surfactant is present in the detergents used to clean the aluminum substrates from the oils used during the manufacturing process. This contaminant is a base, with a pH between 9 and 11 (1% sol) [69].

3.2 Gravimetric tests

3.2.1 Bulk materials

Gravimetric tests of the bulk materials were performed to determine the water uptake behavior of the PBT-GF30 and silicone. The gravimetric test of the PBT-GF30 can be found on **Paper B** for immersion in water inside a climatic chamber at 35, 70 and 130 °C. Fiber-free PBT was also analyzed at 35 °C. In **Paper C** the water uptake behavior of the silicone adhesive for temperatures of the climatic chamber of 70, 90 and 130 °C was determined. In **Paper C**, in addition to water, an attempt was also made to establish the surfactant uptake behavior of silicone. However, it was seen that the silicone does not distinctly absorb surfactant after cured, and that is the motive behind the higher importance given to water as the immersion fluid in this section. In **Paper D** the water uptake of PBT-GF30 at 90 °C was determined.

Specimen manufacturing

In **Paper B**, to study PBT-GF30 and fiber-free PBT, the ISO 294-3 standard [70] was followed. This standard relies on the use of 1 mm thick 60x60 mm^2 plates, Figure 3.1.

The most important detail in these plates is that the thickness is much smaller than the side length, so that the water diffusion in the material can be considered unidirectional, through the thickness.

For the PBT-GF30 and PBT, 1 mm thick plates were obtained from injection molding and, afterwards, the specimens were cut to the desired size. Also in **Paper B**, smaller plates, 1 mm thick 30x30 mm^2 plates, Figure 3.2, were validated against standard specimens at 70 °C. The main advantages of the smaller specimens are: (i) lowering the amount of material used to $\frac{1}{4}$ and (ii) being easier to store immersed

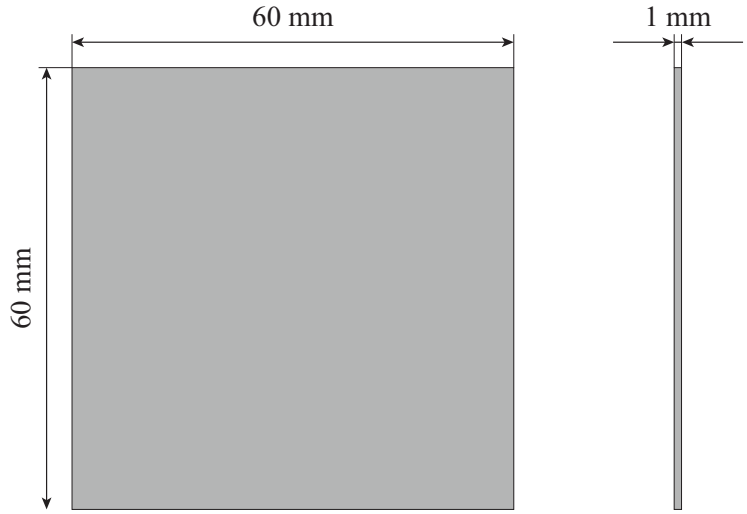


Figure 3.1: Specimens used for the gravimetric study of the bulk materials following the ISO 294-3 standard [70].

in smaller containers, also requiring less water to reach full immersion. Those were the plates used in **Paper C** to study the water uptake of silicone adhesives and in **Paper D** to study the water uptake of PBT-GF30 at 90 °C.

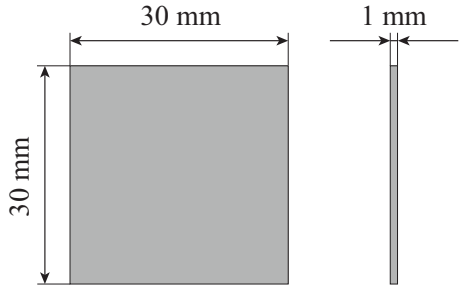


Figure 3.2: Reduced scale specimens used for the gravimetric study of the bulk materials.

For the silicone, the specimens were cut from an 1 mm-thick plate of adhesive prepared according to the French NF T 76-142 standard [71]. A mold is lined with a 1 mm thick silicone frame. The frame is used not only to impose the thickness of the adhesive layer but also to ensure hydrostatic pressure minimizing the amount of defects in the plate. The adhesive is then placed inside the frame and cured using a hot-plate press.

Experimental procedure

The bulk plates of material were fully dried in silica before they were immersed in distilled water. When dried, the surface of the specimens was treated using sandpaper to remove surface contamination. Afterwards, the mass of the plates was recorded and they were immersed in distilled water. When immersed, it is very important that the plates are not in contact with each other or the container, to ensure the complete surface area was in contact with the immersion fluid. The container is then placed on a climatic chamber (Memmert GmbH, Büchenbach, Germany) with the desired environmental temperature.

After immersion, the mass of the specimens was periodically measured until a stable value was reached. At this point, it was assumed that the specimen was saturated. For each time step t, the water uptake was given by:

$$M_t = \frac{m_t - m_0}{m_0} \cdot 100 \quad (\%) \tag{3.1}$$

where m_t is the mass of the specimen at the current time step, t, and m_0 is the initial mass of the specimen, measured prior to water immersion.

When the mass of the specimens was going to be measured, they were cleaned using a paper towel just to remove the excess fluid at the surface, not aiming to remove the water inside the specimen. Additionally, the specimens were only exposed to ambient conditions for the time required to execute the mass measurement. Afterwards, they were immediately re-immersed in water.

All mass measurements were conducted using a microbalance with 0.1 mg of accuracy (KernToledo, Balingen, Germany).

For the gravimetric studies of silicone and PBT-GF30 immersed in water in a container in the climatic chamber at 130 °C, it must be noted that the lid was kept open and water was added periodically. This was done to avoid pressurization of the container.

3.2.2 Adhesive joints

In **Paper E**, it was aimed to isolate the effect of the interphase or interface on the water uptake behavior of adhesive joints. Therefore, gravimetric studies were performed. Joints with different thicknesses were prepared and the test was executed at 70 °C. The idea behind using different adhesive thicknesses in the joints was that, knowing the water uptake behavior of the adhesive and substrate, if a

difference was detected, it should be the same regardless of adhesive thickness, since the interface/interphase, is assumed to be exactly the same, Figure 3.3.

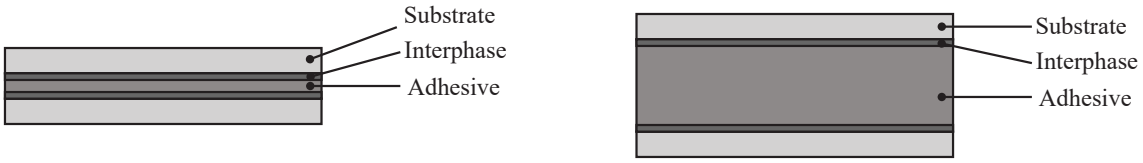


Figure 3.3: Interphase on thinner and thicker adhesive joints.

Specimen manufacturing

In these tests, the aim was to increase the adhesive/substrate ratio. Therefore, taking the conventional SLJs as a reference, rectangular joints (RJ), isolating the overlap, were prepared, Figure 3.4.



Figure 3.4: Rectangular joints manufactured for the gravimetric study of adhesive joints.

These joints have an overlap of 25x20 mm^2, which are the same dimensions of the substrate area. The substrates are always 2 mm thick. Aluminum and PBT-GF30 were used and different adhesive thicknesses were prepared. The PBT-GF30 substrates were cleaned with acetone and the aluminum substrates were treated with sandpaper, cleaned with acetone and anodized using a 9% (m/m) phosphoric acid solution following the ASTM D3933 standard [72]. To ensure the desired adhesive thickness, calibrated tape was used. Thicknesses of 0.5, 1 and 2 mm were manufactured. The substrates and calibrated tape were placed in a mold. Afterwards, adhesive is spread in both sides of the substrates and the two sides are bonded. The mold is then introduced in the hot-plate press at 120 °C and 20 bar for 25 minutes. After curing, to ensure all of the substrate area is covered by adhesive, the excess substrate, used to place the calibrated tape, is trimmed, Figure 3.5.

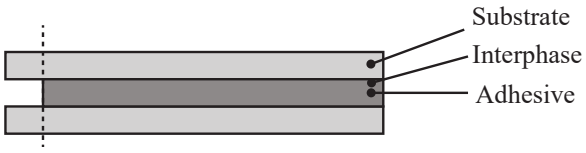


Figure 3.5: Trim RJs to make sure the adhesive is in the same plane of the end of the substrate for every side.

Experimental procedure

After manufacturing, the joints were fully dried in silica. After drying, the joints were measured, in terms of geometry and mass, and were placed in a container with distilled water. When immersed in water, the same precautions detailed for the gravimetric test of the bulk materials must be followed, ensuring the material is not in contact with other joints or the container. The container is placed in a climatic chamber (Memmert GmbH, Büchenbach, Germany) to ensure the immersion temperature.

The joints' mass was periodically measured using a microbalance with 0.1 mg of accuracy (KernToledo, Balingen, Germany).

3.3 Mechanical tests

3.3.1 Bulk tensile tests

Bulk tensile tests were conducted for the PBT-GF30 substrate and silicone adhesive.

The PBT-GF30 substrates were tested:

- **Paper B**: As supplied (without drying or aging) at controlled temperatures of 35, 70 and 130 °C;
- **Paper B**: At room temperature (RT) after drying at RT;
- **Paper B**: At RT, periodically during water immersion at temperatures of the climatic chamber of 35, 70 and 130 °C (for each specimen tested in these conditions, its water content was determined prior to the test);
- **Paper D**: At RT after drying, after saturating and after re-drying after saturation at temperatures of the climatic chamber of 70, 90 and 130 °C.

The silicone adhesive was always tested at RT:

- **Paper C**: After drying, after saturating and after re-drying after saturation at temperatures of the climatic chamber of 70, 90 and 130 °C;
- **Paper C**: Neat, and with different amounts of contaminant (water or surfactant) mixed prior to the adhesive curing: 2%, 5% and 10% (m/m).

Specimen manufacturing

Bulk tensile tests are usually performed with "dogbone" specimens following the BS 2782 standard [73], Figure 3.6.

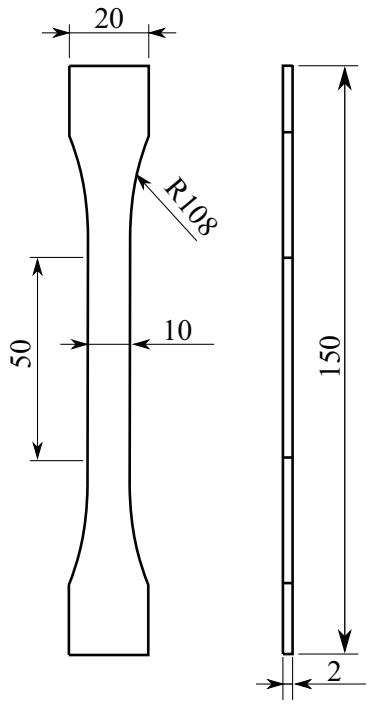


Figure 3.6: Standard "dogbone" specimens for bulk tensile tests.

However, in **Paper B** and **Paper C**, it was intended to determine the effect of immersion in water on the mechanical properties of the PBT-GF30 and silicone, respectively. Therefore, to reduce immersion time and the container required to introduce the samples, as well as the amount of fluid required to fully immerse the samples, reduced scale specimens were used, Figure 3.7.

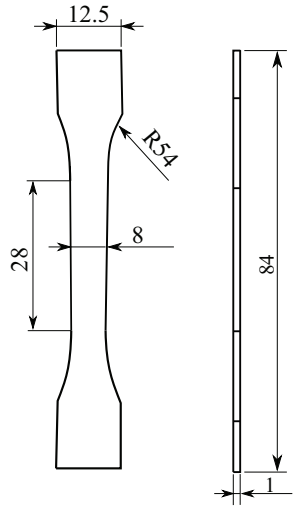


Figure 3.7: Reduced scale "dogbone" specimens for bulk tensile tests.

These smaller specimens were validated in **Paper B** against standard specimens, using PBT-GF30 and conducting the test at room temperature [74]. Additionally, these reduced scale specimens have been used by other authors [31; 75]. Since these specimens were proven to be valid and they represent a smaller waste of material when compared to other samples, they were used for all of the bulk tensile tests required in this work. Additionally, this makes the comparisons between tests of the same material easier to perform since the samples are similar and, using the same test speed, the strain rate variable is similar, decreasing the differences between conditions that may be caused by test samples with different geometries. For the silicone in particular, since the strain-to-failure is considerable, smaller specimens also make it simpler to finish the tensile test before the displacement limit of the machine is reached.

For the PBT-GF30 samples, the specimens were cut from a previously injection-molded plate. For the silicone samples, first, a silicone plate was prepared and, afterwards, the specimens were cut using a punch-matrix system.

To produce the silicone plates, the French NF T 76-142 standard [71] was followed. The process consists on lining a mold with a silicone frame with the desired thickness of the plate. The frame is used not only to establish the adhesive layer thickness, but also to ensure hydrostatic pressure, reducing the amount of defects found in the final specimen. The adhesive is, then, placed inside the silicone frame and the mold is placed on the hot-plate press, following the adequate curing cycle to cure the adhesive.

Experimental procedure

To execute the bulk tensile tests, an Instron® 3367 universal testing machine was used. This machine has a load cell capacity of 30kN.

The two types of specimens, standard and reduced scale, were generally tested at room temperature and ambient humidity. However, in **Paper B**, they were also tested at controlled temperatures, as stated above. These tests were achieved attaching a climatic chamber to the universal testing machine. Prior to testing in the latter conditions, the specimens were kept in the climatic chamber for enough time to reach the constant temperature desired.

3.3.2 Single lap joint (SLJ) tests

SLJs were prepared with aluminum and PBT-GF30 substrates. PBT-GF30 were used in **Paper D** and **Paper E** and aluminum substrates were used in **Paper E** and **Paper F**.

In **Paper D**, the SLJs were used to access the effect of humidity and temperature on the properties of the joints. Therefore, for temperatures of the climatic chamber of 70, 90 and 130 °C, the SLJs are tested dried, aged and dried after aging. In **Paper E**, SLJs were used to compare the strength and failure mode of joints with aluminum and PBT-GF30 substrates before and after aging. In **Paper F** SLJs with different levels of contamination (uncontaminated, 1 spray, 4 sprays and 10 sprays) were tested to understand how the strength and failure path of the joints is affected by surface contamination.

Specimen manufacturing

The adhesive thickness used was, generally, 1 mm. However, in **Paper E**, both for PBT-GF30 and aluminum substrates additional adhesive thicknesses of 0.5 mm and 2 mm were manufactured. The substrate thickness was always 2 mm. The geometry used was based on the ASTM D1002 [76] and ISO 4587:1995 [77] standards and is represented in Figure 3.8.

The surface preparation of the PBT-GF30 consisted on cleaning with acetone. The aluminum substrates were treated with sandpaper, cleaned with acetone and anodized. The anodizing process consists of immersing the material in an aqueous phosphoric acid solution, with a concentration of 9% (m/m) according to the ASTM D3933 standard [72].

After the surface was treated, the substrates were placed in a mold [78] and the adhesive thickness was ensured using packing shims. The adhesive was then carefully applied to both substrates to avoid adhesion issues and the final joints were placed in a hot-plate press in the required conditions to cure the adhesive, at 120 °C and 20 bar for 25 minutes.

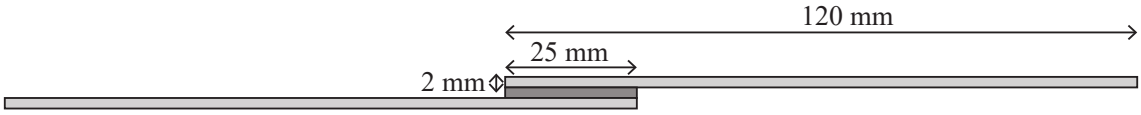


Figure 3.8: Single lap joints manufactured.

In **Paper F** the joints were contaminated using surfactant prior to bonding. The contamination process, carried out after anodizing, consisted of spraying the substrates with an aqueous solution of the surfactant (10 g/L) at a constant distance of 300 mm from the substrate. The different contamination levels were achieved through the number of sprays applied (none, 1, 4 or 10). To ensure the repeatability of the process, the spray nozzle was aligned to the middle of the substrate. The objective of the spray contamination was achieving a more uniform contaminant distribution, while being able to establish different contamination levels with representative behaviors. After the surfactant solution was applied, the specimens were dried at 70 °C for 12h to evaporate the water and ensure only the surfactant was in the overlap prior to the adhesive application.

Experimental procedure

To test the SLJs, they were vertically placed and fastened using two grips. The gripping pressure is achieved by using four M6 bolts (with a thread pitch of 1mm) and applying 20 Nm of torque to the bolts. Additionally, metal tabs are places beneath each substrate of the SLJ to keep them horizontal when handled. Two pins are also used to control the center placement of the SLJs when testing. Load–displacement curves were obtained for all SLJs tested using an Instron® 3367 universal testing machine with a load cell capacity of 30kN.

3.3.3 Double cantilever beam (DCB) tests

Three different sorts of DCBs were used in this work: (i) standard DCBs with high strength steel substrates, (ii) DCBs with aluminum substrates and (iii) DCBs with PBT-GF30 substrates. The standard DCBs with high strength steel were used

in **Paper D** to determine the mode I fracture toughness of the adhesive. The DCBs with PBT-GF30 substrates were used in **Paper D** to study the effect of water aging and immersion temperature on the behavior of DCB joints at temperatures of the climatic chamber of 70, 90 and 130 °C when dried, aged and dried after aging. The DCBs with aluminum substrates were used in **Paper F** to study the effect of surface contamination on the behavior of DCBs, using different levels of contamination (uncontaminated, 1 spray, 4 sprays and 10 sprays).

Specimen manufacturing

Standard high-strength steel DCB joints were manufactured following the geometry in Figure 3.9. The objective of these substrates is avoiding plastic deformation, measuring a reliable value for the G_{Ic} of the adhesive. The substrates were grit blasted and degreased with acetone before the application of the adhesive. The adhesive thickness was 1 mm, which was achieved using calibrated tape. The initial crack length was 45 mm, and it was achieved using a 0.1 mm thick sharp razor blade. The adhesive was spread on both substrates and the joints were placed in a mold and, afterwards, on a hot-plate press to achieve the cure of the adhesive.

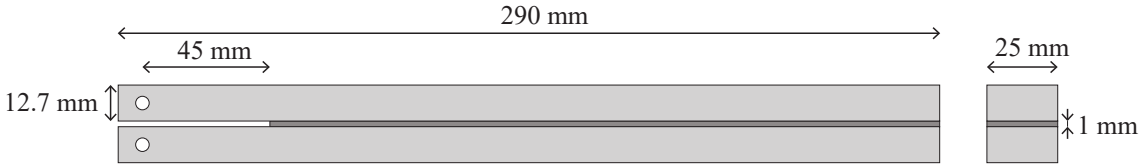


Figure 3.9: Schematic representation of the of the geometry of the standard DCBs with high strength steel substrates, dimensions in mm.

DCBs with aluminum substrates were manufactured according to the geometry in Figure 3.10. The bondline thickness was 1 mm and the same procedures followed for the steel substrates were performed. When contamination studies were performed, the same procedure used to contaminate the SLJs were carried out. In this case the pre-crack was of 5 mm.

DCBs with PBT-GF30 substrates were manufactured following the geometry in Figure 3.11. The same substrates used for the SLJs were used. The bondline thickness was 1 mm and was achieved using calibrated tape. Generally, the same procedures used for the other DCB joints were followed, apart from the substrate preparation, which was only cleaned with acetone. The initial crack length was 10 mm. Finally, after the adhesive was cured, the steel end-blocks used to perform the

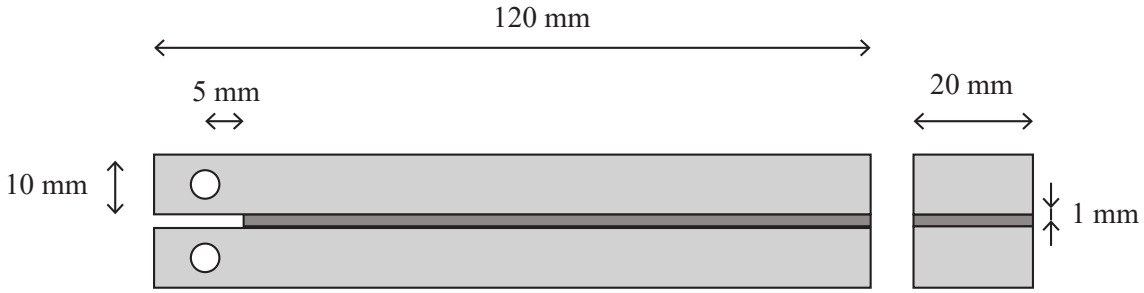


Figure 3.10: Schematic representation of the DCB specimens with aluminum substrates, dimensions in mm.

test were bonded using a cyanoacrylate adhesive on each specimen end, following the ISO 15024 standard [79].

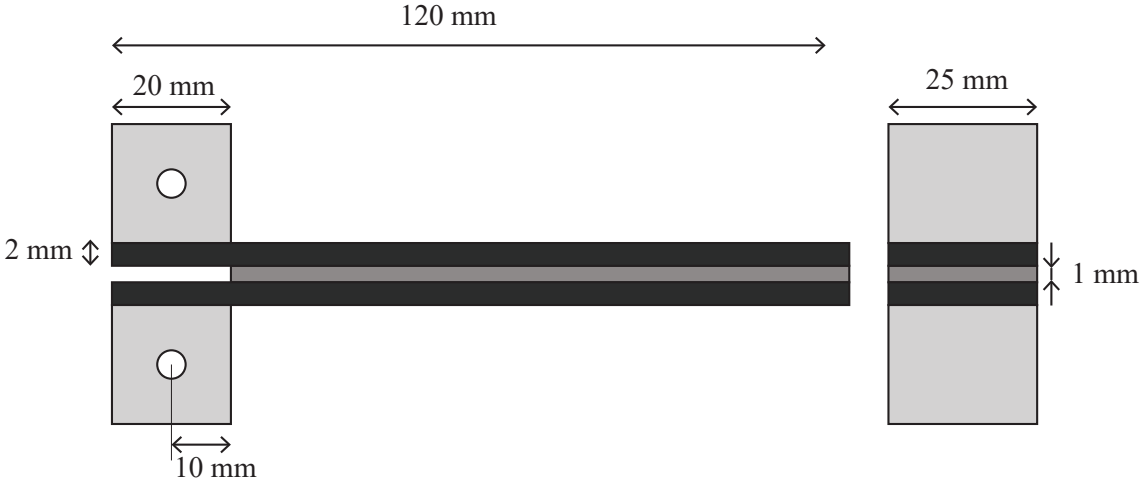


Figure 3.11: Schematic representation of the geometry of the DCBs with PBT-GF30 substrates, dimensions in mm.

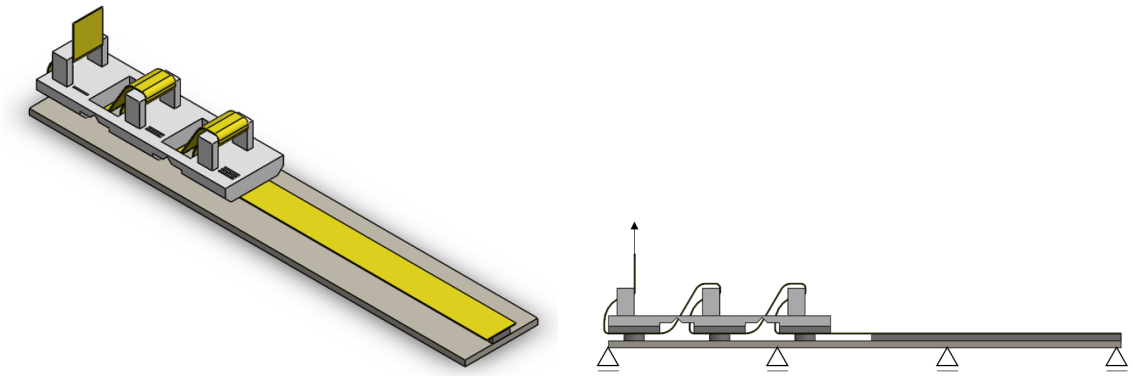
Experimental procedure

The DCBs were tested using an Instron® 3367 universal testing machine, which has a load cell capacity of 30kN.

For the DCBs with PBT-GF30 and aluminum substrates, the load-displacement curves were determined using the universal testing machine. However, the DCBs with high strength steel, used to determine the G_{Ic}, were analyzed using a J-integral approach. Therefore, a digital image correlation (DIC) analysis was followed.

3.3.4 Joints for the patent proposed

The testing method for which a patent (**Patent G**) was submitted, requires a joint that comprehends three pull-off tests and one peel test, Figure 3.12a. This method allows the determination of the strength and fracture toughness of the adhesive using one single continuous loading step, Figure 3.12b, and it was validated in **Paper H**. To ensure the continuity and sequence of the test, as well as the vertical load, a 0.03 mm thick steel strip was used.



(a) (b)

Figure 3.12: Schematic representation of the joint tested a) and of the testing method b).

Specimen manufacturing

The joint used for the test is shown in Figure 3.13. The part (1), correspondent to the pull-off tests, was manufactured from polycarbonate (PC). The strip identified with the number (2) corresponds to 0.03 mm thick steel. The adhesive overlaps are identified by (3) and the substrate identified by (4).

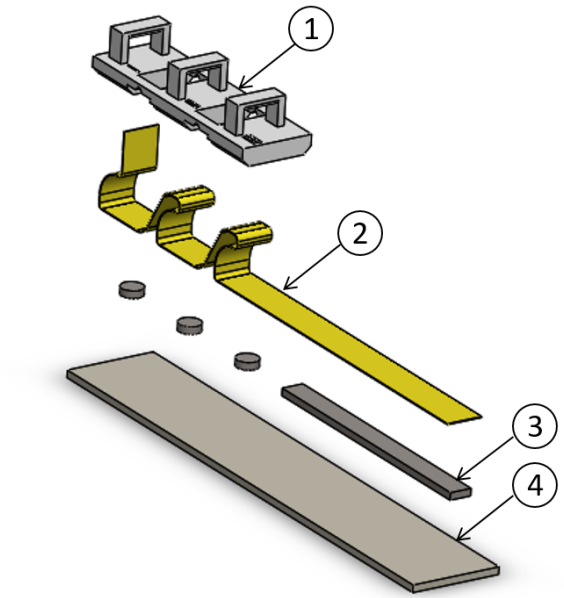
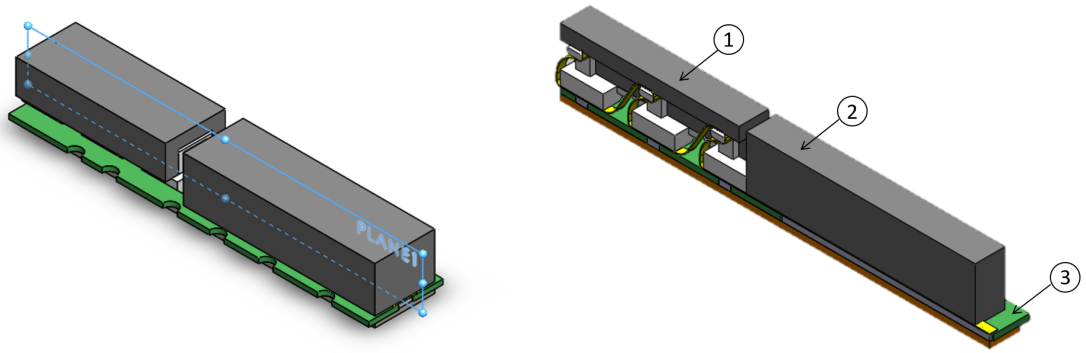
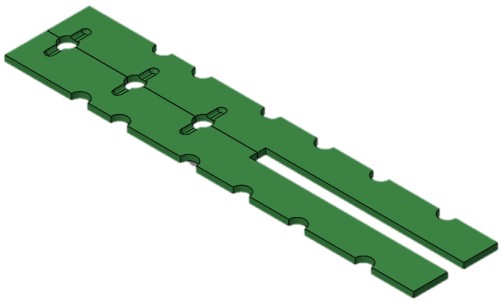


Figure 3.13: Schematic representation of the different parts of the joint used for the test.

To manufacture the joints, ensure alignment and a good quality overlap, an assembly was used, Figure 3.14. The aluminum blocks identified by (1) and (2) were used to apply pressure to the overlap and guarantee the alignment of the joint. The polytetrafluoroethylene (PTFE) mask (3), Figure 3.14c, was used to ensure the dimensions of the overlap.



(a) (b)



(c)

Figure 3.14: Assembly used to assist joint manufacturing a), cut view, considering the cut by plane 1 b) and the mask used to ensure the overlap area c).

For the manufacture of the joint, first, the substrate was treated with sandpaper and cleaned with acetone. Afterwards, the mask, cut in half (as shown in Figure 3.14c), was placed on top of the substrate, Figure 3.14b, inside a mold, Figure 3.15. In the mold, pins were placed to guarantee the alignment of the assemblies. The pull-off testing part was treated with low pressure oxygen plasma. The steel strip was primed using a silicone primer, looped around the pull-off test part as shown in Figure 3.12 and hold in place using an epoxy adhesive. Then, the silicone adhesive was placed in the designated cut-offs of the mask (Figure 3.14c). The pull-off test part was placed on top of the adhesive with the help of the pressure block identified by (1) in Figure 3.14b. The steel strip was placed on top of the adhesive for the peel test. Lastly, the pressure block for the peel test was placed, the mold closed and inserted in a hot-plate press to cure the adhesive.

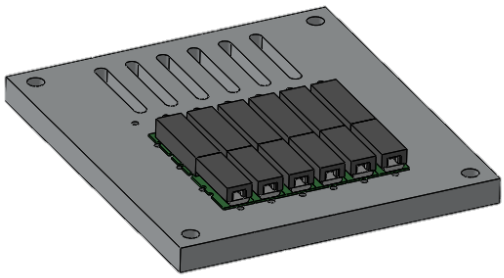


Figure 3.15: Schematic representation of the joints and assemblies used to assist joint manufacturing in a mold.

Experimental procedure

To conduct the tests, a setup that restrains the specimen vertically but not horizontally was required, Figure 3.16. This testing setup consists of two lateral supports (1), used to fix the bars (2), which are manufactured from polished steel to decrease friction with the rollers of the part where the specimens are attached (3). The attachment of the specimens was performed using bolts in the six designated gaps, as shown using two bolts in the figure. The setup was attached to an Instron® 3367 universal testing machine, with a load cell capacity of 30kN.



Figure 3.16: Test setup attached to the universal testing machine to test the specimens.

3.4 Complementary tests

3.4.1 Dynamic mechanical analysis (DMA)

In **Paper C**, a DMA was conducted on the neat adhesive to determine its glass transition temperature. For that, 2 mm thick specimens with 6 by 20 mm plates were prepared. The DMA was conducted on a 242 E Artemis (NETZSCH-Gerätebau

GmbH) machine from -110 to 130 °C.

3.4.2 Glass transition temperature measurement using an in-house developed apparatus

In **Paper B**, an in-house developed apparatus based on the concept of the DMA [80] was used to determine the glass transition temperature (T_g) of the PBT-GF30 and of the fiber-free PBT. The specimens used are 2 mm thick 10 by 25 mm plates. A hole of 3.5 mm was made in the center of the specimen to attach it to the machine. The apparatus works by measuring the damping of the sample which is vibrating at the resonance frequency as the temperature increases. A dummy specimen is kept inside the machine solely to measure the temperature of the material. The T_g is the temperature at which the maximum damping and, therefore, the minimum amplitude is recorded.

3.4.3 Differential Scanning Calorimetry (DSC)

The DSC analysis was conducted in **Paper B** to understand the thermal degradation of the PBT and PBT-GF30, using 1 mm thick disks with 6 mm diameter. These tests were carried on a NETZSCH DSC 214 Polyma DSC21400A-0655-L machine in the temperature range from -20 to 300 °C in a N_2 atmosphere.

3.4.4 Fourier Transform Infrared Spectroscopy (FTIR)

FTIR analysis was conducted on **Paper B** and **Paper C**.

In **Paper B** the main objective is determining the immersion temperature at which chemical changes start occurring in PBT-GF30. For that, the material was analyzed prior to water immersion and after saturation at temperatures of the climatic chamber of 35, 79, 80, 85, 90 and 130 °C.

In **Paper C** the same analysis was conducted, using unaged silicone and silicone after saturation at temperatures of the climatic chamber of 70, 90 and 130 °C. Additionally, it was intended to understand if the addition of water or surfactant prior to the curing of the adhesive had an influence on its chemical profile. Therefore, neat adhesive and adhesive with 2, 5 and 10% of water (m/m) and 2, 5 and 10% of surfactant (m/m) were analyzed. The profile of the neat surfactant was also studied.

The tests were conducted using a PerkinElmer Spectrum Two machine (Waltham, MA, USA). Wave lengths of 1000-500 cm^{-1} with a KBr window and $LITaO_3$ detector

(15,700-370 cm^{-1}). The spectra was recorded in attenuated total reflectance (ATR). The specimens used to study chemical changes due to water uptake were removed from water and kept in room conditions for about 30 minutes prior to test.

3.4.5 Scanning electron microscopy (SEM)

SEM analysis was conducted in **Paper C** and **Paper F**. In **Paper C** the objective was understanding how water absorbed after curing has an effect on the morphology of the adhesive. Therefore, unaged adhesive, as well as adhesive aged at temperatures of the climatic chamber of 70, 90 and 130 °C were studied. Additionally, it was aimed to understand the influence of water and surfactant added prior to curing on the morphology of the material. Therefore, adhesive with 2, 5 and 10% of contaminant (water or surfactant) was analyzed.

In **Paper F** the object of study was the contaminant on an adhesive joint. Therefore the surface of the joint prior to the application of contaminant and contaminated was analyzed. Finally, the fracture surface of a contaminated joint with the highest level of surface contamination was studied.

SEM analysis was conducted on two different microscopes: JEOL JSM 6301F/Oxford INCA Energy 350/Gatan Alto 2500 (Tokyo, Japan) and FEI Quanta 400 FEG ESEM /EDAX Genesis X4M (Hillsboro, Oregon, United States). The analysis were carried out at CEMUP (University of Porto, Portugal). The analyzed samples were coated with an Au/Pd thin film, by sputtering, for 120 seconds with a current of 15 mA using SPI Module Sputter Coater. The aged specimens were removed from water and kept at room temperature for 12 hours prior to the SEM analysis.

Chapter 4

Numerical methods

In this chapter, the main characteristics of the numerical models conducted are presented. The simulations are divided in two main groups: the gravimeric simulation used to mimic the water uptake behavior of materials, and the mechanical simulation, used to model the mechanical tests. In this section, first, the main attributes used in the generality of the simulations are presented and, then, the peculiarities of the simulations of joints under different aging conditions and with surface contamination are presented. The finite element analysis (FEA) was performed using the software *Abaqus*.

4.1 Gravimetric simulation

The main purposes of this simulation are: (i) mimic the experimental results obtained for the bulk plates of material, (ii) from the model developed for the bulk plates, create models with the same diffusion parameters to simulate the water uptake behavior of more complex geometries. The water uptake behavior of materials was simulated using a heat transfer analogy. Therefore, the coefficient of diffusion is correspondent to the thermal conductivity and the water uptake to the temperature. To stipulate the water uptake at saturation, it is assumed that, as soon as the material is placed in water, the nodes in direct contact with the fluid saturate. Therefore, the nodal temperature attributed to the exterior nodes of the joint in the beginning of the simulation is the water uptake at saturation.

4.1.1 Bulk materials

To simulate the bulk material plates, in **Paper B**, the exact simulation would require a three-dimensional model, Figure 4.1. For the three-dimensional model a 20-node quadratic heat transfer brick (DC3D20) was used.

However, a three-dimensional model would require a significant amount of computational resources. Therefore, to decrease computation time and simplify the model, a two-dimensional model was proposed, Figure 4.2. The two-dimensional model used 4-node linear heat transfer quadrilateral (DC2D4) elements.

The two-dimensional model was validated against the three-dimensional model with good results in **Paper B**. Additionally, a third two-dimensional model, considering only water uptake through the thickness was done, also with good results. This shows that, first, the water uptake can be considered unidirectional. And, consequently, the difference between the two-dimensional and three-dimensional model is negligible, since the governing dimension is the thickness.

4.1.2 Adhesive joints

In this section, the simulation of the water uptake of the rectangular joints used in **Paper E** as well as the single lap joints used in **Paper D** and **Paper E** and DCB joints in **Paper D**.

The numerical simulations of the adhesive joints were conducted following the

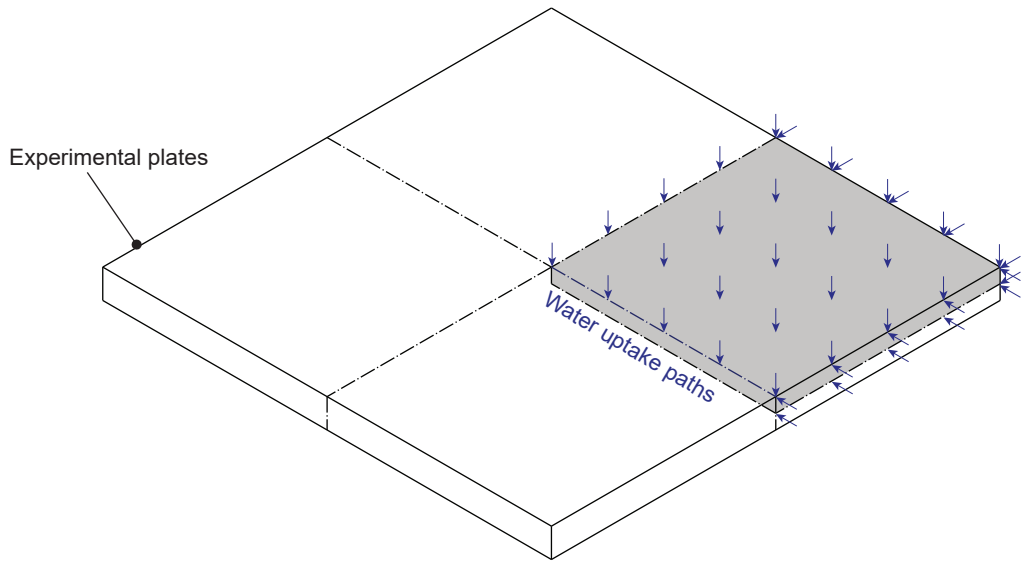


Figure 4.1: Three-dimensional model used to simulate the water uptake behavior of bulk plates.

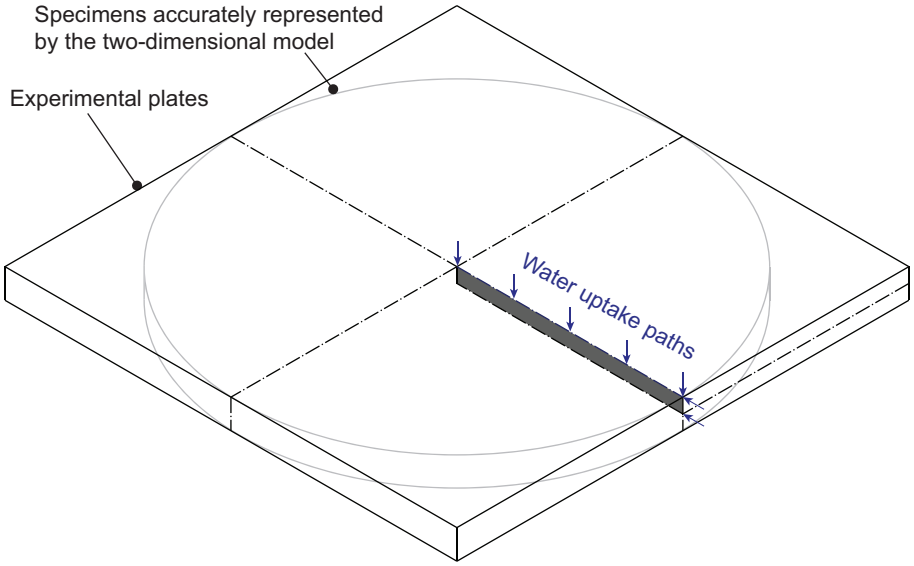


Figure 4.2: Two-dimensional approximation used to simulate the water uptake behavior of bulk plates.

same train of thought described for the bulk material. The numerical models consider the ideal condition in which no water ingresses through the interface. Therefore, these models only consider the water uptake through the adhesive, for joints with aluminum substrates, and the water that ingresses through the adhesive and substrate, for the joints with PBT-GF30 substrates.

Joints with aluminum substrates consider only the water uptake perpendicular to the bondline thickness, Figure 4.3. Therefore, a two-dimensional model is appropriate to simulate this behavior. Additionally, taking advantage of symmetry, only one forth of the adhesive overlap needs to be simulated. The elements used in this model were 4-node linear heat transfer quadrilateral (DC2D4). This model is valid both for SLJs and RJs, since the analysis is conducted only on the adhesive, and the only difference is that the SLJ has a longer substrate.

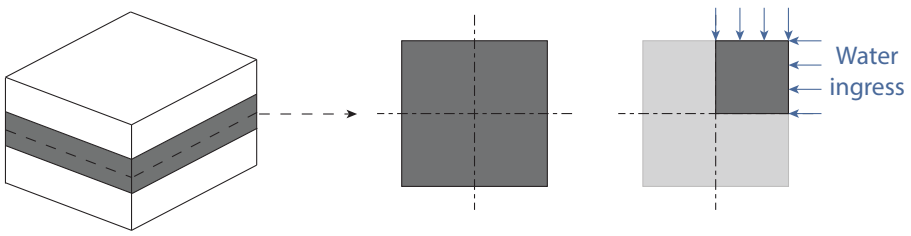


Figure 4.3: Numerical model developed for the gravimetric study of RJs with aluminum substrates.

Joints with PBT-GF30 substrate consider the water uptake through the substrate and adhesive. Therefore, to accurately simulate the joint, a three-dimensional model is required. Taking advantage of symmetry only one eight of the joint was simulated, using 20-node quadratic heat transfer brick (DC3D20) elements. Figure 4.4 shows the concept for RJs. However, it can also be used to SLJs. To DCBs it should be considered that the joint has one less symmerty plane, requiring the simulation of one quarter of the joint. Since water can ingress through the substrate and adhesive, a contact was introduced between the two materials to take into account the water that ingresses the adhesive, from the substrate.

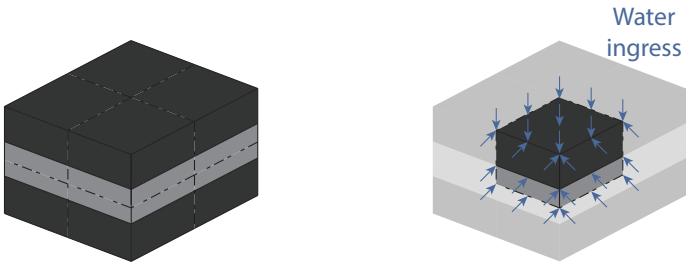


Figure 4.4: Numerical model developed for the gravimetric study of RJs with PBT-GF30 substrates.

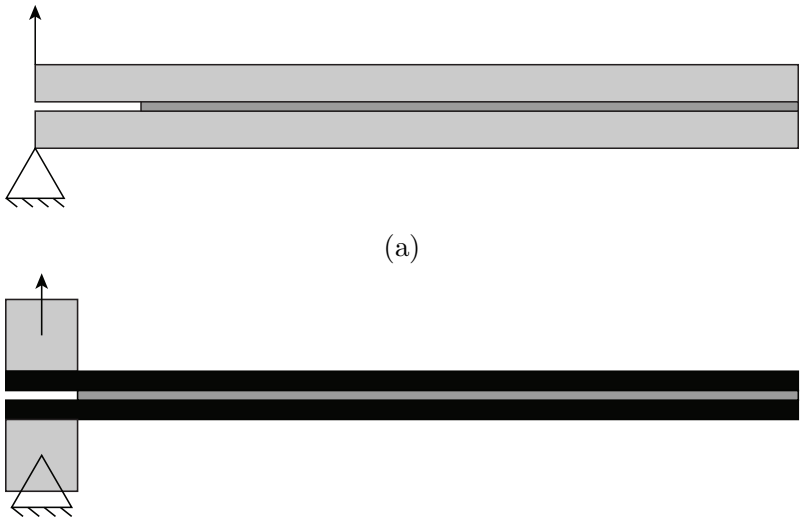
4.2 Mechanical simulation

The mechanical tests simulated were SLJs and DCBs, in **Paper D** and **Paper F**. The testing method patented in **Patent G** was also simulated in **Paper H**.

4.2.1 Double cantilever beam (DCB) and single lap joints (SLJ)

In those simulations, generally, the substrates were simulated as elastic elements, using a 4-node bilinear plain strain quadrilateral, reduced integration, hourglass control (CPE4R). The adhesive was simulated using 4-node-two-dimensional cohesive elements (COH2D4).

The boundary conditions introduced to the DCB models with metallic substrates (aluminum and high strength steel) and PBT-GF30 substrates are shown in Figures 4.5a and 4.5b, respectively.



(a)

(b)

Figure 4.5: Boundary conditions of the numerical model developed for the DCBs with metallic a) and PBT-GF30 b) substrates.

The boundary conditions of the SLJs, either with metallic or PBT-GF30 substrates are presented in Figure 4.6.



Figure 4.6: Boundary conditions of the numerical model developed for the SLJs.

Dried, aged and dried after aging conditions

In **Paper D**, the numerical simulation of dried, aged and dried after aging joints was performed. In those models, the mechanical properties of the adhesive and substrate were adjusted to the properties of those materials at each humidity condition and temperature analyzed. In these simulations the plasticity of the substrate was also considered.

The mechanical properties of the adhesive and substrate were determined in **Paper B**, **Paper C** and **Paper D**, through bulk tensile tests.

Surfactant contaminated conditions

When the contaminated conditions were analyzed, the substrates and adhesive were simulated as elastic elements and the cohesive elements were placed in the interphase between the adhesive and substrate, where the failure occurred, Figure 4.7. The properties of neat adhesive and substrate were known and the properties

of the interphase were changed to match the experimental results and obtain an estimation of their values.

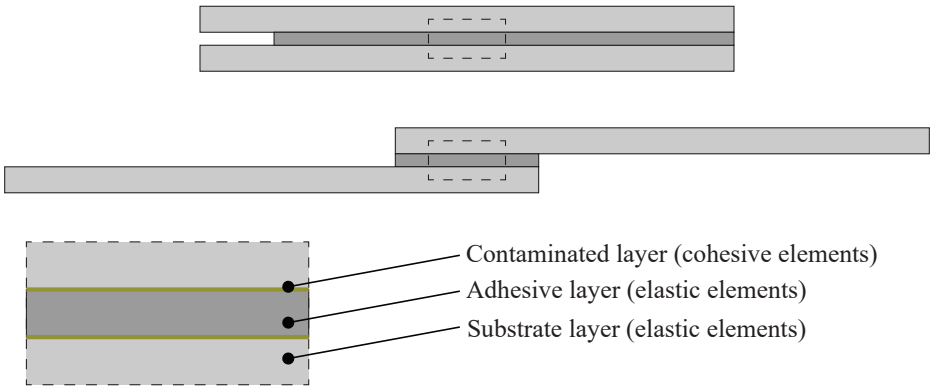


Figure 4.7: Numerical model developed for contaminated adhesive joints.

4.2.2 Patent tests

The patent joint consists of three pull-off tests followed by a peel test. These tests are going to be simulated separately since the first requires a thee-dimensional model and the second can be simulated using a two-dimensional model.

Pull-off test

The pull-off tests were simulated through a three-dimensional (3D) model, Figure 4.8. The substrate was simulated using a small block, just modeling the portion of the substrate below the pull-off part. The substrate was restricted in all directions, except the direction in which the pull-off test setup allows movement. A simplification was made to the model, since the two models are equivalent when the test is perfectly aligned. The horizontal movement of the pull-off testing part was restricted where in contact with the strip and the base of the part was pulled as it would be by the strip.

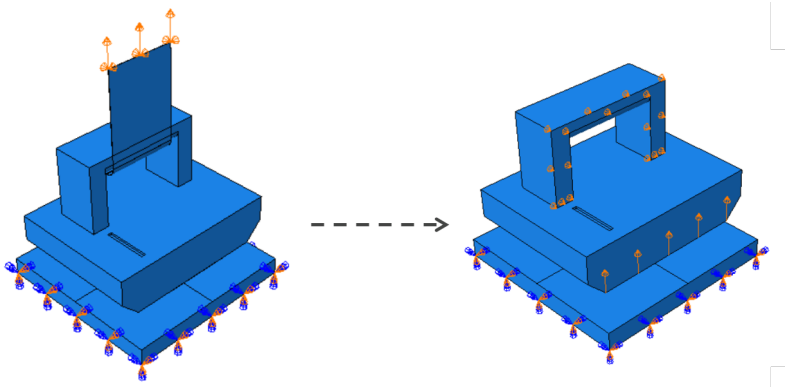


Figure 4.8: Numerical model used to simulate pull-off tests.

The elements used in the adhesive were 8-node three-dimensional cohesive elements (COH3D8), in the pull-off part, 10-node quadratic tetrahedrons, 3D stress elements (C3D10) and, in the substrate, 8-node linear bricks, using reduced integration, hourglass control (C3D8R).

Peel test

The peel tests can be simulated using a two-dimensional (2D) model, considering an out-of-plane dimension of 6 mm, which was the overlap width. The displacement was simulated in the left edge of the steel strip. The substrate was pinned in the vertical direction.



Figure 4.9: Numerical model used to simulate peel tests.

In the adhesive, 4-node two-dimensional cohesive elements (COH2D4) were used. In the steel strip and substrate the elements used were 4-node bilinear plane strain quadrilateral elements, with reduced integration, hourglass control (CPE4R).

Chapter 5

Conclusions

This work is a combination of tasks and, therefore, the conclusions are going to be divided in three main sections: (i) conclusions from water aging studies; (ii) conclusions from surfactant contamination studies; (iii) patent developed.

Conclusions from water aging studies

Bulk materials (silicone and PBT-GF30)

- The water uptake of silicone and PBT-GF30 for all of the temperatures analyzed follows the Fick's law of diffusion, and the coefficient of diffusion as a function of temperature can be described by the Arrhenius law;

- When comparing PBT-GF30 and fiber-free PBT, the latter absorbs more water and at a quicker rate, since it is composed of only the more hydrophilic matrix, without the presence of the more hydrophobic glass fibers;

- For the PBT-GF30 tested periodically during water immersion at different temperatures, the strength only changes between the dry and humid conditions, remaining around the same value regardless of the amount of humidity within the specimen. This happens because for all water uptake values found globally in the specimen, the surface is saturated, having only different degrees of water penetration. Therefore, failure always starts in the damaged saturated edge. With increasing temperature of water immersion, there is a higher decrease in strength and stiffness of the material;

- Silicone adhesive and PBT-GF30 substrates were tested dried, saturated and dried after saturation in water, at climatic chamber temperatures of 70, 90 and

130 °C. Silicone slightly, but almost negligibly, increases strength and stiffness when water aged, however, these changes are reversible upon re-drying. The increase of environmental temperature decreases strength and stiffness of the material. PBT-GF30 decreases strength and stiffness when aged, and also when temperature increases. This changes appear to be reversible for 70 °C, but not 90 and 130 °C;

- Testing unaged PBT-GF30 at controlled temperatures it was clear that temperature has a significant influence on the strength and stiffness of the material, decreasing them, and increasing ductility;

- Silicone does not show changes in its FTIR profile due to interactions with water at any of the immersion temperatures. However, PBT-GF30 exhibits changes in the FTIR profile after immersion in water at high temperatures, above a temperature between 80 and 85 °C;

- Finally, 1 mm thick plates with a surface area of 30x30 mm^2 can be used to characterize the water uptake of bulk materials.

Adhesive joints with silicone adhesive and PBT-GF30 substrates

- Considering SLJs and DCBs tested dried, water aged and dried after aging at climatic chamber temperatures of 70, 90 and 130 °, for SLJs and DCBs at 70 ° and SLJs in general, the joints exhibited a slightly better performance after they where water aged, when compared to the dried conditions, due to the slight increase in strength of the adhesive in this condition;

- However, the DCBs, when aged at 90 °C and both aged and dried after aging at a climatic chamber temperature of 130 °C failed on the substrate, due to the chemical degradation of the PBT-GF30 at immersion temperatures above 85 °C. This happened for the DCBs and not the SLJs because the substrate loading of the DCBs was more severe;

- As for the substrate and adhesive, with increasing temperature, there was a decrease in the mechanical behavior of the joints.

Effect of the interphase on joints with silicone adhesive and PBT-GF30 and aluminum substrates

- From the results drawn after water immersion at 70 °C, the water gain of joints with PBT-GF30 can be inferred from the numerical model that considers the water gain of the substrate and adhesive, since the effect of the interphase on the water gain of these joints is negligible. This translates into joints before and after aging having cohesive failure in the adhesive, with failure loads that fall within the standard deviation for all adhesive thicknesses in the aged and dried conditions;

- For joints with aluminum substrates and silicone adhesive, the interphase has a significant effect on the water gain, which translates into a significantly lower failure load of the joint when aged at 70 °C for two months and a shift from cohesive failure in the adhesive to adhesive failure after aging;

- The environmental resistance of the PBT-GF30/silicone interphase appears to be higher than that of the aluminum/silicone interphase since the water absorbed through the interphase can not be clearly identified in the gravimetric tests and after aging at 70 °C for two months failure is still cohesive in the adhesive, and for the aluminum/silicone joints adhesive failure is recorded.

Conclusions from surfactant contamination studies

Bulk silicone

- The surfactant added to the adhesive prior to its curing changes the the FTIR profile of the final adhesive, showed by the difference in the C-H bond;

- The absorption of surfactant during the curing process of the adhesive significantly decreases its strength and stiffness, also changing the morphology of the cured material;

- This behavior is attributed to this particular contaminant since, if the same exercise is done with water addition prior to the adhesive curing, this only contributes to the creation of voids, which does not happen with surfactant. Water does not change the morphology of the adhesive or its chemical profile, only decreasing the strength of the material because of the increase of void volume.

Joints with silicone adhesive and aluminum substrates

- The contamination of the substrate surface with surfactant prior to the application of the adhesive decreases the strength of the joint, both for SLJs and DCBs. Additionally, as the amount of surfactant increases, the strength of the joint decreases;

- As the amount of surfactant at the surface increases, failure moves from cohesive through the middle of the adhesive, to cohesive close to the interface, to adhesive. This is attributed to, for the uncontaminated condition, the interphase being stronger, and the failure of the joint being cohesive. However, for low amounts of surface contamination, the adhesive at the interphase absorbs surfactant during curing, decreasing its strength and shifting the failure path to this region. For large amounts of contaminant, the surfactant acts as a physical barrier between adhesive and substrate, promoting adhesive failure.

Patent developed

- This method allowed the determination of the strength and fracture toughness of the adhesive;

- The strength determined for the adhesive was 2.7±0.2 MPa and its fracture energy release rate 3.0±0.4 N/mm;

- The determined strength of the adhesive is lower than the one obtained using bulk tensile tests, which can be attributed to testing a joint instead of bulk material since, typically, in a joint, the constraint of the substrates leads to a lower determined strength of brittle adhesives;

- The fracture energy release rate determined using the peel test was similar to the one determined using standard DCB joints;

- The loading of the pull-off test was purely tensile and there was no plastic deformation of the substrates in the peel test.

Chapter 6

Future work

This work can be continued and complemented in the future following different approaches to study in more detail additional topics left unanswered.

First, since the main objective was understanding the effects of aging and surface contamination on the quality of the joint, a permeability study could be done in the same surfactant contaminated conditions for the joint with aluminum and for the PBT-GF30 joint dried and re-dried after aging to understand if aging cycles have an influence on the permeability of the material.

Regarding the humidity analysis, a complementary study on cyclic aging of the joint could be performed to understand if consecutive aging cycles would result on the same water uptake behavior as the first, and their effect on the properties of the joint.

Regarding the contamination study, the effect of contamination on the adhesive could be further explored by performing a complementary analysis to understand if the surfactant has affected the cross-linking of the adhesive and its final curing degree.

Finally, it would be interesting to change the materials to repeat some studies and analyze different phenomena that were not observed during this study. For instance, if the humidity study with aluminum and PBT-GF30 substrates was repeated with an adhesive that suffers swelling, the residual stresses at the interface could be studied. Also in this study, if the adhesive used suffered chemical degradation with aging, it would be possible to study the extension of water aging through the FTIR profile of adhesive throughout the joint.

Regarding the contamination study more contaminants found in the manufacturing process could be studied, also combining the study with different surface treatments to the substrate, such as anodizing, etching, primer application, laser

treatment, or others. A water aging study of surfactant contaminated joints could also be performed.

Regarding the patent joint, changes could be made to reduce the size and make it suitable for a wider variety of substrates, or adapt its use to different joint geometries, such as grooves. Finally, testing different contaminated conditions would be important.

References

[1] L. F. M. da Silva, A. Öchsner, and R. D. Adams. *Handbook of adhesion technology*, volume 1. Springer, 2018.

[2] A. Nijs, M. Selezneva, Y. Swolfs, N. Hirano, I. Taketa, T. Karaki, I. Verpoest, and L. Gorbatikh. Notch-sensitivity of hybrid carbon-fibre/self-reinforced polypropylene composites. *Composites Science and technology*, 200:108422, 2020.

[3] J Comyn. Durability of structural adhesives. *Applied Science, London*, 1983.

[4] A. Q. Barbosa, L. F. M. da Silva, and A. Öchsner. Hygrothermal aging of an adhesive reinforced with microparticles of cork. *Journal of Adhesion Science and Technology*, 29(16):1714–1732, 2015. ISSN 0169-4243.

[5] G. M. S. O. Viana, M. Costa, M. D. Banea, and L. F. M. da Silva. A review on the temperature and moisture degradation of adhesive joints. *Proceedings of the Institution of Mechanical Engineers, Part L: Journal of Materials: Design and Applications*, 231(5):488–501, 2017. ISSN 1464-4207.

[6] I. D. Maxwell and R. A. Pethrick. Dielectric studies of water in epoxy resins. *Journal of Applied Polymer Science*, 28(7):2363–2379, 1983. ISSN 0021-8995.

[7] J. Zhou and J. P. Lucas. Hygrothermal effects of epoxy resin. Part I: the nature of water in epoxy. *Polymer*, 40(20):5505–5512, 1999. ISSN 0032-3861.

[8] L. W. Jelinski, J. J. Dumais, A. L. Cholli, T. S. Ellis, and F. E. Karasz. Nature of the water-epoxy interaction. *Macromolecules*, 18(6):1091–1095, 1985. ISSN 0024-9297.

[9] D. A. Powers. Interaction of water with epoxy. *Sandia Report SAND2009-4405, Albuquerque, New Mexico*, 2009.

[10] R. A. Pethrick. Design and ageing of adhesives for structural adhesive bonding–a review. *Proceedings of the Institution of Mechanical Engineers, Part L: Journal of Materials: design and applications*, 229(5):349–379, 2015. ISSN 1464-4207.

[11] J. Crank. *The mathematics of diffusion*. Oxford university press, 1979. ISBN 0198534116.

[12] A. Malpot, F. Touchard, and S. Bergamo. Effect of relative humidity on mechanical properties of a woven thermoplastic composite for automotive application. *Polymer Testing*, 48:160–168, 2015. ISSN 0142-9418.

[13] Z. A. Mohd Ishak, T. S. A. Tengku Mansor, B. N. Yow, U. S. Ishiaku, and J. Karger-Kocsis. Short glass fibre reinforcedpoly (butylene terephthalate) Part 1–Microstructural characterisation and kinetics of moisture absorption. *Plastics, rubber and composites*, 29(6):263–270, 2000. ISSN 1465-8011.

[14] A. Boubakri, N. Haddar, K. Elleuch, and Y. Bienvenu. Impact of aging conditions on mechanical properties of thermoplastic polyurethane. *Materials & Design*, 31(9):4194–4201, 2010. ISSN 0261-3069.

[15] S. Popineau, C. Rondeau-Mouro, C. Sulpice-Gaillet, and M. E. R. Shanahan. Free/bound water absorption in an epoxy adhesive. *Polymer*, 46(24):10733–10740, 2005. ISSN 0032-3861.

[16] Y. Li, J. Miranda, and H.-J. Sue. Hygrothermal diffusion behavior in bismaleimide resin. *Polymer*, 42(18):7791–7799, 2001. ISSN 0032-3861.

[17] H. G. Carter, K. G. Kibler, and J. D. Reynolds. *Fundamental and operational glass transition temperatures of composite resins and adhesives*. ASTM International, 1978.

[18] H. G. Carter and K. G. Kibler. Langmuir-type model for anomalous moisture diffusion in composite resins. *Journal of Composite Materials*, 12(2):118–131, 1978. ISSN 0021-9983.

[19] M. E. Gurtin and C. Yatomi. On a model for two phase diffusion in composite materials. *Journal of Composite materials*, 13(2):126–130, 1979. ISSN 0021-9983.

[20] A. Mubashar, I. A. Ashcroft, G. W. Critchlow, and A. D. Crocombe. Moisture absorption–desorption effects in adhesive joints. *International Journal of Adhesion and Adhesives*, 29(8):751–760, 2009. ISSN 0143-7496.

[21] Y. C. Lin and X. Chen. Moisture sorption–desorption–resorption characteristics and its effect on the mechanical behavior of the epoxy system. *Polymer*, 46(25): 11994–12003, 2005. ISSN 0032-3861.

[22] W. K. Loh, A. D. Crocombe, M. M. A. Wahab, and I. A. Ashcroft. Modelling anomalous moisture uptake, swelling and thermal characteristics of a rubber toughened epoxy adhesive. *International journal of adhesion and adhesives*, 25 (1):1–12, 2005. ISSN 0143-7496.

[23] F. Cavodeau, M. Brogly, S. Bistac, T. Devanne, T. Pedrollo, and F. Glasser. Hygrothermal aging of an epoxy/dicyandiamide structural adhesive–influence of water diffusion on the durability of the adhesive/galvanized steel interface. *The Journal of Adhesion*, pages 1–25, 2018. ISSN 0021-8464.

[24] M. P. Zanni-Deffarges and M. E. R. Shanahan. Diffusion of water into an epoxy adhesive: comparison between bulk behaviour and adhesive joints. *International Journal of Adhesion and Adhesives*, 15(3):137–142, 1995. ISSN 0143-7496.

[25] K. F. Drain, J. Guthrie, C. L. Leung, F. R. Martin, and M. S. Otterburn. The effect of moisture on the strength of polycarbonate-cyanoacrylate adhesive bonds. *International journal of adhesion and adhesives*, 5(3):133–136, 1985. ISSN 0143-7496.

[26] A. J. Kinloch. Interfacial fracture mechanical aspects of adhesive bonded joints—a review. 1979. ISSN 0021-8464.

[27] P. Cognard. *Collage des Composites: Construction Aerospatiale, Automobile et Ferroviaire*. Ed. Techniques Ingénieur, 2004.

[28] R. Grangeat. Durabilité des assemblages collés en environnement humide-Instrumentation par capteurs à fibre optique. 2019.

[29] B. De'Nève, M. Delamar, T. T. Nguyen, and M. E. R. Shanahan. Failure mode and ageing of steel/epoxy joints. *Applied Surface Science*, 134(1-4):202–212, 1998. ISSN 0169-4332.

[30] P. Bonniau and A. R. Bunsell. A comparative study of water absorption theories applied to glass epoxy composites. *Journal of Composite Materials*, 15(3):272–293, 1981. ISSN 0021-9983.

[31] G. Viana, M. Costa, M. D. Banea, and L. F. M. da Silva. Behaviour of environmentally degraded epoxy adhesives as a function of temperature. *The Journal of Adhesion*, 93(1-2):95–112, 2017.

[32] S. Sugiman, A. D. Crocombe, and I. A. Aschroft. Experimental and numerical investigation of the static response of environmentally aged adhesively bonded joints. *International Journal of Adhesion and Adhesives*, 40:224–237, 2013. ISSN 0143-7496.

[33] Y. Hua, A. D. Crocombe, M. A. Wahab, and I. A. Ashcroft. Modelling environmental degradation in EA9321-bonded joints using a progressive damage failure model. *The Journal of Adhesion*, 82(2):135–160, 2006. ISSN 0021-8464.

[34] J. Cognard. Blistering of glass-epoxy amine adhesive joints in water vapour at high pressure. An indication of interfacial crumpling. *The Journal of Adhesion*, 47(1-3):83–93, 1994. ISSN 0021-8464.

[35] M. Costa, G. Viana, L. F. M. da Silva, and R. D. S. G. Campilho. Environmental effect on the fatigue degradation of adhesive joints: a review. *The Journal of Adhesion*, 93(1-2):127–146, 2017. ISSN 0021-8464.

[36] M. Costa, G. Viana, L. F. M. da Silva, and R. D. S. G. Campilho. Effect of humidity on the fatigue behaviour of adhesively bonded aluminium joints. *Latin American Journal of Solids and Structures*, 14(1):174–187, 2017. ISSN 1679-7825.

[37] R. S. Ashofteh and H. Khoramishad. The influence of hygrothermal ageing on creep behavior of nanocomposite adhesive joints containing multi-walled carbon nanotubes and graphene oxide nanoplatelets. *International Journal of Adhesion and Adhesives*, 94:1–12, 2019. ISSN 0143-7496.

[38] P. Moy and F. E. Karasz. Epoxy-water interactions. *Polymer Engineering & Science*, 20(4):315–319, 1980. ISSN 0032-3888.

[39] B. De'Nève and M. E. R. Shanahan. Water absorption by an epoxy resin and its effect on the mechanical properties and infra-red spectra. *Polymer*, 34(24): 5099–5105, 1993. ISSN 0032-3861.

[40] T. S. Ellis and F. E. Karasz. Interaction of epoxy resins with water: the depression of glass transition temperature. *Polymer*, 25(5):664–669, 1984. ISSN 0032-3861.

[41] Y. Zhang, R. D. Adams, and L. F. M. da Silva. Absorption and glass transition temperature of adhesives exposed to water and toluene. *International Journal of Adhesion and adhesives*, 50:85–92, 2014. ISSN 0143-7496.

[42] G. Z. Xiao and M. E. R. Shanahan. Swelling of DGEBA/DDA epoxy resin during hygrothermal ageing. *Polymer*, 39(14):3253–3260, 1998. ISSN 0032-3861.

[43] R. A. Gledhill and A. J. Kinloch. Environmental failure of structural adhesive joints. *The journal of adhesion*, 6(4):315–330, 1974. ISSN 0021-8464.

[44] S. J. Oh, D. C. Cook, and H. E. Townsend. Characterization of iron oxides commonly formed as corrosion products on steel. *Hyperfine interactions*, 112 (1-4):59–66, 1998. ISSN 0304-3843.

[45] S. M. Cambier, R. Posner, and G. S. Frankel. Coating and interface degradation of coated steel, Part 1: Field exposure. *Electrochimica Acta*, 133:30–39, 2014. ISSN 0013-4686.

[46] M. Eftekhari and A. Fatemi. Tensile behavior of thermoplastic composites including temperature, moisture, and hygrothermal effects. *Polymer Testing*, 51:151–164, 2016. ISSN 0142-9418.

[47] S. B. Kumar, I. Sridhar, and S. Sivashanker. Influence of humid environment on the performance of high strength structural carbon fiber composites. *Materials Science and Engineering: A*, 498(1-2):174–178, 2008. ISSN 0921-5093.

[48] A. Chatterjee and J. W. Gillespie Jr. Moisture absorption behavior of epoxies and their S2 glass composites. *Journal of applied polymer science*, 108(6):3942–3951, 2008. ISSN 0021-8995.

[49] G. Viana, M. Costa, M. D. Banea, and L. F. M. da Silva. Water diffusion in double cantilever beam adhesive joints. *Latin American Journal of Solids and Structures*, 14(2):188–201, 2017. ISSN 1679-7825.

[50] M. K. Antoon, J. L. Koenig, and T. Serafini. Fourier-transform infrared study of the reversible interaction of water and a crosslinked epoxy matrix. *Journal*

of Polymer Science: Polymer Physics Edition, 19(10):1567–1575, 1981. ISSN 0098-1273.

[51] S. G. Hong, N. G. Cave, and F. J. Boerio. The modification of epoxy/metal interphases by adsorbed contaminants. *The Journal of Adhesion*, 36(4):265–279, 1992. ISSN 0021-8464.

[52] C. J. Brotherhood, B. W. Drinkwater, and F. J. Guild. The effect of compressive loading on the ultrasonic detectability of kissing bonds in adhesive joints. *Journal of Nondestructive evaluation*, 21(3):95–104, 2002. ISSN 0195-9298.

[53] C. Jeenjitkaew, Z. Luklinska, and F. Guild. Morphology and surface chemistry of kissing bonds in adhesive joints produced by surface contamination. *International Journal of Adhesion and Adhesives*, 30(7):643–653, 2010. ISSN 0143-7496.

[54] J. Holtmannspötter, J. V. Czarnecki, and H.-J. Gudladt. The use of power ultrasound energy to support interface formation for structural adhesive bonding. *International journal of adhesion and adhesives*, 30(3):130–138, 2010. ISSN 0143-7496.

[55] M. Debski, M. E. R. Shanahan, and J. Schultz. Mechanisms of contaminant elimination by oil-accommodating adhesives Part 1: displacement and absorption. *International Journal of Adhesion and Adhesives*, 6(3):145–149, 1986. ISSN 0143-7496.

[56] M. Debski, M. E. R. Shanahan, and J. Schultz. Mechanisms of contaminant elimination by oil-accommodating adhesives Part 2: A model of the processes involved. *International Journal of Adhesion and Adhesives*, 6(3):150–152.

[57] M. Greiveldinger, M. E. R. Shanahan, D. Jacquet, and D. Verchère. Oil-covered Substrates: A Model Study of the Evaluation in the Interphase During Cure of an Epoxy Adhesive. *The Journal of Adhesion*, 73:179–195, 2000.

[58] S. G. Hong, H. X. Shu, J. J. Lin, and J. D. Young. The effects of a slushing oil on the curing and degradation behavior of an oil-accommodating epoxy adhesive. *Die Angewandte Makromolekulare Chemie: Applied Macromolecular Chemistry and Physics*, 238(1):129–141, 1996. ISSN 0003-3146.

[59] S. Heide-Jørgensen, S. T. de Freitas, and M. K. Budzik. On the fracture behaviour of CFRP bonded joints under mode I loading: Effect of supporting carrier and interface contamination. *Composites Science and Technology*, 160: 97–110, 2018. ISSN 0266-3538.

[60] E. Ito and Y. Kobayashi. Effects of absorbed water on physical properties of polyesters. *Journal of Applied Polymer Science*, 25(10):2145–2157, 1980.

[61] R. S. Stein and A. Misra. Morphological studies on polybutylene terephthalate. *Journal of Polymer Science: Polymer Physics Edition*, 18(2):327–342, 1980.

[62] Z. A. Mohd Ishak and N. C. Lim. Effect of moisture absorption on the tensile properties of short glass fiber reinforced poly (butylene terephthalate). *Polymer Engineering & Science*, 34(22):1645–1655, 1994.

[63] D. V. Rosato, D. V. Rosato, and M. V. Rosato. *Plastic product material and process selection handbook*. Elsevier, 2004.

[64] S. Wels, B. Boettge, R. Bernhardt, S. Klengel, and A. Claudi. Dielectric strength and aging performance of polybutylene terephthalate (PBT) under the influence of temperature and humidity. In *The International Symposium on High Voltage Engineering*, pages 472–482. Springer, 2019.

[65] Y. Liu, H. Liu, and Z. Chen. Post-fire mechanical properties of aluminum alloy 6082-T6. *Construction and Building Materials*, 196:256–266, 2019.

[66] P. M. G. P. Moreira, A. M. P. De Jesus, A. S. Ribeiro, and P. M. S. T. De Castro. Fatigue crack growth in friction stir welds of 6082-T6 and 6061-T6 aluminium alloys: A comparison. *Theoretical and applied fracture mechanics*, 50(2):81–91, 2008.

[67] M. Ericsson and R. Sandström. Influence of welding speed on the fatigue of friction stir welds, and comparison with MIG and TIG. *International journal of fatigue*, 25(12):1379–1387, 2003.

[68] A. Fabrizi, S. Capuzzi, A. De Mori, and G. Timelli. Effect of T6 heat treatment on the microstructure and hardness of secondary $AlSi_9Cu_3$ (Fe) alloys produced by semi-solid SEED process. *Metals*, 8(10):750, 2018.

[69] SysKem Chemie GmbH. Product Specification Cocosalkylaminethoxylate CAS No. : 61791-14-8. Technical Data Sheet, 2020.

[70] ISO DIS 294-3:2018. Plastics-injection moulding os test specimens of thermoplastic materials, part 3: small plates. Standard, International Organization for Standardization, Geneva, CH, November 2018.

[71] NF T76-142. Adhésifs structuraux - Méthode de preparation de plaques d'adhésifs structuraux pour la réalisation d'éprouvettes d'essai de caractérisation. Standard, AFNOR, Laxou, France, November 1988.

[72] ASTM D 3933:1998. Standard Guide for Preparation of Aluminum Surfaces for Structural Adhesives Bonding (Phosphoric Acid Anodizing). Standard, ASTM International, Pennsylvania, United States, May 1998.

[73] BS 2782:2011. Methods of Testing Plastic. Introduction. Standard, British Standard Institution, London, UK, September 2011.

[74] C. S. P. Borges, A. Akhavan-Safar, E. A. S. Marques, R. J. C. Carbas, C. Ueffing, P. Weißgraeber, and L. F. M. da Silva. Effect of water ingress on the mechanical and chemical properties of polybutylene terephthalate reinforced with glass fibers. *Materials*, 14(5):1261, 2021.

[75] M. Costa, G. Viana, C. Canto, L. F. M. Da Silva, M. D. Banea, F. Chaves, R. D. S. G. Campilho, and A. A. Fernandes. Effect of the size reduction on the bulk tensile and double cantilever beam specimens used in cohesive zone models. *Proceedings of the Institution of Mechanical Engineers, Part L: Journal of Materials: Design and Applications*, 230(5):968–982, 2016.

[76] ASTM D1002-99. Standard Test Method for Apparent Shear Strength of Single-Lap-Joint Adhesively Bonded Metal Specimens by Tension Loading (Metal-to-Metal). Standard, ASTM International, Pennsylvania, United States, October 2001.

[77] ISO 4587:2003. Adhesives — Determination of tensile lap-shear strength of rigid-to-rigid bonded assemblies. Standard, International Organization for Standardization, Geneva, CH, March 2003.

[78] M. D. Banea, L. F. M. da Silva, and R. D. S. G. Campilho. Moulds design for adhesive bulk and joint specimens manufacturing. *Assembly Automation*, 2012.

[79] ISO 15024:2001. Fibre-reinforced plastic composites — Determination of mode I interlaminar fracture toughness, GIC, for unidirectionally reinforced materi-

als. Standard, International Organization for Standardization, Geneva, CH, December 2001.

[80] Y. Zhang, R. D. Adams, and L. F. M. da Silva. A rapid method of measuring the glass transition temperature using a novel dynamic mechanical analysis method. *The Journal of Adhesion*, 89(10):785–806, 2013.

Appendix A

Paper A

Review on the effect of moisture and contamination on the interfacial properties of adhesive joints

Check for updates

Original Article

Institution of MECHANICAL ENGINEERS
Journal of MECHANICAL ENGINEERING SCIENCE

Proc IMechE Part C:
J Mechanical Engineering Science
0(0) 1–23
© IMechE 2020
Article reuse guidelines:
sagepub.com/journals-permissions
DOI: 10.1177/0954406220944208
journals.sagepub.com/home/pic
SAGE

Review on the effect of moisture and contamination on the interfacial properties of adhesive joints

CSP Borges[1], EAS Marques[1], RJC Carbas[1], C Ueffing[2], P Weißgraeber[2] and LFM da Silva[1,3]

Abstract

Adhesives play an important role in many key industrial sectors, such as the automotive industry, enabling the construction of lightweight, multi-material structures, combining polymers, composites and metals. However, adhesives are usually polymeric materials, which can be affected by environmental and working conditions, such as moisture and contamination. Although moisture and contamination degrade the adhesive, the failure of a bonded joint is often ultimately interfacial. Therefore, a literature review on the influence of those factors on the interfacial properties of adhesive joints is performed to understand the phenomena that take part in the degradation on adhesive joints when subjected to humid and contaminated environments, which can oftentimes be the case in factory conditions, especially for parts from third-party suppliers. The mechanisms and effects of moisture aging and contamination are presented, as well as experimental testing methods and practical case studies. It is concluded that both moisture and other contaminants may lead to a reduction in joint strength and catastrophic adhesive failure. Moisture absorption can occur through the adhesive, but in an adhesive joint, it can additionally occur through the substrate, the interface between the adhesive and the substrate or in the cracks and pores of the adhesive. After water ingresses into the adhesive, it decreases its mechanical properties and plasticizes it. However, in an adhesive joint, the water diffusion occurs much faster than in bulk adhesive due to the complementary diffusion paths, which typically leads to adhesive failure at the adhesive/substrate interface. Additionally, in an adhesive joint, water may induce the hydrolysis of the substrates or have other chemical interactions with them. Contaminants can diffuse through the joint or remain at the adhesive/ substrate interface. When they diffuse through the joint, they have consequences similar to those of water sorption. However, when they remain at the interface, they can produce locally debonded areas, which may lead to joint failure.

Keywords

Aging, contamination, interface, moisture, diffusion, adhesives, adhesive joints, adhesive bonding

Date received: 8 April 2020; accepted: 30 June 2020

Introduction

Adhesives have been increasingly used in several key industrial sectors due to their many advantages, including for example the unrivaled capacity to join dissimilar materials. These bonded, multimaterial structures exhibit high specific strength and stiffness, key characteristics for the reduction of energy consumption and emissions in vehicles, without compromising the integrity of the structure and the safety of the occupants. Additionally, bonded connections suppress the need for holes and spot welds, which results in a more uniform stress distribution, avoiding stress concentration sites and promoting higher fatigue resistance. This is particularly important when joining composites, which are extremely sensitive to notches.[1–3]

Despite these advantages, a major concern when designing a bonded structure is the environmental conditions it will be exposed to. In fact, one of the major limitations to the wider implementation of adhesive joining is the fact that joint strength

[1]Instituto de Ciência e Inovação em Engenharia Mecânica e Engenharia Industrial (INEGI), Portugal
[2]Robert Bosch GmbH, Corporate Research and Advance Engineering, Renningen, Germany
[3]Departamento de Engenharia Mecânica, Faculdade de Engenharia (FEUP), Universidade do Porto, Porto, Portugal

Corresponding author:
EAS Marques, Instituto de Ciência e Inovação em Engenharia Mecânica e Engenharia Industria Rua Dr. Roberto Frias, s/n Porto 4200-465, Portugal.
Email: emarques@fe.up.pt

degradation might occur in severe environments if preventive measures are not taken. Two of the most important factors that can contribute to joint strength degradation are moisture and contamination.

In many cases, it is desirable to apply adhesives without a time-consuming degreasing procedure and pre-treatment of the substrate, but this can have drastic effects on joint strength. In fact, oil at the interface between the substrate and the adhesive may modify the initial and long term behavior of the adhesive,[4] although it is possible to design adhesives that can operate under these specific conditions.

Adhesive joints, when well prepared, should fail by cohesive failure in the adhesive layer. However, when subjected to environmental attack, the failure typically changes to the interfacial regions.[5] Therefore, the properties of the interface between the adhesive and the substrate in joints subjected to harsh conditions, such as humid and contaminated environments, should be studied and fully understood to produce durable joints. Additionally, most adhesives are hydrophilic and thus they will be strongly susceptible to physical and chemical degradation when operating in environments with high moisture levels.

This is a very wide subject matter that encompasses different scientific areas. This paper attempts to organize some of this knowledge in a way that allows the reader to understand not only the fundamental mechanisms associated with moisture and contamination degradation, but also provides case studies that might be of use in practical applications.

To understand how moisture and contaminants, such as oils used during the manufacturing processes, affect adhesion between adhesive and substrate in an adhesive joint, it is first important to understand the phenomena involved in the adhesion process. Therefore, in the next section, *Interfacial phenomena*, the main theories of adhesion as well as interphase formation are explored. Afterwards, the mechanisms and effects of water ingress and contamination are discussed in the sections *Moisture aging* and *Contamination*, respectively. The following section, *Experimental testing*, discusses sample preparation and testing procedures used to address this topic. Afterwards, *Practical case studies* found in literature are presented and the main *Conclusions* regarding this topic are shown.

Interfacial phenomena

Adhesion theories

Typically, there are four different theories used to describe the adhesion process: the (i) mechanical; (ii) electrostatic; (iii) diffusion and (iv) adsorption theories. The mechanical theory is based on the mechanical interlocking between the adhesive and the substrate, stating that the mechanical connection of the adhesive within the irregularities of the substrate plays an important role on the adhesion between them.[1] The electrostatic theory supports that during the destruction of an adhesive joint, electrical phenomena are observed, presenting the behavior of the interface analogously to the plates of a capacitor, promoting charge transfer and, therefore, improving adhesion. This theory is based on the knowledge that any condensed material has free charges to some extent and, therefore, an electrochemical potential difference will occur across the interface between to materials when in contact.[1,6] The diffusion theory offers a model for polymer-to-polymer adhesion and explores the time and molecular weight dependence of adhesion to polymers, stating that the adhesion of polymers to themselves and to others is caused by diffusion of polymeric molecules across the interface.[1,7–9] The adsorption theory is the more widely applicable and states that, once intimate contact is provided between the adhesive and the substrate, there will be forces of attraction between them. The nature of those forces will depend on the chemical composition of the materials used.

Some authors differentiate these forces into chemical bonds, such as covalent, metallic or ionic; secondary bonds, such as van der Walls and hydrogen bonds and donor-acceptor bonds, such as Bronsted and Lewis acid-base interactions. Chemical bonds present a significantly higher bond energy than secondary bonds, being the donor-acceptor bonds an intermediate group.[1,7,10]

As stated above, intimate contact must be promoted between the two materials within an adhesive joint. This contact is very common between a liquid adhesive and a solid substrate which, to create a close contact on a molecular level, means that the adhesive must properly wet the surface of the substrate. The wettability of a given liquid on a solid surface can be examined through the spreading of a liquid drop onto the solid surface and consecutive measurement of the contact angle. Lower contact angles indicate a better wetting of the surface. This phenomenon is observed when the surface energy of the liquid is lower than that of the solid.[1,10]

Contact angle measurements can be used to determine the surface energy of a surface. To measure the surface wettability of a surface, the aerosol wetting test (AWT) may be applied. This test consists on the evaluation of the droplet pattern produced by a water aerosol on a given surface. The main advantages of this test, especially for industrial applications, are the automation of the process, which allows a precise evaluation of the droplet size and integration in the production process, and the ability to evaluate both small surfaces and the surface of complete components.[11]

Surface free energy can be divided into two components, polar and dispersive, which correlate with surface composition. Commonly, polar and dispersive components are determined through the Owens-

Wendt-Rabel-Kaelbe (OWRK) method.[12,13] For the adhesion phenomena, it is said that surfaces with lower surface energies combined with lower polar components offer the best resistance to adhesion.[14]

An accurate characterization of an adhesive joint cannot simply consider the properties of the substrates and of the bulk adhesive, as there are other layers, boundary layers, that can be found on the surface of the substrates, ending up between the adhesive and the substrate after bonding.[15] Those boundary layers can depend on the manufacturing process (surface treatments, modifications made to the substrates or lubricants used in cutting processes) or on the material that composes the substrate itself and its interaction with the environment. Examples of boundary layers, and in particular weak boundary layers, can be oily contaminants that are left on the surface of the substrates or plasticizers such as those used to improve the flexibility of polyvinyl chloride (PVC) that migrate to the surface and form a liquid, oily layer. Boundary layers that arise due to natural interactions between the material and the surrounding environment or interactions between the materials used are typically different in metals and in polymers. In metals, it is common to observe the appearance of oxide layers. However, in polymeric materials the boundary layers depend on the functional, structural and morphological behavior of the polymer under analysis.

These contaminated or oxidized layers, able to decrease the strength of adhesive joints significantly, can be removed through appropriate surface treatments. The use of a primer can also be adopted to improve adhesion. However, in the manufacturing processes of adhesive joints, a careful and thorough surface preparation can increase the cost and decrease productivity of the process drastically.[5,16] Therefore, it is crucial to understand how contaminants and moisture affect the adhesion process and the performance of the final adhesive joint.

Interphase formation

In adhesive joints, when bonding occurs, there is a formation of a region called interphase, which is a complex polymeric region with heterogeneous morphology and chemical structure, with several layers,[17] morphologically and chemically different from the adhesive. In this transitional layer, gradients in several properties, such as the glass transition temperature (T_g) degree of cross-linking and residual stresses have been identified.[1,18] The properties of the final adhesive joint, such as practical adhesion, critical strain energy release, durability, thermal and hygrothermal aging resistance and corrosion resistance, are also dependent on the properties of this interphase,[18] as well as the properties of the adhesive and substrates used.

Within the interphase, there is a plane of contact between the substrate and the adhesive, which is the interface,[1] and the difference between the two concepts is clarified in Figure 1.

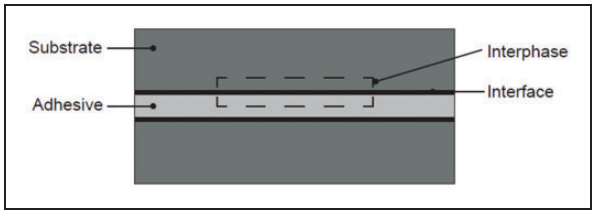


Figure 1. Schematic representation of the interphase and interface of an adhesive joint.

The formation of an interphase can be linked to several phenomena, which are dependent on the adhesive, hardeners, curing agents and their interaction with the substrate and process conditions. Taking the example of epoxy-amine systems, which are among the most studied due to their good mechanical properties, good adhesion to a wide variety of substrates and high chemical resistance,[1,18] the formation of the interphase was found to be related to several different processes: adsorption reactions (of the amines, the epoxides or the substrate), dissolution of the substrate, organometallic complexes or migration of the hardener.[10]

An epoxide is a cyclic ether, therefore, by opening the cycle, chemical connections and hydrogen bonds with the substrate can be formed.[19,20] Preferential adsorption of the curing agent, the amine, is also very commonly described in the literature,[18,21–24] which can also change the curing process by inhibiting chemical reactions between the epoxy and the amines adsorbed on the substrates or by overcuring the epoxy with excess free amino groups close to the substrate, which is also linked to the formation of an interfacial region.[18,22]

Metallic oxides present on the surface of the substrate may also be non-negligibly dissolved, that is, when the liquid adhesive is placed on the surface of the substrate, not only is the amine chemically sorbed by the oxide on the substrate but, as the amine component has a basic nature, it will dissolve the oxide layer. The interaction between amine and oxides also forms organometallic complexes at the surface of the substrate, which subsequently diffuse into the substrate.[19,25] The hardener can also migrate because the chemical affinity of the metal to the hardener is better than to the epoxide groups. In this case, an increase in the degree of cross-linking in the region close to the oxidized metal surface of the substrate can be observed, due to the catalysis of the curing reaction in this region.[18,19] A model of the interactions at the interphase of the adhesive has been developed by Coulaud[19] and is schematically represented in Figure 2.

Although these interactions and phenomena are researched for epoxy-amine systems, other adhesives do not display such a range of studies. Silicone

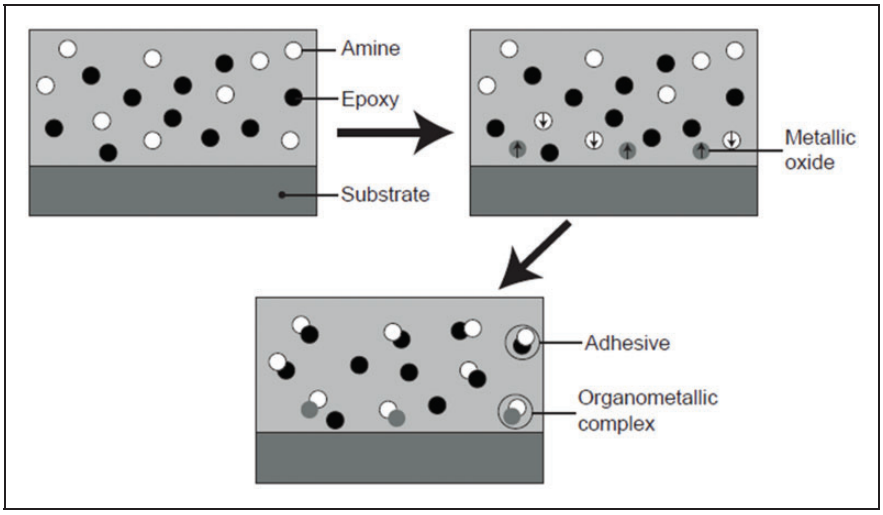


Figure 2. Interphase creation model (adapted from literature[19,26]).

adhesives, for example, are often used as sealants due to their low water uptake and, therefore, frequently exposed to high moisture environments. While the silicone itself does not absorb a significant amount of water, joints with silicone adhesives have been exhibiting adhesive failure in humid conditions, especially at high temperatures.[27–29]

Moisture aging

Mechanisms of moisture aging

In an adhesive joint, water diffusion may occur in four different ways[22]: (i) diffusion into the adhesive; (ii) diffusion into the interface between the adhesive and the substrates; (iii) diffusion by capillarity in the pores and cracks of the adhesive and (iv) diffusion through the substrate.

The analysis of this complex process can start by studying the diffusion of water into the adhesive, where it will be absorbed as free water and as bound water[30,31]: (i) free water occupies the micro cavities of the polymeric chains and does not cause swelling of the adhesive, i.e. volumetric change; (ii) bound water forms single or multiple hydrogen bonds with the molecules that constitute the adhesive and causes swelling of the adhesive.

As the water ingresses into the adhesive, free water and bound water are absorbed, but only the latter causes volumetric changes. Therefore, it can be easily inferred that as both cause mass changes but only one causes swelling, as water sorption occurs, the density of the adhesive will necessarily change.

Bound water can also be divided into type I and type II bound water, according to the activation energy[32]: (i) type I bound water is the dominant form of water sorbed by adhesives and is related to water molecules that form a single hydrogen bond with the adhesive network; (ii) type II bound water has a higher activation energy because it is related to water molecules that form multiple hydrogen bonds with the polymeric chain.

Diffusion of water into an adhesive is usually modelled through the mass variation as a function of time. However, it does not follow a universal model for all materials and conditions studied. Therefore, several models have been proposed to describe the water uptake behavior of materials. The most common model is the Fick's law,[33–37] but the Langmuir model[38–42] and variations of the Fick's law, such as the dual Fick's law[43–45] are also common.

Considering the chemical phenomena happening during water sorption, water mostly forms hydrogen bonds with the non-binding electrons of the polymeric chain and, as water ingresses the polymer, it first connects to polar sites and, then, when at higher concentration, forms clusters.[46] However, the sites where the water bonds with the adhesive are still not clear.[47] It is also known that adhesive plasticization is linked to the strong interaction between the water dispersed and some groups of the polymeric chain of the material. Additionally, resins, such as epoxies, are known to have hydrophilic groups, which means they attract water molecules, and those materials may also suffer from leaching, which is the phenomenon by which some of the solid adhesives are extracted and solve into the solvent which in this case is the immersion environment.[45,48]

Degradation of an adhesive joint due to moisture ingress is, without question, related to the damage caused to the adhesive layer. However, as said, water can also diffuse through the adhesive/substrate interface, through the substrate or by capillarity in the pores and cracks of the adhesive. The latter will be analyzed in more detail in the next paragraphs.

Kinloch et al.[5] stated that adhesive joints become weaker above a critical concentration of water in the adhesive layer. This critical value of water in the adhesive corresponds to a threshold value of humidity of the surrounding environment. The existence of this

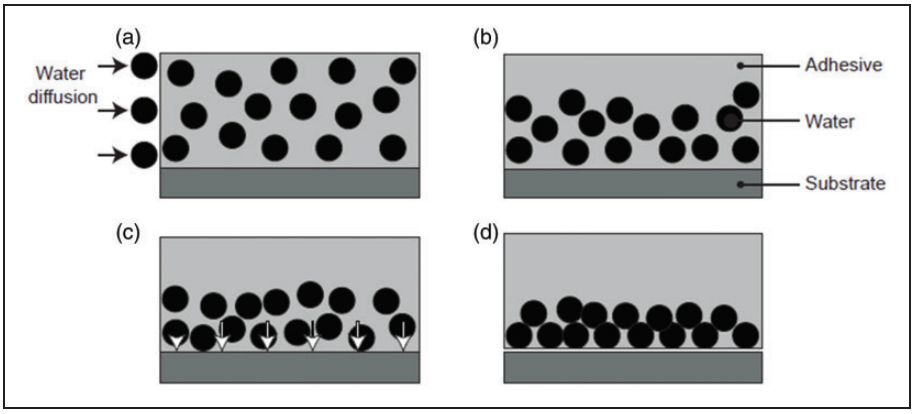


Figure 3. Mechanisms of water damage on the interface adhesive/substrate in an adhesive joint (adapted from literature[26,46]). (a) Water diffusion, (b) Water condensation, (c) Osmotic pressure, (d) Interfacial failure.

threshold is attributed to the existence of capillary condensation.[46]

Cognard et al.[49] commented that, when water vapor is adsorbed by porous solid materials it will condensate when its chemical potential is equal to that of the liquid. If the pores exist along the interface, as they fill with water the interface between the adhesive and the substrate will be weakened. The process by which condensation damages the interface can be divided into four stages (see Figure 3): first, water diffuses into the material (Figure 3a), then, condensation of said water occurs (Figure 3(b)) and the water begins to agglomerate at the interface, creating an osmotic pressure (Figure 3(c)) which leads to the failure of the interface (Figure 3(d)).

The key factor in the damage found in adhesive joints due to moisture ingress is, oftentimes, diffusion through the adhesive/substrate interface, since it may lead to the complete separation of the substrate and the adhesive.[50]

Zanni-Deffarges and Shanahan[51] conducted an experimental work to determine the coefficient of diffusion, D, of an epoxy adhesive bulk and within an adhesive joint, reporting that, in the adhesive joint, D of the adhesive was almost an order of magnitude higher. Therefore, it was concluded that not only was water diffusing through the adhesive, but it was also following different paths, the interface between the adhesive and the substrate. This phenomenon was attributed to capillary diffusion. Considering metallic substrates, to mimic water diffusion three components are considered: substrates, wet adhesive and dry adhesive. The authors suggest that the energy of the dry adhesive/substrate interface is very high, pulling the water diffusion front into the system. It is also noted that the process by which the water diffuses through the interface is more significant than the diffusion through the bulk adhesive, causing premature failure along the bondline, Figure 4. A reason also presented for the water diffusion through the interface can be the structure or polymeric orientation of the adhesive in the regions close to the interface.[51]

Substrates also play a significant role in the aging process since, as exposure time progresses, they can interact with water creating, for example in the case of steel, a corrosion layer or migration of some components of the substrate to the surface of the adhesive. In adhesive joints with steel substrates, it was observed that the adhesive composition changes near the substrate, when compared with the bulk adhesive. De'Nève et al.[52] analyzed an epoxy resin cured with dicyandiamide (DDA) and observed that before aging, the adhesive seemed to have enrichment in hardener near the interface, which caused the failure to be interfacial. A formation of ester groups, due to the interaction between the adhesive and the substrate, was observed with X-ray photoelectron spectroscopy (XPS) prior to aging. The same groups were observed in bulk adhesive after aging. With aging, in the adhesive joint, those groups are saponified into carboxylates due to the corrosion of the substrate. The fracture at this stage occurred near the interface. As aging progressed, failure transferred to a layer of corrosion mixed with adhesive. Using zinc-coated steel substrates, it was observed that zinc moved into the adhesive during aging, which translated into a better performance.

Composite materials are also commonly found as substrates in adhesive joints. For these materials, a similar phenomenon as the one represented in Figure 4 was reported to occur, where water diffusion occurs also at the interface between the matrix and the fiber.[51,53] Therefore, it is highly relevant to study water diffusion through composite materials when analyzing the effect of moisture in adhesive joints for two major reasons: (i) if composite materials are the substrates used in adhesive joints, water will also diffuse through them, consequently reaching the interface and, therefore, the adhesive; (ii) a parallelism can be made between the physical behavior and diffusion mechanisms of the adhesive/substrate interfaces and the fiber/matrix interfaces.

Effects of moisture aging on the interfacial properties

Adhesives exposed to humid environments consistently show a significant decrease in their mechanical properties such as the elastic modulus, strength[54–56]

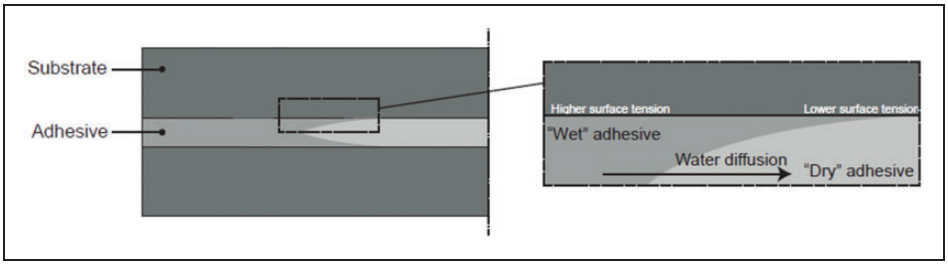


Figure 4. Diffusion front near the metal/adhesive transition. The model suggested by Zanni-Deffarges and Shanahan.[51]

and fracture toughness[46,51,57,58] However, the decrease in strength is usually compensated by an increase in the ductility of the material, leading to higher strain to failure[54–56] and creep strain.[59] The T_g has been also shown to decrease with increasing water content.[47,60–62] This is particularly troubling because the water uptake rate and the diffusion coefficient are known to increase with increasing temperature, even more so when T_g is surpassed.[63–65] Therefore, knowing that maximum water uptake and diffusion rate increase at temperatures above T_g,[65] as water uptake increases T_g, will progressively decrease, bringing the T_g closer to service temperature and, consequently, increasing the diffusion coefficient and the water uptake.[48,63]

As water diffuses into polymeric materials, swelling is known to occur, being reported by several authors.[51,64,66–68] Generally, it has been observed that the change in volume of the adhesive is not proportional to its change in mass because, as mentioned above, the adhesive absorbs moisture as free and as bound water but only the latter influences the change in volume of the material. Additionally, it has been observed that, typically, volume changes linearly with the square root of time at the beginning of the water sorption process, reaching a *plateau* from a given time onwards. This volumetric change is highly affected by temperature, increasing as temperature increases.[64]

Although the properties of the adhesive are degraded by the presence of water, it has been observed that, when in an adhesive joint, premature failure appears to be due to the effect of moisture on the interface, or the interphase, rather than on the adhesive itself.[65]

As said, the volume of the polymeric materials is affected by the presence of water, but the volume of metals remains unchanged, which means that in an adhesive joint with metal substrates the adhesive will expand and increase its volume but still be constricted by the substrates, Figure 5. However, in adhesive joints with composite substrates, a distortion of both the adhesive and the substrate will occur.[51,64,66]

As the adhesive swells, the adhesive layer is also increasingly plasticized by water, introducing stresses near the interface due to the constriction of the substrates. Therefore, stresses are increasingly transferred to this layer, which promotes interfacial failure of the adhesive joint.[26,51,64,66]

Additionally, in adhesive joints, it is common to see that, as water only diffuses into the adhesive through

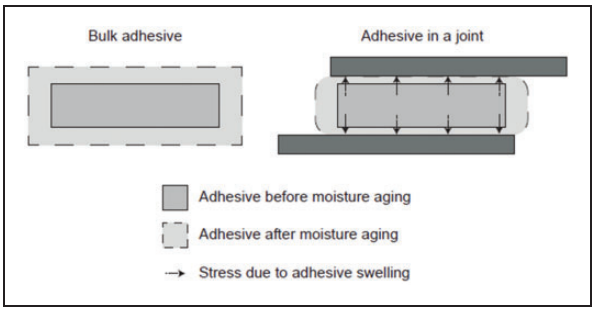


Figure 5. Swelling of the adhesive after being exposed to a humid environment in bulk and in a joint (adapted from Grangeat[26]).

the edges exposed to the environment, at the center of the adhesive layer, the water content will be consistently lower than at the exposed edges, Figure 6.

In joints with unprotected steel substrates, as water diffuses through the interface, localized or general corrosion may occur, with the formation of iron oxides on the interface between the adhesive and the substrate.[70,71] Gledhill et al.[65] studied the variation of properties of adhesive joints immersed in water at different temperatures, observing that at low temperatures, the failure was cohesive. However, from a given temperature, the failure was interfacial, occurring between the iron oxide and the adhesive used.

Composite materials provide a particularly interesting case of study in this context, since they can both be substrates in adhesive joints and provide further information on the behavior of the adhesive/substrate interface through an analogy with the fiber/matrix interface. In those materials, fibers are typically hydrophobic, absorbing significantly less water than the polymeric matrix. However, and in parallelism with substrates in adhesive joints, fibers represent preferential paths for water ingress.[72] Generally, the degradation caused by aging is affected by the nature of the fibers or other inclusions, as it occurs at the interface between the resin and the inclusion, causing the separation of the fibers from the matrix and decreased stress transfer between the two components, lowering the mechanical, thermal and physical properties.[30] This phenomenon is observed for several different types of inclusions, such as long fibers, short fibers and particles. Composite materials commonly used in adhesive joints as substrates, such as carbon

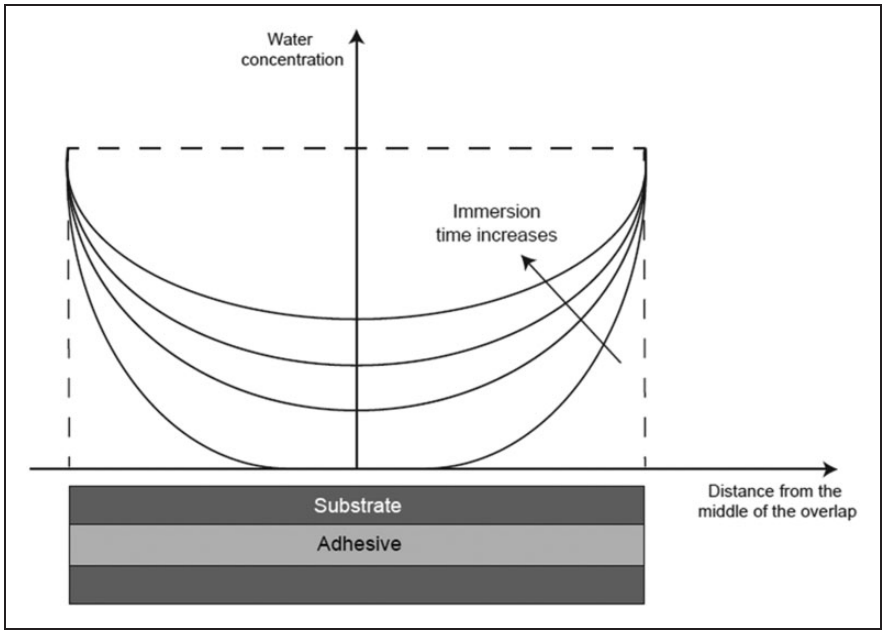


Figure 6. Water concentration distribution assuming a Fickian distribution (adapted from Sargent[69]).

fiber-reinforced polymers (CFRP), were shown to decrease their strength by 25–30% after the first month of exposure, even at temperatures as low as ambient temperature. However, after the first month of exposure, a constant value of strength was recorded.[73]

Water was also shown to diffuse quickly out of epoxy resins at high temperatures.[61] The hygrothermal aging process typically introduces both reversible and irreversible changes to the structure of the polymeric materials, which leads to different levels of damage.[63,74,75] The changes introduced can be fully reversible, meaning that after hygrothermal aging, the materials can be re-dried and their mechanical properties can practically fully restored.[30,76]

However, some of the damage introduced by aging, such as swelling, can be irreversible, especially in specimens aged at high temperatures, which suggests the presence of some chemically attached water. In specimens dried at low temperatures, a difficulty in attaining complete water desorption was observed,[64] which could indicate that only the water that filled the voids of the material is removed, while the water that has already reacted chemically with the adhesive remains, requiring more energy, that is, a higher desorption temperature, to break the chemical bonds.

Contamination

Mechanisms of contamination

Contamination arises in adhesive joints from multiple sources and is one of the major limitations to their use, since it may cause an unpredictable behavior of the joint. When contaminants appear at the interface between adhesives and substrates, they can generally exhibit three types of behaviors: (i) diffuse into the adhesive, (ii) diffuse into the substrate, and (iii) remain at the interface between the adhesive and the substrate causing a physical separation between them.[21]

If contaminants diffuse into the adhesive or the substrate, this can have an influence similar to that of the water. However, the most concerning situation happens if contaminants are located on the surface of the substrate forming a very thin layer, which can be nanometric in scale, which impedes the inter-molecular interactions between the adhesive and the substrate,[77–79] forming areas where the adhesion is weak, that some authors call kissing bonds (KB) or zero volume debonds, Figure 7. In this case, the adhesive and the substrate are in intimate contact, but only form weak adhesion bonds. Nagy et al.[80] state that zero volume debonds occur between compressed, but otherwise unbonded surfaces. The presence of these debonds in adhesively bonded structures is a major point of concern, since they present an area with very reduced bond strength and are almost impossible to detect using typical non-destructive testing equipment.[80]

Marty et al.[82] presented three criteria to the definition of a zero volume debond: (i) shear strength, when testing a single lap joint (SLJ) under tension, is reduced to less than 20% of its nominal value; (ii) failure must be adhesive, i.e. purely at the adhesive/substrate interface; (iii) they must be indistinguishable from perfectly bonded joints with classical amplitude C-scans.

To avoid the formation of these debonded areas, and taking as an example of adhesive joints with metallic substrates and oily contaminants, adhesives must be able to, first, displace the absorbed oil directly

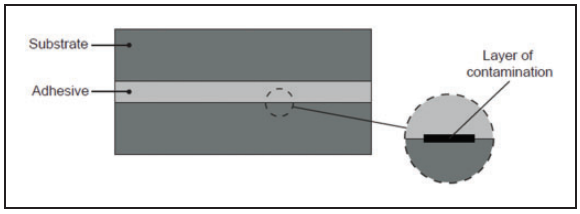


Figure 7. Schematic representation of zero volume debonds (adapted from Yan et al.[81]).

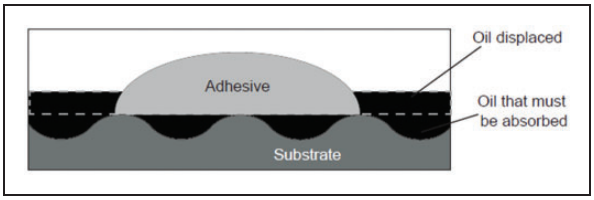


Figure 8. Oil accommodating adhesives (adapted from literature[83,84]).

from the metal surface and, second, absorb the contamination.[21,83] Debski et al.[83] presented a study in which, from the measurement of the surface energy of uncontaminated zinc-coated steel substrates and the same substrates contaminated with mineral oil, it was concluded that, from the thermodynamic point of view, it was probable for the displacement of the essentially apolar oil to occur. However, the substrates have some roughness, in which oil can be trapped. In this case, the adhesive must be able to absorb the contaminant in order to ensure contact between the adhesive and the substrate, Figure 8. In a complementary work,[84] a model that determines the relative importance of each phenomenon involved in the elimination of the contaminant was developed.

Greiveldinger et al.[4] studied the diffusion of an industrial mineral oil into an epoxy resin in an adhesive joint. Initially, the contaminant was placed on the substrate. As the adhesive starts to cure, the oil diffuses into the bulk adhesive. This process occurs very rapidly at the beginning of the curing cycle. Before the curing of the adhesive, the Fourier-transform infrared spectroscopy (FTIR) profile at the interface is very similar to that of the oil. However, at the end of the process, it is very similar to the uncontaminated adhesive. From a given time period of the curing cycle, it is observed that some of the oil leaves the adhesive, which is related to the cross-linking of the adhesive, since the adhesive shrinks slightly on cross-linking, and this compression may result in some of the contaminant being expelled from the adhesive. The cross-linking of the adhesive is very similar with and without the initial presence of oil on the interface as long as the contaminant has mostly been absorbed by the adhesive. In this case, neither the kinetics of cross-linking nor the mechanisms associated with this process exhibit any change.

Contaminants can be a wide variety of materials arising from several contamination sources. However, some of the most relevant for practical study, those that can be critical in the manufacturing process, typically combine high particle mobility with a low cohesive strength, characteristics of release agents, greases and oils.[77]

Effect of contamination on the interfacial properties

Contaminants may influence the different stages of the adhesion process, such as the wettability of the surface, the curing process of the adhesive or the service life. When contaminants are present at the surface of the substrates, which can happen during the manufacturing of the substrate, this may have an immediate consequence of changing the surface energy. For example, for substrates contaminated with tensides, as found in detergents, a decrease in the surface energy will occur, leading to poorer wettability of the substrate by the adhesive and, consequently, lower adhesion strength.[85] The same phenomenon has been observed with the contamination by mold release agents.[79,86,87]

The effect of contaminants on adhesive bonds is a highly complex subject of study, since it will depend on the contaminant, adhesive, substrate and interactions between them. However, two major and different behaviors of the contaminant can be identified. In one case, the contaminant can diffuse through the adhesive or the substrate, disappearing from the adhesive–substrate interface. In the other case, the interface creates a physical barrier between the adhesive and the substrate, significantly reducing the strength of the joint and even resulting in the formation of the previously mentioned zero volume debonds.

Attention will be devoted first to the case, in which the contaminant can be absorbed by the adhesive. One of the best and more thoroughly researched examples of this case is moisture contamination, which has been previously discussed in this review. However, there are other important examples, such as the presence of oil contamination.

Debski et al.[83] determined the T_g of epoxy adhesives neat and contaminated with mineral oil, added by premixing, after different cross-linking periods at high temperature and concluded that the kinetics of the cross-linking process changes with the presence of the contaminant, since for similar cross-linking times, at the same temperature, the higher the mass of contaminant present on the adhesive, the lower the T_g, which is thought to be due to either the absorption of oil by the resin or the evaporation during the cross-linking process. However, at the end of the cross-linking process, regardless of the content of contaminant initially mixed in the adhesive, the T_g is similar.

The influence of oil in the cure of an epoxy adhesive was studied using differential scanning calorimetry (DSC) and thermogravimetric analysis (TGA). From the DSC analysis it was concluded that, with addition of oil content, there is an indication of a different chemical reaction occurring in the curing process, exposed by a decrease of the cure exotherm.

This change of the reaction may also affect the T_g of the adhesive, since the T_g increased with additional oil content. From the TGA it was concluded that peak temperature decreases with increasing oil content, as shown in Figure 9. Moreover, it was recorded a decrease in total weight loss percentage with increasing oil content, which indicates that the presence of oil changes the thermal degradation mechanisms.[88]

The absorption of contaminants by the adhesive, such as in the case of water, may also directly weaken the adhesive on the bondline, which can lead to premature failure of the joint, especially at the free edges, due to a drastic reduction of the peel strength.[89]

In adhesive joints with steel substrates and epoxy adhesives, it was observed that the steel interacts with the adhesive through the amide component. However, with contaminants, the preferential absorption of the curing agent resulted on an adhesive layer very rich in epoxy, incompatible with oil, acting as a barrier to the adsorption of contaminant by the adhesive, remaining at the interface.[21]

If a contaminant cannot be absorbed by the adhesive, due to intrinsic incompatibilities or in cases such as the one discussed above, zero volume debonds may appear at the interface between the adhesive and the substrate. Debonds contribute to unstable crack growth, decreasing the load capacity of the joint.[87] As debonds are areas where there is no connection between the adhesive and the substrate, they will create preferential paths for fracture propagation, contributing to the adhesive failure of the joint, also decreasing its strength, possibly with catastrophic consequences if a sufficiently large area of the joint is affected.[79]

As the consequences of contamination will be very much dependent on the materials and study conditions, the resultant effects are quite complex, and each case can exhibit particularly different effects. To complement this subject, the section *Practical case studies* of this work lists some practical cases related to contamination in more detail.

Experimental testing

In this section, different sample preparation and testing methods suitable for assessing the effect of moisture and contamination on adhesion are discussed in detail. Although sample preparation procedures are inevitably different for moisture aging studies and contamination studies, several testing procedures can be used to analyze the effect of both. Therefore, this section is divided into three sections. The first section is *Moisture aging*, in which the preparation of joints to be aged with water and methods specifically used to analyze them are explored. The second section is *Contamination*, in which the preparation of contaminated samples and testing procedures used to analyze the effect of contamination exclusively are discussed, which are mainly tests to identify zero volume debonds. Lastly, the section *Moisture aging and contamination* is presented, which describes testing methods that can be used to analyze joints in a simultaneously aged and contaminated state.

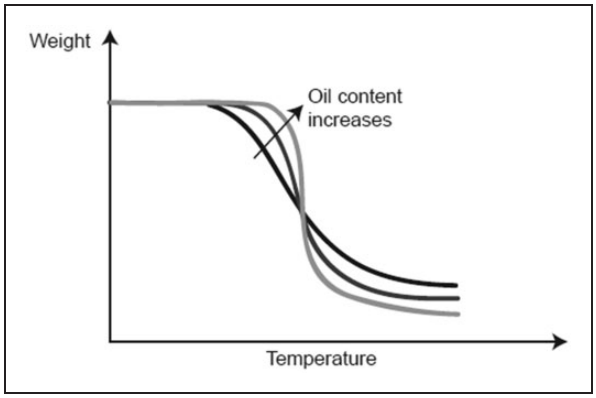


Figure 9. TGA weight loss (adapted from literature[88]).

Moisture aging

The main challenge associated with moisture aging of the adhesive layer in joints, such as SLJs or double cantilever beam (DCBs), is the long period of time needed to achieve the complete saturation of the adhesive layer, mainly due to the small area of adhesive exposed to the environment. Therefore, the use of open-faced joints has been proposed as an alternative to increase the exposed area and decrease the time needed for the adhesive to reach saturation, as shown in Figure 10.

Acknowledging the interfacial nature of the failure of adhesive joints subjected to humidity, this technique can be adopted to speed up the water uptake process and obtain a more uniform degradation of the adhesive layer. Wylde and Spelt[91] and Loh et al.[92] used this technique to study the interfacial fracture energy of aged adhesives and Goglio et al.[90] used it to analyze SLJs immersed in water. The process of joint manufacturing consists of applying the first layer of adhesive onto each substrate, the primary adhesive bonding, Figure 11a, which is followed by drying this layer in an oven to remove any moisture present, Figure 11(b). Afterwards, each substrate with a thin layer of adhesive will be directly exposed to water, until the adhesive is saturated, Figure 11(c). In the final step of the process, two substrates with thin, saturated adhesive layers will be joined using another fresh adhesive, completing the secondary bonding, Figure 11(d).

Fernandes et al.[93] used a similar technique to analyze the fracture toughness of an adhesive after aging. In this work, the objective was to force the failure to occur cohesively on the aged adhesive, to obtain the properties of the adhesive and not the interface. With that in mind, a layer of adhesive was saturated through immersion in water and bonded to the substrates using a fresh layer of adhesive, Figure 12.

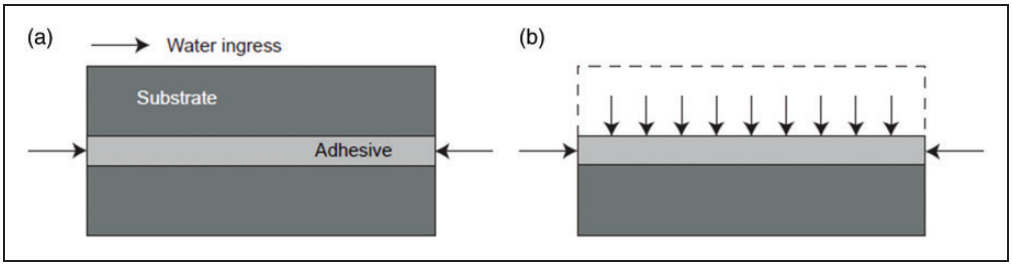


Figure 10. Water ingress in conventional bonded joints and open-faced joints (adapted from Goglio et al. (a) Conventional bonded joint, (b) Open-faced joint.[90]).

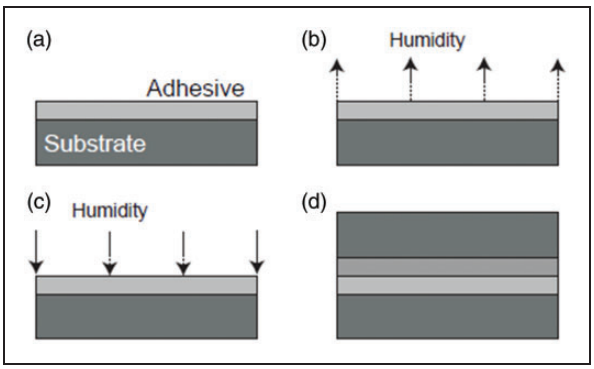


Figure 11. Manufacturing of open-faced SLJs (adapted from Goglio et al.[90]). (a) Primary adhesive bonding, (b) Drying in oven, (c) Exposure to humid environment, (d) Closing the joint with secondary bonding.

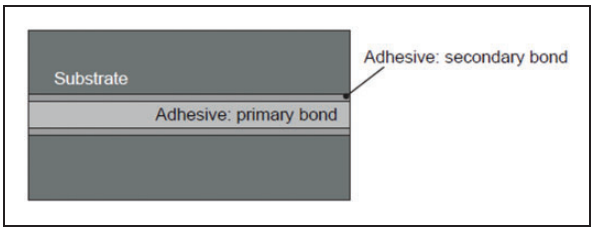


Figure 12. Adaptation of open DCB to force cohesive failure on the adhesive layer (adapted from Fernandes et al.[93]).

Although it is relatively simple to perform gravimetric studies with the bulk adhesive, in an adhesive joint, the mass of water inside the material is usually significantly smaller than the mass of the joint, which makes these studies difficult to perform. These specimens constitute a challenge during the manufacturing process, since the aged layer of adhesive is enclosed in two fresh adhesive layers, which requires a careful alignment of the primary and secondary layers of the adhesive as well as a careful assessment of the bondline thickness, to avoid residual stresses due to asymmetry.

Zanni-Deffarges and Shanahan[51] compared the water diffusion in the same structural epoxy in bulk and in a bonded joint. A cylindrical torsional joint was used to simplify the use of diffusion equations, due to axial symmetry, and because it presents a simple shear field. A gravimetric study was carried out for the bulk adhesive however, as said, that is difficult to perform on the adhesive joint. Therefore, a model considering the variation of the elastic modulus with the water content was contemplated, considering that the elastic modulus of the joint will be given by a combination of the elastic modulus of the dry and the wet adhesive. The coefficient of diffusion D obtained from this method was lower than the one obtained from the gravimetric study; however, it was of the same order of magnitude.

Liljedahl et al.[94] also developed a method to determine the moisture profile in adhesive joints using nuclear reaction analysis (NRA). This process also allowed to understand that the mechanisms of water ingress that occur in an adhesive joint are different from those found in a bulk adhesive, with water ingress progressing much faster in joints. In an adhesive joint, a case II front, where the concentration was approximately linear was found near the exposed edge, followed by a Fickian precursor. Case II diffusion happens when the viscoelastic properties of the material become significant and, in this case, water uptake is linear with time and not with the square root of time ($\sqrt{t}$), which happens for Fickian diffusion.[95] The case II diffusion was attributed to the fact that the substrates provide a constraint against swelling, which causes the water ingress to be higher at the interface.

Fiber Bragg grating (FBG) sensors were used by Mieloszyk et al.[96] to detect moisture contamination in an adhesive joint with composite substrates. These sensors represent a powerful tool to measure strain induced in adhesive bonds with these substrates, as they are highly resistant to corrosion, are small, lightweight and can detect small variations in the water content of the material. Due to its size, FBG sensors can be embedded into the adhesive layer and, with the understanding that as water content increases, the deformation of the adhesive also increases, the moisture presence in the adhesive can be determined indirectly. In this study, the water content in the adhesive at saturation was close to 2% and, even for this low concentration, the FBG sensors were found to be useful to measure the strain of the adhesive. FBG sensors can present an additional interface for preferential water sorption. However, in this study, it is stated that, comparing with the adhesive layer, the sensor is small enough for its effect to be considered negligible.

Ultraviolet (UV) reflection spectroscopy takes advantage of the spectral changes during water sorption allowing to estimate the fraction of hydrogen bonds formed between water and the adhesive. This method was shown to be effective and sufficiently sensitive for use in water sorption studies.[97] By coupling a bifurcated fiber-optic attachment to this equipment, water sorption can be monitored in situ.[97,98]

Contamination assessment

Contamination studies encompass a large range of testing conditions, with many contaminants, which can be applied in different ways such as liquid form or film. When contaminants are in film form or are solid materials, they are simply placed on top of the substrate prior to adhesive bonding. However, when working with liquid contaminants, more precise placement methods must be adopted to understand the amount of contaminant placed on the substrate to obtain comparable experimental tests.

Sato et al.[99] created an apparatus to prepare samples with controlled contamination, Figure 13, where the substrate was translated in a reciprocating movement behind a shielding plate, through which liquid contaminant was sprayed using a pressure-regulated gun.

Akiyama et al.[85] developed a system, inspired by the one described previously to deposit contaminants on the surface of a given substrate. To obtain a uniform layer of contaminant, the substrate was placed on a moving system that displaces at a constant velocity, while the spray nozzle releases the contaminant. The deposition of contaminant was controlled through the number of coating cycles. Afterwards, the amount of contaminant deposited was estimated through the difference of the mass before and after the spray coating of contaminant on a lightweight aluminum foil.

Zero volume debonds must be detected in adhesive structures to avoid unpredictable behavior and its premature failure, since they represent areas with a much lower adhesion strength. However, commonly used non-destructive tests are not very effective since, in this case, they are zero volume and a void is not detectable. Additionally, it is important to detect debonds in structures in service, without damaging them, necessitating the use of non-destructive techniques (NDT).

Infrared thermography is a method based on the reading of the infrared radiation emitted by a structure. That thermal energy, which is emitted in the infrared spectrum by objects, is then transformed into a visible image. When there is a defect that forms a traction-free surface, the emission rate of the dissipation of the thermal energy will be reduced. When applied to adhesive joints, this method was useful to detect non-uniform adhesive layers as well as zero volume defects.[89,100,101]

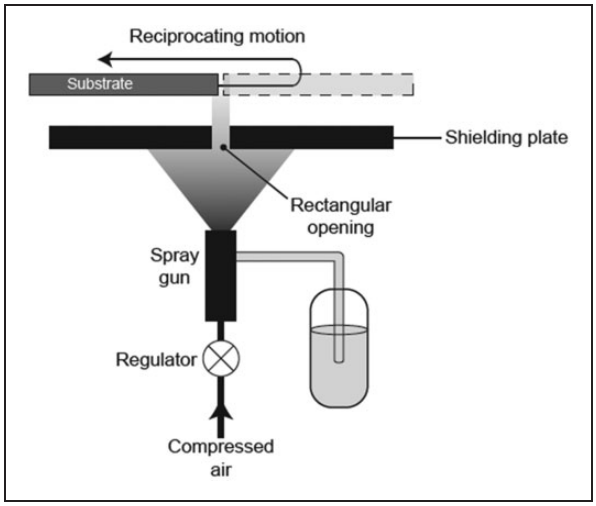


Figure 13. Apparatus for application of controlled layers of contamination (adapted from Sato et al.[99]).

Ultrasonic inspection was also shown to be effective to identify zero volume debonds, partial bonds caused by surface contamination, among others. An analysis of the ratio between normal and transverse interfacial constants of a given imperfect interface was suggested as a method to identify the physical nature of that defect. The ratio can be determined from the ratio between the longitudinal and shear reflection coefficients, considering normal incidence. Nagy et al.[80] showed that this method allows for the distinction between zero volume debonds and partial bonds, due to the significant difference between the ratios for the boundary defects caused by particular shapes and the boundary defects formed at the interface.

Non-linear ultrasonic measurement is based on the hypothesis that when a large amplitude ultrasonic wave propagates through an area containing debonds, non-linearities will be detected on the system. Yan et al.[81,102] tried to test this hypothesis measuring the degree of non-linearity exhibited by perfect bonds and zero volume debonds. If a wave of magnitude A is incident on a zero volume debond, the transmitted waves will be harmonics of the original wave, with the i-th harmonic having an amplitude A_i and frequency $i{\cdot}\omega$. The degree of this harmonic generation defines the extent to which the defect behaves non-linearly. Zero volume debonds caused by contamination are expected to have a smaller increase in the non-linearity of the system than partially closed debonds, because it results only on the addition of a thin layer of contaminant to the system.

Laser-induced breakdown spectroscopy (LIBS) can also be used to study contamination in adhesive joints. LIBS is an analytical method based on atomic emission spectroscopy.[99,103] This method does not require surface preparation, allowing a rapid and in situ analysis of the structures. For the evaluation of the application of this method in adhesive joints, aluminum substrates contaminated with

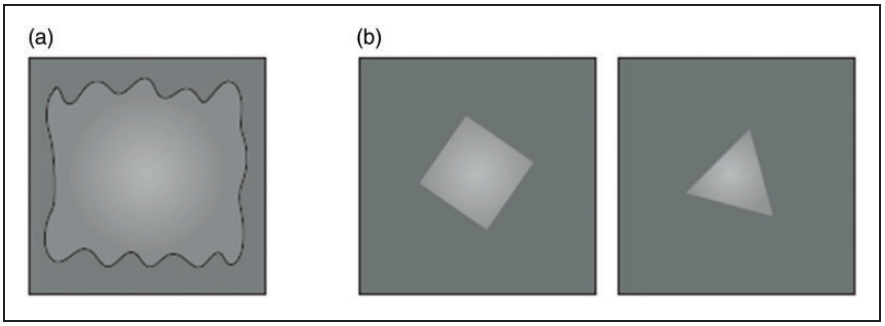


Figure 14. Schematic representation of an adhesive joint using neutron imaging (adapted from Michaloudaki et al.[113]). (a) Adhesive joint with moisture, (b) Adhesive joint with teflon sheets.

silicone oil were used. A surface concentration of silicone oil up to 7 mg/m^2 was found to be enough to reduce the shear strength of the joint. LIBS was able to detect contamination sites for silicone oil concentrations up to 12 mg/m^2, which is not enough to detect all the contamination sites that may cause a decrease in strength of the bond, but still constitutes an interesting evaluation method to discard joints that most certainly will fail due to influence of silicone oils.[99]

Greiveldinger et al.[4] developed a heated attenuated total reflection (ATR) cell to study the evolution of the adhesive/substrate interphase. This process requires the substitution of the substrate used in the real adhesive joint for the ATR crystal, which may introduce errors in the study since several authors reported that the diffusion of the contaminant into the adhesive also depends on the substrate.[83,84] However, this can be a significant test used to understand whether the contaminant is able to diffuse into an adhesive or if it will remain on the interface during the curing cycle.

Composite bell peel (CBP) was assessed as a destructive test to evaluate interfacial adhesion of adhesive bonds with CFRP substrates by Teixeira de Freitas et al.[104] This test was able to detect successfully a weak bond undetectable with C-scan, identifying a sudden decrease in peel strength and change in the failure mode from cohesive to adhesive. Compared with a DCB test, this test has the inconvenience of having delamination of the flexible composite substrate.

Acoustic emission (AE) is a process based on equipment that can detect changes in elastic waves prevenient from a crack propagating in a material or from a light impact.[89] AE combined with peel tests has been used to distinguish good quality bonds from weak bonds because the energy released recorded by AE for cohesive failure is much higher than for adhesive failure.[104] Therefore, this method is presented as a potential candidate to evaluate the quality of adhesive bonds in service, for early detection of weak bonds.

Leaky lamb waves can be used to detect zero volume debonds. These waves are modified acoustic waves that travel parallel to the bondline. Their properties are influenced by the properties of the adhesive layer, easily detecting debonds. However, they are not very effective for the detection of weak bonds.[89,105]

Surface energy can be used to understand the suitability of a given material for adhesive bonding. Typically, this test can simply be made by measuring the contact angle of a drop of a given liquid on the substrate used. Lower contact angles indicate better wetting of the surface and a lower surface energy of the liquid when compared to the substrate.[1,10,106,107] The better the wettability of a substrate's surface, the better the bondability of that substrate. Therefore, to evaluate the effect of a given contaminant on the bondability of a substrate, the contact angle of the contaminated and uncontaminated surface can be compared.

Heslehurst et al.[89] observed that when an adhesive bondline is degraded, the out-of-plane deformation of the joint is modified locally. Therefore, the analysis of this deformation might be an interesting approach for the identification of a weakened bondline. Holographic interferometry was used for the analysis of both debonds and weak bonds, proving to be a successful method to do so, exhibiting a global irregularity of the fringe pattern over the defective bondline areas.

Moisture and contamination

FTIR can be used to understand whether chemical changes have been observed in the specimen. More precisely, it is used to characterize the interaction of a cross-linked epoxy matrix with water sorption[63,76] or with the contaminant.[79,85,88] Antoon et al.[76] used FTIR to study the reversible interaction of water and a cross-linked epoxy matrix, detecting that the absorption bands of the epoxy resin change with sorbed moisture, which is attributed to solvent-induced modifications of the electronic environment, caused by water molecules. Polymer swelling can also affect the spectrum through the introduction of conformational changes or bond distortion, influencing the vibrational spectrum.[108] Wapner et al.[109] used FTIR-transmission-microscopy as a new technique to measure the water uptake of lap joint with silicon wafers, used as infra-red transparent substrates, and an epoxy-amine adhesive. The analysis was done as a function of distance to the edge of the joint, allowing the profile of unidirectional concentration of water as

a function of the distance to the edge of the joint to be traced. An increase of the coefficient of diffusion in an adhesive joint, when compared to bulk material, was also recorded, which shows the importance of the accurate analysis of the behavior of the adhesive in real joints. Regarding contamination studies, Jeenjitkaew et al.[79] used FTIR to study the presence of functional groups from the contaminants concluding there is not a chemical reaction between the contaminant and adhesive, but there is a migration of thickening agent when using adhesives that cure at high temperature.

Hong et al.[88] used both FTIR and DSC analysis to trace the curing profiles of uncontaminated and contaminated specimens and concluded that the presence of oil contaminants only has a limited effect on the curing rate of the epoxy adhesive.

DSC shows the heat effect of a given reaction as a function of temperature.[110] Zheng et al.[111] used DSC to analyze the failure mode of SLJs, concluding that environmental exposure does not influence the curing extent and T_g of the adhesive and that the degradation was, therefore, caused by interfacial degradation. Calvez et al.[112] used this method to analyze the curing process of an epoxy adhesive, observing that complete cross-linking is achieved.

Acoustic transmission uses a combination of ultrasonic and acoustic methods and it has been used to analyze the strength loss in composite materials due to moisture absorption. Its applicability in the study of adhesive joints is related to the determination of the bondline strength. This method requires an ultrasonic pulse to be induced as a stress wave, which will produce acoustic emissions if the material forms microcracks.[89]

Neutron imaging was also been proposed as a NDT to detect defects in adhesive joints.[113] Neutron radiography, similarly, to X-ray radiography, requires a variation in attenuation to achieve object contrast on the final image. However, in X-ray radiography, the contrast is obtained for objects with different densities, and in neutron radiography the contrast is obtained as a function of scattering and capture possibilities. Adhesive joints with moisture and with Teflon sheets at the interface, to simulate contamination, were analyzed with this method. A clear white zone where the Teflon sheet is located can be observed, as well as the moisture diffused within the adhesive. This method appears to be quite reliable, but it will depend on the nature of the adhesive, substrate and contaminant.

TGA is a particularly interesting method to perform both in moisture and contamination studies. TGA is a method that studies one or more properties of a given sample, when subjected to a controlled heating. When an aged sample is subjected to TGA, the sample is progressively heated and, at about 100°C, the water that has not formed chemical bonds with the material and is just occupying the free spaces in its chain reaches its evaporation temperature and is released from the material, showing a significant drop in mass of the specimen under analysis.[114] As temperature continues to increase, a second drop is recorded, related to the water that is bound with the structure of the material, mainly through hydrogen bonds. Regarding the studies of the effect of contamination, Hong et al.[88] used TGA to analyze an adhesive with and without oil contamination, which was shown to change the weight loss peak, decreasing with increasing oil content.

X-ray photoelectron spectroscopy (XPS) is used to measure the elemental composition of surface. This analysis can be used simultaneously for the analysis of the effects of moisture and other contaminants. The surface sensitivity of this method enables the measurement of thickness and the assessment of the distribution of thin contaminant films on a flat surface, up to about 5 nm.[107,115]

Time-of-flight secondary ion mass spectrometry (ToF-SIMS) can also be used in this analysis. This method has a very significant sensitivity, mass resolution and spatial resolution, which allows monolayer imaging of chemical information of the material.[116,117] However, both ToF-SIMS and XPS require vacuum, which could evaporate the substance under analysis.

Practical case studies

Moisture aging

To analyze the effect of water in bulk adhesives, Maxwell et al.[118] performed dielectric measurements of amine-cured epoxy adhesives as a function of water content. The measurements were carried out at frequencies between 200 Hz to 200 kHz and temperatures between −60 and 70 °C. In this work, both free and bound water were identified. Additionally, as the relaxation was found to have activation energy close to what is predicted from the breaking of hydrogen bonds, the nature of the connections between water and the adhesive was suggested to be of this type.

Jelinski et al.[119] also studied the interaction between water and epoxy resins. It was concluded that water interacts with specific sites on the epoxy backbone, being impeded in its movement and having a discrete array of possible positions instead of behaving like a gas in an inert matrix. However, the authors assumed that water acted simply as a plasticizer, not identifying any specific hydrogen-exchange mechanisms. This interaction was further investigated by Powers,[75] that concluded, corroborating the work of Maxwell et al.,[118] that water absorbed into epoxy resins associates with polar centers in the polymer, being able to break hydrogen bonds in the polymeric chain, causing the material to swell. It is also stated that the openings on the polymeric chain created by the absorption of water cause more water absorption

centers to be available, enabling further water sorption. The damage caused by water sorption has an irreversible component, which is believed to be due to the hydrolysis of linkages in epoxy.

Regarding the effect of water in the interface of adhesive joints, Drain et al.[120] analyzed polycarbonate-polycarbonate and steel-steel adhesive joints, bonded using a cyanoacrylate adhesive. When bonding polycarbonate substrates, no interface can be identified due to the dissolution of the composite in the ethylcyano-acrylate monomer, present in the adhesive. Therefore, the behavior of this bond, when compared with steel substrates, revealed a higher water resistance, since the diffusion of water through the interface is inhibited. As it was observed by Drain et al.,[120] the interface plays a key role on the water sorption behavior and the degradation of the adhesive joints and, therefore, must be studied.

The kinetics of water diffusion was analyzed by Gledhill et al.[65] through the study of joints with steel substrates and an epoxy adhesive. The authors concluded that this process could be predicted using thermodynamic considerations and that it was governed by the water diffusion through the interface. The main mechanism for failure of the joints was found to be the displacement of adhesive on the surface with metal oxide. Furthermore, it was said that the catastrophic effect of water on adhesive joints could be avoided if the integrity of the interface was preserved when in contact with moisture. However, thermodynamic considerations infer that if only secondary forces act at the interface, water will always desorb an organic adhesive from a surface with metal oxide. Therefore, to avoid the damage of the joint induced by water, it should be either impeded to reach the interface with a concentration higher than what is needed to displace the adhesive, or stronger interfacial forces, resistant to water, should be forged.

Viana et al.[74] studied water diffusion in DCBs, immersing them in water and periodically testing them until their properties were constant, at which point the material was considered to be saturated. If only diffusion in the adhesive was considered, the adhesive was found to reach saturation sooner than expected. Afterwards, two numerical models were created, the first one dimensional and the second two dimensional. The first model simulated the adhesive in the DCB joint as beam elements considering one-dimensional diffusion, and the diffusion coefficient was then fitted to match the experimental results. The second model considered a layer of adhesive and two thin interfacial layers. The diffusion coefficient was also fitted but, this time, one coefficient was attributed to the interface and other to the adhesive. It was concluded that the coefficient attributed to the interface was one to two orders of magnitude higher than the coefficient set for the one-dimensional case, causing water diffusion to occur preferentially through the interface. In an additional work, Viana et al.[121] showed that with increasing water content, the failure was increasingly interfacial, a phenomenon also promoted by high temperatures.

The failure mode of adhesive joints after being subjected to water aging was found to change from cohesive to adhesive failure, especially in polished surfaces, coupled with a decrease in joint strength[65,66,122–125] Additionally, Cognard et al.[122] concluded that after water immersion the failure, which was initially cohesive, becomes adhesive, especially on polished surfaces. In the long term, debonding of the adhesive joints subjected to both liquid water and water vapor was recorded. A threshold of humidity for which water vapor accelerated the cracks was also determined and justified based on the theory of Michalske for the weakening of bonds due to water.[126] Therefore, it is assumed that two different processes occur in the debonding of adhesives, one that occurs at high speed and characterizes the initial strength of the joint, and another at low speed that is related to its durability. In an additional work, Cognard et al.[46] observed blisters in water vapor in an epoxy-amine adhesive when subjected to high temperature and pressure. Those blisters, when analyzed microscopically, appear to come from smaller ones which spread along the interface adhesive/substrate, and increase under the osmotic pressure created.

McGeorge[123] analyzed a complex adhesive composite joint, loaded in shear, subjected to different aging conditions. It was concluded that the shear strength decreases with water sorption, combined with an increase in ductility. After saturation, specimens were subjected to further aging cycles with mechanical loading and high temperature, at high humidity, which did not cause any additional damage on the more carefully prepared adhesive joint, which had a primer with fiber glass reinforcement and an epoxy anticorrosion primer. For adhesive joints that did not follow all the steps of the surface preparation, further crack development was recorded. After re-drying the specimens, the shear strength increases but it does not return to the initial value. The authors also suggested that small overlap lengths can lead to high scatter of results and, therefore, misleading conclusions.

Legghe et al.[124] studied the water sorption behavior of an epoxy film, fitting both Fick and Langmuir models to the experimental results, with the best approximation for the experimental results being obtained from the Langmuir model. The effect of water sorption on the adhesion strength between the adhesive and steel was also investigated through the performance of pull-off tests on epoxy coated steel specimens immersed in water. In this study, it was observed that, as adhesive thickness increased, the difference between the time a loss of adhesion was observed and the time expected for the water to reach the interface, only considering diffusion through the adhesive, also increased, indicating the presence of

another mechanism, such as interfacial stresses due to the swelling of the adhesive or diffusion of water through the interface. After re-drying, the adhesion properties were somewhat restored although they continued to be lower than those of the dry material, showing the presence of irreversibility in the process.

Leger et al.[66] studied the aging of a SLJ using a crash-resistant epoxy adhesive immersed in water at 70 °C. In this work, a numerical model is developed to simulate the water diffusion in the adhesive and consequent residual strength, using a coupled elasto-plastic law to predict its mechanical behavior. It is concluded that water ingress induces stresses in the adhesive. However, these stresses are not very critical, if the exterior load imposed leads to crack initiation and final fracture. It is also stated, based on the numerical simulation, that the interface will be the most favorable place for crack propagation, being the most damaged area of the adhesive.

Sugiman et al.[125] analyzed the effect of adhesive thickness, combined with aging of the adhesive joint, on the strength of SLJs using dissimilar substrates, one steel and one glass fiber-reinforced polyester (GFRP). It was concluded that, for dry conditions, with increasing adhesive thickness, the failure changes from adhesive to mixed failure. However, after aging the joint for 15 days at 60 °C, the failure occurred at the adhesive/substrate interface for all the adhesive thicknesses tested, ranging from 0.1 to 0.5 mm. In dry conditions, the adhesive mainly remained bonded to the steel substrate but, in wet conditions, the interfacial failure happened at the adhesive/steel interface. For the numerical simulation, it was considered that the water diffused through the adhesive joint from all the sides exposed to water and through the GFRP. This process was concluded after chronic 15 days and although the adhesive close to GFRP was saturated, the adhesive close to the steel substrate was not. The difference in water content between the faces of the adhesive increased with increasing adhesive thickness. Over the overlap length, it was also noted that although the edges of the adhesive were saturated, the center was not.

Surface preparation and different surface treatments were also shown by several authors to play a key role in the water sorption characteristics of an adhesive joint.[69,112,127,128]

Sargent[69] determined the effect of the immersion in distilled water at 35 °C on adhesive joints with aluminum substrates and phenolic and epoxy-based adhesives for over seven years. The adhesive–adherend combination was found considerably stable even with a significant water concentration, since periodic peel strength tests showed constant joint behavior and no corrosion was found on the substrate. It was furthermore concluded that the pre-treatment performed on the substrate was one of the key factors that contribute to the durability of an adhesive joint, avoiding corrosion.

Kinloch et al.[127] studied the influence of temperature and humidity on adhesive joints with epoxy adhesive and aluminum alloy substrates, subjected to different surface treatments: grit blasting and degreasing (GBD), chromic-acid etching (CAE) and phosphoric-acid anodizing (PAA). Matching the results obtained by Sargent,[69] it was concluded that the surface treatment plays a crucial role in the durability of the adhesive joint. With XPS and electron microscopy analysis, it was observed that the joints that showed the poorest durability failed in the interphase between the oxide and the adhesive. This happened for GBD pre-treated joints that also showed poor wetting and macro-voids at the interface, leading to a lower value of G_{th} (the threshold below which there is no crack propagation). PAA pre-treated joints failed through the oxide layer due to its weakening caused by the humid environment, also followed by a decrease in G_{th}. The specimens with the CAE pre-treatment showed no interfacial failure and no decrease in G_{th}.

Calvez et al.[112] studied the durability of joints with galvanized steel substrates and an epoxy adhesive, when subjected to moisture-induced aging. SLJs were manufactured and tested. Afterwards, SEM, FTIR and DSC analysis were carried out to examine the failure surfaces and determine the locus of failure. Throughout the testing period, the adhesive showed physical and chemical modifications and the substrate exhibited progressively a higher corroded area. The failure changed from mixed failure (cohesive and interfacial) to interfacial and, for long exposure times, to the surface layer of corrosion products. A three-step process was also proposed to explain the loss of adhesion after moisture aging: (i) hydrolysis of the adhesive and interface at high stress areas; (ii) hydrolysis of the center of the joint and beginning of the corrosion of the substrates; and (iii) rupture in a weak boundary layer due to growth of the corrosion products.

Li et al.[128] studied SLJs with aluminum-lithium substrates subjected to different surface treatments, analyzing their behavior at a humid environment at high temperature. The surfaces were treated with sandpaper, sandblasting, chemical etching and PAA. A combination of mechanical and PAA treatments was also analyzed. It was concluded that the exposure to hot-humid environments causes the degradation of the adhesive joint while also changing the failure mode. Out of the surfaces treated with a single procedure, the surfaces treated with PAA revealed the lowest decrease in strength after hygrothermal aging. The best behavior reported was for joints treated using both mechanical and PAA treatments, although a decrease in strength was detected for excessive surface roughness. Figure 15 explains why a medium level of surface roughness (Figure 15(b)) increases the path followed by water along the interface when compared with low levels of surface roughness (Figure 15(a)), which contributes to a decrease in

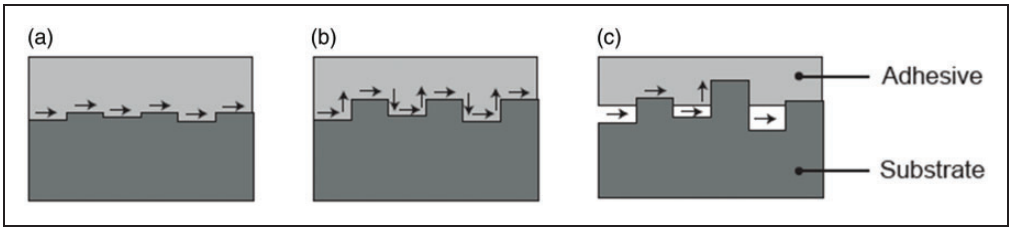


Figure 15. Effect of surface roughness of the substrates on water diffusion (adapted from Li et al.[128]). (a) Low roughness, (b) Medium roughness, (c) High roughness.

water diffusion rate. However, high roughness can also be disadvantageous if it impedes the mechanical interlocking of the adhesive (Figure 15(c)). In this case, water is free to diffuse between the adhesive and the substrate.

In conclusion, the present work indicates that water diffusion in adhesive joints is mainly governed by diffusion through the interface. Typically, a change from cohesive failure to adhesive failure at the adhesive/substrate interface coupled with a strength reduction was commonly reported to occur in adhesive joints, after moisture degradation. Additionally, polished surfaces were found to facilitate the decohesion process, as they do not provide the mechanical interlocking of the adhesive on the substrate. It is important to notice that surfaces with very high roughness also represented a problem as they impede the adhesive from fully wetting the substrate, creating preferential paths for water diffusion. Corrosion of metallic substrates due to water ingress was also a common occurrence, found to damage the adhesion levels. However, proper surface treatments were found to suitable for minimizing this effect, as well as water diffusion through the substrate, leading to a significant reduction of the influence of water on joint strength.

Contamination

Contamination processes encapsulate a wide variety of behaviors, depending on the adhesive/substrate interaction, the contaminant/adhesive and contaminant/substrate interaction and on the different surface treatments used. The aim of this section is a holistic perspective of the effect of contamination in adhesive joints, and therefore, case studies with different substrates (such as aluminum, steel and CFRP) subjected to different surface preparations, different adhesives (such as adhesives with and without fillers, oil-accomodating adhesives and common epoxy adhesives) and different contaminants (such as oils, silicones, fuels, mold release agents and tensides) are discussed. To avoid excessive subdivision, the studies analyzed regarding contamination are presented in chronological order.

Hong et al.[21] used XPS analysis to study the adhesive/substrate interface between cold-rolled steel, electrogalvanized steel and aluminum substrates and an epoxy adhesive with a polyamide curing agent, with and without contamination. Steel substrates were contaminated using a ''ship-out'' oil and aluminum substrates were contaminated using an aerospace hydraulic fluid. Without contamination, electrogalvanized steel and aluminum interacted with the adhesive mainly through the free amines of the curing agent, exhibiting a preferential adsorption of this agent. With contaminants, the preferential adsorption of the curing agent resulted on an epoxy-rich adhesive layer, incompatible with oil, acting as a barrier to the adsorption of contaminant by the adhesive. In aluminum substrates, the adsorption of curing agent decreases. Adhesive displaced the oil in cold-rolled steel substrates without the observation of protonation of the curing agent (which is the addition of a proton to an atom, molecule or ion), which indicates that there is residual contamination associated with the substrate.

In a complementary study, Hong et al.[88] studied the effect of aliphatic slushing oil, a ship-out oil, on the curing and degradation behavior of an epoxy designed for oil-accommodation using DSC, TGA and FTIR analysis. It was concluded that the presence of oil does not influence the curing rate of the epoxy, with contaminated and uncontaminated specimens consuming around the same amount of epoxide groups during the curing process. However, it can affect the final properties of the adhesive, such as the T_g.

Olsson-Jacques et al.[115] analyzed aluminum substrates bonded with an epoxy adhesive with contamination of an aviation fuel, applied between the grit blasting and the bonding steps, using Boeing wedge tests. The aviation fuel is composed by a mixture of alkanes, de-icing fluid and water insoluble compounds, among other constituents. It was concluded that the fuel is adsorbed by the surface of the substrate. When the contaminant is applied before the adhesive, it does not have a high influence on the durability of the joint; however, if it is applied before the silane coupling agent, it leads to catastrophic failure of the adhesive joint. This silane coupling agent can also shift the failure mode from adhesive to cohesive. The contaminant also leads to slight shifts in the fracture path.

Ogawa et al.[129] studied the fracture mechanism and oil-absorption of oil-accommodating epoxy based adhesives. For that purpose, shear and T-peel tests were carried out using steel substrates and the fracture

surfaces were analyzed with SEM. In this study, the oil concentration was calibrated from the absorbance between the adhesive containing oil and the neat adhesive, which is due to the C–H stretching vibration in the methylene chains of the oil. Peel and shear strength decreased with the contamination of oil in the joints. Both cured and uncured adhesive specimens were immersed in oil and analyzed. Uncured adhesive showed a much higher capability of absorbing oil than cured adhesive, leading to the conclusion that if a joint is contaminated prior to the curing of the adhesive, it should be able to absorb the contamination, removing it from the adhesive/substrate interface. However, if the adhesive is already cured it can only be expected to absorb limited quantities of oil, leaving much of it present on the grooves of the steel plate, creating conditions favorable for the appearance of debonds.

Anderson et al.[130] tested the effect of silicone contamination on several combinations of adhesives and substrates. Different paints and primers were also analyzed. Experimental tests were mostly performed using a tensile button-to-plate configuration. The main conclusions of this work were that the sensitivity to silicone contamination of the strength of the bonded system depends on the substrate material, with lower sensitivity for cases in which the silicone can diffuse into the substrate, and on the curing temperature of the adhesive or primer, with lower sensitivity for cases where the curing temperature is higher. The strength of the adhesive bond was shown to decrease considerably with contamination. Cleaning the surfaces after contamination can slightly restore strength, although it never fully returns to the initial, uncontaminated values, even after severe treatments such as grit blasting. The bonds that exhibited a higher sensitivity to silicone contamination were high strength bonds to metal substrates. The use of a silane primer, in those cases, can reduce or eliminate the sensitivity to contamination, and this effect is improved by exposing the silane-treated substrate to high temperatures.

Jeenjitkaew et al.[79] studied the effect of a mold release agent, artificial sweat and cutting oil lubricant on chromic acid etched aluminum substrates with two different epoxy adhesives. The joints were analyzed using field emission scanning electron microscopy (FESEM) with an energy dispersive X-ray spectrometer (EDS), a wavelength dispersive spectrometer (WDS), FTIR and mechanical tests. The mold release agent stayed at the interface creating zero volume debonds, causing interfacial failure in the contaminated area and decreasing significantly the strength of the joint. The percent decrease in joint strength was close to the percent of area contaminated. In this case, contact angle also showed a significant increase, which indicates a decrease in wettability and, consequently, bondability. The other contaminants migrated to the adhesive, almost fully disappearing from the interface and not interfering with the properties of the joint. Failure of these joints was cohesive on the adhesive, which is in accordance with the failure exhibited by the non-contaminated control samples. Nevertheless, the cutting oil introduced voids and cavities near the interface.

Jeenjitkaew et al.[131] performed an additional study with the same materials, but included hardened steel substrates. These substrates were bonded with one of the epoxy adhesives and contaminated with PTFE film, PTFE spray and mold release agent. In this study, double lap joints (DLJs) were tested quasi-statically and a numerical simulation of those joints was performed. For joints with hardened steel substrates, PFTE film and mold release agent caused a significant decrease in shear strength, when compared with the control specimens, also creating debonds and causing interfacial failure. Specimens contaminated with PTFE stray exhibited mixed failure, with a shear strength between that of the control samples and that of the samples contaminated with PTFE film or mold release agent. The numerical model developed used solid elements for the adhesive and the substrates and cohesive elements for the interface. Where zero volume debonds appeared experimentally, uncoupled elements were used. The results of the simulation were found to be in good agreement with the experimental results.

Zheng et al.[111] studied the effect of stamping lubricant on the strength of adhesive joints with aluminum substrates bonded with an epoxy-modified acrylic adhesive, through SLJ tests. It was concluded that below a certain level of contamination, a limited effect was noticed on the strength of the joint. However, for higher levels, contamination significantly decreases the strength of the joint. A limit concentration of lubricant was also established, above which the lubricant evaporation leads to pores in the adhesive layer. Joints were also exposed to a neutral salt spray, which reacted with the substrates causing corrosion of the substrates and, consequently, degradation in bond adhesion and a decrease of the joint strength. The lubricant, in this case, was found to be beneficial, protecting the substrates from corrosion.

Heide-Jørgensen et al.[86] developed an analytical model which can mimic DCB tests with contaminants on the surface, creating zero volume debonds. The analytical model of the weak interface consists of a beam, where the areas with adhesive are modelled by springs. In an additional study, Heide-Jørgensen et al.[87] studied the mode I fracture behavior of adhesive joints with CFRP substrates, bonded with an epoxy film adhesive, with and without debonds along the crack propagation path, using DCB tests. The debond was introduced through the placement of a release film on the surface of the CFRP while curing and promoted unstable crack growth. In the areas where debonds were found, the load–displacement

curve displays sudden drops in load with increasing displacement.

Akiyama et al.[85] studied the effect of different contaminants on adhesive joints with aluminum substrates bonded with epoxy and acrylic adhesives: silicone oil, mineral oil, a fluorine release agent and surfactants. The contaminants were applied to the aluminum surface using a spray. For this study, SLJ and DCB tests were performed and the fracture surfaces were evaluated using FTIR and atomic force microscopy (AFM). Uncontaminated control specimens exhibited cohesive failure in the adhesive. Surfactants or tensides, which are found in detergents, reduced the adhesion strength, which might be due to the decrease in surface energy they induce or with the low diffusion into the adhesive. Two of the surfactants used, sodium dodecyl sulfate and stearic acid, completely changed the failure from cohesive in the adhesive to adhesive. Mineral oil had no influence on the adhesion strength. Silicone oil did not affect the adhesion strength with the acrylic adhesive especially developed for oily surface adhesion, exhibiting cohesive failure in the adhesive, but lowered the strength of joints with epoxy adhesives, also exhibiting adhesive failure. It was shown that, for the epoxy adhesives, the effect was more noticeable when the oil was more viscous, which indicates physical adsorption on aluminum, confirmed in the AFM analysis. Mold release agent exhibited a significant influence on the strength of SLJ using epoxy adhesives, which exhibited adhesive failure, having a lower, but also noticeable influence on the joints using the acrylic adhesive, which exhibited mixed failure.

Summarizing the results from this section, it can be stated that contaminants were either found to diffuse to the adhesive and substrate or stay at the adhesive/substrate interface. In the first case, the influence of the contaminant on joint strength is significantly lower than in the second, with the process observed being similar to water sorption. However, the works reported in the literature demonstrated that if the absorption cannot occur due to the interaction between the adhesive, substrate and contaminant, this can lead to the creation of preferential paths through the surface, even producing zero volume debonds which lead to the catastrophic failure of the joint.

Moisture aging and contamination

Although more limited in number, the literature presents several studies, in which the effect of moisture and contamination is analyzed in the experimental procedure. This section describes these works, presented in chronological order.

Doyle et al.[48] studied the effect of several immersion environments on the properties of adhesive joints with aluminum substrates and an epoxy adhesive. Water-based environments, such as de-ionized water, a urea solution and simulated ocean water, and non-polar solvent systems, such as fuel and hydraulic fluid, exhibited different effects on the adhesive. All environments induced a plasticization of the resin, which lowers T_g and benefits further water ingress. However, water-based environments also promoted the growth of an oxide layer in the aluminum substrate, contributing to the opening of the bondline, also enabling additional water ingress. This ultimately results in the complete failure of the joint. Time-domain reflectometer (TDR) analysis was performed to determine the point at which failure occurs. Dichloromethane was also studied and it was found that it leads to a significant chemical degradation, to the point where some of the epoxy resin was extracted and solved into this solvent. In all immersion environments, a decrease in shear and cleavage energy was determined. A good correlation was found between the dielectric permittivity, the shear strength, and the cohesive energy.

Peterson et al.[132] studied the effect of the cleanliness of the surface of aluminum substrates on adhesion with silicone rubber in order to determine the minimum surface energy of the substrate to ensure good adhesion. Therefore, substrates with different levels of contamination of paraffin or silicone oil were prepared and compared using contact angle measurement and EDX. SLJs were manufactured after the application of the primer and silicone rubber onto clean substrates, with different surface energies, i.e. different levels of cleanliness. The SLJs were tested before and after immersion in boiling water for 100 h. It was concluded that after aging, for joints with the same surface energy, the percentage of joints that fail adhesively increases, coupled with a decrease in the shear strength of the joint. Both before and after aging, when the surface energy is lower, a higher percentage of joints fails adhesively, as expected.

Müller et al.[133] studied the strength of SLJs with steel substrates bonded with three different epoxy adhesives. These joints were immersed in water, oil and a solution of mineral and industrial fertilizers for 90 days. Control samples of the three adhesives kept in an uncontaminated environment consistently exhibited cohesive failure in the adhesive, not displaying a significant reduction in shear strength. Adhesive joints immersed in contaminant environments showed a significant decrease in shear strength at starting at about half of the immersion time. The failure mode of the joints also evolved from cohesive to mixed failure and finally to adhesive failure for two of the adhesives, while the other consistently exhibited cohesive failure. The significant decrease in strength of the adhesive was observed to be simultaneous with the initiation of adhesive failure as well as the appearance of under corrosion of the adhesive layer. Diffuse seepage of the immersion bath into the adhesive was also identified and considered as a cause for the decrease in strength of the adhesive bond.

Markatos et al.[134] studied the effect of pre-bond contamination of a silicon-based release agent and moisture on adhesive joints with CFRP substrates through DCB tests. Both cases led to the creation of zero volume debonds, not detectable by conventional NDT, as concluded from C-scans. A small increase in moisture content exhibited a small increase in mode I fracture toughness, while for higher content of water and for joints with the silicon-based release agent, a decrease in fracture toughness was registered. For concentrations of silicon over 7%, a complete lack of adhesion was recorded.

Hoffman et al.[135] evaluated the effect of pre-bond contamination with moisture, release agent, fingerprints and de-icing fluid using centrifuge tests. Joints were manufactured using CFRP substrates and an aluminum stamp, bonded with a film of epoxy adhesive. Contaminations were divided into production and repair scenarios, being the production scenarios the release agent and moisture and the repair scenario de-icing fluid. Fingerprints were considered in both production and repair scenarios. A significant reduction in adhesion strength was recorded for all contaminants, being lower for the higher concentration of contaminants, with moisture as the most severe case of contamination. When adhesive failure was identified, the adhesive remained mainly on the metallic stamp, which indicates that the bond between the metallic stamp and the adhesive is stronger than that between the adhesive and the CFRP.

Yerra et al.[136] analyzed the effect of contamination of oil and water droplets on carbon fiber-reinforced nylon 66, joined in SLJs using an epoxy-based adhesive and an acrylic-based adhesive. Contamination was found to have a more significant effect on the acrylic adhesive than on the epoxy. A decrease in strength and stiffness, paired with an increase in strain to failure was found as water ingresses the epoxy adhesive and hydrolysis occur. However, oil contamination resulted in a stiffness increase and a decrease in strain to failure, which is attributed to the cross-linking performance of the epoxy. Failure was cohesive for specimens with oil contamination and adhesive for water contamination. With acrylic adhesives, a decrease in strength, greater than 50%, was observed for oil contamination. However, the stiffness did not change suggesting that there is no chemical interaction with the polymeric chain. Failure for joints with the acrylic adhesive was always interfacial.

Overall, an analysis of the literature shows that most studies that analyze both the effect of moisture aging and contamination, chose to do so separately, presenting results similar to the ones reported in the two previous sections. However, it was found that when paired, the processes will lead to a cumulative damage of the adhesive joints, that is, joints with the same level of contamination will fail at lower strength and with increasingly adhesive failure (if the failure caused by contamination was not already fully adhesive) after moisture aging. In addition, joints with higher levels of contamination, after being subjected to the same moisture aging of less contaminated joints, also present lower strength and progressively more adhesive failure.

Conclusions

A literature review on the effect of moisture and contamination on adhesive joints was performed. It was concluded that both moisture diffusion and contamination can contribute to a reduction in joint strength and a higher likelihood of interfacial failure.

Moisture absorption by adhesives was shown to be divided into free and bound water. The first only fills the free spaces on the polymeric chain, while the second forms chemical bonds with said chain, through hydrogen bonds. However, when in an adhesive joint, water can also diffuse through the interface between the adhesive and the substrate, both by capillarity in the pores and cracks of the adhesive and through the substrate.

Adhesives suffer degradation of their mechanical properties after water sorption, decreasing elastic modulus, strength, and toughness, although strain to failure increases with water content. Adhesives are also plasticized by water ingress, decreasing its T_g. However, the decrease in properties of the adhesive is not the main cause for premature failure of adhesive joints, since the interface between the adhesive and substrate is damaged and failure occurs mainly through the interface. Water may also cause the degradation of the substrate and corrosion on metallic surfaces.

Regarding contaminants, they typically can diffuse into the adhesive or substrate or remain at the adhesive/substrate interface. If the contaminant diffuses, a process similar to water contamination occurs. However, if the contaminant remains at the interface, locally debonded areas between the adhesive and substrate may appear contributing to the catastrophic failure of the joint. To address this issue, oil-accommodating adhesives were developed. These adhesives must be able to displace oil from the substrate surface as well as absorb oil to eliminate it from the interface.

Contaminants may also contribute to the decrease in wettability of the substrate surface. When absorbed by the adhesive, contaminants can affect the curing process of the adhesive, potentially affecting T_g. Additionally, it can affect the strength of the adhesive (similarly to what happens when water is absorbed), especially at the free edges. When debonded areas appear, they contribute to unstable crack growth and to interfacial failure of the adhesive joints, resulting on a significant decrease of the joint strength.

Finally, several methods to detect moisture aging and contamination were discussed and case studies regarding these topics, from previous studies, were introduced.

Declaration of Conflicting Interests

The author(s) declared no potential conflicts of interest with respect to the research, authorship, and/or publication of this article.

Funding

The author(s) disclosed receipt of the following financial support for the research, authorship, and/or publication of this article: The authors wish to acknowledge and thank the funding and support provided by *Robert Bosch GmbH, Corporate Research and Advance Engineering, Renningen*.

ORCID iDs

CSP Borges https://orcid.org/0000-0001-7721-7118
EAS Marques https://orcid.org/0000-0002-2750-8184
RJC Carbas https://orcid.org/0000-0002-1933-0865
LFM da Silva https://orcid.org/0000-0003-3272-4591

References

1. da Silva L, Öchsner A and Adams R. *Handbook of adhesion technology*. New York, NY: Springer Science & Business Media, 2018.
2. Adams R, et al. *Structural adhesive joints in engineering*. New York, NY: Springer Science & Business Media, 1997.
3. da Silva L, Pirondi A and Öchsner A. *Hybrid adhesive joints*. vol 6, New York, NY: Springer Science & Business Media, 2011.
4. Greiveldinger M, et al. Oil-covered substrates: a model study of the evaluation in the interphase during cure of an epoxy adhesive. *J Adhes* 2000; 73: 179–195.
5. Kinloch AJ. Interfacial Fracture Mechanical Aspects of Adhesive Bonded Joints – A Review, *The Journal of Adhesion* 10: 193–219.
6. Deryagin BV and Krotova NA. *Electrical theory of adhesion of films to solid surfaces*. In: *Dokl. Akad. Nauk. SSSR*. Vol. 61, 1948, pp.849–852.
7. Kinloch A. *Adhesion and adhesives: science and technology*. New York, NY: Springer Science & Business Media, 2012.
8. Voiutskii S. *Autohesion and adhesion of high polymers*. New York: Interscience Publishers, 1963.
9. Wake W. *Adhesion and the formulation of adhesives*. Barking: Applied Science Publishers, 1982.
10. Adams R. *Adhesive bonding: science, technology and applications*. 2005: Elsevier.
11. Wilken R, Markus S, Amkreutz M, et al. *Method and device for testing a surface quality*. EP1893974 B1, 2008.
12. Kaelble D. Dispersion-polar surface tension properties of organic solids. *J Adhes* 1970; 2: 66–81.
13. Owens DK and Wendt R. Estimation of the surface free energy of polymers. *J Appl Polym Sci* 1969; 13: 1741–1747.
14. Lugscheider E and Bobzin K. The influence on surface free energy of PVD-coatings. *Surface Coat Technol* 2001; 142: 755–760.
15. Sharpe L. The interphase in adhesion. *J Adhes* 1972; 4: 51–64.
16. Jadhav P, Molligan D, Andersen S, et al. *Effect of surface preparation on environmental durability of adhesive-bonded metallic surfaces*. 2007.
17. Crompton J. Interfacial properties and stability in bonded aluminium. *J Mater Sci* 1989; 24: 1575–1581.
18. Barthés-Labrousse M-G. Mechanisms of formation of the interphase in epoxy-amine/aluminium joints. *J Adhes* 2012; 88: 699–719.
19. Coulaud M. *Rôle des interfaces et interphases dans les assemblages collés*. PhD Thesis, INSA, Lyon, 2007.
20. Monternot H, Bénazet D and Ancenay H. *Guide du collage*. France: CETIM Senlis, 1978.
21. Hong S, Cave N and Boerio F. The modification of epoxy/metal interphases by adsorbed contaminants. *J Adhes* 1992; 36: 265–279.
22. Comyn J. *Durability of structural adhesives*. London: Applied Science, 1983.
23. Brockmann W, et al. Adhesion in bonded aluminium joints for aircraft construction. *Int J Adhes Adhes* 1986; 6: 115–IN1.
24. Bockenheimer C, Valeske B and Possart W. Network structure in epoxy aluminium bonds after mechanical treatment. *Int J Adhes Adhes* 2002; 22: 349–356.
25. Possart W, et al. Formation and structure of epoxy network interphases at the contact to native metal surfaces. *Comptes Rendus Chimie* 2006; 9: 60–79.
26. Grangeat R. *Durabilité des assemblages collés en environnement humide-Instrumentation par capteurs à fibre optique*. 2019.
27. Baghdachi J, Martin G and Mahoney K. *One-part, primerless windshield adhesive*. SAE Technical Paper, 1990.
28. Sun YK, Wan DT, Bao YW, et al. Study of tensile bond strength for structural silicone sealants after artificial accelerated aging. In: *Key engineering materials*. Vol. 768. Trans Tech Publ, 2018, pp.13–18.
29. Vandereecken P and Maton I. *Ways of improving the interfacial durability of silicone adhesives in building applications*, in *durability of building and construction sealants and adhesives*. 4th Vol. Conshohocken, PA: ASTM International, 2012.
30. Barbosa A, da Silva L and Öchsner A. Hygrothermal aging of an adhesive reinforced with microparticles of cork. *J Adhes Sci Technol* 2015; 29: 1714–1732.
31. Viana G, et al. A review on the temperature and moisture degradation of adhesive joints. *Proc IMechE, Part L: J Materials: Design and Applications* 2017; 231: 488–501.
32. Zhou J and Lucas J. Hygrothermal effects of epoxy resin. Part I: the nature of water in epoxy. *Polymer* 1999; 40: 5505–5512.
33. Pethrick R. Design and ageing of adhesives for structural adhesive bonding–a review. *Proc IMechE, Part L: J Materials: Design and Applications* 2015; 229: 349–379.
34. Crank J. *The mathematics of diffusion*. Oxford: Oxford University Press, 1979.
35. Malpot A, Touchard F and Bergamo S. Effect of relative humidity on mechanical properties of a woven thermoplastic composite for automotive application. *Polymer Test* 2015; 48: 160–168.
36. Mohd Ishak Z, et al. Short glass fibre reinforcedpoly (butylene terephthalate) Part 1–Microstructural characterisation and kinetics of moisture absorption. *Plastics, Rubber Compos* 2000; 29: 263–270.
37. Boubakri A, et al. Impact of aging conditions on mechanical properties of thermoplastic polyurethane. *Mater Des* 2010; 31: 4194–4201.

38. Popineau S, et al. Free/bound water absorption in an epoxy adhesive. *Polymer* 2005; 46: 10733–10740.
39. Li Y, Miranda J and Sue HJ. Hygrothermal diffusion behavior in bismaleimide resin. *Polymer* 2001; 42: 7791–7799.
40. Carter H, Kibler K and Reynolds J. Fundamental and operational glass transition temperatures of composite resins and adhesives. In: *Advanced composite materials—environmental effects*. Conshohocken, PA: ASTM International, 1978.
41. Carter H and Kibler K. Langmuir-type model for anomalous moisture diffusion in composite resins. *J Compos Mater* 1978; 12: 118–131.
42. Gurtin M and Yatomi C. On a model for two phase diffusion in composite materials. *J Compos Mater* 1979; 13: 126–130.
43. Mubashar A, et al. Moisture absorption–desorption effects in adhesive joints. *Int J Adhes Adhes* 2009; 29: 751–760.
44. Lin Y and Chen X. Moisture sorption–desorption–resorption characteristics and its effect on the mechanical behavior of the epoxy system. *Polymer* 2005; 46: 11994–12003.
45. Loh W, et al. Modelling anomalous moisture uptake, swelling and thermal characteristics of a rubber toughened epoxy adhesive. *Int J Adhes Adhes* 2005; 25: 1–12.
46. Cognard J. Blistering of glass-epoxy amine adhesive joints in water vapour at high pressure. An indication of interfacial crumpling. *J Adhes* 1994; 47: 83–93.
47. Moy P and Karasz F. Epoxy-water interactions. *Polym Eng Sci* 1980; 20: 315–319.
48. Doyle G and Pethrick R. Environmental effects on the ageing of epoxy adhesive joints. *Int J Adhes Adhes* 2009; 29: 77–90.
49. Cognard P. *Collage des Composites: Construction Aerospatiale, Automobile et Ferroviaire*. Ed. Techniques Ingénieur, 2004.
50. Cavodeau F, et al. Hygrothermal aging of an epoxy/dicyandiamide structural adhesiveinfluence of water diffusion on the durability of the adhesive/galvanized steel interface. *J Adhes*. Epub ahead of print 20 December 2018. DOI: 10.1080/00218464.2018.1556100.
51. Zanni-Deffarges M and Shanahan M. Diffusion of water into an epoxy adhesive: comparison between bulk behaviour and adhesive joints. *Int J Adhes Adhes* 1995; 15: 137–142.
52. De'Nève B, et al. Failure mode and ageing of steel/epoxy joints. *Appl Surface Sci* 1998; 134: 202–212.
53. Bonniau P and Bunsell A. A comparative study of water absorption theories applied to glass epoxy composites. *J Compos Mater* 1981; 15: 272–293.
54. Viana G, et al. Behaviour of environmentally degraded epoxy adhesives as a function of temperature. *J Adhes* 2017; 93: 95–112.
55. Sugiman S, Crocombe A and Aschroft I. Experimental and numerical investigation of the static response of environmentally aged adhesively bonded joints. *Int J Adhes Adhes* 2013; 40: 224–237.
56. Hua Y, et al. Modelling environmental degradation in EA9321-bonded joints using a progressive damage failure model. *J Adhes* 2006; 82: 135–160.
57. Costa M, et al. Environmental effect on the fatigue degradation of adhesive joints: a review. *J Adhes* 2017; 93: 127–146.
58. Costa M, et al. Effect of humidity on the fatigue behaviour of adhesively bonded aluminium joints. *Latin Am J Solids Struct* 2017; 14: 174–187.
59. Ashofteh R and Khoramishad H. The influence of hygrothermal ageing on creep behavior of nanocomposite adhesive joints containing multi-walled carbon nanotubes and graphene oxide nanoplatelets. *Int J Adhes Adhes* 2019; 94: 1–12.
60. De'Nève B and Shanahan M. Water absorption by an epoxy resin and its effect on the mechanical properties and infra-red spectra. *Polymer* 1993; 34: 5099–5105.
61. Ellis T and Karasz F. Interaction of epoxy resins with water: the depression of glass transition temperature. *Polymer* 1984; 25: 664–669.
62. Zhang Y, Adams R and da Silva L. Absorption and glass transition temperature of adhesives exposed to water and toluene. *Int J Adhes Adhes* 2014; 50: 85–92.
63. Chatterjee A and Gillespie Jr J. Moisture absorption behavior of epoxies and their S2 glass composites. *J Appl Polym Sci* 2008; 108: 3942–3951.
64. Xiao G and Shanahan M. Swelling of DGEBA/DDA epoxy resin during hygrothermal ageing. *Polymer* 1998; 39: 3253–3260.
65. Gledhill R and Kinloch A. Environmental failure of structural adhesive joints. *J Adhes* 1974; 6: 315–330.
66. Leger R, Roy A and Grandidier J. A study of the impact of humid aging on the strength of industrial adhesive joints. *Int J Adhes Adhes* 2013; 44: 66–77.
67. McKague E Jr, Reynolds J and Halkias J. Swelling and glass transition relations for epoxy matrix material in humid environments. *J Appl Polym Sci* 1978; 22: 1643–1654.
68. Wright W. The effect of diffusion of water into epoxy resins and their carbon-fibre reinforced composites. *Composites* 1981; 12: 201–205.
69. Sargent J. Durability studies for aerospace applications using peel and wedge tests. *Int J Adhes Adhes* 2005; 25: 247–256.
70. Oh S, Cook D and Townsend H. Characterization of iron oxides commonly formed as corrosion products on steel. *Hyperfine Interact* 1998; 112: 59–66.
71. Cambier S, Posner R and Frankel G. Coating and interface degradation of coated steel, Part 1: Field exposure. *Electrochim Acta* 2014; 133: 30–39.
72. Eftekhari M and Fatemi A. Tensile behavior of thermoplastic composites including temperature, moisture, and hygrothermal effects. *Polym Test* 2016; 51: 151–164.
73. Kumar S, Sridhar I and Sivashanker S. Influence of humid environment on the performance of high strength structural carbon fiber composites. *Mater Sci Eng A* 2008; 498: 174–178.
74. Viana G, et al. Water diffusion in double cantilever beam adhesive joints. *Latin Am J Solids Struct* 2017; 14: 188–201.
75. Powers D. *Interaction of water with epoxy*. Sandia Report SAND2009-4405. New Mexico: Albuquerque, 2009.
76. Antoon M, Koenig J and Serafini T. Fourier-transform infrared study of the reversible interaction of water and a crosslinked epoxy matrix. *J Polym Sci: Polymer Physics Edition* 1981; 19: 1567–1575.
77. Holtmannspötter J, Czarnecki J and Gudladt HJ. The use of power ultrasound energy to support interface

formation for structural adhesive bonding. *Int J Adhes Adhes* 2010; 30: 130–138.
78. Brotherhood C, Drinkwater B and Guild F. The effect of compressive loading on the ultrasonic detectability of kissing bonds in adhesive joints. *J Nondestruct Eval* 2002; 21: 95–104.
79. Jeenjitkaew C, Luklinska Z and Guild F. Morphology and surface chemistry of kissing bonds in adhesive joints produced by surface contamination. *Int J Adhes Adhes* 2010; 30: 643–653.
80. Nagy P. Ultrasonic classification of imperfect interfaces. *J Nondestruct Eval* 1992; 11: 127–139.
81. Yan D, Drinkwater B and Neild S. Experimental and theoretical characterization of kissing bonds in adhesive joint using non-linear ultrasonic measurement. In: *AIP conference proceedings*, Kingston, Rhode Island, 26-31 July 2009. American Institute of Physics.
82. Marty P, Desai N and Andersson J. NDT of kissing bond in aeronautical structures. In *16th world conference on NDT*, Montreal, Canada, 30 August-3 September 2004.
83. Debski M, Shanahan M and Schultz J. Mechanisms of contaminant elimination by oil-accommodating adhesives Part 1: displacement and absorption. *Int J Adhes Adhes* 1986; 6: 145–149.
84. Debski M, Shanahan M and Schultz J. Mechanisms of contaminant elimination by oil-accommodating adhesives Part 2: A model of the processes involved. *Int J Adhesion Adhes* 1986; 6: 150–152.
85. Akiyama H, et al. Influence of surface contaminants on the adhesion strength of structural adhesives with aluminium. *J Adhes*. Epub ahead of print 7 April 2019. DOI: 10.1080/00218464.2019.1598393.
86. Heide-Jørgensen S and Budzik M. Crack growth along heterogeneous interface during the DCB experiment. *Int J Solids Struct* 2017; 120: 278–291.
87. Heide-Jørgensen S, de Freitas S and Budzik M. On the fracture behaviour of CFRP bonded joints under mode I loading: Effect of supporting carrier and interface contamination. *Compos Sci Technol* 2018; 160: 97–110.
88. Hong S, et al. The effects of a slushing oil on the curing and degradation behavior of an oil-accommodating epoxy adhesive. *Die Angewandte Makromolekulare Chemie:* Appl Macromol Chem Phys 1996; 238: 129–141.
89. Heslehurst R. Observations in the structural response of adhesive bondline defects. *Int J Adhes Adhes* 1999; 19: 133–154.
90. Goglio L, Rezaei M and Rossetto M. Moisture degradation of open-faced single lap joints. *J Adhes Sci Technol* 2014; 28: 1382–1393.
91. Wylde J and Spelt J. Measurement of adhesive joint fracture properties as a function of environmental degradation. *Int J Adhes Adhes* 1998; 18: 237–246.
92. Loh W, et al. Environmental degradation of the interfacial fracture energy in an adhesively bonded joint. *Eng Fract Mech* 2002; 69: 2113–2128.
93. Fernandes P, et al. The influence of water on the fracture envelope of an adhesive joint. *Theoretical Appl Fract Mech* 2017; 89: 1–15.
94. Liljedahl C, et al. Characterising moisture ingress in adhesively bonded joints using nuclear reaction analysis. *Int J Adhes Adhes* 2009; 29: 356–360.
95. Hopkinson I, et al. Fickian and Case II diffusion of water into amylose: a stray field NMR study. *Carbohydrate Polym* 1997; 34: 39–47.
96. Mieloszyk M and Ostachowicz W. Moisture contamination detection in adhesive bond using embedded FBG sensors. *Mech Syst Signal Process* 2017; 84: 1–14.
97. Weir M, Bastide C and Sung C. Characterization of interaction of water in epoxy by UV reflection spectroscopy. *Macromolecules* 2001; 34: 4923–4926.
98. Sung N, Prokopowicz G, Paik HJ, et al. UV reflection spectroscopy for in situ polymer characterization via bifurcated fiberoptic probe. In: *Polymeric materials science and engineering fall meeting 1994*, Washington, D.C., 1994.
99. Sato T, et al. Detection of contaminants on pre-bond surface by LIBS. *J Adhes* 2018; 94: 689–700.
100. Meola C and Carlomagno G. Recent advances in the use of infrared thermography. *Measure Sci Technol* 2004; 15: R27.
101. Tighe RC, Dulieu-Barton JM and Quinn S. Identification of kissing defects in adhesive bonds using infrared thermography. *Int J Adhes Adhes* 2016; 64: 168–178.
102. Yan D, Drinkwater B and Neild S. Measurement of the ultrasonic nonlinearity of kissing bonds in adhesive joints. *Ndt & E Int* 2009; 42: 459–466.
103. Cremers DA, Multari RA and Knight AK. Laser-Induced Breakdown Spectroscopy. In Meyers RA (ed) *Encyclopedia of Analytical Chemistry* 2016, pp.1–28.
104. de Freitas S, Zarouchas D and Poulis J. The use of acoustic emission and composite peel tests to detect weak adhesion in composite structures. *J Adhes* 2018; 94: 743–766.
105. Bar-Cohen Y and Mal A. End product nondestructive evaluation of adhesive-bonded composite joints. In: *ASM International, Engineered materials handbook*, Ohio, United States: ASM International, Materials Park, 1990, pp.777–784.
106. Dillingham R and Oakley B. Surface energy and adhesion in composite–composite adhesive bonds. *J Adhes* 2006; 82: 407–426.
107. Rider A, Olsson-Jacques C and Arnott D. Influence of adherend surface preparation on bond durability. *Surface Interface Analys: An International Journal devoted to the development and application of techniques for the analysis of surfaces, interfaces and thin films* 1999; 27: 1055–1063.
108. Bernstein H. The average XH stretching frequency as a measure of XH bond properties. *Spectrochim Acta* 1962; 18: 161–170.
109. Wapner K and Grundmeier G. Spatially resolved measurements of the diffusion of water in a model adhesive/silicon lap joint using FTIR-transmission-microscopy. *Int J Adhes Adhes* 2004; 24: 193–200.
110. Rogers R and Morris E. On estimating activation energies with a differential scanning calorimeter. *Analytical Chem* 1966; 38: 412–414.
111. Zheng R, et al. Effects of a sheet metal stamping lubricant on static strength of adhesive-bonded aluminum alloys. *J Adhes Sci Technol* 2015; 29: 1382–1402.

112. Calvez P, et al. Mechanisms of interfacial degradation of epoxy adhesive/galvanized steel assemblies: relevance to durability. *J Adhes* 2012; 88: 145–170.
113. Michaloudaki M, Lehmann E and Kosteas D. Neutron imaging as a tool for the non-destructive evaluation of adhesive joints in aluminium. *Int J Adhes Adhes* 2005; 25: 257–267.
114. Silva-Pereira E. *Exploring chirality of unnatural amino acids and peptides on water sorption and stratum corneum uptake*. Reading, UK: University of Reading, 2019.
115. Olsson-Jacques C, et al. Effect of contaminant on the durability of epoxy adhesive bonds with Alclad 2024 aluminium alloy adherends. *Surface Interface Analysis* 1996; 24: 569–577.
116. Sodhi RN. Time-of-flight secondary ion mass spectrometry (TOF-SIMS):—versatility in chemical and imaging surface analysis. *Analyst* 2004; 129: 483–487.
117. Benninghoven A. Chemical analysis of inorganic and organic surfaces and thin films by static time-of-flight secondary ion mass spectrometry (TOF-SIMS). *Angewandte Chemie Int Edition English* 1994; 33: 1023–1043.
118. Maxwell I and Pethrick R. Dielectric studies of water in epoxy resins. *J Appl Polym Sci* 1983; 28: 2363–2379.
119. Jelinski L, et al. Nature of the water-epoxy interaction. *Macromolecules* 1985; 18: 1091–1095.
120. Drain K, et al. The effect of moisture on the strength of polycarbonate-cyanoacrylate adhesive bonds. *Int J Adhes Adhes* 1985; 5: 133–136.
121. Viana G, et al. Moisture and temperature degradation of double cantilever beam adhesive joints. *J Adhes Sci Technol* 2017; 31: 1824–1838.
122. Cognard J. Influence of water on the cleavage of adhesive joints. *Int J Adhes Adhes* 1988; 8: 93–99.
123. McGeorge D. *On the long term properties of steel-composite interfaces for marine applications. in fourth international conference on composite materials for offshore operations*. Houston TX, 2005.
124. Legghe E, et al. Correlation between water diffusion and adhesion loss: Study of an epoxy primer on steel. *Progr Organic Coat* 2009; 66: 276–280.
125. Sugiman S, Effect of adhesive thickness on the strength of steel-composite joints aged in wet environment. In: *IOP conference series: materials science and engineering*, Bangka-Belitung Province, Indonesia, 29-30 August 2018. IOP Publishing.
126. Michalske T and Bunker B. Slow fracture model based on strained silicate structures. *J ApplPhys* 1984; 56: 2686–2693.
127. Kinloch A, Little M and Watts J. The role of the interphase in the environmental failure of adhesive joints. *Acta Mater* 2000; 48: 4543–4553.
128. Li J, et al. Surface treatment for improving durability of aluminum-lithium adhesive-bonded joints under hot-humid exposure. *Coatings* 2019; 9: 346.
129. Ogawa T and Hongo M. Fracture mechanism and oil absorption of an oil-accommodating adhesive. *J Adhes Sci Technol* 1997; 11: 1197–1209.
130. Anderson G, et al. The effects of silicone contamination on bond performance of various bond systems. *J Adhes* 2010; 86: 1159–1177.
131. Jeenjitkaew C and Guild F. The analysis of kissing bonds in adhesive joints. *Int J Adhes Adhes* 2017; 75: 101–107.
132. Petersson L, et al. Effect of surface cleanliness of aluminium substrates on silicone rubber adhesion. *J Phys D: Appl Phys* 2010; 44: 034011.
133. Müller M. Research of liquid contaminants influence on adhesive bond strength applied in agricultural machine construction. *Agronomy Res* 2013; 11: 147–154.
134. Markatos D, et al. Degradation of mode-I fracture toughness of CFRP bonded joints due to release agent and moisture pre-bond contamination. *J Adhes* 2014; 90: 156–173.
135. Hoffmann M, et al. Determination of adhesion strength of pre-bond contaminated composite-to-metal bonded joints by centrifuge tests. *Compos Part B: Eng* 2018; 147: 114–121.
136. Yerra V and Pilla S. Understanding resilience to contamination in the joint interface for a resistive welded joint in fiber reinforced thermoplastics. SAE Technical Paper, 2019.

Appendix B

Paper B

Effect of water ingress on the mechanical and chemical properties of polybutylene terephthalate reinforced with glass fibers

materials

MDPI

Article

Effect of Water Ingress on the Mechanical and Chemical Properties of Polybutylene Terephthalate Reinforced with Glass Fibers

Catarina S.P. Borges [1], Alireza Akhavan-Safar [1], Eduardo A.S. Marques [1,*], Ricardo J.C. Carbas [1], Christoph Ueffing [2], Philipp Weißgraeber [2] and Lucas F.M. da Silva [1,3]

[1] Instituto de Ciência e Inovação em Engenharia Mecânica e Engenharia Industrial (INEGI), 4200-465 Porto, Portugal; cspborges@fe.up.pt (C.S.P.B.); aakhavan-safar@inegi.up.pt (A.A.-S.); rcarbas@fe.up.pt (R.J.C.C.); lucas@fe.up.pt (L.F.M.d.S.)
[2] Robert Bosch GmbH, Corporate Research and Advance Engineering, 71272 Renningen, Germany; Christoph.Ueffing@de.bosch.com (C.U.); Philipp.Weissgraeber@de.bosch.com (P.W.)
[3] Departamento de Engenharia Mecânica, Faculdade de Engenharia (FEUP), Universidade do Porto, 4200-465 Porto, Portugal
* Correspondence: emarques@fe.up.pt

Abstract: Short fiber reinforced polymers are widely used in the construction of electronic housings, where they are often exposed to harsh environmental conditions. The main purpose of this work is the in-depth study and characterization of the water uptake behavior of PBT-GF30 (polybutylene terephthalate with 30% of short glass fiber)as well as its consequent effect on the mechanical properties of the material. Further analysis was conducted to determine at which temperature range PBT-GF30 starts experiencing chemical changes. The influence of testing procedures and conditions on the evaluation of these effects was analyzed, also drawing comparisons with previous studies. The water absorption behavior was studied through gravimetric tests at 35, 70, and 130 °C. Fiber-free PBT was also studied at 35 °C for comparison purposes. The effect of water and temperature on the mechanical properties was analyzed through bulk tensile tests. The material was tested for the three temperatures in the as-supplied state (without drying or aging). Afterwards, PBT-GF30 was tested at room temperature following water immersion at the three temperatures. Chemical changes in the material were also analyzed through Fourier-transform infrared spectroscopy (FTIR). It was concluded that the water diffusion behavior is Fickian and that PBT absorbs more water than PBT-GF30 but at a slightly higher rate. However, temperature was found to have a more significant influence on the rate of water diffusion of PBT-GF30 than fiber content did. Temperature has a significant influence on the mechanical properties of the material. Humidity contributes to a slight drop in stiffness and strength, not showing a clear dependence on water uptake. This decrease in mechanical properties occurs due to the relaxation of the polymeric chain promoted by water ingress. Between 80 and 85 °C, after water immersion, the FTIR profile of the material changes, which suggests chemical changes in the PBT. The water absorption was simulated through heat transfer analogy with good results. From the developed numerical simulation, the minimum plate size to maintain the water ingress unidirectional was 30 mm, which was validated experimentally.

Keywords: aging; moisture; diffusion; contamination; Fickian distribution; polybutylene terephthalate; short glass fiber; housing for electronic components

check for updates

Citation: Borges, C.S.P.; Akhavan-Safar, A.; Marques, E.A.S.; Carbas, R.J.C.; Ueffing, C.; Weißgraeber, P.; da Silva, L.F.M. Effect of Water Ingress on the Mechanical and Chemical Properties of Polybutylene Terephthalate Reinforced with Glass Fibers. *Materials* **2021**, *14*, 1261. https://doi.org/10.3390/ma14051261

Academic Editor: Seeram Ramakrishna

Received: 18 January 2021
Accepted: 26 February 2021
Published: 7 March 2021

Publisher's Note: MDPI stays neutral with regard to jurisdictional claims in published maps and institutional affiliations.

Copyright: © 2021 by the authors. Licensee MDPI, Basel, Switzerland. This article is an open access article distributed under the terms and conditions of the Creative Commons Attribution (CC BY) license (https://creativecommons.org/licenses/by/4.0/).

1. Introduction

Composite materials, and especially fiber-reinforced polymers (FRP), have been increasingly representing a low-weight alternative to conventional materials such as steel, as they present high specific properties such as stiffness and strength [1,2]. Additionally, they contribute to the reduction of the cost of the manufacturing process. FRPs can use both long and short fiber inclusions. Short fiber reinforced polymers (SFRP) are more suitable

for manufacturing processes such as injection molding and promote an improvement of the mechanical properties than the fiber-free polymer.

One of the challenges related to the use of multiple polymeric materials, and their composites, is their sensibility to environmental conditions, such as corrosive environments, high temperatures, or humidity [3]. FRP can even be subjected to severe environmental conditions when they are used in infrastructures immersed in water such as fixed or floating composite bumper systems, for instance in bridges or in structures to support solar panels in water [4]. For these applications, new materials have been developed, such as cellulose nanocrystals cement paste [5], which can significantly improve the fracture behavior of the cement as well as retard the hydration of the cement, making it more suitable for these severe applications. However, since these materials are still under development, further research is needed. Moisture generally promotes degradation of the polymer, which can happen even when subjected to usual atmospheric humidity [6,7]; therefore, it is crucial to understand how the properties of composite materials change when exposed to water.

Water can be absorbed by the polymer as free and bound water. Free water occupies the free spaces on the structure of the material, the polymeric chain, which means it does not change the volume of the material. Bound water can increase the volume of the material, as it forms chemical bonds with the polymer's molecular chain [3,6,8,9]. The bound water is also responsible for the decrease in glass transition temperature, T_g. Free water can start forming hydrogen bonds with the structure of the material, turning into bound water, a change that is promoted by high temperatures and longer exposure times [10,11].

Water diffusion is commonly described with good approximation by Fick's law [12–15]. However, materials can exhibit Fickian or non-Fickian behavior, typically depending on the relation between the diffusion and relaxation rate. If the diffusion rate is much quicker than the relaxation rate, the material tends to exhibit Fickian behavior; however, if the relaxation rate influences the water uptake, non-Fickian behavior is usually identified [16–18]. In composite materials, it is often considered that the glass fibers are hydrophobic, absorbing significantly less water than the polymeric matrix, which is considered hydrophilic. However, they present preferential paths for the water ingress, and the interface between fiber and matrix is usually degraded. Therefore, degradation of thermoplastic composites is highly dependent on the specific composition of the matrix, the type of fiber, the fiber/matrix interface, and the volume fraction of fibers [13].

Regarding the mechanical properties, moisture degradation is generally responsible for a decrease in the strength and stiffness of thermoplastic materials. This process also contributes to a higher ductility of the polymer, verified by an increase in strain at failure, especially for temperatures above T_g when the motion of the polymer's molecular chain increases [13,18,19].

PBT (polybutylene terephthalate) is a particularly interesting polyester due to its rapid crystallization, good processing characteristics for short extrusion and injection molding, excellent mold flow, and improved flexibility, since it has two additional methylene units in the main chain when compared to polyethylene terephthalate (PET) [17,20,21]. However, PBT has limited toughness at low temperatures and high deformation rates. Additionally, with hygrothermal aging, it tends to undergo hydrolysis and become more brittle [22]. Hygrothermal aging is the process in which the deterioration of a given material occurs due to the action of moisture and temperature, as discussed above [21].

PBT reinforced with 30% short glass fiber, PBT-GF30, is widely used in the housing for electronic components due to its good properties and suitability for manufacture through injection molding. Its fast crystallization rate enhances moldability and, consequently, leads to parts with good surface quality [23,24].

However, while this material has many manufacturing advantages, it was identified that there are few recycling options. Research is being carried out in this field, most studies being performed fairly recently, since this is a material that suffered a great expansion in the past years due to its applicability in the automotive and electric sectors, among others [25]. The processes discussed are mainly focused on the depolymerization of PBT

in supercritical methanol [26]. This research is important because when designing a new product, it is important not only take into consideration the long -term properties and durability of a component, but also be environmentally responsible for ensuring sustainable and responsible economic development, which not only benefits the environment but also the longevity and efficiency of the product [27–29].

In the housing for electronic components, PBT-GF30 can be subjected to humid environments at different temperatures. Therefore, it is important to know its water uptake behavior to predict the conditions at which the electronic components can be at risk and in contact with humidity. Additionally, this knowledge allows a more accurate design of the components for each specific application prior to its manufacturing, which reduces manufacturing costs of the component. As it has been said, one of the main issued regarding PBT usage is the recycling of the product; therefore, the low production cost of the components can be combined with a high waste management cost, which must be taken into account.

The moisture uptake of PBT and its glass fiber composites, with different volume fractions of fibers, was shown to follow the Fick's law for water absorption regardless of the temperature of the water where the material is immersed [30]. Ishak et al. [21] also concluded that for short glass fibers, the desorption behavior is Fickian. In the same study, it was observed that the coefficient of diffusion decreased with increasing volume fraction of fibers. This occurrence was connected to the random orientation of the fibers, which retards the water ingress in the hydrophilic matrix. The equilibrium moisture increases with decreasing fiber content, which was attributed to increase in volume fraction of the hygroscopic PBT matrix. For fiber-free PBT and PBT with 18% short glass fiber, the coefficient of diffusion was determined. The coefficient of diffusion increased with increasing temperature, following an Arrhenius relationship.

Ishak et al. [21] also studied the effect of moisture aging on fiber-free PBT and PBT with 10% short glass fiber in volume at two different levels of relative humidity, 81.2 and 100%. Water has a significantly higher influence when the samples were subjected to a relative humidity of 100%. However, there are additional conclusions that can be drawn across all results. First, all the composites fractured in a brittle way, and a decrease in strength after aging was observed, which can be related to the yielding effect of absorbed water. For reinforced PBT, it was stated that failure occurs also due to the degradation of the interface between the fibers and the matrix. However, the glass fibers contributed to an improvement of the retention and recoverability of the tensile properties. With scanning electron microscopy (SEM) analysis, Ishak et al. [31] also observed hydrolysis of the matrix through the appearance of micro-voids and the absence of plastic deformation and degradation at the fiber–matrix interface. Additionally, regarding the variation of the mechanical properties of fiber-free PBT and PBT with 30% short glass fiber specimens saturated in humidity testing, after aging at 30 °C, both PBT and PBT-GF30 exhibited a slight decrease in strength compared to the unaged state. However, after aging at 90 °C, only 21% of the initial strength remained for fiber-free PBT and 36% for PBT-GF30.

Ishak et al. [32] studied the behavior of short fiber reinforced PBT immersed in water at 30, 60 and 90 °C for fiber contents between 0 and 18% in volume. For high temperature (90 °C), the toughness of the material decreases significantly. At this higher temperature, fiber-free PBT and PBT with 18% short glass fiber were analyzed through the determination of the pH and FTIR profile of the water where it has been immersed. Regarding the measurement of the pH, it was determined that it decreased after the immersion of PBT composites. Additionally, it has been observed that the difference between the initial pH and pH after 750 h of water immersion was higher for lower fiber contents. However, until slightly above 100 h of immersion, the pH decreased for both cases to the same value. Afterwards, the pH of the water where PBT with GF was immersed increased again due to the appearance of OH^- ions in the water. These results were confirmed through FTIR analysis of the water. The water where PBT was immersed revealed the presence of carboxylic groups associated with the hydrolysis of PBT. In the water where PBT-GF30 was immersed, there were also groups associated with the hydrolysis of glass fiber. These

results indicate a hydrolysis of the fiber at high temperatures for long immersion times, which had been also detected by Hsu et al. [33].

Bergeret et al. [34] studied the effect of moisture on the properties of PET, PBT and PA6,6 reinforced with short glass fibers with different surface treatments. Regarding the PBT, when aged, the lack of chemical linkages between the glass fibers and PBT matrix creates a weak fiber/matrix interface and consequently, a fragile composite in a hygrothermal environment. Rosato et al. [23] also notes that although after 24 h fiber-free PBT only absorbs 0.1% of water, this material is not suitable for hot–humid environments at temperatures above 52 °C. Gardner et al. [35] studied the long-term resistance of fiber-free PBT, aging the material up to three years at relative humidities between 11 and 100% and temperatures between 66 and 93 °C and concluded that, above 50 °C, PBT loses half of its tensile strength in three to four years.

The main purpose of this work was the complete characterization of the water uptake behavior of PBT-GF30 and its effect on the properties of the material, while also considering the effect of temperature. It was also expected to understand how the experimental methods adopted to perform this characterization influence the results, comparing them with other studies. Numerically, it was intended to create a simple model to simulate the water uptake behavior of PBT-GF30. With the simulation established, the minimum plate length–thickness ratio for the water flow to be one dimensional was determined. Additionally, the mechanical performance of the bulk tensile tests was simulated to complement the experimental results.

2. Experimental Details

Housings for electronic components, composed of PBT-GF30, can be subjected to elevated temperatures between room temperature (RT) and temperatures of 130 °C during the manufacturing, packaging, transport, and storage processes. In this work, three different temperatures were analyzed, from a temperature slightly above RT, 35 °C, to the maximum temperature reported in the manufacturing process, 130 °C. The intermediate temperature was chosen to be 70 °C since it is also an interesting reference temperature of the process, being a relevant temperature for transport and packaging.

2.1. Materials

In this work, the PBT-GF30 short fiber, a polymeric matrix composite, was analyzed. To understand the effect of fiber content on the water uptake behavior of the material, fiber-free PBT was also used in this work. The material for the injection molded plates and respective data sheets were obtained from the manufacturer.

2.2. Specimen Manufacturing

For each test performed, suitable specimens were machined from plates of PBT-GF30 and PBT, previously obtained from injection molding. T_g measurement specimens and standard "dogbone" specimens were obtained from 2 mm thick plates, and the gravimetric test specimens, differential scanning calorimetry (DSC) specimens, reduced-scale "dogbone" specimens, and FTIR specimens were obtained from 1 mm thick plates.

2.2.1. Glass Transition Temperature

The water uptake behavior of the polymer is known to change if the temperature under analysis is above or below T_g. Therefore, the first step was to determine T_g. The determination of the glass transition temperature was carried out using rectangular specimens with 10×25 mm^2 and 2 mm thickness. A hole with a 3.5 mm diameter was made in the center on the specimen to attach it to the apparatus used for T_g measurement.

2.2.2. Differential Scanning Calorimetry (DSC) and Fourier Transform Infrared Spectroscopy (FTIR)

For DSC and FTIR analysis, tests were performed using 1 mm thick disks with a 6 mm diameter. These specimens are typically used for DSC. However, due to their small size, they were also used for FTIR to minimize the time required to saturate the sample.

2.2.3. Gravimetric Analysis

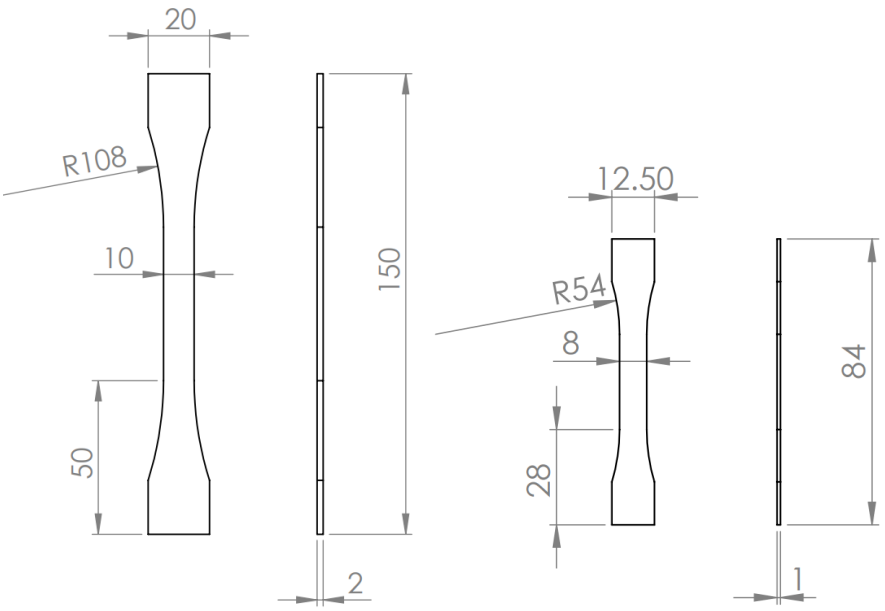
Plates used for the gravimetric study were manufactured based on the ISO 294-3 standard [36]. Therefore, plates of 60 × 60 mm^2 and 1 mm thick were used.

The thickness is significantly smaller than all other dimensions so that it represents the preferential water absorption path and the water flow can be considered as one dimensional. However, these specimens require quite a large amount of material. Therefore, in Section 4, a study is conducted to attempt to obtain similar results with smaller plates.

2.2.4. Bulk Tensile Tests

Standard "dogbone" bulk tensile specimens have large dimensions, and to study the effect of water on the mechanical properties of PBT-GF30, they should be immersed in water, which would require large water containers and long immersion times. Therefore, reduced-scale specimens were used to accelerate this process.

Standard "dogbone" specimens follow the British standard BS 2782 [37] (Figure 1a). The reduced-scale "dogbone" specimens have the dimensions shown in Figure 1b and have been used in previous studies [38,39].



(**a**) (**b**)

Figure 1. "Dogbone" specimens used for bulk tensile tests (dimensions in mm). (**a**) Standard specimens. (**b**) Reduced-scale specimens.

2.3. Experimental Procedures

2.3.1. Glass Transition Temperature

T_g was measured using an in-house developed apparatus based on the DMA dynamic mechanical analysis concept [40]. The apparatus works by the measurement of the damping of a sample, which is kept vibrating at the resonance frequency as the temperature is increased. Temperature is measured using a dummy specimen, which is placed in the same oven of the specimen for damping measurement. As the specimen approaches T_g, the damping of the sample rises significantly, and the amplitude of the vibration approaches zero. As T_g is surpassed, the amplitude increases again. Therefore, T_g can be determined

through the minimum of amplitude, or maximum of damping. For each condition, at least three specimens were tested.

2.3.2. Differential Scanning Calorimetry (DSC)

The analysis of the DSC spectra of PBT and PBT-GF 30 was used to study the thermal behavior of the materials. These tests were carried out using a NETZSCH DSC 214 Polyma DSC21400A-0655-L machine. In the DSC test, the temperature changed between 20 and 300 °C; then, the samples were cooled from 300 to −20 °C and finally heated from −20 to 300 °C, which was the range considered for the analysis. The heating and cooling were performed at 10 °C/min in a N_2 atmosphere. Three specimens were tested.

2.3.3. Gravimetric Analysis

Before the immersion in water, the PBT and PBT-GF30 specimens were fully dried in silica for two weeks at 35 °C in order to ensure no water was found on the material. After the specimens were dried, their surface was manually treated with sandpaper (grade 800) to remove any contaminants on the surface and minimize surface roughness. The initial mass of the specimen was measured. Afterwards, the polymeric and composite plates were immersed in water, ensuring the plates were completely surrounded by water and not in direct contact with the container or other specimens so that the area of water absorption was not compromised. The temperature of water immersion was controlled by placing the containers with water in a cimatica chamber (Memmert GmbH, Büchenbach, Germany).

The mass of the plates was periodically measured until saturation was achieved. All mass measurements were performed using a microbalance with 0.1 mg of accuracy (KernToledo, Balingen, Germany). Before weighing the aged samples, their surface was cleaned using a paper towel. The water, or moisture, uptake of each specimen, for each time step is given by

$$M_t = \frac{m_t - m_0}{m_0} \times 100 \quad (\%) \tag{1}$$

where m_t is the mass of the specimen at the current time step and m_0 is the initial mass of the specimen. This process was repeated for 35, 70, and 130 °C. For 130 °C a water container was kept open inside the climatic chamber, and small amounts of water were periodically added. The specimens were considered to be saturated when the water content was stable, showing that the material was unable to absorb more water. For each condition, at least four specimens were tested.

2.3.4. Bulk Tensile Tests

For the material in the as-supplied state, standard "dogbone" specimens were tested at room temperature, and reduced-scale "dogbone" specimens were tested at room temperature and at 35, 70, and 130 °C and after aging at the three temperatures.

The tensile tests were performed at the rate of 1 mm/min using an Instron® 3367 universal testing machine with a load cell capacity of 30 kN.

For the tests at controlled temperature, the specimens were inserted in a climatic chamber, which was integrated in the universal testing machine. Prior to testing, each specimen was placed in the climatic chamber for a set period of time (10 min for the lower temperatures and 20 min for 130 °C) to ensure a uniform temperature distribution.

For the tests with water uptake for the three temperatures, the specimens were dried, as described for the gravimetric test specimens, and treated with sandpaper to create a uniformly rough surface; their mass was measured as mentioned above; and, finally, they were immersed in water. The specimens were tested periodically through the time needed to saturate the samples. Whenever the mechanical properties were measured, after a given immersion time, the surfaces of the specimens were dried with a paper towel, the mass was measured, and the tensile test was performed at RT.

For each condition, at least three specimens were tested.

2.3.5. Fourier Transform Infrared Spectroscopy (FTIR)

The analysis of the FTIR spectra of dry samples and samples saturated at 35, 70, and 130 °C allows one to determine the extension of the effects of moisture aging, since if chemical relations are established between the PBT-GF30 and irreversible damage that occurs in the material, the intensity of the absorption bands for relevant groups changes. The specimens were simulated numerically and kept in water for a sufficient amount of time to reach saturation. The FTIR analysis was carried out using a PerkinElmer Spectrum Two machine (Waltham, MA, USA). Wave lengths of 4000–500 cm^{-1} were used at a scanning velocity of 0.2 cm^{-1} . These tests were performed with a $LiTaO_3$ detector (15,700–370 cm^{-1}) and a KBr window. The spectra were obtained in attenuated total reflectance (ATR), which creates spectra equivalent to transmittance. Bulk specimens with a thickness of 1 mm were used. To narrow the range of temperatures at which changes in the FTIR profile occur in the material, other temperatures were, afterwards, analyzed. Three specimens were tested.

3. Experimental Results

3.1. Glass Transition Temperature

Representative curves obtained from the T_g measurement are shown in Figure 2, and the values of the T_g are presented in Table 1.

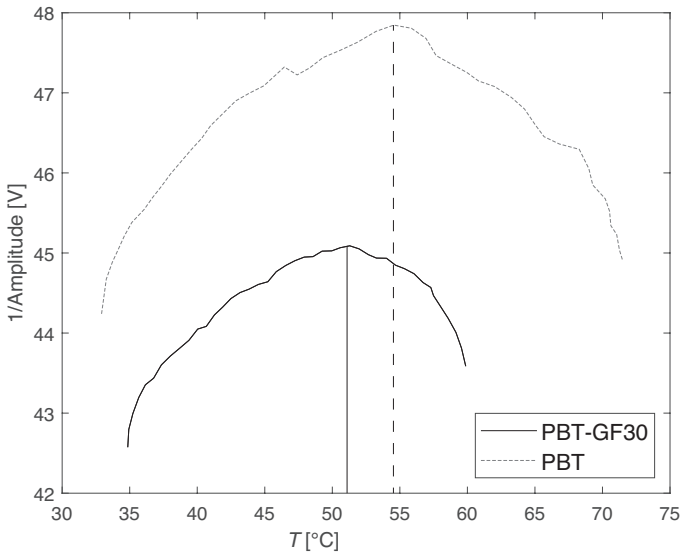


Figure 2. Glass transition temperature measurement results: representative curves.

Table 1. Glass transition temperature measurement results.

Material	T_g (°C)
PBT-GF30	49 ± 4
PBT	54 ± 6

The three levels of temperature analyzed are 15 °C below T_g (35 °C), 20 °C above T_g (70 °C), and 80 °C above T_g (130 °C). These results are in accordance with the values reported by different authors, falling in the expected range between 40 and 60 °C [41–44].

3.2. Differential Scanning Calorimetry (DSC)

The results from DSC analysis are presented in Figure 3.

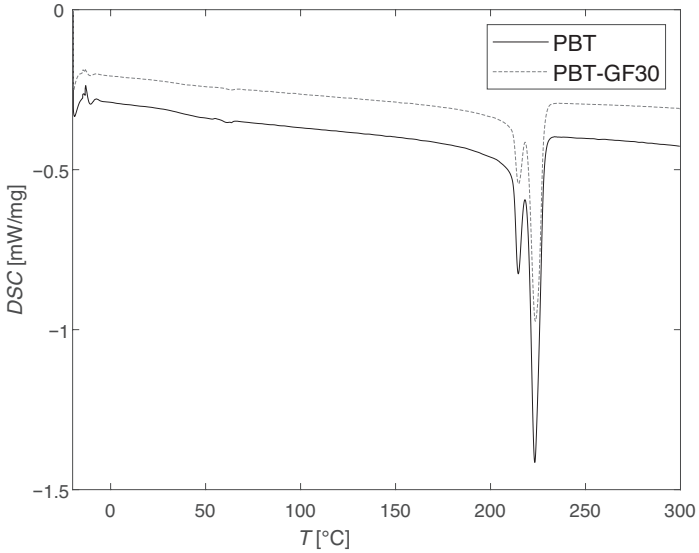


Figure 3. Differential scanning calorimetry (DSC) results: representative curves, where a peak is shown at around 220 °C.

It can be observed that both the PBT and the PBT-GF30 display a disturbance in the curve slightly above 50 °C, which corresponds to T_g, and only display significant degradation for temperatures above 200 °C, with a peak slightly above 220 °C, which corresponds to the melting temperature of the material. Therefore, in the range of temperatures analyzed, the chemical degradation is not significant. Similar results for DSC were found by Ma et al. [45] and Souilem et al. [46] for fiber-free PBT.

3.3. Gravimetric Analysis

A Fick's law of diffusion can be fitted to the experimental results for the four conditions studied. The Fick's law is given by [47]

$$M_t = \left[1 - \frac{8}{\pi^2}\sum_{n=0}^{\infty}\frac{1}{(2n+1)^2}\exp\left(\frac{-D(2n+1)^2\pi^2 t}{4h^2}\right)\right]M_\infty \quad (2)$$

where t represents time starting from the immersion and h represents the thickness of the specimen. Therefore, a script was run in Matlab to determine the best fit of the coefficient of diffusion, D, and infinite water uptake, M_∞. For that, the least square method was used. The values determined for each material and each temperature, T, are given in Table 2.

Table 2. Water uptake properties of the materials analyzed.

Material	T (°C)	D (m ^{2}/s)	M_∞ (%)
PBT	35	4.80×10^{-13}	0.61
PBT-GF30	35	3.15×10^{-13}	0.47
PBT-GF30	70	3.90×10^{-12}	0.50
PBT-GF30	130	1.37×10^{-11}	0.56

The experimental results and analytical curves obtained with the determined D and M_∞ can be seen in Figure 4.

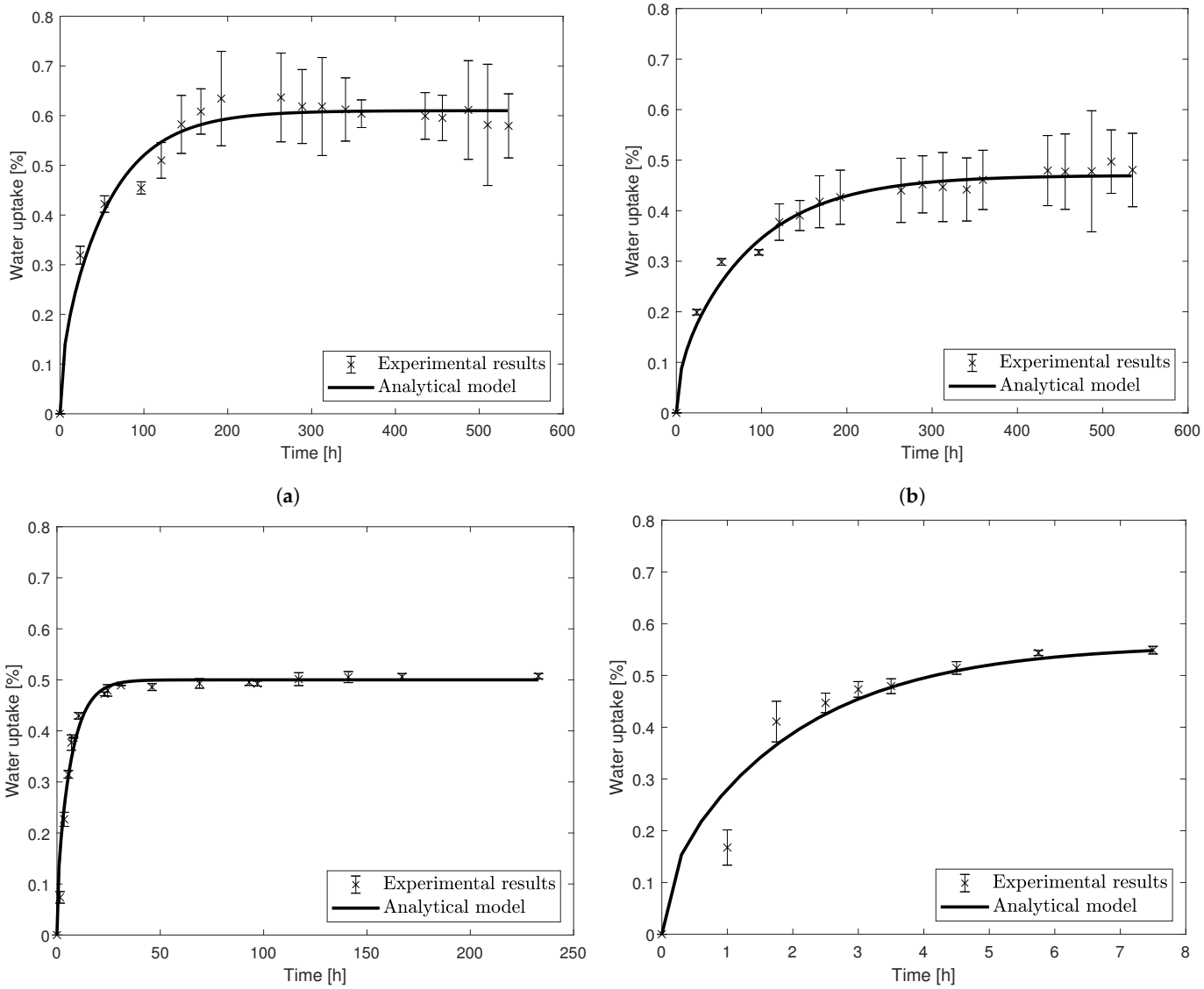


Figure 4. Experimental results and numerical details for the gravimetric tests. (**a**) PBT at 35 °C. (**b**) PBT-GF30 at 35 °C. (**c**) PBT-GF30 at 70 °C. (**d**) PBT-GF30 at 130 °C.

A comparison of the Fick's law for the three different temperatures and for PBT-GF30 is given in Figure 5.

The results obtained show that fiber-free PBT absorbs more water than PBT with 30% of glass fibre. This may be due to the decrease in sites where the water molecules can form hydrogen bonds with the material, since those bonds are formed between the PBT matrix and water. Additionally, the material has lower porosity due to the portion of the material occupied by glass fibre, decreasing the water absorbed in the free volume of the polymeric chain of the PBT matrix. However, considering only this fiber/matrix ratio, the infinite water uptake of PBT-GF30 should be 70% of the infinite water uptake of fiber-free PBT, but the experimentally determined ratio is 77%, which implies that there are other factors playing a role in this, apart from the usual measurement accuracy consideration. These factors can be due, for instance, to capillarity effects along the fiber/matrix interface. Regarding the coefficient of diffusion, it is also higher for fiber-free PBT when compared with PBT-GF30. However, they have the same order of magnitude.

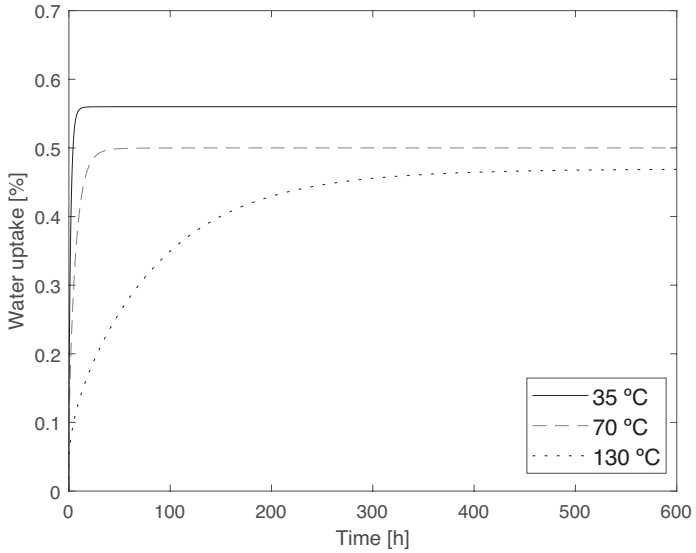


Figure 5. Comparison between the water uptake behavior of PBT-GF30 for 35, 70, and 130 °C, where it can be observed that the water uptake increases significantly with temperature, and the maximum water uptake also increases with temperature.

PBT-GF30 absorbs a higher water content as temperature increases, the temperature-related absorption being smaller than that recorded between fiber-free PBT and PBT-GF30. Moreover, as temperature increases, the water absorption is significantly quicker, with the coefficient of diffusion being about two orders of magnitude higher. This phenomena occurs because at a higher temperature, there is an increase in energy and movement of the molecules, increasing the rate of diffusion. The infinite water uptake and coefficient of diffusion as a function of temperature can be seen in Figure 6.

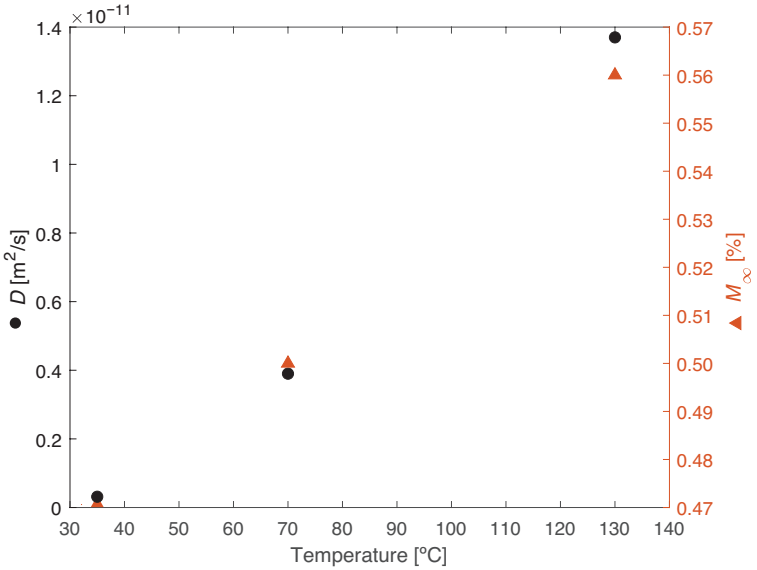


Figure 6. Diffusion parameters for PBT-GF30 as a function of temperature, showing an increase in the coefficient of diffusion and maximum water uptake.

The coefficient of diffusion can often be represented as a function of temperature by an Arrhenius relation, given by

$$D = D_0 \exp\left(\frac{-E_A}{RT}\right) \quad (3)$$

where D_0 is the permeability index, function of temperature, E_A the activation energy for diffusion, R the universal gas constant, and T temperature. Rearranging Equation (3), it can be established that:

$$\ln(D) = -\frac{E_A}{R} D_0 \frac{1}{T} \quad (4)$$

Therefore, if D as a function of T follows an Arrhenius relation, $ln(D)$ and $1/T$ will have a linear relation, Figure 7. From these results, M_∞ as a function of temperature is given by a linear relation with a coefficient of determination, R^2, of 0.9985. The coefficient of determination of the linear relation between $ln(D)$ and $1/T$ is 0.9996.

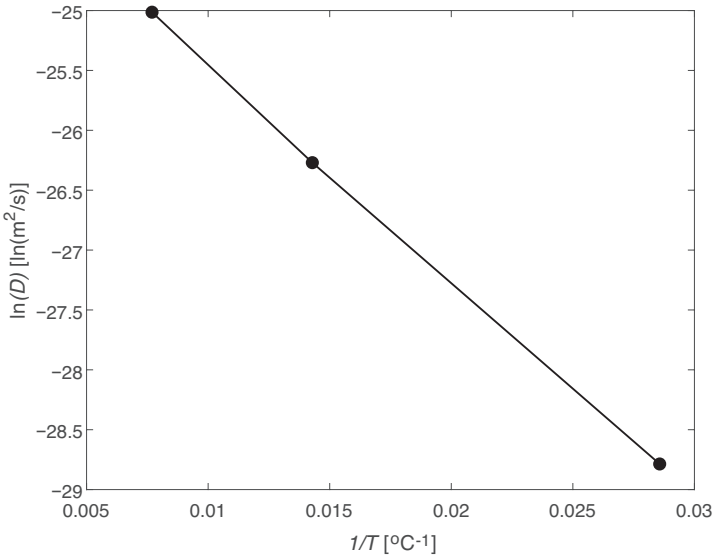


Figure 7. Arrhenius relation for the coefficient of diffusion.

Among the results found in the literature, Bastioli et al. [48], studied the water uptake of fiber-free PBT at 37 °C and identified a coefficient of diffusion of 4.40 × 10^{-13} and an infinite mass of 0.65%, which is close to the results obtained for PBT at 35 °C. Ishak et al. [32], at 30 °C, identified a coefficient of diffusion of 1.90 × 10^{-13} for fiber-free PBT and 1.00 × 10^{-13} for PBT-GF30. Closer to the highest temperature studied in the present paper, at 100 °C, Ishak et al. [21] identified an infinite mass of 0.71% and a coefficient of diffusion of 4.05 × 10^{-11} for a content of fibers close to 30% (at about 28.5%).

3.4. Bulk Tensile Tests

3.4.1. Validation of the Reduced-Scale "Dogbone" Specimens

The representative stress vs. strain curves for standard and reduced-scale "dogbone" specimens can be observed in Figure 8, and the results are shown in Table 3.

Table 3. Mechanical properties of standard and reduced-scale "dogbone" specimens at room temperature, showing that the results for stiffness and tensile strength have a small error.

Property	Standard Specimens	Reduced-Scale Specimens	Error
Young's modulus (GPa)	8.6 ± 0.1	8.2 ± 0.1	4.6%
Tensile strength (MPa)	112 ± 1	105 ± 1	6.3%

It can be concluded that the reduced-scale specimens can be used to characterize the material as a function of temperature and immersion time. However, it is important to understand that the results obtained from standard specimens and reduced-scale specimens are not exactly the same. In previous studies [38] using the same specimens, strength

increased compared to the standard "dogbone" specimens. Additionally, it was stated that the differences in Young's modulus and strength were greater for more brittle materials. In this study, the difference in Young's modulus and strength for the stronger and more ductile material were about 9 and 8%, respectively, and, for the more flexible and less ductile material, about 45 and 23%, respectively. In the present work, the error was of 5 and 6% for Young's modulus and strength, respectively, which is lower that what was recorded for the previous work.

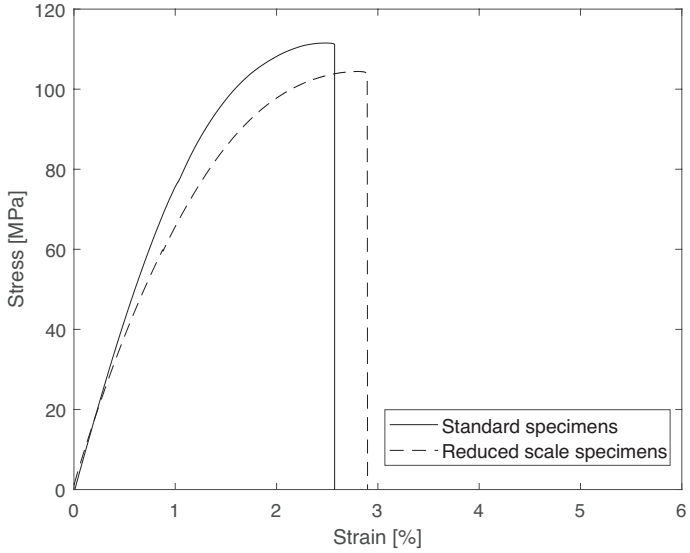


Figure 8. Validation of the reduced-scale "dogbone" specimens: representative stress vs. strain curves.

3.4.2. Bulk Tensile Tests for Different Temperatures

Representative stress–strain curves for the three temperatures analyzed are given in Figure 9, and the results are shown in Table 4.

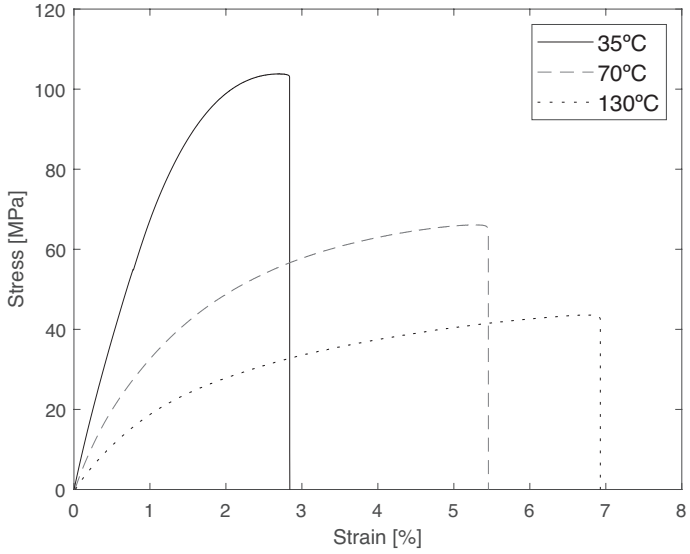


Figure 9. Bulk tensile tests at different temperatures: representative stress vs. strain curves, showing that stiffness and strength decrease with the testing temperature.

From the experimental results, there is a clear decrease in both tensile strength and Young's modulus with increasing temperature, (Figure 10). This decrease follows a similar trend for strength and Young's modulus, being more severe between 35 and 70 °C, since

T_g is within these values. This behavior is typical of viscoelastic materials, whose properties depend on temperature. This happens because at a higher temperature, there is an increase in the mobility of the polymeric chain, which allows the accommodation of higher deformations; however, it contributes to a decrease in stiffness and strength.

Table 4. Bulk tensile tests at different temperatures and stiffness tensile strengths, showing the stiffness and strength decrease with testing temperature.

Property	35 °C	70 °C	130 °C
Young's modulus (GPa)	8.2 ± 0.1	4.6 ± 0.1	2.3 ± 0.1
Tensile strength (MPa)	105 ± 1	66 ± 1	44 ± 1

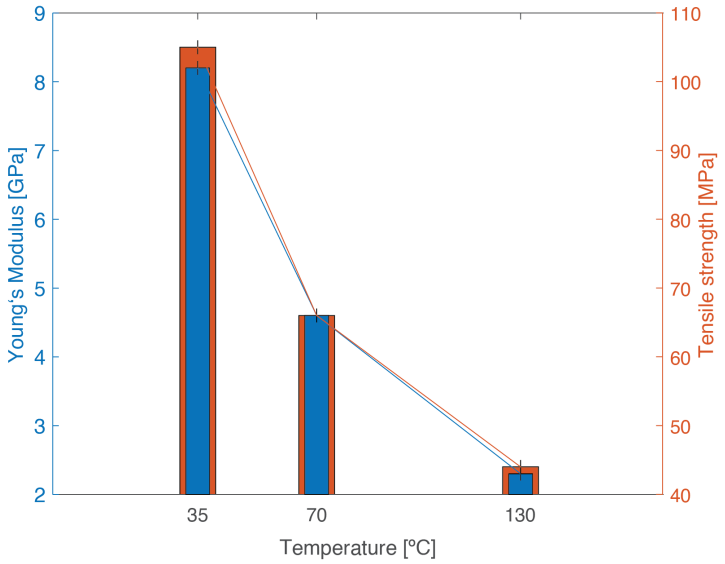
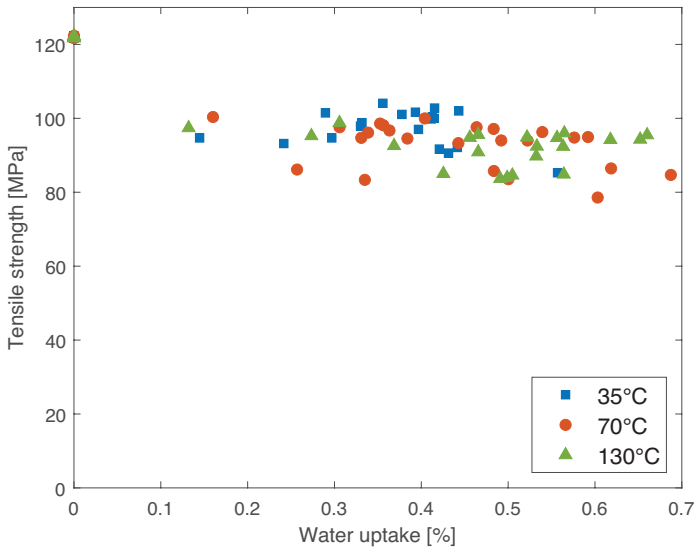


Figure 10. Tensile strength and stiffness of PBT-GF30 as a function of temperature, showing a decrease in both properties with increasing temperature.

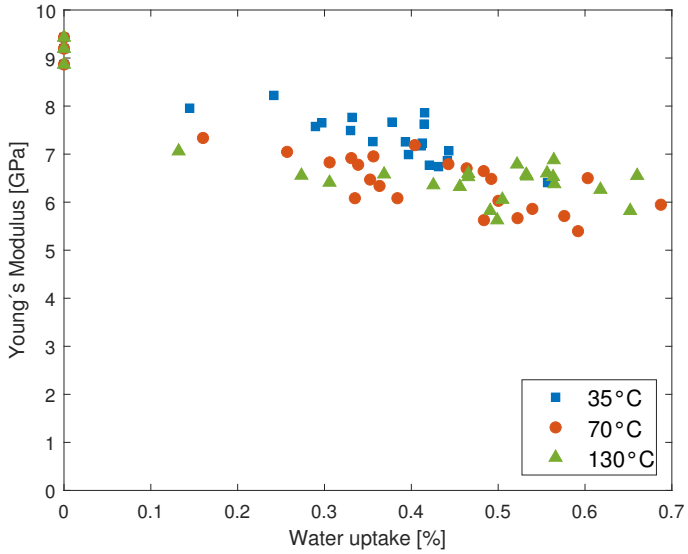
3.4.3. Bulk Tensile Tests after Aging at Different Temperatures

The results for tensile strength and Young's modulus as a function of water uptake for 35, 70, and 130 °C are given in Figure 11.



(**a**)

Figure 11. *Cont.*



(**b**)

Figure 11. Tensile strength and stiffness of PBT-GF30, aged at 35, 70, and 130 °C as a function of water uptake. (**a**) Tensile strength. (**b**) Young's modulus.

It can be concluded that there is not a clear trend in any of the temperatures analyzed for the evolution of strength and Young's modulus as a function of water uptake. However, it is clear that there is a decrease in both mechanical properties from the dry to the humid condition, since the material with humidity typically exhibits a relaxation on the polymeric chain. Additionally, the drop in mechanical properties is more significant for higher temperatures. Further explanation for these results can be found in Sections 4.2 and 3.5. It is also important to highlight that in these tests, at RT, temperature does not play a role in the decrease in mechanical properties, only humidity, since when the specimen is tested, after weighing and correctly assembling on the universal testing machine, it is already at RT.

3.5. Fourier Transform Infrared Spectroscopy (FTIR)

The transmittance spectra obtained with the FTIR analysis can be seen in Figure 12.

From the FTIR analysis, it can be concluded that there is no significant change in the dry, 35, or 70 °C condition. However, for 130 °C, there is a difference in the range of from 3500 to 3000 cm^{-1}, which is related to hydrogen bonds and may be caused by the establishment of chemical bonds with water or the hydrolysis of the material. This may be related to the larger decrease in mechanical properties for the higher temperatures.

To complete the analysis and narrow the temperature range at which profile change happens, water immersion at other temperatures between 70 and 130 °C were analyzed. The first intermediate temperature analyzed was 90 °C. The analyzed range was gradually refined, leading to the conclusion that the change in FTIR profile of the material occurs between 80 and 85 °C. Figure 13 presents the results for 35, 70, and 80 °C, showing that no chemical bonds are formed until 80 °C is reached. Figure 14 exhibits the results obtained for those temperatures. From the curves for 80, 85, and 90 °C, further conclusions can be drawn. The peak in the curve for 85 °C, corresponding to the OH^{-} ions, in the zoomed area, is at 78% of the peak obtained for 90 °C. Since the curve for 90 °C is similar to that obtained at higher temperatures and the curve obtained at 80 °C is similar to the curve obtained at lower temperatures, it can be speculated that the exact transition temperature is closer to 80 °C than to 85 °C. However, to determine the exact values, further immersion temperatures need to be analyzed.

The chemical changes recorded can be either due to hydrolysis of the PBT or the creation of chemical bonds with water as bound water. In the first scenario, alcohol

and acid functions should be formed, and analysing the FTIR spectra, the appearance of this functions can be seen at around 1750 cm^{-1}. However, they are also present for low temperatures. Therefore, chemical bonds with water can be considered the most probable cause of the OH^- peak.

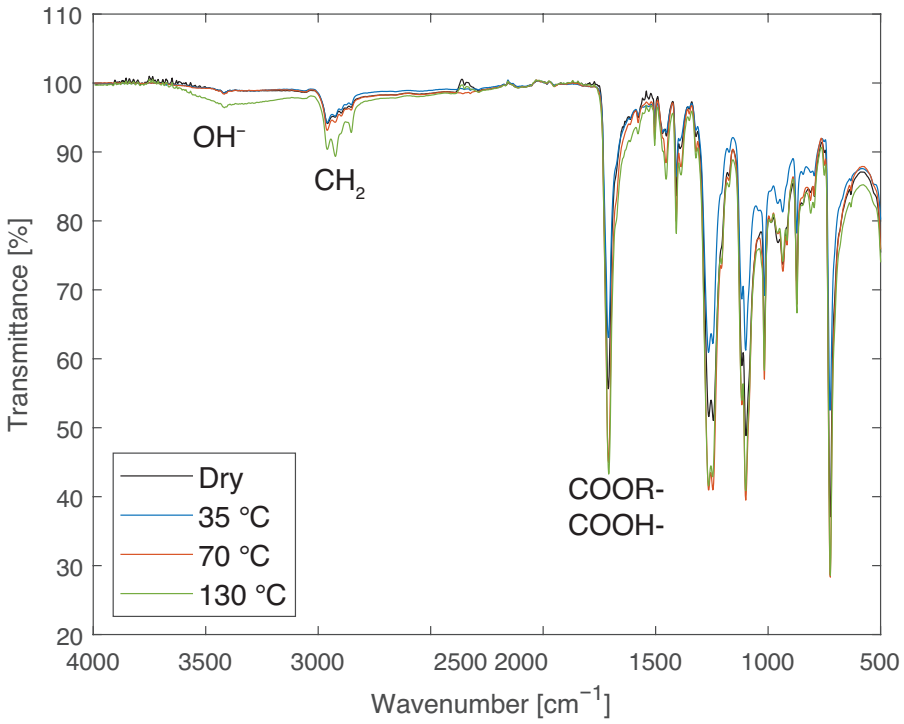


Figure 12. FTIR results of PBT-GF30 dry and after aging in water at 35, 70, and 130 °C, showing chemical changes found in the region related to OH^- for 130 °C.

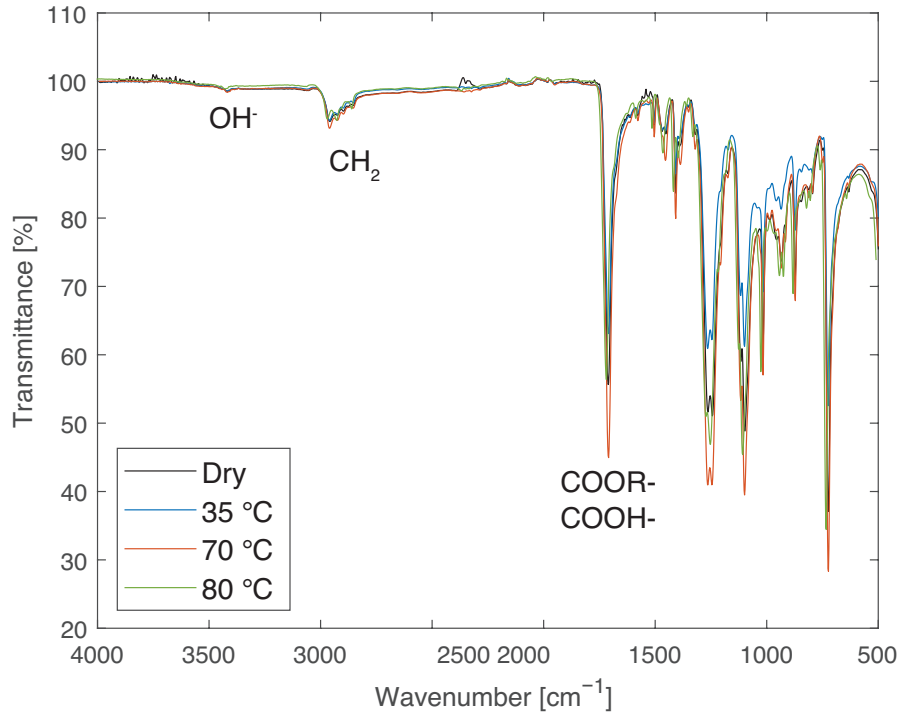


Figure 13. FTIR results of PBT-GF30 after aging in water at 35, 70, and 80 °C, showing no chemical changes found at these temperatures in the region related to OH^-.

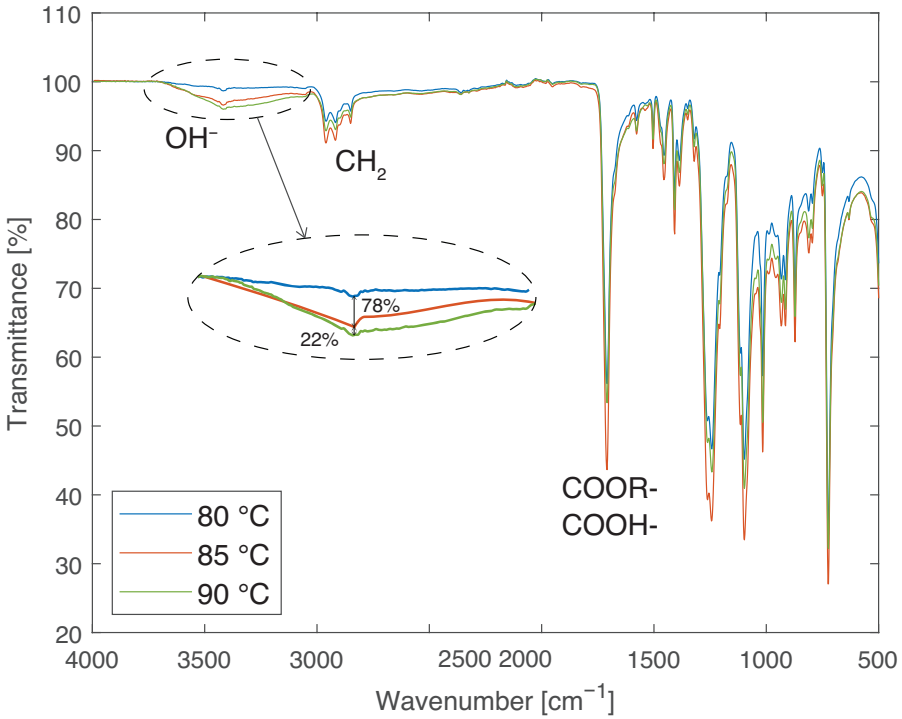


Figure 14. FTIR results of PBT-GF30 after aging in water at 80, 85, and 90 °C, showing chemical changes in the region related to OH^- appearing between 80 and 85 °C.

4. Numerical Simulation

4.1. Gravimetric Analysis

The main purpose of the developed numerical models of gravimetric studies was to create a methodology that is able to precisely reproduce experimental results. For this, first, two-dimensional approximation of the experimental tests was analyzed. This approximation is used to simplify the geometrically more accurate three-dimensional numerical model of the plate, significantly decreasing computation time. Afterwards, a second numerical model was developed to understand if the assumption that the water uptake is unidirectional is fair for these specimens in order to validate the analytical model. Finally, the experimental results were numerically reproduced.

4.1.1. Evaluation of the Numerical Model Adopted

The specimens used in the experimental study are squares with a 60 mm side and 1 mm thickness. If one takes advantage of the symmetries in this structure, the section that must be simulated is that marked in dark grey in Figure 15. This model is referred to as three dimensional. In this model, water ingress must be considered through the surfaces S_1, S_2, and S_3.

However, this three-dimensional model is computationally heavy, both when running the simulation and the post-processing operations. Therefore, a simplified two-dimensional model was developed in an effort to obtain similar results but with reduced computational time. This two-dimensional model only considers the slice represented in dark grey in Figure 15. Water uptake in this specimen is considered to occur through edges E_1 and E_2.

This slice represents an oversimplified model of the experimental tests, which would only accurately represent circular specimens, as presented in Figure 15. Although the corners present in the experimental specimen are neglected, if the results are not significantly affected by this simplification, it has the potential to lead to an important reduction of computation time. Therefore, the two-dimensional and three-dimensional models were run, and their results compared.

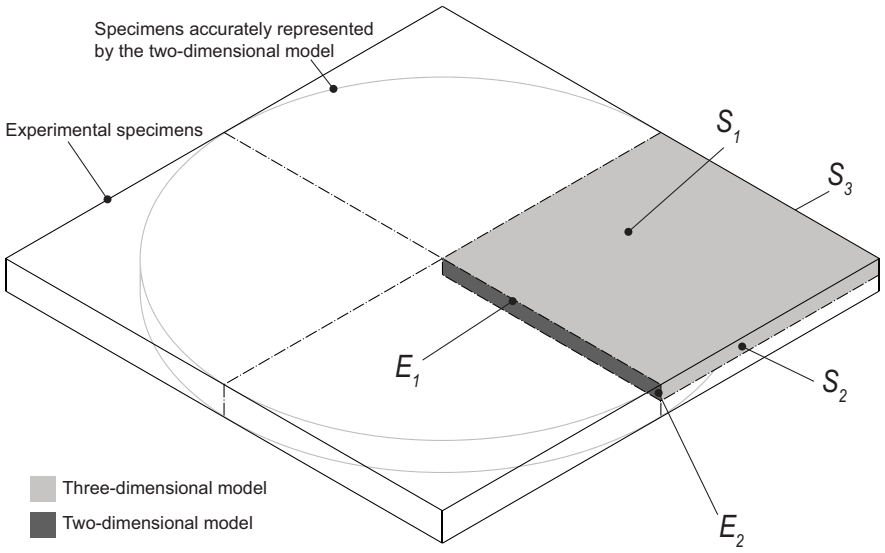


Figure 15. Schematic representation of the numerical model.

To simulate water diffusion, a heat transfer analogy was used, where the coefficient of diffusion can be compared to the thermal diffusivity. It is also considered that once the material is immersed in water, the first layer of nodes instantaneously saturates, which means a boundary condition is applied with the value of water uptake at saturation. For the two-dimensional model, a uniform mesh of $5 \cdot 10^{-5}$ m was used, and for the three-dimensional model, a mesh size of $2 \cdot 10^{-4}$ m was used. Due to the large computational time of the three-dimensional model, it was only run until the saturated level was reached. The elements used are heat transfer elements: for the two-dimensional model, a 20-node quadratic heat transfer brick (DC3D20), and for the three-dimensional model, a 4-node linear heat transfer quadrilateral (DC2C4). The results of water uptake as a function of time for the two models can be seen in Figure 16. From these results, it can be concluded that a two-dimensional approximation can be used. The plates used in this work have a thickness significantly smaller than the other dimensions of the specimen, with a 1:60 ratio. Therefore, it seems fair to assume that water is absorbed mainly through the thickness. However, to ensure this is an appropriate approximation, a numerical simulation was conducted. With this purpose, the two-dimensional model represented in Figure 15 was compared to a model similar to it but taking into account that the side surfaces were isolated, i.e., water uptake only occurs through E_1. This model is referred to as two-dimensional model with unidirectional ingress. The two models were run, and a comparison between them can also be observed in Figure 16. From this numerical study, it can be concluded that a unidirectional water ingress occurred in the experimental tests.

From Figure 16, it is clear that there is a slight difference between the two-dimensional and the three-dimensional models, which is due to the aforementioned simplification of the corners. However, it is clear that the two-dimensional model is quite capable of accurately describing the water uptake behavior and, due to the lower computation time, this was the model adopted for the remaining work.

4.1.2. Simulation of the Experimental Results

A numerical simulation was conducted to mimic the water absorption behavior of the PBT and PBT-GF30 plates, using a two-dimensional model considering water uptake through the exposed surfaces, similar to that previously described as a two-dimensional model. For each simulation, the coefficient of diffusion and maximum water uptake were set to the values presented in Table 2. A comparison between the analytical model established to describe the water absorption behavior and the results of the numerical simulation is shown in Figure 17.

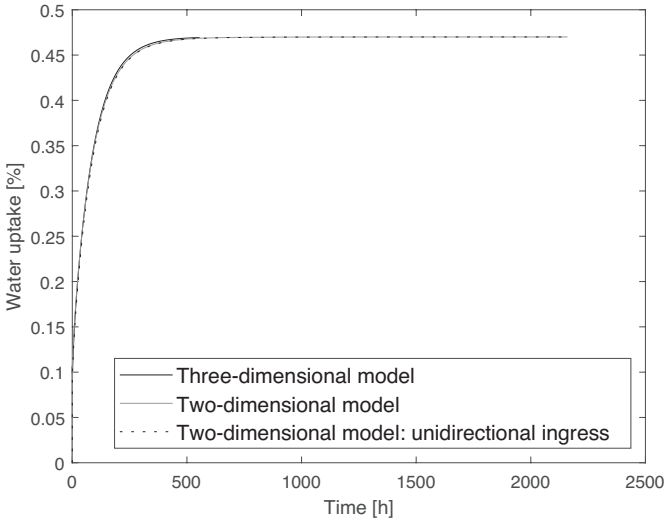


Figure 16. Comparison between the three-dimensional, two-dimensional, and two-dimensional with unidirectional ingress models, using data from PBT-GF30 at 35°C, showing that a two-dimensional model can be used.

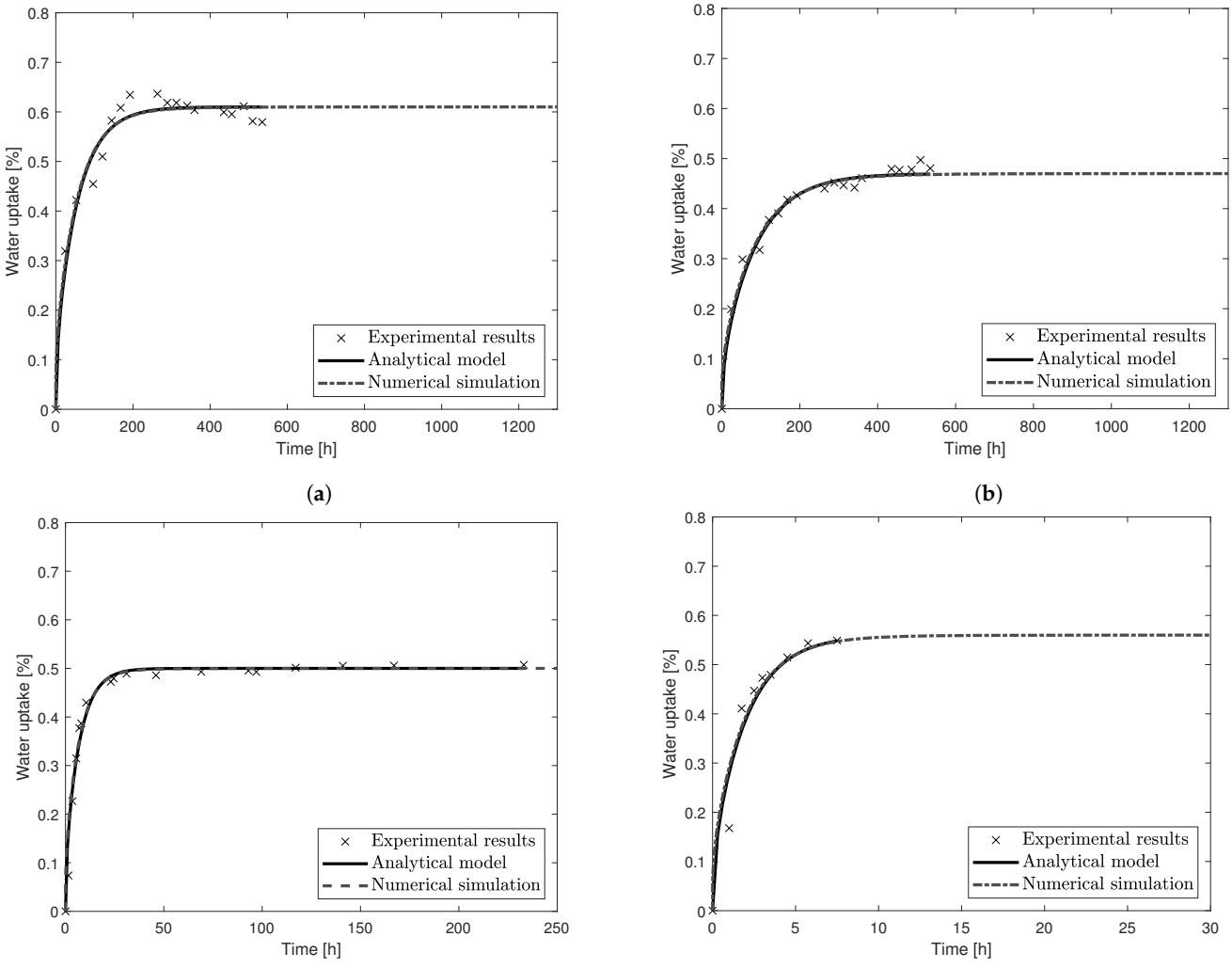


Figure 17. Numerical simulation of water uptake for the gravimetric tests compared with the analytical model and experimental results, showing that the simulation fits the analytical model. (**a**) PBT at 35 °C. (**b**) PBT-GF30 at 35 °C. (**c**) PBT-GF30 at 70 °C. (**d**) PBT-GF30 at 130 °C.

It can be concluded that the developed numerical simulation exhibits a very good correlation with the obtained experimental results .

4.1.3. Minimum Plate Side Length–Thickness Ratio for the Water Flow to Be One Dimensional

In this study, one of the concerns identified regarding the experimental procedures was the large amount of material required to manufacture the plates for the gravimetric study. Since the plates were obtained from injection-molded PBT and PBT-GF30, it would be beneficial to use smaller plates so that the defects introduced to the surface by injection molding could be avoided, thereby avoiding sandpaper treatment. Additionally, in multi-material structures, or in parts where there is an aim to characterize a smaller portion of the material, smaller plates would also be beneficial. However, the water flow in these smaller plates must remain unidirectional and, from the numerical point of view, it is beneficial to maintain the valid two-dimensional approximation.

Therefore, as a first step, a three-dimensional model, described above, was compared for different side lengths, which differ by 10 mm (60, 50, 30, 20, and 10 mm), always maintaining a thickness of 1 mm (Figure 18). The mesh size of these models was changed for each plate, in a manner proportional to the side length, to maintain the number of elements.

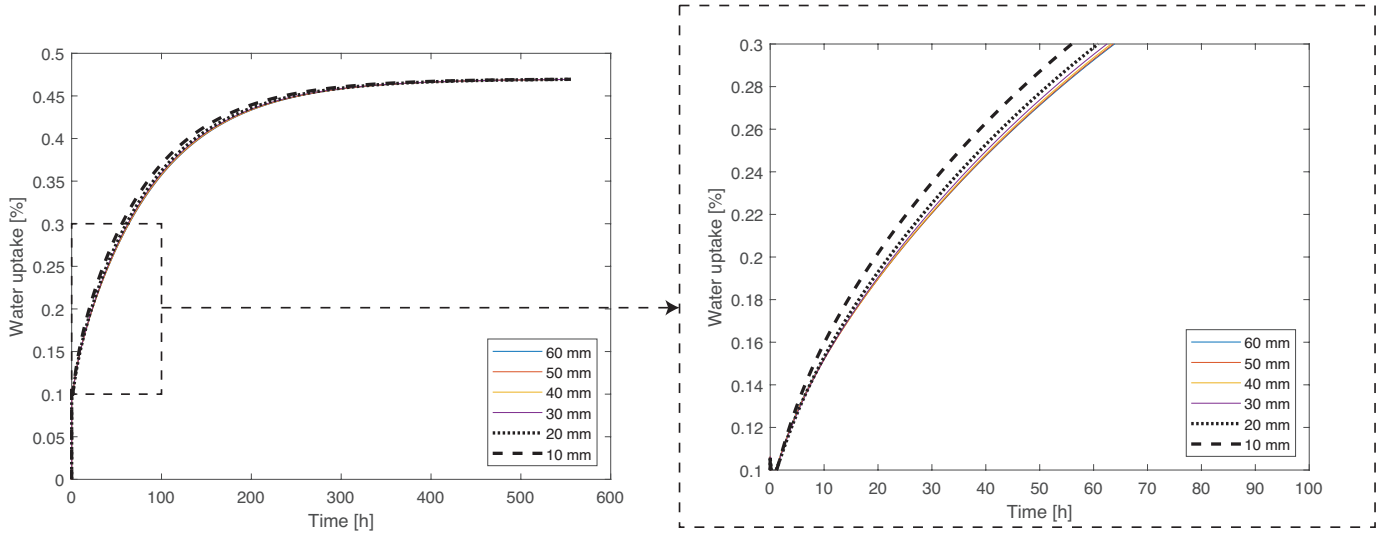


Figure 18. Numerical simulation of the water uptake of specimens with different sizes at 35 °C, showing that the results are in agreement for the 60 and 30 mm side lengths.

The side length of 10 mm was discarded from consideration at an early stage, since the difference between the 60 mm and 10 mm plates is significant, with a maximum error of 6%. The size of 20 mm presents lower discrepancy in the results, with a maximum error of 2%. However, a plate with a 30 mm of side was considered to present the best compromise between the fidelity of the water uptake process, with a maximum error of 1%, and the amount of material necessary for its manufacture. Afterwards, the model was used to determine if the two-dimensional approximation used previously remained valid and if the water flow remained unidirectional, which is the case, as can be observed in Figure 19.

At this point, it is understood that, from the numerical point of view, a plate with a 30 mm side length would be suitable to characterize the water uptake behavior of PBT-GF30. Although the coefficient of diffusion and water uptake at saturation used to conduct this simulation are obtained with water immersion at 35 °C, the same correlation would be found for 70 and 130 °C.

Experimental validation was performed at 70 °C to avoid the long immersion time required to saturate the material at 35 °C and to avoid chemical changes that would occur

at 130 °C. Figure 20 shows that the water uptake behavior obtained with plates with a 30 mm side length have similar experimental results to those with a 60 mm side length.

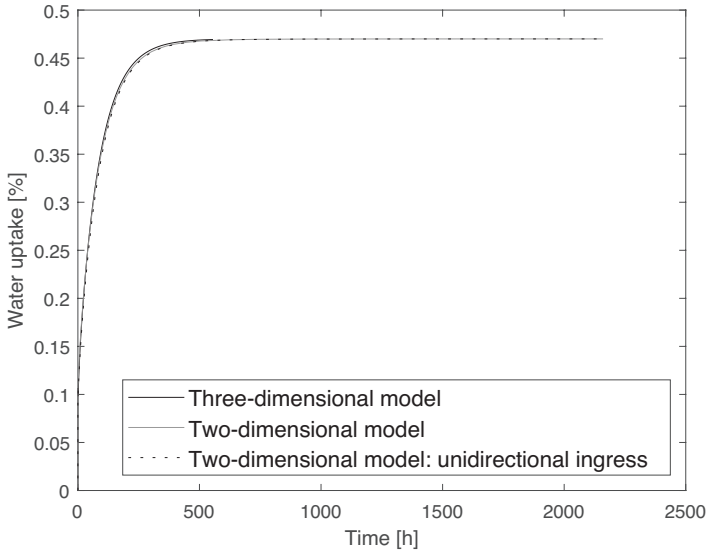


Figure 19. Comparison between the three-dimensional, two-dimensional, and two-dimensional with unidirectional ingress models for a plate with a 30 mm side length, using data from PBT-GF30 at 35 °C. As can be observed, the two-dimensional model remains valid.

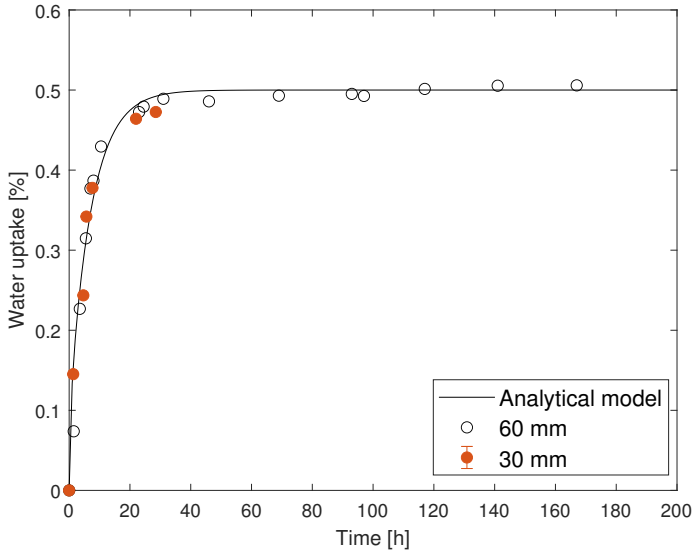


Figure 20. Experimental validation of a plate with a size of 30 mm, showing that this plate size is sufficient for water uptake behavior characterization.

From these results, it is concluded that plates with a side length of 30 mm and a 1 mm thickness can be used to perform gravimetric studies.

4.2. Simulation of the Bulk Tensile Tests

The bulk tensile tests at room temperature using the reduced-scale specimens were simulated in Abaqus using one-eighth of the specimen, taking full advantage of symmetry. One of the edges was pinned, and displacement was applied to the opposite side. In this model, a uniform mesh of 0.2 mm was used, and both the elastic and plastic properties of the material were considered. The mesh and stress in the time increment before plasticization starts can be observed in Figure 21. The elements used are 3D stress, an 8-node linear brick, and reduced integration (C3D8R). This simulation was conducted from the properties

obtained in the as-supplied state when tested at room temperature as a given condition to evaluate stress distribution for bulk tensile tests.

It can be observed that there is a stress gradient from the edges to the middle of the specimen, with stress being higher at the edges. Therefore, it can be assumed that the specimen starts to fail at those edges, damaged by water uptake.

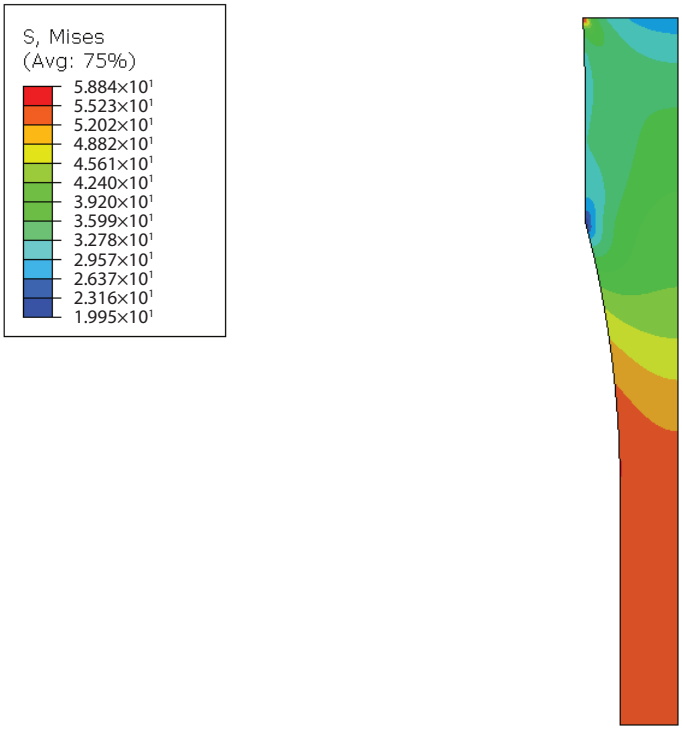


Figure 21. Numerical simulation of the bulk tensile tests using reduced-scale specimens, showing higher stress near the edge of the specimen.

Reduced-scale specimens were also simulated in Abaqus. Taking advantage of symmetry, only one-eighth of the specimen was represented. Additionally, the same boundary conditions described above for the gravimetric analysis simulation were used. In Figure 22, water distribution was achieved after one day and a half of water immersion at 35 °C. The global water uptake level at this point in the specimen was 0.26% according to the numerical simulation.

From these two simulations, it can be observed that as the water ingresses the material, the first region to saturate is the outer layer, which is also the region where the stress for a given time increment of the bulk tensile test is higher. The core of the material, as shown in Figure 22, has a significantly smaller water content. However, the specimen starts to fail at the saturated edge, which is almost immediately saturated after water immersion. Consequently, all humid states depend on the same condition to initiate failure, which is failure of the saturated edge. This translates into similar strength of all humid conditions.

The authors that also studied the effect of water uptake on the mechanical properties of PBT and its short fiber composites conducted slightly different experiments, which may have led to different results. The differences are mainly regarding immersion time and specimen thickness.

Bergeret et al. [34], when analyzing PBT with 15% short glass fiber using "dogbone" immersed in water at 120 °C, concluded that for short immersion times, the strength of the material decreased, reaching a stable *plateau*. After a longer immersion time, strength was found to undergo a second drop. In the first decrease, for short immersion times, strength decreased to just above 80 MPa, which is similar to the results obtained in this work.

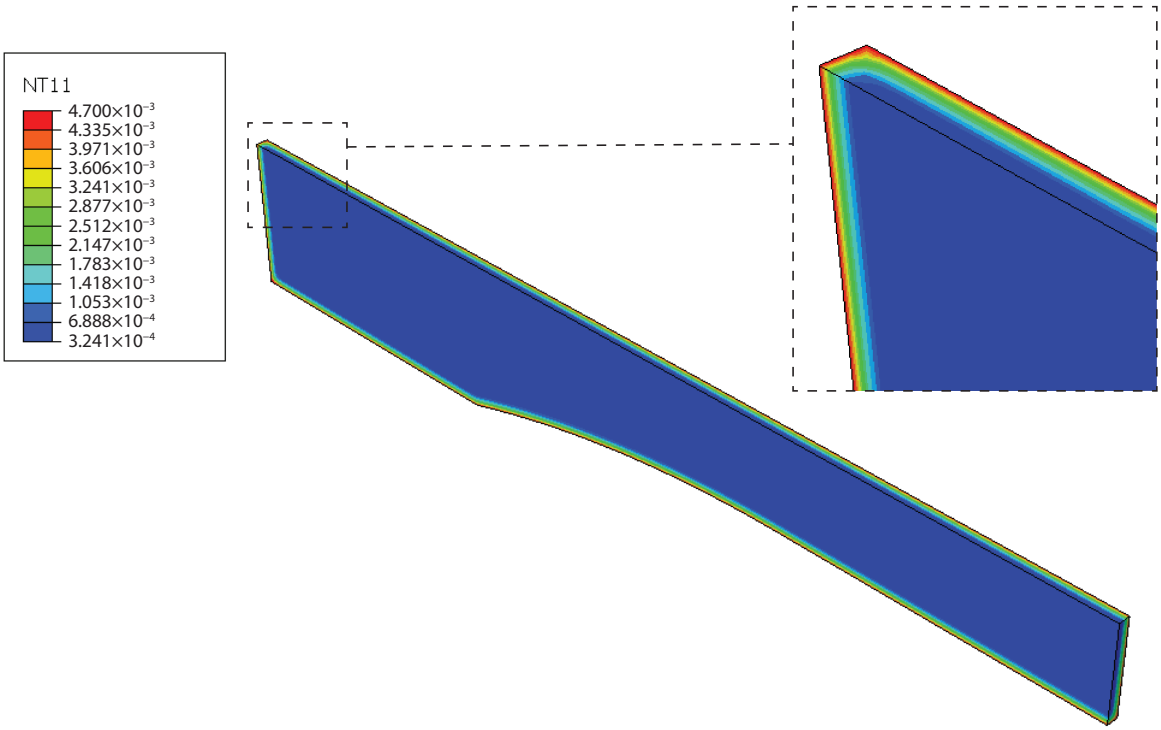


Figure 22. Numerical simulation of the water uptake, NT11, for reduced-scale specimens at 35 °C at the end of 21.2 h, showing that at this stage, only the outer layers are saturated.

Ishak et al. [31], as discussed above in Section 1, reported a decrease to 21% in the initial strength and to 36% for PBT-GF30 (when compared to the unaged state) after water immersion at 90 °C. In this study, specimens were tested at 20 °C when saturated. However, the immersion time may correspond to the second drop in strength. Additionally, the decrease in strength described by this work for 30 °C is compatible to that identified in the present work for 35 °C.

Rosato et al. [23] and Gardner et al. [35], as mentioned above in Section 1, also noted that the strength of PBT exposed to environments of 100% of relative humidity can be significantly decreased after very long exposure times. After three to four years, the tensile strength was reduced to about 50%.

The other variable that may influence the results is temperature. Although it is common for tests to be performed at room temperature after water immersion at a higher temperature, the specimens used in the present study have a smaller thickness to decrease immersion time, which may lead to a quicker decrease in temperature between the time the specimen is removed from the climatic chamber and the end of the test. Therefore, temperature plays a less significant role, leading to a higher strength and Young's modulus.

5. Conclusions

The main conclusions drawn from this work are that the diffusion for all conditions tested follows a Fickian law. Fiber-free PBT absorbs more water than PBT-GF30, which may be not only attributed to the portion of the hydrophilic matrix and hydrophobic fibers but also to the capillarity between the fiber and the matrix. Regarding the rate of water ingress, it is slightly higher for material without fiber inclusions. However, the main influence on this rate occurs due to temperature following an Arrhenius relation. The effect of temperature on the mechanical properties of PBT-GF30 is more significant than the effect of humidity.

For humid conditions at a given temperature, the mechanical properties obtained through tensile testing specimen do not change as a function of water uptake due to the fact that the outer layer of the specimen material is saturated in every case, corresponding to the region of maximum stress during the test.

Regarding chemical degradation of the material, after water immersion at a temperature between 80 and 85 °C, there is the establishment of chemical connections between water and PBT or hydrolysis of PBT (degradation of the polymer chain), which produces alcohol and carboxylic groups, both exhibiting OH groups.

Additionally, with this work, it was possible to conclude that plates with a 30 mm side length can be used to trace the water absorption profiles of a material with similar results to those obtained following the standard larger plates. This is valid for 1 mm-thick plates.

Author Contributions: Conceptualization, C.S.P.B., E.A.S.M. and C.U.; methodology, C.S.P.B., A.A.-S., P.W. and R.J.C.C.; software, A.A.-S. and C.S.P.B.; investigation, C.S.P.B. and R.J.C.C.; original draft preparation, C.S.P.B. and E.A.S.M.; writing—review and editing, C.U., P.W. and L.F.M.d.S.; supervision, L.F.M.d.S.; project administration, L.F.M.d.S.; funding acquisition, C.U. and P.W. All authors have read and agreed to the published version of the manuscript.

Funding: This research received no external funding.

Institutional Review Board Statement: Not applicable.

Informed Consent Statement: Not applicable.

Data Availability Statement: No new data were created or analyzed in this study. Data sharing is not applicable to this article.

Acknowledgments: The authors wish to acknowledge and thank the funding and support provided by Robert Bosch GmbH, Corporate Research and Advance Engineering, Renningen.

Conflicts of Interest: The authors declare no conflict of interest.

References

1. Brigante, D. *New Composite Materials*; Springer: Berlin, Germany, 2014.
2. Yao, S.S.; Jin, F.L.; Rhee, K.Y.; Hui, D.; Park, S.J. Recent advances in carbon-fiber-reinforced thermoplastic composites: A review. *Compos. Part B Eng.* **2018**, *142*, 241–250.
3. Barbosa, A.; da Silva, L.; Öchsner, A. Hygrothermal aging of an adhesive reinforced with microparticles of cork. *J. Adhes. Sci. Technol.* **2015**, *29*, 1714–1732.
4. Fang, H.; Bai, Y.; Liu, W.; Qi, Y.; Wang, J. Connections and structural applications of fibre reinforced polymer composites for civil infrastructure in aggressive environments. *Compos. Part B Eng.* **2019**, *164*, 129–143.
5. Ghahari, S.; Assi, L.N.; Alsalman, A.; Alyamaç, K.E. Fracture properties evaluation of cellulose nanocrystals cement paste. *Materials* **2020**, *13*, 2507.
6. Borges, C.; Marques, E.; Carbas, R.; Ueffing, C.; Weißgraeber, P.; da Silva, L.F.M. Review on the effect of moisture and contamination on the interfacial properties of adhesive joints. *Proc. Inst. Mech. Eng. Part C J. Mech. Eng. Sci.* **2020**. doi:10.1177/0954406220944208.
7. Boubakri, A.; Haddar, N.; Elleuch, K.; Bienvenu, Y. Impact of aging conditions on mechanical properties of thermoplastic polyurethane. *Mater. Des.* **2010**, *31*, 4194–4201.
8. Viana, G.; Costa, M.; Banea, M.; da Silva, L. A review on the temperature and moisture degradation of adhesive joints. *Proc. Inst. Mech. Eng. Part L J. Mater. Des. Appl.* **2017**, *231*, 488–501.
9. Viana, G.; Costa, M.; Banea, M.; da Silva, L. Moisture and temperature degradation of double cantilever beam adhesive joints. *J. Adhes. Sci. Technol.* **2017**, *31*, 1824–1838.
10. Zhou, J.; Lucas, J.P. Hygrothermal effects of epoxy resin. Part I: The nature of water in epoxy. *Polymer* **1999**, *40*, 5505–5512.
11. Zhou, J.; Lucas, J.P. Hygrothermal effects of epoxy resin. Part II: Variations of glass transition temperature. *Polymer* **1999**, *40*, 5513–5522.
12. Eftekhari, M.; Fatemi, A. Tensile, creep and fatigue behaviours of short fibre reinforced polymer composites at elevated temperatures: A literature survey. *Fatigue Fract. Eng. Mater. Struct.* **2015**, *38*, 1395–1418.
13. Eftekhari, M.; Fatemi, A. Tensile behavior of thermoplastic composites including temperature, moisture, and hygrothermal effects. *Polym. Test.* **2016**, *51*, 151–164.
14. Shen, C.H.; Springer, G.S. Moisture absorption and desorption of composite materials. *J. Compos. Mater.* **1976**, *10*, 2–20.
15. Rangaraj, S.V.; Smith, L.V. Effects of moisture on the durability of a wood/thermoplastic composite. *J. Thermoplast. Compos. Mater.* **2000**, *13*, 140–161.
16. Loh, W.; Crocombe, A.; Wahab, M.A.; Ashcroft, I. Modelling anomalous moisture uptake, swelling and thermal characteristics of a rubber toughened epoxy adhesive. *Int. J. Adhes. Adhes.* **2005**, *25*, 1–12.
17. Ito, E.; Kobayashi, Y. Effects of absorbed water on physical properties of polyesters. *J. Appl. Polym. Sci.* **1980**, *25*, 2145–2157.

18. Chow, C.; Xing, X.; Li, R. Moisture absorption studies of sisal fibre reinforced polypropylene composites. *Compos. Sci. Technol.* **2007**, *67*, 306–313.
19. Malpot, A.; Touchard, F.; Bergamo, S. Effect of relative humidity on mechanical properties of a woven thermoplastic composite for automotive application. *Polym. Test.* **2015**, *48*, 160–168.
20. Stein, R.; Misra, A. Morphological studies on polybutylene terephthalate. *J. Polym. Sci. Polym. Phys. Ed.* **1980**, *18*, 327–342.
21. Ishak, Z.M.; Lim, N. Effect of moisture absorption on the tensile properties of short glass fiber reinforced poly(butylene terephthalate). *Polym. Eng. Sci.* **1994**, *34*, 1645–1655.
22. Mohd Ishak, Z.; Ishiaku, U.; Karger-Kocsis, J. Hygrothermal aging and fracture behavior of styrene-acrylonitrile/acrylate based core–shell rubber toughened poly (butylene terephthalate). *J. Appl. Polym. Sci.* **1999**, *74*, 2470–2481.
23. Rosato, D.V.; Rosato, D.V.; Rosato, M.V. *Plastic Product Material and Process Selection Handbook*; Elsevier: Amsterdam, The Netherlands, 2004.
24. Wels, S.; Boettge, B.; Bernhardt, R.; Klengel, S.; Claudi, A. Dielectric strength and aging performance of polybutylene terephthalate (PBT) under the influence of temperature and humidity. In *The International Symposium on High Voltage Engineering*; Springer: Berlin, Germany, 2019; pp. 472–482.
25. Huang, J.; Yang, J.; Chyu, M.K.; Wang, Q.; Zhu, Z. Continuous-distribution kinetics for degradation of polybutylene terephthalate (PBT) in supercritical methanol. *Polym. Degrad. Stab.* **2009**, *94*, 2142–2148.
26. Jie, H.; Ke, H.; Wenjie, Q.; Zibin, Z. Process analysis of depolymerization polybutylene terephthalate in supercritical methanol. *Polym. Degrad. Stab.* **2006**, *91*, 2527–2531.
27. Muo, I.; Azeez, A.A. Green entrepreneurship: Literature review and agenda for future research. *Int. J. Entrep. Knowl.* **2019**, *7*, 17–29.
28. Blažková, I. Sectoral and firm-level determinants of profitability: A multilevel approach. *Int. J. Entrep. Knowl.* **2018**, *6*, 32–44.
29. Kliestik, T.; Misankova, M.; Valaskova, K.; Svabova, L. Bankruptcy prevention: New effort to reflect on legal and social changes. *Sci. Eng. Ethics* **2018**, *24*, 791–803.
30. Ishak, Z.M.; Ariffin, A.; Senawi, R. Effects of hygrothermal aging and a silane coupling agent on the tensile properties of injection molded short glass fiber reinforced poly(butylene terephthalate) composites. *Eur. Polym. J.* **2001**, *37*, 1635–1647.
31. Ishak, Z.M.; Ishiaku, U.; Karger-Kocsis, J. Hygrothermal aging and fracture behavior of short-glass-fiber-reinforced rubber-toughened poly(butylene terephthalate) composites. *Compos. Sci. Technol.* **2000**, *60*, 803–815.
32. Mohd Ishak, Z.; Tengku Mansor, T.; Yow, B.; Ishiaku, U.; Karger-Kocsis, J. Short glass fibre reinforcedpoly (butylene terephthalate) Part 1–Microstructural characterisation and kinetics of moisture absorption. *Plast. Rubber Compos.* **2000**, *29*, 263–270.
33. Hsu, A.; Jemian, W.; Wilcox, R. Solvent effect of water on S-glass. *J. Mater. Sci.* **1976**, *11*, 2099–2104.
34. Bergeret, A.; Ferry, L.; Ienny, P. Influence of the fibre/matrix interface on ageing mechanisms of glass fibre reinforced thermoplastic composites (PA-6, 6, PET, PBT) in a hygrothermal environment. *Polym. Degrad. Stab.* **2009**, *94*, 1315–1324.
35. Gardner, R.; Martin, J. Effect of relative humidity on the mechanical properties of poly (1, 4-butylene terephthalate). *J. Appl. Polym. Sci.* **1980**, *25*, 2353–2361.
36. ISO 294-3. Plastics-Injection Moulding os Test Specimens of Thermoplastic Materials, Part 3: Small Plates. 2002. Available online: https://www.iso.org/standard/32205.html (accessed on March 2016).
37. Institution, B.S. Methods of Testing Plastic. Introduction. BS 2782:2011. 2011. Available online: https://shop.bsigroup.com/ProductDetail?pid=000000000030244347 (accessed on September 2019).
38. Costa, M.; Viana, G.; Canto, C.; da Silva, L.; Banea, M.; Chaves, F.; Campilho, R.; Fernandes, A. Effect of the size reduction on the bulk tensile and double cantilever beam specimens used in cohesive zone models. *Proc. Inst. Mech. Eng. Part L J. Mater. Des. Appl.* **2016**, *230*, 968–982.
39. Viana, G.; Costa, M.; Banea, M.; da Silva, L. Behaviour of environmentally degraded epoxy adhesives as a function of temperature. *J. Adhes.* **2017**, *93*, 95–112.
40. Zhang, Y.; Adams, R.; da Silva, L. A rapid method of measuring the glass transition temperature using a novel dynamic mechanical analysis method. *J. Adhes.* **2013**, *89*, 785–806.
41. Konishi, T.; Miyamoto, Y. Smectic structure and glass transition in poly (butylene terephthalate). *Polym. J.* **2010**, *42*, 349–353.
42. Pyda, M.; Nowak-Pyda, E.; Mays, J.; Wunderlich, B. Heat capacity of poly (butylene terephthalate). *J. Polym. Sci. Part B Polym. Phys.* **2004**, *42*, 4401–4411.
43. Yin, H.; Dittrich, B.; Farooq, M.; Kerling, S.; Wartig, K.A.; Hofmann, D.; Huth, C.; Okolieocha, C.; Altstädt, V.; Schönhals, A.; et al. Carbon-based nanofillers/Poly (butylene terephthalate): Thermal, dielectric, electrical and rheological properties. *J. Polym. Res.* **2015**, *22*, 140.
44. Ensinger. TECADUR PBT GF 30. Material Data Sheet, December 2007, Germany. Available online: https://www.ensingerplastics.com/en/shapes/products/tecadur-pbt-gf30-natural (accessed on November 2020).
45. Ma, M.; Niu, L.; Ma, J.; Ma, J.; Jiao, T. Fabrication and Thermal Degradation Kinetics of PBT/BEO/Nano-Sb_2O_3 Composites. *J. Nanomater.* **2020**, *2020*. https://doi.org/10.1155/2020/6641702
46. Souilem, S.; Doulache, N.; Khemici, M.; Gourari, A. TSDC and DSC study of effects of physical aging on polybutylene terephthalate (PBT). *Int. J. Polym. Anal. Charact.* **2014**, *19*, 175–188.
47. Fick, A. On liquid diffusion. *J. Membr. Sci.* **1995**, *100*, 33–38.
48. Bastioli, C.; Guanella, I.; Romano, G. Effects of water sorption on the physical properties of PET, PBT, and their long fibers composites. *Polym. Compos.* **1990**, *11*, 1–9.

Appendix C

Paper C

Influence of water and surfactant contamination on the mechanical and chemical properties of a silicone adhesive before and after curing

Influence of water and surfactant contamination on the mechanical and chemical properties of a silicone adhesive before and after curing

C.S.P. Borges[1], R. Brandão[2], A. Akhavan-Safar[1], E.A.S. Marques[1], R.J.C. Carbas[1], C. Ueffing[3], P.Weißgraeber[4], F. Schmid[3], L.F.M. da Silva[2]

1 Instituto de Ciência e Inovação em Engenharia Mecânica e Engenharia Industrial (INEGI), Portugal
2 Departamento de Engenharia Mecânica, Faculdade de Engenharia (FEUP), Universidade do Porto, Portugal
3 Robert Bosch GmbH, Corporate Research and Advance Engineering, 71272 Renningen, Germany
4 Chair of Lightweight Design, University of Rostock, Germany

Abstract: This work aims to analyze the mechanical and chemical effects that contaminants can have prior to curing of the silicone adhesive, if they are in the substrate or surrounding environment at adhesive application, as well as after curing when they appear during the service life of the joint. In this case, the contaminants are water and a surfactant present in detergents used to clean oils from aluminum surfaces. For this, 2%, 5%, and 10% of contaminant was added to the adhesive prior to curing and neat adhesive after curing was immersed in contaminant at different temperatures. For all cases, the effect on the mechanical properties was evaluated through bulk tensile tests, the effect on the chemical profile was evaluated using Fourier-transform infrared spectroscopy (FTIR) and the morphology of the materials was studied with scanning electron microscopy (SEM). The water immersion increased slightly the mechanical properties of the adhesive, which returned to their initial value upon redrying. However, high immersion temperatures introduce irreversible damage in the material. Water added prior to curing introduces voids in the adhesive, decreasing its strength. The surfactant added prior to curing changes the adhesive morphology, showing a variation in the C-H bond. These changes translate into a lower strength and stiffness of the mixture.
Keywords: Adhesives, silicone, aging, contamination, moisture, diffusion

1 Introduction

Adhesive joints are an alternative to classical joining methods in several industrial sectors, such as the automotive, aerospace and electronics. When compared to bolting or riveting, adhesives have the advantage of not needing the introduction of holes in the component, which is particularly important when joining notch sensitive composite materials, and contributes to a more uniform stress distribution [1]. When compared to welding, adhesives have the advantage of not needing the local heating of the components, which may lead to local degradation of the material and residual stresses in the final component. The application of adhesives relies on a careful surface preparation, since they are sensitive to moisture and other contaminants that can be accommodated on the substrate. Additionally, during their service life, due to their polymeric nature, adhesives are also able to absorb environmental moisture or other contamination.

The adhesive analyzed in this study was a silicone, used to bond a housing for electronic components used in the automotive industry. Silicones have both organic and inorganic groups, which gives them a combination of particular properties when compared to ordinary organic rubbers since, due to the Si-O bond, silicones have a higher

heat resistance, chemical stability, electrical insulation and weatherability [2]. This array of properties makes silicone a great candidate for particular applications that require not only joining components but also the sealing of the assembly. Hence, it becomes clear that it is important to understand the effect of water and contamination both prior to the adhesive curing, if they are found in the substrate or in the manufacturing environment, and after curing, if the silicone adhesive is supposed to seal the component from that fluid. As contaminants, water and a surfactant that can be used or clean cutting oils from aluminum substrates prior to adhesive bonding were analyzed.

Silicones are usually considered when designing sealant joints, since they are generally more hydrophobic than other polymers used as adhesives. However, it must be considered that they are not completely resistant to water absorption [3]. After the curing process of the adhesive, water can be absorbed by the adhesive as free water or bound water. Free water only fills the micro cavities in the polymeric chain of the adhesive, as bound water forms hydrogen bonds with the chain, which can cause chemical changes in the material [4–6]. The diffusion of water into a polymeric material is usually described through the variation of mass as a function of time. There is no universal law to describe this water uptake behavior, however, in most cases, the Fick's law is used with good approximation [7–11]. The Fick's law of diffusion is defined as a function of two variables: water uptake at saturation (or infinite water uptake), M_∞, which is the point at which even immersed in water the mass of the sample will stop increasing since the material can not absorb more water, and the coefficient of diffusion, D, which translates the diffusion rate.

Dai et al. [12] investigated the ingress of deionized water, NaCl and HNO_3 on filled silicone rubber using temperatures between 20 and 60 °C. It was concluded that the water uptake of these silicones can be defined by the Fick's law of diffusion and that the coefficient of diffusion increases with increasing temperature, as stated above, while the infinite mass uptake is relatively insensitive to the change. Khalilullah et al. [3] studied the moisture absorption of silicone/phosphor composites at different temperatures, between 30 and 80 °C and different relative humidities, between 30% and 80%, and also concluded that the material follows a Fickian model, adding that the diffusivity follows the Arrhenius law of diffusion, increasing with temperature and relative humidity.

The Fick's law of diffusion is not the only one used to describe the behavior of the ingress of water in silicones. Lutz et al. [13] studied the water diffusion in high temperature vulcanized silicone rubber (HTV-SR) and found that the behavior followed a Langmuir model. Similar findings were reported by Fang et al. [14].

Generally, adhesives exposed to humid environments experience a decrease in their mechanical properties, such as strength, stiffness and toughness. The decrease in strength is usually paired with an increase in ductility and, consequently, strain to failure and creep strain [15–18]. This behavior is particularly pronounced at higher temperatures, due to the relaxation of the polymeric chain and to the ratio between bound and free water, which increases with temperature [19]. Han et al. [20] characterized the degradation of an epoxy adhesive, performing gravimetric studies and micro indentation to access the mechanical properties of the material. It was concluded that water diffusion causes meso-scale degradation of the mechanical properties of the material and that as the local water uptake increased led to more extensive degradation.

However, for silicones that is not the behavior reported in literature. Fan et al. [21] studied the effect of moisture on the mechanical properties of phosphor/silicone composites, through the exposure of different samples to a controlled temperature of 55 °C and

85% of relative humidity (RH). The tensile strength and Young's modulus of materials with 0% and 10% of phosphor over an aging time of 42 days were studied. Over the aging time, the specimens were periodically removed from the water container and tested. For all the samples analyzed, the pure silicone, with 0% of phosphor, was stronger and more flexible. However, both materials increased in strength and stiffness over the aging period. It was observed that the increase in strength of the pure silicone is higher than that of phosphor/silicone composites. This was also related to the hydrolisis of phosphor particles, which increases their surface roughness, promoting an uneven contact between the particles and silicone that culminates in gaps between them and decreases the rate of tensile strength increase. Regarding the Young's modulus, it was seen that the increase for the composite is more pronounced than for pure silicone. This was attributed to the hydrolysis of the phosphor particles, which accelerated the stiffening of the material. Ali and Hackman [22] studied the loss of hydrophobicity of high temperature vulcanized (HTV) silicone rubber using the contact angle between saline water and silicone, and concluded that, during immersion, this property decreases sharply, to 15% of its initial value, after 3000h of immersion at 98 °C.

Most studies conducted on this topic regard the effect of water contamination, however, it must be noted that, the conclusions drawn regarding water diffusion into the material can be extrapolated to other contaminants, such as surfactants, remembering that this will occur with different laws of diffusion and different chemical effects on the structure of the material.

As two substrates are bonded using an adhesive, there is a formation of a zone called interphase. This region is different from the adhesive and substrate, both morphologically and chemically [1, 23]. The interphase is a transitional region with gradients of glass transition temperature, crosslinking and residual stresses, presenting a layered structure [24], which makes it a complex zone, with heterogeneous morphology. The properties of the adhesive joint are dependent on the properties of the adhesive, the substrate and the interphase [23].

If there is contamination at the surface of the substrates prior to bonding, it can either be absorbed by the substrate, by the adhesive (pior to curing or during the curing process), or remain at the adhesive/substrate interface. The second situation is the most concerning one, since the contaminant may act as a physical separation between the adhesive and substrate, constraining the inter-molecular interactions between them and creating weak bonds or, in the worst scenario, debonding [6, 25–27]. To avoid this, the adhesive must have the capacity of absorbing some of the contaminant present at the substrate surface. However, this absorption, specially before the curing process is complete, may have severe consequences to in the final adhesive properties, particularly at the interphase. The effect of contamination on adhesives is a highly complex topic, since it depends on the contaminant, adhesive and interactions between them. In this study, a silicone adhesive and water and surfactant contamination are analyzed. However, to the authors' best knowledge, there is not significant research performed on silicone adhesives, and the work developed on surfact contamination, although it is more extensive, it is also limited. Therefore, for this literature review, the scope was extended to further material classes.

Debski et al. [28] studied the effect of mineral oil, added pre-mixing to epoxy adhesives, on the glass transition temperature, T_g of the materials. It was concluded that the cross-linking kinetics changes with the addition of contaminant, since for the same cross-linking time and temperature, the higher the amount of oil mixed, the lower the T_g. Hong et al. [29] analyzed the effect of oil on the curing of an epoxy adhesive through differential

scanning calorimetry (DSC) and determined that, with the increase of oil content, there is a decrease in the cure exotherm, which indicates changes in the chemical reaction of the curing. Akiyama et al. [30] studied the influence of surface contamination on joints with aluminum substrates and acrylic and epoxy adhesives. Different contaminants were used, among which four surfactants: stearic acid, oleic acid, sodium dodecyl sulfate (SDS), and dodecyl trimethyl ammonium chloride (DTAC). The adhesion strength was shown to decrease with surfactant contamination and two possible motives were pointed out, the first was that the surface energy of the surface was significantly affected by the presence of contaminant lowering the wettability of the substrate and the second is that the surfactants have low diffusivity into the adhesive, remaining at the interface. However, this hypotesis was not further analyzed since the effect of the surfactant on the adhesive is not known.

As said, most projects developed regarding the effect of contamination on adhesive joints concern epoxy adhesives. Therefore, it is important to wide the scope of research and understand the effect on silicone adhesives.

In this work, the effect of water and surfactant contamination prior to curing was analyzed by adding 2, 5 or 10% of the contaminant to the uncured adhesive and the effect after curing is studied by immersing the neat silicone adhesive in the contaminant in a climatic chamber at 70, 90 and 130 °C for water and 70 °C for surfactant. These three temperatures were chosen because they represent the higher temperatures of interest from the manufacturing, packaging and service life of the final component and these phenomena are enhanced by increasing temperature. Additionally, 130 °C represents the highest peak temperature that can be recorded during these processes. For the surfactant only the lower temperature was used since the fluid is not stable at the higher temperatures. The mechanical properties were evaluated through bulk tensile tests, chemical profiles were analyzed using Fourier-transform infrared spectroscopy (FTIR), for comparison purposes, FTIR of the contaminant profile was also carried out. The morphology of the materials was detailed with scanning electron microscopy (SEM) with energy dispersive spectroscopy (EDS). A dynamic mechanical analysis (DMA) was also carried out to understand if there is a transition temperature in the temperature range analyzed.

2 Experimental details

2.1 Materials

The adhesive used in this study is a two-part silicone adhesive. The adhesive/catalyst ratio used was 1:1 and the mixture was performed using a speed mixer and cured at 120 °C for 25 minutes.

The water contamination was performed using distilled water.

The surfactant contamination was performed using Cocosalkylaminethoxylate manufactured by SysKem Chemie GmbH (Wuppertal, Germany). This surfactant is used to clean aluminum surfaces from oils needed during the manufacturing process. In the following sections, the group of surfactant and water are going to be referred to, generally, as contaminant.

2.2 Specimen manufacturing

The specimens for the different studies were cut from adhesive plates. For this, first, the adhesive and hardener must be mixed. The mass required of each part was measured using a microbalance with 0.1 mg of accuracy (KernToledo, Balingen, Germany) and then mixed using a Hauschild SpeedMixer® DAC 150.1 FVZ-K (Hauschild GmbH & Co.KG, Hamm, Germany) at 2000 rpm for 15 seconds. For the plates manufactured to study the effect of surfactant and water after the curing of the adhesive, after these steps the adhesive was introduced in the mold, as described below. However, when the effect prior to curing was the object of study the process is more complex. The mass of contaminant desired is introduced in the mixture (since the mass of the uncured adhesive plate is 50 g, for the 2% of contaminant 1 g is added, 2.5 g for 5% and 5 g for 10%) and is mixed for an additional 5 seconds at the same speed.

The adhesive plate was manufactured following the French NF T 76-142 standard [31]. The process consists on introducing the adhesive on a mold lined with a silicone frame with the thickness desired for the plate. The frame ensures hydro-static pressure and this process decreases the amount of defects found in the final specimen. Afterwards, the mold is placed on a hot plates press following the curing cycle required to cure the adhesive.

Plates with thicknesses of 2 mm and 1 mm were produced. The 2 mm thick plates were utilized for the DMA of the neat adhesive and bulk tensile tests, FTIR and SEM analysis where contaminant was added prior to the adhesive curing. The 1 mm thick plates were used for the gravimetric analysis and bulk tensile tests performed after water immersion. The main purpose of the 1 mm thick specimens for these two procedures is the reduction of the immersion temperature required to fully saturate the specimen.

2.2.1 Dynamic mechanical analysis (DMA)

DMA was conducted with the neat adhesive after manufacturing, i.e., without the introduction of water or contamination either prior to curing or after curing. For this, 2 mm thick specimens with 6 by 20 mm were prepared from the plates previously manufactured.

2.2.2 Gravimetric study

In the plates used for the gravimetric study, the thickness must be significantly smaller than the other dimensions so that is represents the preferential water uptake direction. The specimens used were square plates with a side length of 30 mm, since in previous work by the same authors [32] it has been determined that this size gives the same diffusion curve as the plates with side length of 60 mm that follow the ISO 294-3 standard [33] with a smaller material waste and higher storage capability when immersed in water.

2.2.3 Bulk tensile tests

Bulk tensile test specimens were cut using a punch-matrix system from the previously manufactured adhesive plates. The specimens were reduced scale, Figure 1, since they have been known to accurately represent the tensile behavior of polymeric materials [32]. These reduced scale specimens are easier to store in water and decrease the overall extension imposed to the testing machine, since this silicone is a very resilient material.

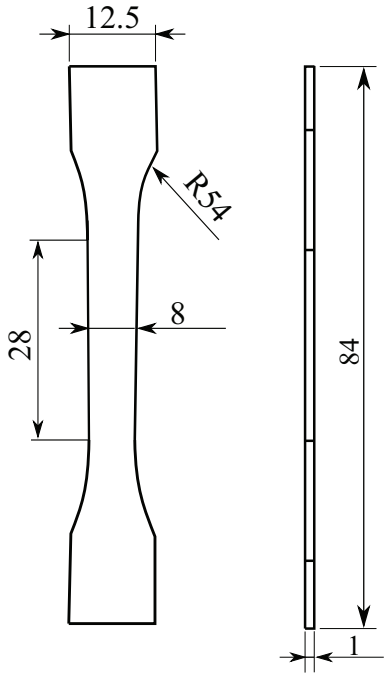


Figure 1: Reduced scale specimens used for bulk tensile testing.

2.2.4 Fourier-transform infrared spectroscopy (FTIR) and scanning electron microscopy (SEM)

FTIR analysis were conducted using the specimens tested in the bulk tensile tests for the correspondent condition, cutting into the specimen to remove the superficial layer of material and, therefore, surface contamination. For the SEM analysis, the fracture surfaces of the specimens after the bulk tensile test were analyzed.

2.3 Testing procedures

2.3.1 Dynamic mechanical analysis (DMA)

The DMA was conducted in a 242 E Artemis (NETZSCH-Gerätebau GmbH) machine scanning a range of temperatures from -110 °C to 130 °C at a rate of 3 °C/min. The material was analyzed for a frequency of 1 and 10 Hz. Three specimens were tested.

2.3.2 Gravimetric study

The gravimetric test has the main purpose of understanding how the contaminant diffuses into the specimen, after adhesive curing.

For the gravimetric analysis, the specimens were, first, dried in silica at 70 °C for two weeks. Afterwards, their mass was measured and this is considered the initial mass, m_0. Afterwards, the specimens were immersed in contaminant in a climatic chamber (Memmert GmbH, Büchenbach, Germany) at the respective study temperature (70, 90 or 130 °C for water and 70 °C for the surfactant). At this point, it is crucial to ensure that the plates are fully covered in the immersion fluid and not in contact with the container or other plates, so that the surface is completely in contact with the surrounding contaminant and the absorption area is not compromised. To ensure the specimens remained under the contaminant, they were attached to 10x10x10 mm^3 stainless steel blocks.

The mass of the specimens was measured periodically until a constant mass value was reached. When that happened, it was considered that the specimen was saturated, i.e., it reaches its maximum contaminant absorption level. When the mass of the specimens was going to be measured, the surface was cleaned with a paper towel just to remove excess fluid at the surface, not intending to remove fluid that may be free in the interior of the material. The mass measurements were conducted using a microbalance with 0.1 mg of accuracy (KernToledo, Balingen, Germany).

The contaminant uptake of the specimens for each time step was determined from:

$$M_t = \frac{m_t - m_0}{m_0} \cdot 100(\%) \tag{1}$$

where m_t is the mass at the time considered.

For the higher temperature, 130 °C it must be noted that, to avoid pressurization of the container, the lid was kept open and the water was added periodically. When adding water it was made sure that only a maximum of 7% (V/V) of the container volume was added in new water to ensure the temperature gradient was not very significant. However, it must be considered that a gradient in temperature can be periodically identified. Additionally, it must be kept in mind that the temperature displayed refers to the temperature of the climatic chamber where the fluid container is placed and, for the higher temperature, it does not coincide with the fluid temperature since the vapor temperature of water is 100 °C. For each condition, at least four specimens were tested.

2.3.3 Bulk tensile tests

The specimens were dried in silica at the controlled temperature (70, 90 or 130 °C), and then tested for the dried condition. Afterwards, they were immersed in water in a climatic chamber at the same temperature until saturation was achieved, and tested for the aged condition. Finally, they were redried at the same temperature and tested for the dried after aging condition. All tests were conducted at room temperature.

Bulk tensile tests were performed using a universal testing machine Instron® 3367, which has a load capacity of 30 kN, at a constant rate of 5 mm/min. Since the specimens are very reduced and thin, the addition of an extensometer would interfere with the results of the test. Additionally, the use of Digital Image Correlation (DIC) measurement required the painting of the specimen prior to the test which, since it is a time-consuming process, in the dried conditions could include ambient water in the specimen and, in the aged condition, could remove water from the specimen. Therefore, the displacement obtained from the grips of the machine was used, after tuning with controlled specimens through DIC to ensure a correct measurement of displacement. For each condition, at least three specimens were tested.

2.3.4 Fourier-transform infrared spectroscopy (FTIR)

FTIR analysis was conducted using a PerkinElmer Spectrum Two machine (Waltham, MA, USA). Wave lengths of 4000–500 cm^{-1} were scanned with intervals of 0.2 cm^{-1} and the tests were carried out in a machine with a KBr window and a $LiTaO_3$ detector (15,700–370 cm^{-1}). The spectra was recorded in attenuated total reflectance (ATR), which establishes spectra equivalent to transmittance. The specimens were removed from water and kept at room conditions for about 30 minutes prior to the performance of the FTIR analysis.

2.3.5 Scanning electron microscopy (SEM)

SEM analysis was conducted on two different microscopes: JEOL JSM 6301F/Oxford INCA Energy 350/Gatan Alto 2500 (Tokyo, Japan) and FEI Quanta 400FEG ESEM / EDAX Genesis X4M (Hillsboro, Oregon, United States). The analysis were carried out at CEMUP (University of Porto, Portugal). The samples were coated with an Au/Pd thin film, by sputtering, for 120 s with a current of 15 mA using the SPI Module Sputter Coater. The specimens were removed from water and kept at room conditions for about 12 hours prior to the performance of the SEM analysis, during this time, the specimens were cleaned using ultrasounds.

3 Experimental results

In this section, the different experimental results for each test are presented and some comments are made about the individual conclusions drawn from them. However, the complete analysis of these phenomena must take into consideration the full scope of tests performed for each conditions, which is presented in the *Discussion* section.

3.1 Dynamic mechanical analysis (DMA)

The DMA results are shown through a representative curve in Figure 2. The two curves represented refer to the same specimen (out of the three tested) for the two frequencies tested, 1 and 10 Hz. The transition temperature obtained, determined from the inflection points of the curves recorded, is at -56.3±0.9 °C, considering both the results for 1 and 10 Hz. This is a value of glass transition temperature (T_g), commonly found for silicones. It can be concluded that on the range of temperatures under analysis (70 to 130 °C) there is no preponderant transition temperature.

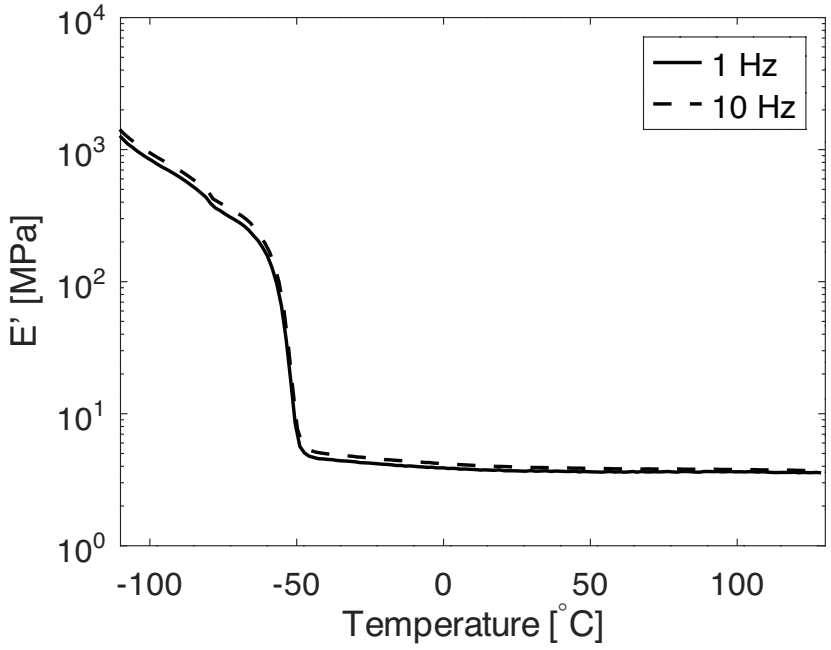


Figure 2: Representative curves obtained for the DMA for the same specimen, registered for 1 Hz and 10 Hz.

3.2 Gravimetric study

3.2.1 Effect of water after curing

The gravimetric study for the silicone immersed in water in a climatic chamber at 70, 90 and 130 °C can be seen in Figure 3.

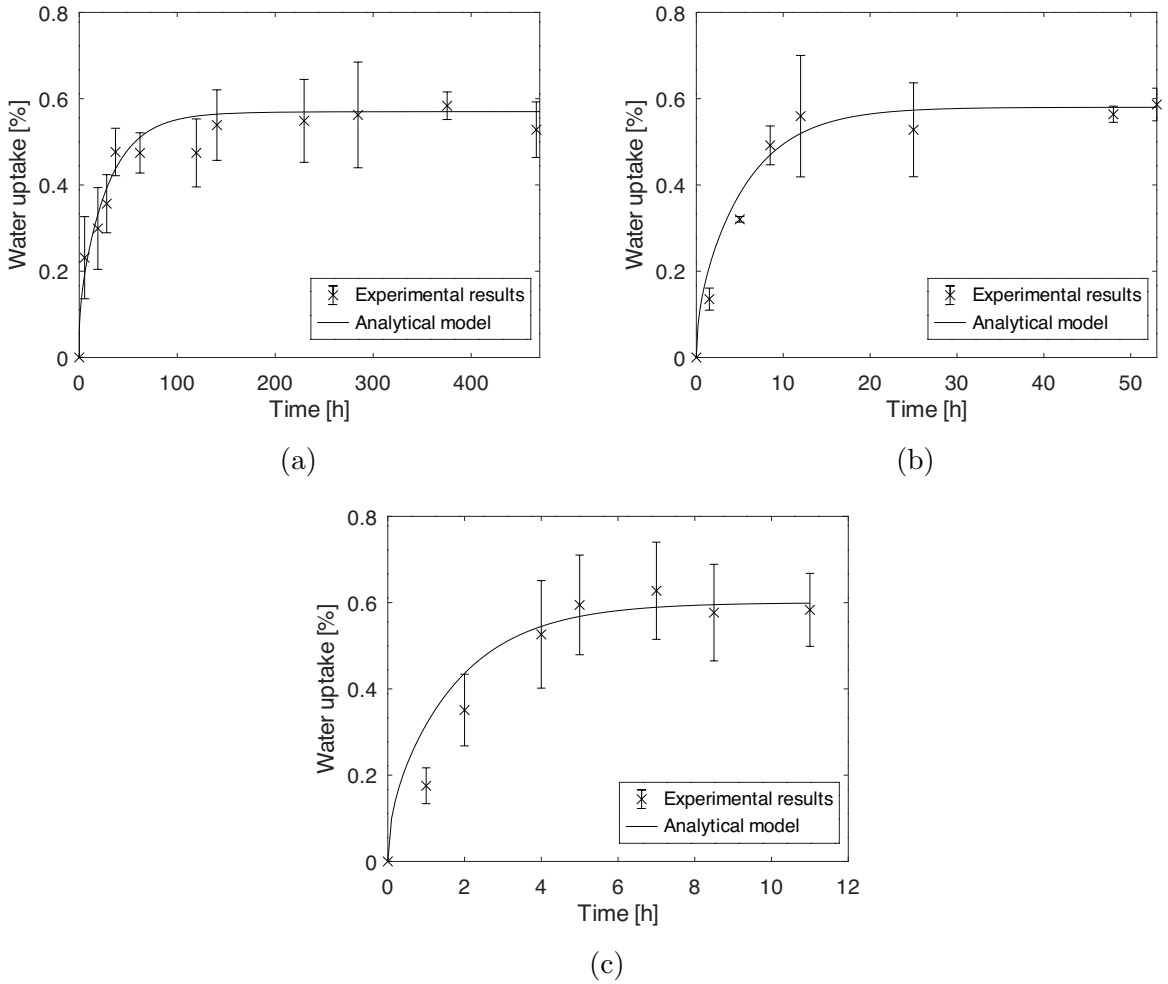


Figure 3: Water uptake as a function of time and respective analytical model following Fick's law of diffusion, for climatic chamber temperatures of 70 °C (a), 90 °C (b) and 130 °C (c).

The analytical model represented is obtained from the second Fick's law of diffusion:

$$M_t = \left[1 - \frac{8}{\pi^2} \sum_{n=0}^{\infty} \frac{1}{(2n+1)^2} \, exp\left(\frac{-D(2n+1)^2\pi^2 t}{4h^2}\right)\right] M_\infty \tag{2}$$

where t is the time (starting from immersion) and h is the thickness of the specimen. The values determined for each temperature are given in Table 1. In this table, as well as for the data treatment of the coefficient of diffusion as a function of temperature, it must be noted that, although the highest temperature of the climatic chamber was 130 °C, the temperature of immersion was 100 °C.

As temperature increases, there is also a slight increase of the maximum water content the silicone can absorb, due to the relaxation of the polymeric chain of the material.

Table 1: Parameters of the Fick's law of diffusion as a function of temperature.

Temperature [°C]	D [m^2/s]	M_∞ [%]
70	$9.1 \cdot 10^{-13}$	0.57
90	$4.8 \cdot 10^{-12}$	0.58
100	$9.8 \cdot 10^{-12}$	0.60

Additionally, it is clear that, as the immersion temperature increases, the coefficient of diffusion also increases. Usually, this increase follows an Arrhenius relation, which is given by:

$$D = D_0 \, exp\left(\frac{-E_A}{RT}\right) \tag{3}$$

where D_0 is the permeability index, E_A is the activation energy for diffusion, R is the universal gas constant and T is temperature. Rearranging the equation:

$$\ln(D) = -\frac{E_A}{R} D_0 \frac{1}{T} \tag{4}$$

Which means that the law that describes D as a function of temperature is approximately a line in a graph where the abscissa axis corresponds to the inverse of temperature and the ordinate axis corresponds to $\ln(D)$, Figure 4.

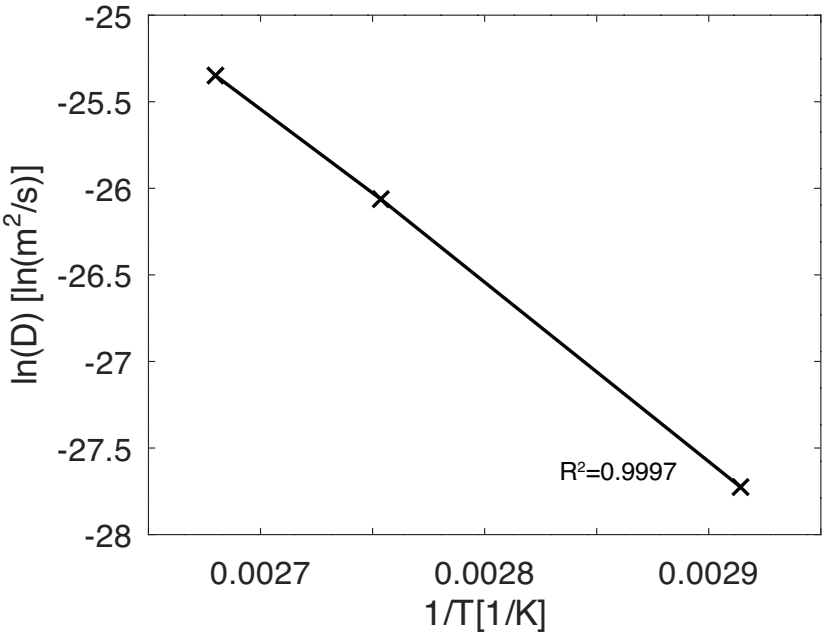


Figure 4: Relation between D and immersion temperature.

3.2.2 Effect of surfactant after curing

The gravimetric study for the silicone immersed in surfactant at 70 °C can be seen in Figure 5.

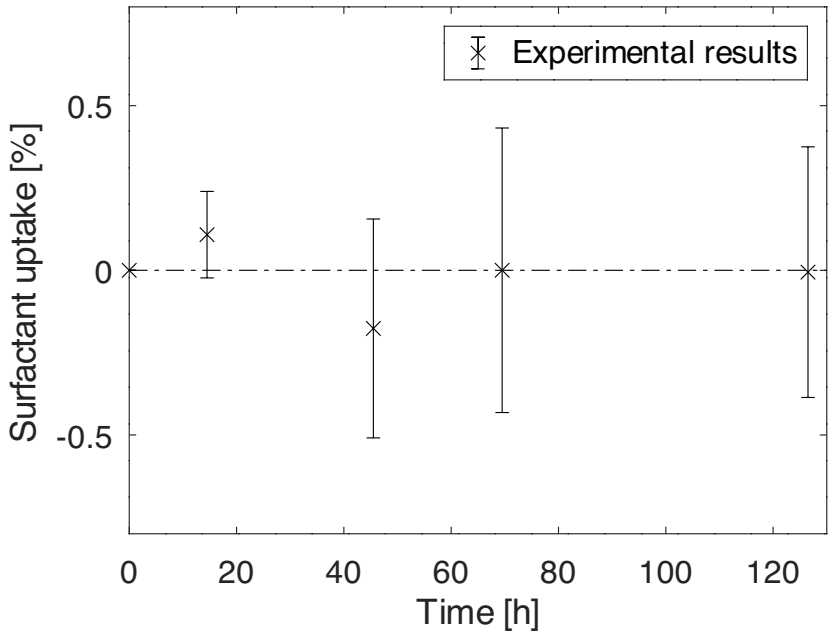


Figure 5: Surfactant uptake as a function of time, for 70 °C.

The average mass of the specimen is approximately the same along the time period analyzed. However, there is a high standard deviation, which is related to the contaminant that remained on the surface of the specimen after cleaning lightly with a paper towel and, in other time increments, a more careful surface cleaning of the specimen led to lower mass recorded. This means that there may be a small amount of surfactant being absorbed by the silicone. However, this effect is not detectable thorough a gravimetric test. Nonetheless, since the results show that, on average, there is no surfactant ingress on the material, the mechanical and chemical analysis of the silicone after immersion in contaminant are not going to be carried out.

3.3 Bulk tensile tests

Bulk tensile test results are going to be divided according to what they aim to analyze. The effect of water prior to curing was evaluated by mixing water into the adhesive before curing, the same is valid for the surfactant. The effect of water after curing was evaluated from the specimens immersed in water in a climatic chamber at 70, 90 and 130 °C.

3.3.1 Effect of water after curing

The representative curves for the three humidity conditions tested (dried, saturated and dried after saturation) at the three different climatic chamber temperatures (70, 90 and 130 °C) are shown in Figure 6.

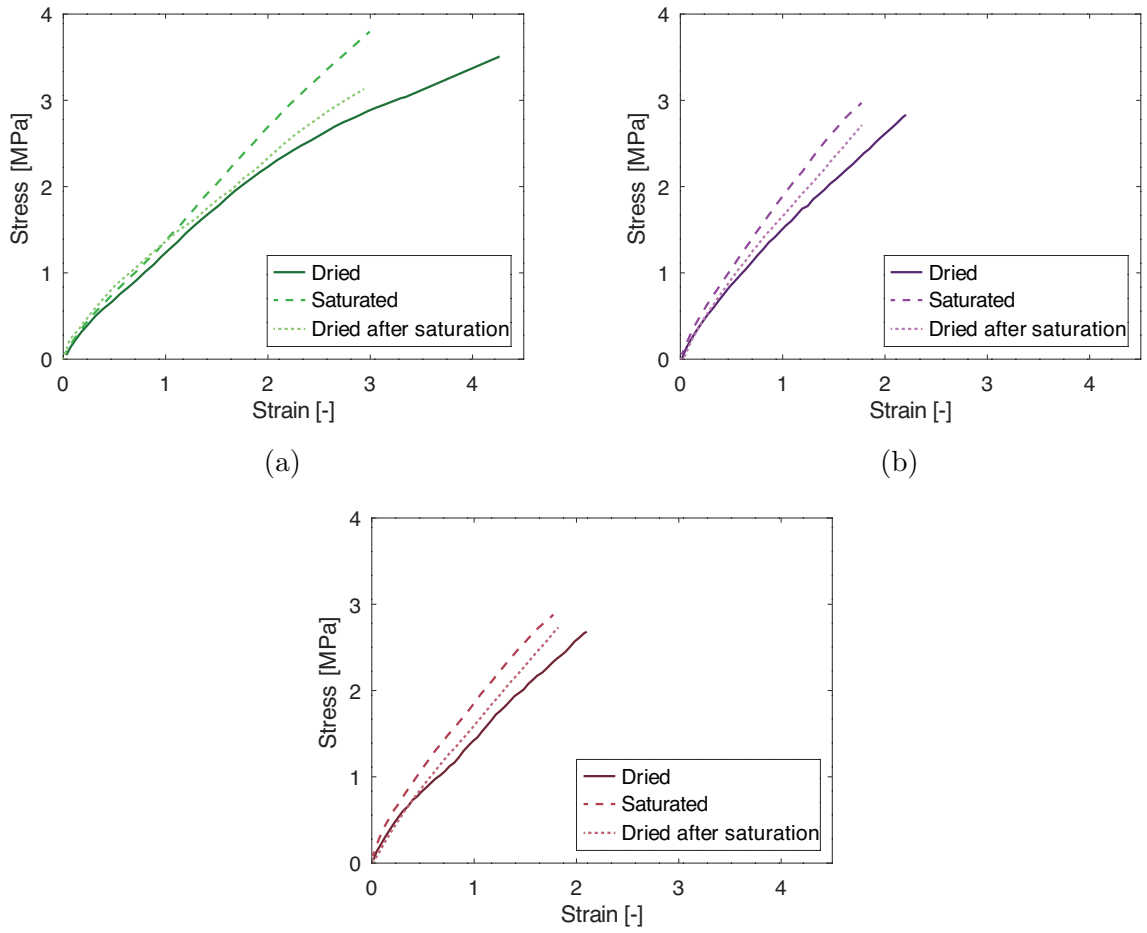


Figure 6: Representative stress-strain curves after the specimens are subjected to drying, saturation and drying after saturation at climatic chamber temperatures of 70 °C (a), 90 °C (b) and 130 °C (c).

The results for each temperature and condition are fairly similar, with the aged condition with a slightly higher strength, which is similar to the results obtained by Fan et al. [21] The same results were disclosed in the work of other authors, such as Pan et al. [34] which alerts that, as the adhesive gets stiffer with aging time, it can cause reliability problems in the joint due to stress concentrations. This increase in strength and stiffness after exposure to water or high humidity environments has been attributed to a completion of their cure process when exposed to there environments [35].

Kochanke et al. [36] did an extensive study using an addition curing silicone, such as the one used in this work, without the addition of adhesion promoters. In this work, it was concluded that immersion in water can further increase cross-linking density of the polymer, related to the consumption of excess Si-H groups, generally found in their formulation. This phenomena would justify an increase in stiffness and could explain an increase in strength. However, this work reports an increase in stiffness but not strength. No tests were performed after the material was redried, however, if the explanation of further cross-linking is correct, the increase in stiffness should remain the same.

Comparing the strength of the tree conditions at each temperature tested, Figure 7, it is possible to infer that strength slightly increases when the material is immersed in water (from the dried to the aged condition), being restored when the specimen is dried,

which would not confirm further cross-linking. However, this change would have to be confirmed for instance by periodically testing specimens during its water absorption and desorption or increasing the number of specimens tested.

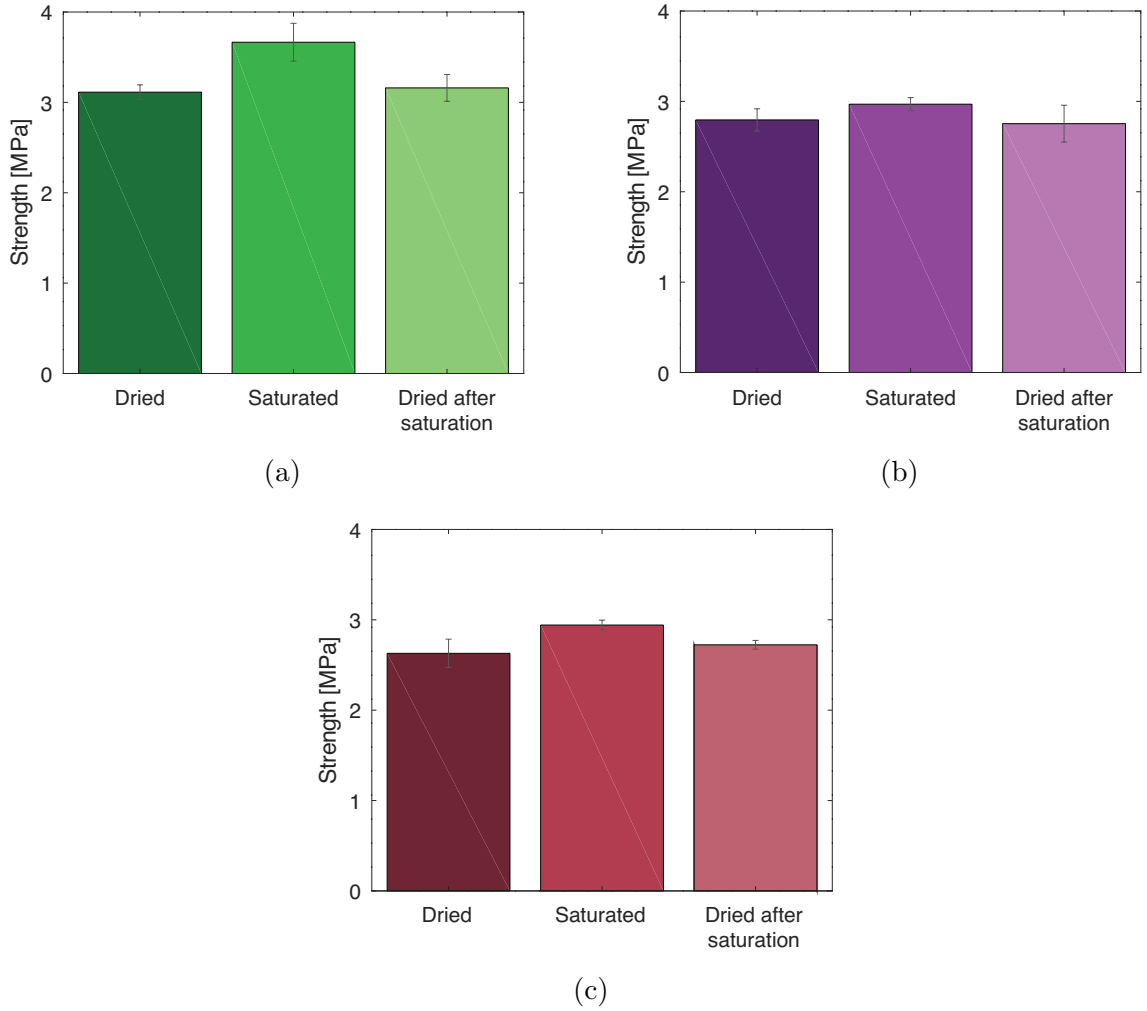


Figure 7: Strength of the specimens dried, saturated and dried after saturation for each climatic chamber temperature: 70 °C (a), 90 °C (b) and 130 °C (c).

Comparing the strength for the three different temperatures for each condition tested, Figure 8, for the dried condition strength decreases with increasing temperature and, for the other conditions it decreases from 70 °C to the other temperatures, being similar between chamber temperatures of 90 and 130 °C. It must be recalled that the tests were not performed at the temperatures indicated, but at room temperature after drying, saturation and redrying at those temperatures. Therefore, it can be considered that the damage introduced to the material slightly increases as the temperature to which it was subjected also increases.

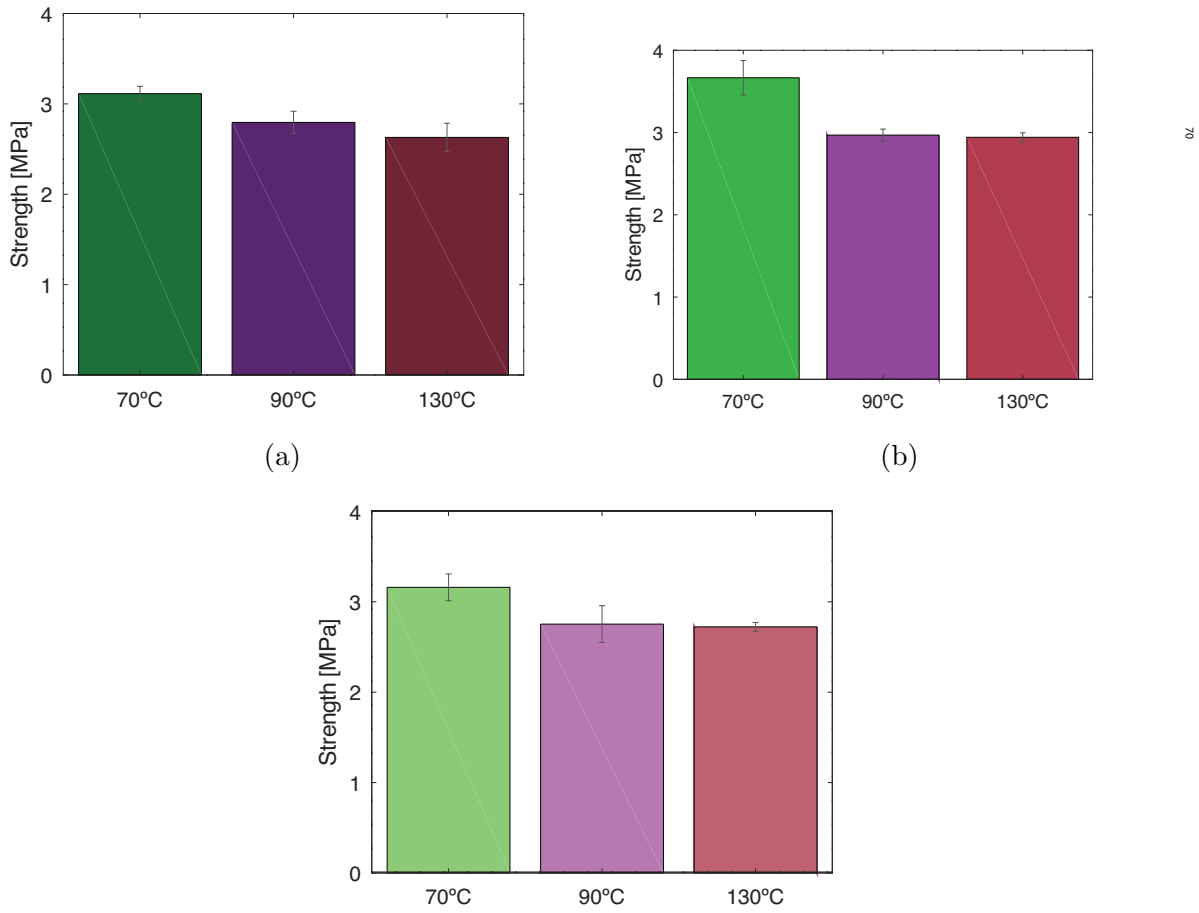
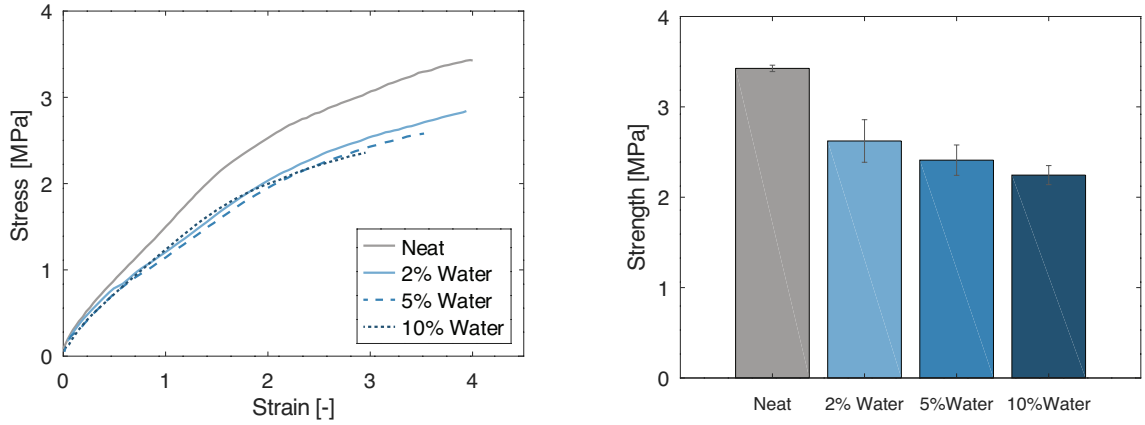


Figure 8: Strength of the specimens at climatic chamber temperatures of 70 °C, 90 °C and 130 °C for each condition: dried (a), saturated (b) and dried after saturation (c).

3.3.2 Effect of water prior to curing

Representative stress-strain curves of the material as a function of the amount of water added prior to curing, as well as the strength for the different conditions analyzed can be seen in Figures 9a and 9b, respectively.



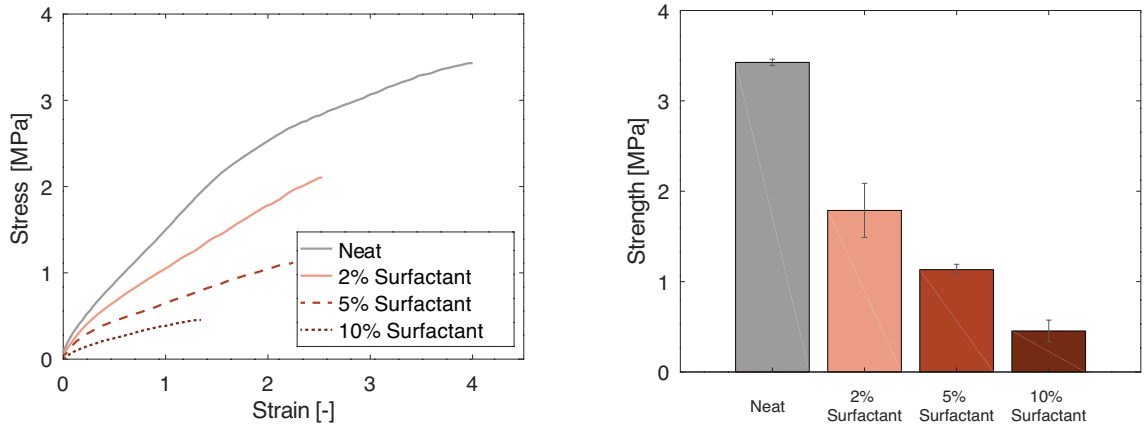
(a) (b)

Figure 9: Representative stress-strain curves for the adhesive with addition of water prior to curing (a) and strength for the different amounts of water added (b).

The strength, as shown, decreases as the water content added to the mixture prior to curing increases. However, the stiffness is lower than for the neat adhesive, but very similar between the specimens with water. Therefore, it may lead to the conclusion that, although there is degradation of the mechanical properties due to the inclusion of water, it does not change the properties of the material matrix itself. The strength and stiffness decrease as water is included but between the conditions with water, strength appears to decrease only due to an increase in the amount of voids added.

3.3.3 Effect of surfactant prior to curing

Representative stress-strain curves of the adhesive with surfactant added prior to curing and strength for the different amounts of surfactant are shown in Figures 10a and 10b, respectively.



(a) (b)

Figure 10: Representative stress-strain curves for the adhesive with addition of surfactant prior to curing (a) and strength for the different amounts of surfactant added (b).

Unlike what was observed for the addition of water, with the addition of surfactant the decrease in strength of the specimens is accompanied by a decrease in stiffness, which

leads one to believe that there is a morphological or chemical variation of the material, both of which are going to be analyzed through SEM and FTIR.

3.4 Fourier-transform infrared spectroscopy (FTIR)

3.4.1 Effect of water after curing

The effect of water after curing of the adhesive was analyzed form the FTIR profile of specimens dried after saturation at the three different immersion temperatures analyzed, Figure 11.

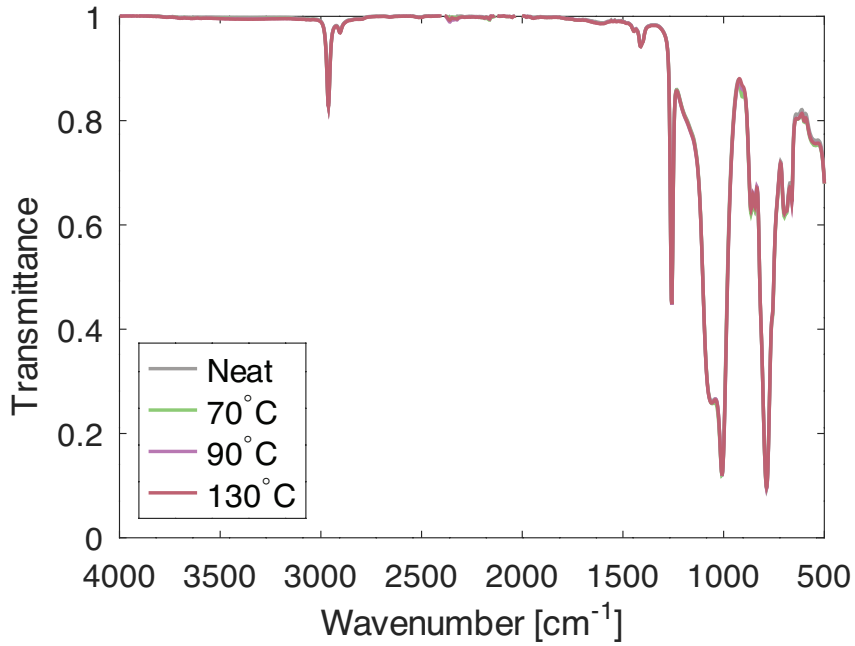


Figure 11: Representative curves obtained for the FTIR analysis of the specimens immersed in water, dried after saturation as a function of immersion temperature.

From the curves presented, it is clear that, for all immersion temperatures, there is no irreversible chemical damage introduced to the material, since the profiles after aging perfectly overlap with the profile of the neat adhesive. Which means that, after water immersion at the three temperatures, the material retains its initial chemical structure.

3.4.2 Effect of water prior to curing

The chemical profiles, obtained from FTIR, of the material with water added in different quantities are presented in Figure 12 and compared to the neat adhesive.

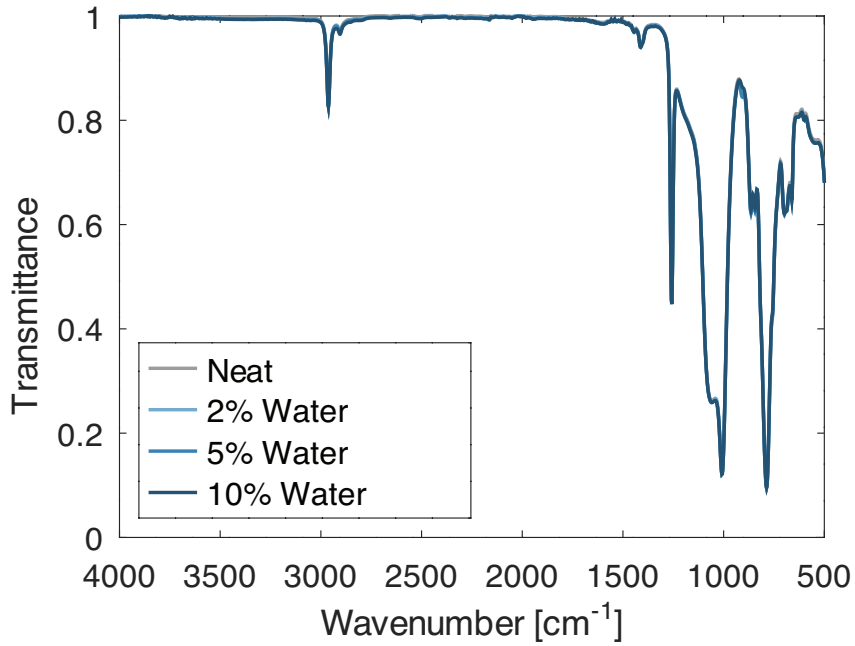


Figure 12: Representative curves obtained for the FTIR analysis as a function of water added prior to curing.

It can be concluded that the chemical profile of the material does not change when water is introduced prior to curing, which means that, as predicted, water does not form chemical bonds with the adhesive and it does not appear to influence the curing of the adhesive. From Figures 11 and 12 it can be seen that either in the case where water is added prior to the curing of the adhesive or after it is cured, no changes occur in the FTIR profile of the material, since they all the curves overlap with the "Neat" one.

3.4.3 Effect of surfactant prior to curing

The FTIR profiles of the neat adhesive and adhesive with different quantities of surfactant added can be seen in Figure 13.

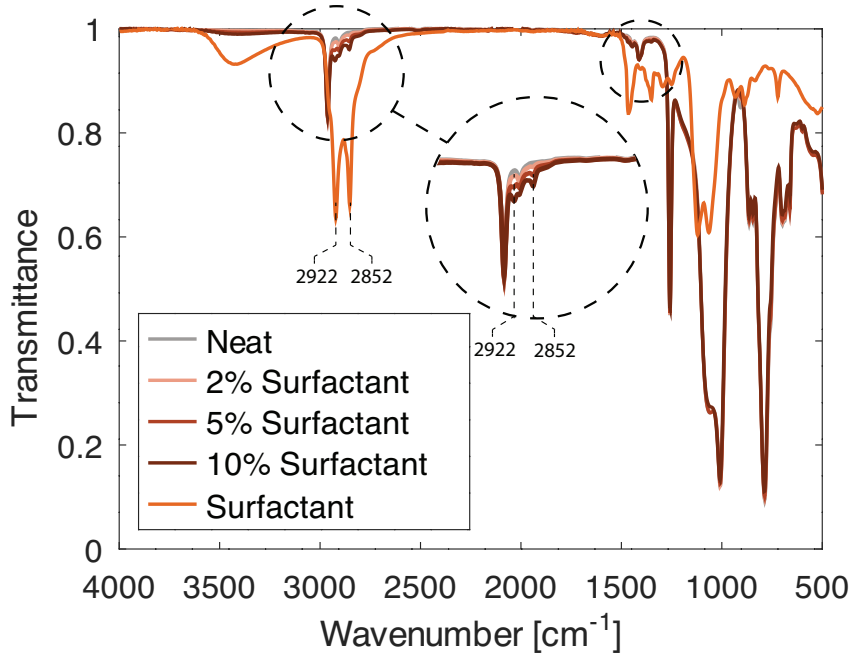


Figure 13: Representative curves obtained for the FTIR analysis as a function of surfactant added prior to curing.

The profile of the contaminant exhibits two peaks at around 2922 cm^{-1} and 2852 cm^{-1}, which could be assigned to C-H bonds and their stretching vibrations. And, as the amount of contaminant added to the adhesive increases, small peaks appear in the profile of the adhesive at the same wavenumbers. In agreement with this, the absorption at about 1450 cm−1 increases, which can be assigned to associated bending vibrations for C-H. The peak associated with stretching vibrations is more pronounced since its absorption coefficient is larger than those of the corresponding bending vibrations. The fingerprint region, from about 900 to 1300 cm^{-1} remains unchanged. The recorded IR spectra can be described as a (concentration-dependent) addition of the two starting materials silicone adhesive and contaminant. Neither newly appearing absorption bands nor the disappearance of existing absorption bands were observed. Therefore, it can be assumed that the contamination is incorporated into the adhesive bulk without significant interactions occurring.

Considering the peaks that increase in the adhesive as the amount of contaminant increases, Figure 14 , it is clear that its increase follows a linear relation, both for 2922 cm^{-1} and 2852 cm^{-1}, with a correlation coefficient of 0.9863 and 0.9971, respectively. It must be considered that the increase in the peak is related to a decrease in the value of transmittance.

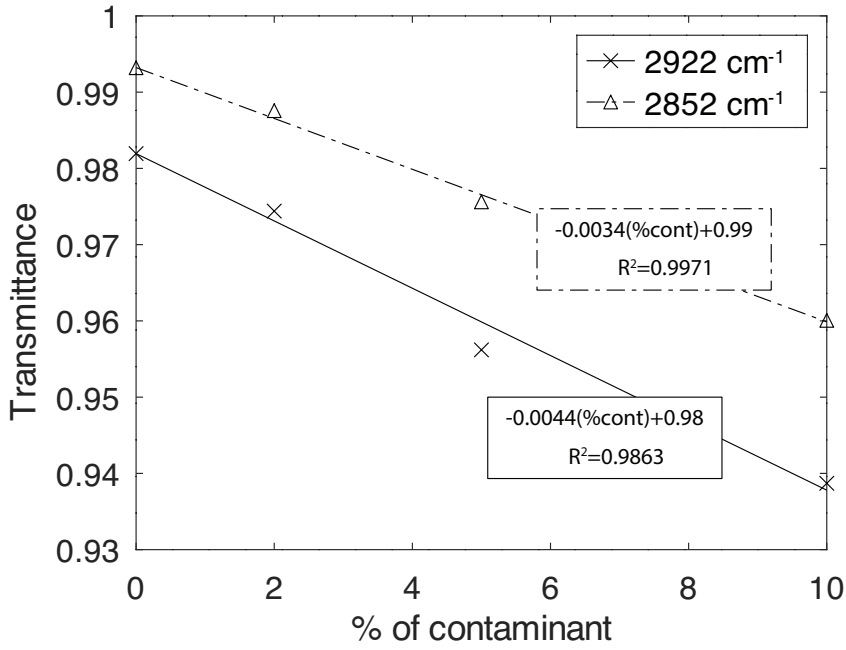
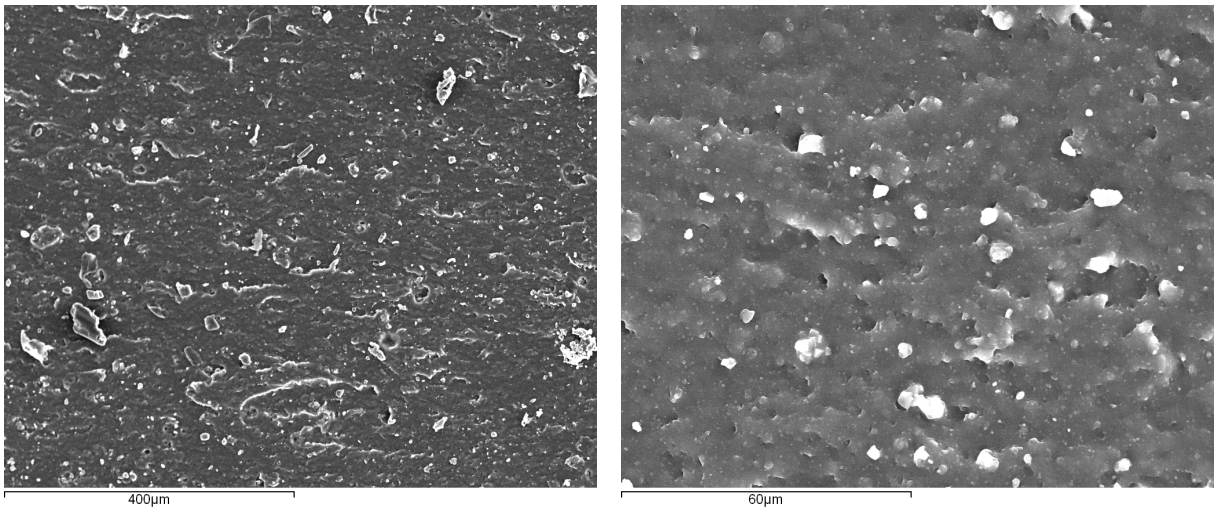


Figure 14: Relevant peaks obtained for the FTIR profile as a function of the amount of contaminant.

3.5 Scanning electron microscopy (SEM)

The SEM images of the neat adhesive, without the addition of water or surfactant, are shown in Figure 15.



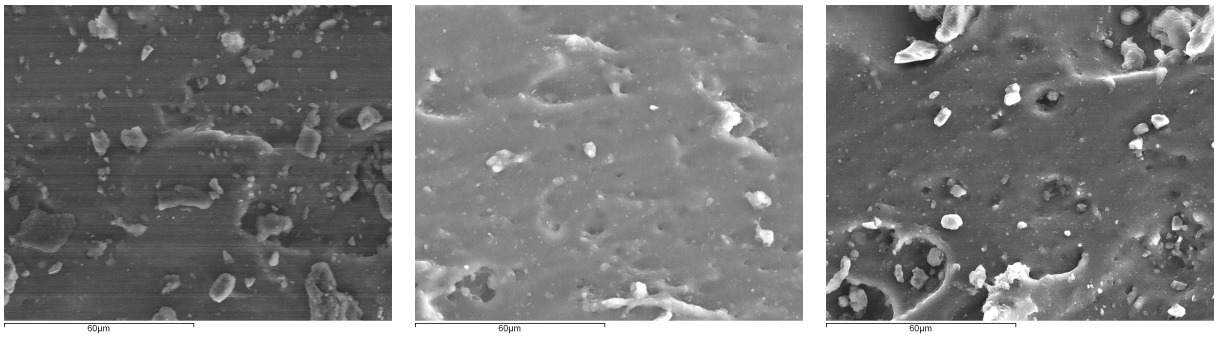
(a) (b)

Figure 15: SEM image of the neat adhesive with lower (a) and higher (b) magnification.

This surface is typical of silicone materials, and is going to be used as a reference surface then compared to contaminated conditions, either after curing of the adhesive or prior to curing.

3.5.1 Effect of water after curing

The fracture surfaces of the specimens that were immersed in water after the curing of the neat adhesive are shown in Figure 16.



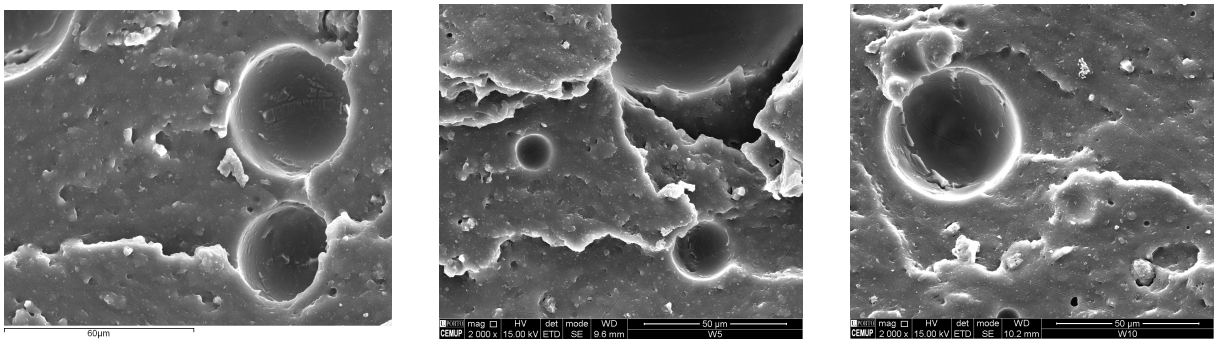
(a) (b) (c)

Figure 16: SEM image of the adhesive after water immersion at climatic chamber temperatures of 70 °C (a), 90 °C (b) and 130 °C (c).

The fracture surfaces of the material appear to be increasingly smoother from neat adhesive to the adhesive immersed at climatic chamber temperatures of 70 °C, 90 °C and finally 130 °C. However, the morphology of the material does not change abruptly from the neat condition, prior to water immersion, to the aged specimens, with the specimen that was saturated at 70 °C being more similar to the neat adhesive than to the other immersion temperatures. This shows that, probably, the main differences denoted for the failure surface are not related to the water ingress but to the temperature at which it happens.

3.5.2 Effect of water prior to curing

The fracture surfaces of the specimens to which water was added prior to curing are shown in Figure 17. It must be noted that, when different machines were used to obtain the SEM images, the magnification were adapted to the focal length so that the images between machines are easily comparable.



(a) (b) (c)

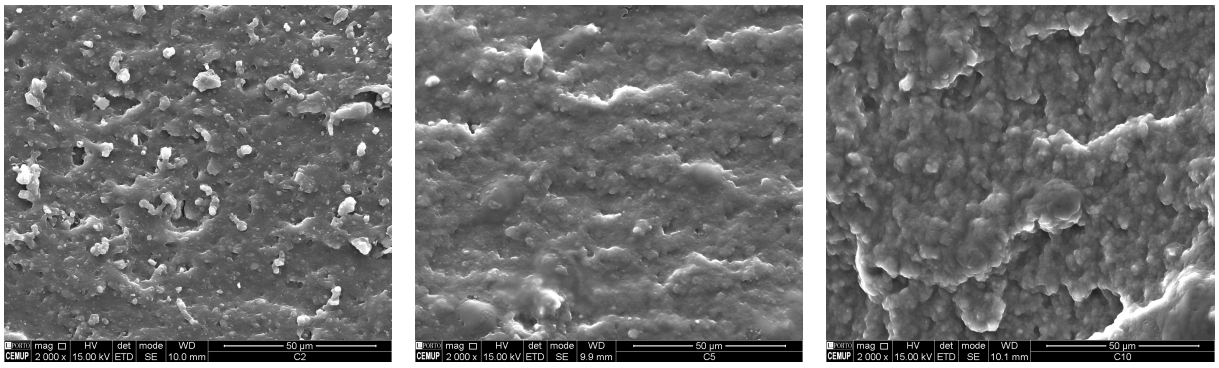
Figure 17: SEM image of the adhesive with the addition of 2% (a), 5% (b) and 10% (c) of water prior to curing.

With the addition of water to the adhesive prior to curing, the matrix of the adhesive is very similar to the neat adhesive and the same for the three amounts of water included.

However, as water is added, it goes to specific locations in the adhesive and, as the temperature is raised to 120 °C to cure the adhesive, the water evaporates and forms voids. These voids induce fracture of the specimen by perforation through the voids, evidenced by the fracture surfaces passing through them.

3.5.3 Effect of surfactant prior to curing

The fracture surfaces of the specimens to which surfactant was added prior to curing are shown in Figure 18.



(a) (b) (c)

Figure 18: SEM image of the adhesive with the addition of 2% (a), 5% (b) and 10% (c) of surfactant prior to curing.

It is clear that the morphology of the adhesive changes from the neat condition to the contaminated ones, with a change intensification increasing surfactant content, which is also an indicator of chemical changes in the structure of the adhesive.

4 Discussion

4.1 Effect of water after curing

The gravimetric studies performed, Figure 3, exhibit that the coefficient of diffusion increases with increasing temperature, which was attributed to the relaxation of the polymeric chain at higher temperatures, and also explains the increase in maximum water uptake. However, from the FTIR analysis, Figure 11 it was seen that there is no change in the chemical profile of the adhesive, particularly in the region associated with OH^- bonds, indicating that water was absorbed as free water, and did not establish chemical bonds with the adhesive. From the bulk tensile tests, Figures 6 and 7, it was observed that strength increased slightly, for all temperatures analyzed, as the specimens were aged. However, the increase was reversed as the specimens were redried.

From the data collected, its can be concluded that the changes introduced by water to the silicone adhesive are reversible, not changing the chemical profile or irreversibly damaging the material. Hoque et al. [37] studied the water absorption and desorption of pure silicone and silicone with phosphorous and concluded that the water absorbed by the material was fully removed upon redrying.

From the work of Kochanke et al. [36] it was concluded that water uptake further increases cross-linking of the silicone, which would result in an increase in stiffness and

possibly strength. However, since when redrying the specimens the mechanical properties were restored, a higher cross-linking density cannot be reported in the present work. The slight increase can be attributed to the water absorbed slightly toughening the very flexible structure of the silicone, but this would have to be confirmed by further mechanical and chemical testing. Additionally, further cross-linking could result in an increase in stiffness, particularly at the highest temperatures, for longer immersion times.

The SEM images of the fracture surface of the specimens tested after saturation, Figure 16, appear to be smoother with increasing immersion temperature. Additionally, for all conditions tested (dried, saturated and dried after saturation), strength decreased with the increase of the temperature to which the material was subjected, Figure 8. Combined with the conclusion that the effect produced on the material by water is reversible, these results show that exposure to high temperatures has an effect on the strength and failure surface of the material.

4.2 Effect of water prior to curing

The introduction of water to the adhesive prior to curing of the adhesive decreases its strength and stiffness, Figure 9a. However, the stiffness appears to be fairly insensitive to the amount of water added and the decrease in strength between the specimens with water addition is not very pronounced, although there is a clear decreasing trend with increasing water content mixed.

From the SEM analysis, Figure 17, it was shown that when water is added to the silicone adhesive prior to curing, it segregates in preferential locations, evaporating as the adhesive temperature is increased and forming voids. However, it does not appear to establish chemical interactions or damage the surrounding adhesive. The analysis of the FTIR profile of the silicone with different amounts of water added, also compared against the profile of the neat adhesive, Figure 12 showed that the water inclusion did not change the molecular structure of the material, which corroborates the conclusion that there is no expressive interaction between the silicone matrix and segregated water during the curing and cross-linking of the adhesive. This explains the results found for the bulk tensile tests, since it shows that the increase in the amount of water added to the adhesive only contributes to a higher unoccupied volume of adhesive, with the voids acting as a punched volume, causing the adhesive to fail progressively earlier with increasing water content, although the stiffness is similar.

Although the water prior to curing does not have a severe impact on the mechanical properties of the adhesive, the appearance of voids during curing and its presence during the service life of an adhesive bond, could lead to a higher water uptake through the pores of the material or even positioning of the voids close to the interface, enhancing the water absorbed between adhesive and substrate and causing failure of the joint.

4.3 Effect of surfactant prior to curing

The introduction of surfactant prior to the curing of the adhesive showed a severe impact on the mechanical properties of the silicone, translated both in a decrease of stiffness and strength, Figure 10a. From the FTIR profile, Figure 13, it was seen that the contaminant inclusion contributes to an increase of the amplitude of vibration of the C-H bond, also detecting changes in the vibration of the bond angle. This implies that, as the surfactant is added to the adhesive, its chemical instability increases, changing the

cross-linking reactions and resulting in weaker adhesive. If the surfactant content was progressively increased to more than 10%, it is expected that it would reach a concentration at which the silicone would not cure. From the SEM analysis, these conclusions were supported, since a change in the molecular structure of the adhesive is expected to promote a difference in the morphology of the material, exposed in Figure 18.

These findings lead to the conclusion that, if surfactant contamination is found at the substrates prior to bonding, it could not only lead to a physical separation between the adhesive and substrate, resulting in a weaker bond, but also, even if removed from the interface by adhesive absorption, lead to an interphase much weaker that the neat adhesive at the middle of the overlap. Which would prevent adhesive failure, but would contribute to a failure close to the substrate at a load level much lower that predicted from the neat adhesive properties.

5 Conclusions

The main conclusions drawn from this work are that:

- When water is absorbed by silicone adhesives after aging, it contributes to a slight increase in strength and stiffness of the material. However, there is no change the chemical profile of the material;

- The increase of temperature at which the specimens are dried and aged decreases its strength and changes the morphology of the fracture surface, indicating damaging of the adhesive;

- The presence of water prior to the curing of the silicone adhesive does not cause chemical changes to the adhesive, only contributing to the appearance of voids after curing;

- The surfactant added prior to curing is absorbed by the adhesive during cross-linking, changing the chemical profile of the final adhesive, showed by the difference in the C-H bond;

- The absorption of contaminant during the curing process significantly influences the mechanical properties of the adhesive, decreasing its strength and stiffness and alters its morphology.

Acknowledgments

The author(s) disclosed receipt of the following financial support for the research, authorship, and/or publication of this article: The authors wish to acknowledge and thank the funding and support provided by Robert Bosch GmbH, Corporate Research and Advance Engineering, Renningen. The authors also gratefully acknowledge the funding provided by Fundação para a Ciência e Tecnologia (FCT), Portugal for the Ph.D. Grant 2020.06055.BD.

References

[1] L. F. M. da Silva, A. Öchsner, and R. D. Adams. *Handbook of adhesion technology*. Springer Science & Business Media, 2018.

[2] S. C. Shit and P. Shah. A review on silicone rubber. *National Academy Science Letters*, 36(4):355–365, 2013.

[3] I. Khalilullah, T. Reza, L. Chen, A. K. M. Mazumder, Monayem H., J. Fan, C. Qian, G. Zhang, and X. Fan. In-situ characterization of moisture absorption and hygroscopic swelling of silicone/phosphor composite film and epoxy mold compound in LED packaging. In *2017 18th International Conference on Thermal, Mechanical and Multi-Physics Simulation and Experiments in Microelectronics and Microsystems (EuroSimE)*, pages 1–9. IEEE, 2017.

[4] A. Q. Barbosa, L. F. M. da Silva, and A. Öchsner. Hygrothermal aging of an adhesive reinforced with microparticles of cork. *Journal of Adhesion Science and Technology*, 29(16):1714–1732, 2015.

[5] G. M. S. O. Viana, M. Costa, M. D. Banea, and L. F. M. da Silva. A review on the temperature and moisture degradation of adhesive joints. *Proceedings of the Institution of Mechanical Engineers, Part L: Journal of Materials: Design and Applications*, 231(5):488–501, 2017.

[6] C. S. P. Borges, E. A. S. Marques, R. J. C. Carbas, C. Ueffing, P. Weißgraeber, and L. F. M. da Silva. Review on the effect of moisture and contamination on the interfacial properties of adhesive joints. *Proceedings of the Institution of Mechanical Engineers, Part C: Journal of Mechanical Engineering Science*, 235(3):527–549, 2021.

[7] Richard A. Pethrick. Design and ageing of adhesives for structural adhesive bonding–a review. *Proceedings of the Institution of Mechanical Engineers, Part L: Journal of Materials: design and applications*, 229(5):349–379, 2015.

[8] J. Crank. *The mathematics of diffusion*. Oxford university press, 1979.

[9] A. Malpot, F. Touchard, and S. Bergamo. Effect of relative humidity on mechanical properties of a woven thermoplastic composite for automotive application. *Polymer Testing*, 48:160–168, 2015.

[10] Z. A. Mohd Ishak, T. S. A. Tengku Mansor, B. N. Yow, U. S. Ishiaku, and J. Karger-Kocsis. Short glass fibre reinforcedpoly (butylene terephthalate) Part 1–Microstructural characterisation and kinetics of moisture absorption. *Plastics, rubber and composites*, 29(6):263–270, 2000.

[11] A. Boubakri, N. Haddar, K. Elleuch, and Y. Bienvenu. Impact of aging conditions on mechanical properties of thermoplastic polyurethane. *Materials & Design*, 31(9):4194–4201, 2010.

[12] J. Dai, X. Yao, H. Y. Yeh, and X. Liang. Moisture absorption of filled silicone rubber under electrolyte. *Journal of applied polymer science*, 99(5):2253–2257, 2006.

[13] B. Lutz, Z. Guan, L. Wang, F. Zhang, and Z. Lü. Water absorption and water vapor permeation characteristics of HTV silicone rubber material. In *2012 IEEE International Symposium on Electrical Insulation*, pages 478–482. IEEE, 2012.

[14] S. Fang, Z. Jia, H. Gao, and Z. Guan. Influence of fillers on silicone rubber for outdoor insulation. In *2007 Annual Report-Conference on Electrical Insulation and Dielectric Phenomena*, pages 300–303. IEEE, 2007.

[15] G. Viana, M. Costa, M. D. Banea, and L. F. M. da Silva. Behaviour of environmentally degraded epoxy adhesives as a function of temperature. *The Journal of Adhesion*, 93(1-2):95–112, 2017.

[16] S. Sugiman, A. D. Crocombe, and I. A. Aschroft. Experimental and numerical investigation of the static response of environmentally aged adhesively bonded joints. *International Journal of Adhesion and Adhesives*, 40:224–237, 2013.

[17] Y. Hua, A. D. Crocombe, M. A. Wahab, and I. A. Ashcroft. Modelling environmental degradation in EA9321-bonded joints using a progressive damage failure model. *The Journal of Adhesion*, 82(2):135–160, 2006.

[18] R. S. Ashofteh and H. Khoramishad. The influence of hygrothermal ageing on creep behavior of nanocomposite adhesive joints containing multi-walled carbon nanotubes and graphene oxide nanoplatelets. *International Journal of Adhesion and Adhesives*, 94:1–12, 2019.

[19] J. Zhou and J. P. Lucas. Hygrothermal effects of epoxy resin. Part I: the nature of water in epoxy. *Polymer*, 40(20):5505–5512, 1999.

[20] X. Han, E. Pickering, A. Bo, and Y. Gu. Characterisation on the hygrothermal degradation in the mechanical property of structural adhesive: A novel meso-scale approach. *Composites Part B: Engineering*, 182:107609, 2020.

[21] J. Fan, Z. Wang, X. Zhang, Z. Deng, X. Fan, and G. Zhang. High moisture accelerated mechanical behavior degradation of phosphor/silicone composites used in white light-emitting diodes. *Polymers*, 11(8):1277, 2019.

[22] M. Ali and R. Hackam. Effects of saline water and temperature on surface properties of HTV silicone rubber. *IEEE Transactions on Dielectrics and Electrical Insulation*, 15(5):1368–1378, 2008.

[23] M.-G. Barthés-Labrousse. Mechanisms of formation of the interphase in epoxy-amine/aluminium joints. *The Journal of Adhesion*, 88(8):699–719, 2012.

[24] J. S. Crompton. Interfacial properties and stability in bonded aluminium. *Journal of materials science*, 24(5):1575–1581, 1989.

[25] C. Jeenjitkaew, Z. Luklinska, and F. Guild. Morphology and surface chemistry of kissing bonds in adhesive joints produced by surface contamination. *International journal of adhesion and adhesives*, 30(7):643–653, 2010.

[26] C. J. Brotherhood, B. W. Drinkwater, and F. J. Guild. The effect of compressive loading on the ultrasonic detectability of kissing bonds in adhesive joints. *Journal of Nondestructive evaluation*, 21(3):95–104, 2002.

[27] J. Holtmannspötter, J. V. Czarnecki, and H.-J. Gudladt. The use of power ultrasound energy to support interface formation for structural adhesive bonding. *International journal of adhesion and adhesives*, 30(3):130–138, 2010.

[28] M. Debski, M. E. R. Shanahan, and J. Schultz. Mechanisms of contaminant elimination by oil-accommodating adhesives Part 1: displacement and absorption. *International Journal of Adhesion and Adhesives*, 6(3):145–149, 1986.

[29] S. G. Hong, H. X. Shu, J. J. Lin, and J. D. Young. The effects of a slushing oil on the curing and degradation behavior of an oil-accommodating epoxy adhesive. *Die Angewandte Makromolekulare Chemie: Applied Macromolecular Chemistry and Physics*, 238(1):129–141, 1996.

[30] H. Akiyama, T. Fukata, T. Sato, S. Horiuchi, and C. Sato. Influence of surface contaminants on the adhesion strength of structural adhesives with aluminium. *The Journal of Adhesion*, 96(15):1311–1325, 2020.

[31] NF T76-142. Adhésifs structuraux - Méthode de preparation de plaques d'adhésifs structuraux pour la réalisation d'éprouvettes d'essai de caractérisation. Standard, AFNOR, Laxou, France, November 1988.

[32] C. S. P. Borges, A. Akhavan-Safar, E. A. S. Marques, R. J. C. Carbas, C. Ueffing, P. Weißgraeber, and L. F. M. da Silva. Effect of Water Ingress on the Mechanical and Chemical Properties of Polybutylene Terephthalate Reinforced with Glass Fibers. *Materials*, 14(5):1261, 2021.

[33] ISO 294-3. Plastics — Injection moulding of test specimens of thermoplastic materials — Part 3: Small plates. Standard, International Organization for Standardization, Geneva, CH, March 2002.

[34] Y. Pan, F. Zhu, J. Fan, J. Tao, X. Lin, F. Wang, and L. Shi. Investigation of mechanical properties of silicone/phosphor composite used in light emitting diodes package. *Polymers*, 10(2):195, 2018.

[35] F. de Buyl. Silicone sealants and structural adhesives. *International Journal of Adhesion and Adhesives*, 21(5):411–422, 2001.

[36] A. Kochanke, K. Krämer, C. Üffing, and A. Hartwig. Influence of high-temperature and high-humidity aging on the material and adhesive properties of addition curing silicone adhesives. *International Journal of Adhesion and Adhesives*, 111:102980, 2021.

[37] M. A. Hoque, R. K. Bradley, J. Fan, and X. Fan. Effects of humidity and phosphor on silicone/phosphor composite in white light-emitting diode package. *Journal of Materials Science: Materials in Electronics*, 30(23):20471–20478, 2019.

Appendix D

Paper D

The influence of humidity and immersion temperature on the properties and failure mode of PBT-GF30/silicone bonded joints

Composite Structures 289 (2022) 115421

Contents lists available at ScienceDirect

Composite Structures

journal homepage: www.elsevier.com/locate/compstruct

The influence of humidity and immersion temperature on the properties and failure mode of PBT-GF30/silicone bonded joints

R. Brandão [a], C.S.P. Borges [b], E.A.S. Marques [b,*], R.J.C. Carbas [b], A. Akhavan-Safar [b], F. Schmid [c], C. Ueffing [c], P. Weißgraeber [d], L.F.M. da Silva [a]

[a] Departamento de Engenharia Mecânica, Faculdade de Engenharia (FEUP), Universidade do Porto, Portugal
[b] Instituto de Ciência e Inovação em Engenharia Mecânica e Engenharia Industrial (INEGI), Portugal
[c] Robert Bosch GmbH, Corporate Research and Advance Engineering, Renningen, Germany
[d] Chair of Lightweight Design and Materials, University of Rostock, Germany

ARTICLE INFO

Keywords:
Adhesives
Adhesive joints
PBT-GF30
Silicone
Aging
Moisture
Diffusion
Double cantilever beam
Single lap joint

ABSTRACT

The housing of automotive electrical components are commonly manufactured from polybutylene terephthalate with 30% of glass fiber (PBT-GF30). These housings can be subjected to severe conditions of temperature and humidity that can catalyze the degradation of their properties. In order to connect the different parts of the housing, a silicone adhesive is used, which also serves as a sealant preventing moisture from entering the final component. Therefore, to understand if the joint serves its purpose correctly, the effects of temperature and water uptake in joints with PBT-GF30 substrates and silicone adhesive were studied. Single lap joints (SLJ) and double cantilever beam (DCB) joints were tested at three different temperatures (70, 90 and 130 °C) and in three different conditions (dried, aged in water and dried after aging). To understand if water immersion introduced irreversible damage to the joints, the re-dried condition was also analyzed. The tensile properties of the bulk substrate and adhesive for all conditions were also determined. It has been seen that, generally, since the adhesive has a higher strength when aged, this leads to a better joint performance at this condition. However, at 90 °C and 130 °C there was chemical degradation of the PBT-GF30 after aging, which lead to failure approaching the substrate in those conditions for the SLJ. This was attributed to the release of chemical compounds that stay at the adhesive/substrate interface. In the DCB, since the loading of the substrate is even more severe, there was substrate failure. Finally, a numerical model was created for all conditions tested, which showed that the joints can be simulated by the properties of the bulk adhesive and substrate, showing that the effect of the interface is not preponderant.

1. Introduction

The bonding of two components can be done resorting to several different methods, such as riveting, bolting or welding. However, riveting and bolting require the introduction of holes in the parts being bonded, which is particularly concerning when joining notch sensitive composite materials, and welding requires the local heating of the components, which may introduce a region of degraded properties. Therefore, adhesive bonding is an interesting solution, also creating a more uniform stress distribution and sealing the final bond, specially if silicone adhesives are employed [1].

Silicone adhesives are used for non-structural and semi-structural applications that require flexible bonding, resistance to extreme environments and high durability of the adhesive bond. They showcase extreme flexibility at low temperatures, since their glass transition temperature (T_g) in often below zero. Standard formulations remain flexible up to −60 °C, special one-part formulations (with condensation cure) can go down to −90 °C and special two-part formulations down to −115 °C [2]. Since silicones are often used as sealants, adhesive joints with silicone adhesives are often subjected to humid environments.

The substrates under analysis are manufactured from polybutylene terephthalate with 30% of short glass fibers (PBT-GF30). This material is used in the housings for electronic components used in the automotive industry due to its rapid crystallization and suitable processing characteristics for injection molding, good flow and flexibility [3–5].

Water can diffuse into the adhesive joints through the adhesive, substrate or adhesive/substrate interface. As well as through pores and cracks of the final assembly [6]. Adhesives are usually polymeric materials, which can absorb water as free water, that fills the free

* Corresponding author.
E-mail address: emarques@fe.up.pt (E.A.S. Marques).

https://doi.org/10.1016/j.compstruct.2022.115421
Received 6 August 2021; Received in revised form 7 February 2022; Accepted 22 February 2022
Available online 10 March 2022
0263-8223/© 2022 Published by Elsevier Ltd.

spaces in the polymeric chain, or bound water, which establishes chemical bonds with that chain, causing chemical degradation of the material [7–9]. Water uptake in polymeric materials can usually be described, through water uptake as a function of time, by the Fick's law of diffusion [10–12]. This law is suitable for cases where the diffusion rate is much higher than the relaxation rate of the polymer [13]. However, there are situations for which this law is not suitable. The main factors that benefit a non-Fickian diffusion are the viscoelastic nature of the polymers and cracks that may arise in the material, increasing its free volume and changing the uptake behavior [14]. Other options for laws of diffusion can be the Langmuir model [15–17] and variations of the Fick's law, such as the dual Fick's law [18]. Most diffusion laws used focus on the fact that the material absorbs water and its mass increases. However, it is possible that the compound loses mass due to its dissolution on the immersion environment, in this case, water [19]. In the present study, both the matrix of the substrate and the adhesive are polymeric materials, being the substrate PBT-GF30, and the adhesive silicone.

Borges et al. [20] conducted an extensive study regarding the water uptake behavior of the same PBT-GF30 used in the present study, also investigating how the mechanical and chemical properties of the material are affected by water. Three temperatures were studied (35, 70 and 130 °C) and it was showed that the uptake follows the Fick's law of diffusion, increasing the maximum water absorption, M_∞ with increasing temperature as a result of a relaxation of the polymeric matrix. Regarding, the diffusion coefficient, D, it increased significantly with temperature, following the Arrhenius relation. Similar results were obtained by other authors [21,22]. This phenomenon was linked to the increased energy and motion of the molecules paired with the relaxation of the chain, which increases the diffusion rate. The effect of temperature and water on the mechanical properties of the material was also analyzed by Borges et al. [20] following two different procedures: the specimens prior to moisture aging were tested at controlled temperature and the aged specimens were tested at room temperature after aging at different temperatures. As most polymeric materials, PBT-GF30 significantly decreases its mechanical properties when tested at high temperature. Additionally, it also follows the common trend of decreasing its strength and stiffness with increasing moisture content [1,19,20,23].

For silicones, on the other hand, this is not the case. Oldfield and Symes [24] tested several silicone adhesives in different environments (hot-dry and hot-wet environment), leaving the silicones at different locations on aluminum boxes that allowed free circulation of ambient air around the elastomers but excluded light and rain. The hot-dry place had an annual temperature of 32.3 °C and an annual mean of 43 rainy days, while the hot-wet place had an annual temperature of 28.1 °C and an annual mean of 174 rainy days. The experiment had a considerable period of time (from 2 years up to 20 year) and the authors stated that well-compounded silicone elastomers were mechanically very resistant to hot drying, hot water or tempered environments with some silicones (iron oxide pigmented, heat-vulcanized, dimethyl silicone rubber) exhibiting only reductions of less of 10% in tensile strength, less than 25% reduction in elongation at break and hardness increases of about than 4%, after 20 years of exposure at either site [24]. Fan et al. [25] analyzed the mechanical degradation mechanism of a phosphor/silicone composite over 1008 h of aging at 55 °C, using samples with mass fractions 0% and 10% of phosphor. With aging, the Young's modulus increased for both samples since the moisture permeated into the silicone, the hydrolysis reaction of phosphor powders accelerated the stiffness of the composite.

Although the water immersion of silicones increases its strength, when in a joint it was shown to have an important impact on the decrease of the sealing performance. Wu et al. [26] studied the maximum contact pressure and contact area between silicone rubber and metal surface, conducting compression and hardness tests for several temperatures. The results showed that hardness and compression set increase with aging of silicone rubber. The authors stated that the aging process has a major impact on the sealing performance, with the results indicating that the maximum contact pressure and contact area between silicone rubber and metal surface were significantly reduced after aging, the maximum contact pressure decreasing with increasing aging temperature and 150 °C was the turning point of the aging effect time. In short, the contact area decreased when the aging time and aging temperature increased.

Bowditch et al. [27] stated that when there is water absorption in the joint there can be also chemical degradation of the adhesive, the substrate or the chemical bonds across the interface. The absorbed water often plasticizes the organic adhesives, decreasing its strength. As for the effect of the temperature in the degradation of the material, it is commonly accepted that with increasing temperature there is an increase in the rate of degradation, and, therefore, a decrease in strength and stiffness.

This work aimed to add to the research on joint degradation due to aging, especially since there are not many studies available using silicone adhesives with composite substrates and, since there is chemical degradation of the substrate at temperatures above 85 °C, it is also intended to understand if this chemical change provides further contamination of the interface due to substances that may be released from the substrate when aging.

To understand if the aging creates irreversible effects on the joint, the joints were tested at three different states (dried, aged and dried after aging) at three different temperatures (70 and 90 and 130 °C) to evaluate if they could restore the properties they presented prior to aging, and it was also examined whether this changed with temperature. Single lap joints and double cantilever beam tests were carried out.

Table 1
Strength of the silicone when dried, saturated and dried after saturation at 70, 90 and 130 °C, tested at room temperature [28].

State	T [°C]	Strength [MPa]
Dried	70	3.1 ± 0.1
Saturated	70	3.7 ± 0.2
Dried after saturation	70	3.2 ± 0.1
Dried	90	2.8 ± 0.1
Saturated	90	3.0 ± 0.1
Dried after saturation	90	2.8 ± 0.2
Dried	130	2.6 ± 0.2
Saturated	130	2.9 ± 0.1
Dried after saturation	130	2.7 ± 0.1

2. Experimental details

2.1. Materials

2.1.1. Adhesive

The adhesive used in this study is a commercially available two-component silicone elastomer adhesive, that cures at 120 °C for 25 min. Borges et al. [28] investigated the behavior of this silicone adhesive when dried, saturated and dried after saturation. The properties when dried were determined after drying the material completely at the controlled temperature. The properties when saturated were determined after the specimen was kept in distilled water, at the controlled temperature, for enough time to reach saturation and, the properties dried after saturation were obtained subjecting saturated specimens to a re-drying process in silica at the same temperature. The strength of the material at the different conditions can be observed in Table 1. As for the stiffness, the authors stated that with water intake, the Young's modulus slightly increased.

2.1.2. Substrates

The substrates used in this study are polybutylene terephthalate with 30% short glass fiber (PBT-GF30) and high strength steel. For all states, the general mechanical properties were determined and are presented in the section *Experimental results*.

Table 2
Water uptake properties of the materials previous determined.

Material	T [°C]	D [m^2/s]	M_∞ [%]
PBT-GF30	70	3.90×10^{-12}	0.50
PBT-GF30	130	1.37×10^{-11}	0.50
Silicone adhesive	70	9.1×10^{-13}	0.57
Silicone adhesive	90	4.8×10^{-12}	0.58
Silicone adhesive	130	9.8×10^{-12}	0.60

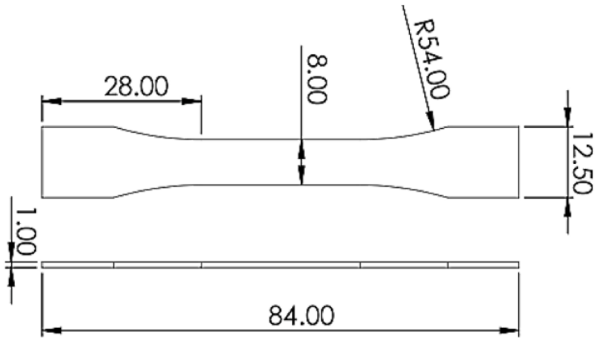


Fig. 1. Schematic representation of the bulk tensile test specimens' geometry, dimensions in mm.

2.2. Specimen manufacturing

2.2.1. Gravimetric analysis

A gravimetric study was conducted on PBT-GF30 substrates at a temperature of 90 °C. Borges et al. [20] conducted a similar study for the temperatures of 70 and 130 °C, which are also the temperatures analyzed in this paper. Similarly, Borges et al. [28] performed the identical study for 70, 90 and 130 °C but for the silicone adhesive of this work. All the values for the coefficient of diffusion, D, and the infinite water uptake, M_∞, are available in Table 2.

Regarding the plates used in this study, 30 × 30 mm^2 and 1 mm thick plates were used. Normally, 60 × 60 mm^2 and 1 mm plates are used, according to ISO 294-3 standard [29]. However, Borges et al. experimentally compared the two geometries and concluded that both had similar diffusion curves [20]. Thus, in order to decrease the amount of PBT-GF30 used, the smaller plates were used.

2.2.2. Bulk tensile tests

To study the effect of water and temperature on the mechanical properties of the PBT-GF30, bulk tensile test were performed for each condition to obtain the Young's Modulus (E), strength (σ) and plastic behavior. However, the standard bulk dogbone specimens have high dimensions, and must be immersed in water, which would require large water containers and long immersion times. Therefore, reduced-scale specimens were used to expedite this process and decrease material and water waste. These specimens were utilized in previous works and were proven to be valid against standard specimens [20,23]. The dimensions of the reduced scale dogbone specimens are shown in Fig. 1.

2.2.3. Single lap joints (SLJ)

Single lap joints with 1 mm thick adhesive and 25 mm of overlap length were manufactured. The adhesive thickness was chosen to mimic that of the housing for electronic components. In order to achieve that, packing shims were used to provide the necessary spacing between the two substrates. The schematic representation of the geometry used based in ASTM D1002 [30] and ISO 4587:1995 [31] standards is shown in Fig. 2. The mold used for the manufacturing is similar to the one used in previous works [32]. The mold was, afterwards, placed in a hot-plates press at 120 °C and 20 bar for 25 min. This ensures both the correct curing and the pressure needed to avoid voids along the overlap, producing good quality joints.

2.2.4. Double cantilever beam (DCB)

The same substrates with 2 mm thickness and 25 mm width were used for the DCBs. The bond line thickness was set at 1 mm with the use of spacers (calibrated metal tape), which were positioned between the substrates prior to the application of the adhesive. To ensure a pre-crack in the adhesive, a 0.1 mm razor blade was inserted mid-thickness. Before testing, stainless steel end-blocks were attached with cyanoacrylate adhesive on each specimen end respecting the ISO 15024 standard, which specifies that the crack-opening mode due to a load applied perpendicularly to the plane of delamination using the DCB specimen can be achieved with the use of hinges or load block [33]. The schematic representation of the geometry of the DCB joints is presented in Fig. 3. The mold used is similar to that of the SLJ, which was also placed in the hot-plates press to ensure the correct curing of the adhesive.

The joints with composite substrates have plastic deformation during testing. Therefore, to accurately simulate the process, the mode I fracture toughness of the adhesive must be determined from standard specimens. To determine that the fracture toughness in mode I, high strength steel substrates were used. The same adhesive thickness of 1 mm was applied, being ensured with the use of spacers. The value of the crack length, a_0 was 45 mm allowing a stable crack propagation. A pre-crack was introduced with a sharp blade positioned mid-thickness. The geometry of the DCB is shown in Fig. 4.

Prior to the application of the adhesive, the joint surfaces of the PBT-GF30 were degreased with acetone while the high strength steel were grit blasted and then degreased with acetone.

2.3. Experimental procedures

All tests were conducted with an *INSTRON*® 3367 universal test machine (Norwood, MA, USA), with a capacity of 30 kN. The tests were performed at room temperature and constant displacement rate of 2 mm/min. At least three specimens were tested for each condition

2.3.1. Gravimetric analysis

Before the immersion in water, the PBT-GF30 specimens were completely dried in silica at RT for two weeks to guarantee that the material does not contain humidity. Afterwards, the surfaces were treated with sand paper to remove any impurities and ensure minimum roughness so that the diffusion behavior is not influenced by the surface. Before immersion, the masses of the specimens were determined. It was ensured that when the specimens were immersed, they were completely submerged in water and the surface was only in contact with water. The water temperature, at 90 °C, was controlled by placing the water container in a climatic chamber (Memmert GmbH, Büchenbach, Germany). The mass was measured periodically until saturation was reached. Before all mass measurements, the specimens were dried with a paper towel to remove excess water from their surface. All mass measurements were performed on a microbalance with 0.1 mg accuracy (KernToledo, Balingen, Germany). The water uptake for each step is determined by:

$$M_t = \frac{m_t - m_0}{m_0} \times 100\ (\%) \quad (1)$$

where m_t is the mass of the specimen at the current step, and m_0 the initial mass. When the water uptake of the specimens reached a stable value, they were considered saturated.

2.3.2. Bulk tensile tests

In this work, bulk tensile tests of the PBT-GF30 were performed in three different states (dried, aged and dried after aging) and at three temperatures (70, 90 and 130 °C). All specimens were placed in a climatic chamber for enough time to reach saturation. This time was determined from the diffusion law previously determined through the gravimetric analysis. To create a uniformly rough surface, the dogbone

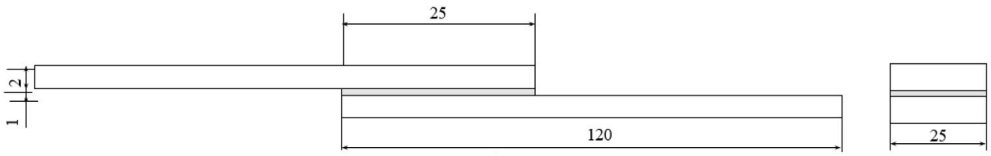


Fig. 2. Schematic representation of the geometry of the SLJs with PBT-GF30 substrates, dimensions in mm.

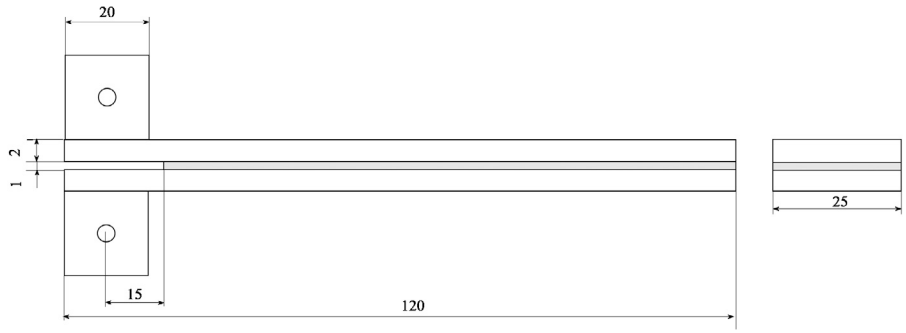


Fig. 3. Schematic representation of the geometry of the DCBs with PBT-GF30 substrates, dimensions in mm.

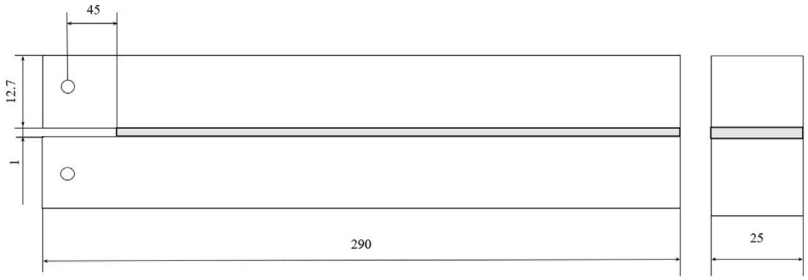


Fig. 4. Schematic representation of the geometry of the standard DCBs with high strength steel substrates, dimensions in mm.

specimens were treated with sandpaper and mass was measured. Prior to testing, they were dried with paper towel. The tests were conducted in ambient conditions, at room temperature. For each test performed, load–displacement ($P-\delta$) curves were obtained up to failure. For each condition, at least three specimens were tested.

2.3.3. Single lap joints (SLJ)

Prior to testing, the SLJ were positioned and secured vertically using two grips (pressure was created using four M6 bolts and applying 20 Nm of torque with a torque wrench). Metal tabs were positioned below one side of each substrate of the SLJs to secure the specimens were horizontal when assembled. In addition, two center pins were utilized during testing to ensure proper positioning of the substrate, as well as to provide greater grip, minimizing or preventing the specimens from slipping. Load–displacement (P-δ) curves were recorded for all SLJs tested, allowing the determination of the tensile strength. For all states, the specimens were kept in the climatic chamber (either in distilled water for the aged condition or in silica for the dried ones) right until the testing procedure.

2.3.4. Double cantilever beam (DCB)

Load–displacement (P-δ) curves were determined for all DCBs with PBT-GF30 substrates tested.

As stated previously, due to the plastification of the PBT-GF30 substrates when in a DCB joint, it was not possible to determine the fracture toughness of the adhesive in mode I using these substrates. Therefore, it was assessed using standard joints with high strength steel substrates. The G_{IC} was determined using the J-integral method. The J-integral, introduced by Rice et al. is a continuous mechanical value that indicates the resistance of a material to crack propagation under a constant stress, and it is a mean of reporting the toughness of the material in geometries containing flaws [34]. It is measured at the onset of fracture and is defined as the critical value of fracture toughness. It has also an excellent applicability for modeling with current finite element modeling tools [35,36].

Defining the energy release rate from the concept of force from beam theory for a DCB [34]:

$$G_{IC} = 12\frac{(P_u a)^2}{E_a h^3} + P_u\theta_0 \tag{2}$$

or

$$G_{IC} = P_u\theta_p \tag{3}$$

where P_u is the load applied per unit length at adjacent extremities, a is the crack length, h is the substrate thickness, E_a is the Young's modulus of the substrate and θ_p is the relative rotation of the substrate at the loadline as shown in Fig. 5.

The J-integral is defined along an arbitrary path surrounding the beginning of the adhesive layer [37]:

$$G_n = \int_0^{\delta_{nc}} t_n(\delta_n)d\delta_n \tag{4}$$

where δ_n and δ_{nc} are the normal opening and the normal end opening of the cohesive law at the tip of the initial crack and t_n is current normal traction. G_{IC} is the value of G_n at the tip of the crack. As for $t_n(\delta_n)$ is obtained by differentiation of Eq. (4) with respect to δ_n, giving the cohesive law [37].

$$t_n(\delta_n) = \frac{\partial G_1}{\partial \delta_n} \tag{5}$$

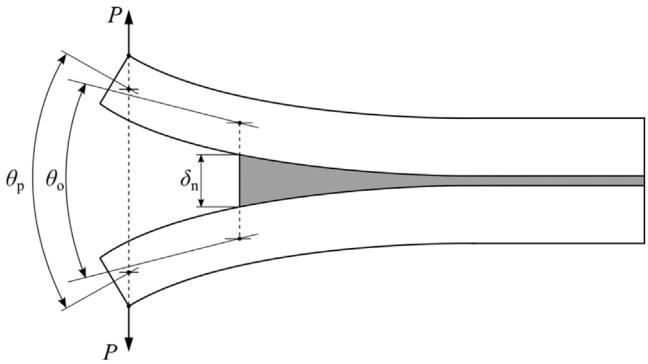


Fig. 5. DCB specimen under loading, with description of the analysis parameters.

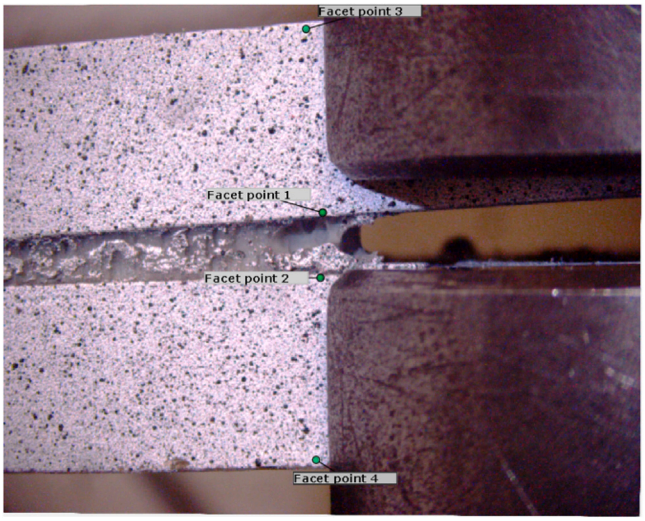


Fig. 6. Points taken by the optical method for measuring θ_p.

For the determination of δ_n and θ_p, a digital image correlation (DIC) software, *GOM*, was used. This software has the ability of following manually defined target points and gives the displacement relative to an imposed coordinate system. This method was previously used by Campilho et al. [38].

The technique used to create the target points consists on painting the specimen with white ink and, afterwards, black ink is carefully sprayed in order to obtain a speckled pattern as is shown in Figs. 6 and 8. Two points (p_1, p_2) were used to obtain the current opening between the two substrates at the crack tip, t_A, and during the upload of the video is defined as (t_A^{CT}). Two points on top of the specimen (p_1, p_3) and two points on the bottom of the specimen (p_2, p_4) were used to obtain θ_p. The points used for one of the specimens in DIC software are shown in Fig. 6. To correspond the points in Figs. 6 and 8, it must be considered that Facet point i corresponds to p_i.

The value of t_A^{CT} in S.I units (mm) is given by:

$$t_A^{CT} = |p1 - p2| \tag{6}$$

and δ_n comes as:

$$\delta_n = t_A^{CT} - t_A \tag{7}$$

where t_A is the initial thickness of the adhesive, which is 1 mm. Therefore, δ_n starts with an initial value of 0.

The relative rotation between two substrates was defined using two vectors u and t using all the four points (p_1, p_2, p_3, p_4). Both vectors are collinear with the top and bottom substrates [39].

$$\vec{u} = (p_{1x} - p_{3x}, p_{1y} - p_{3y}) \tag{8}$$

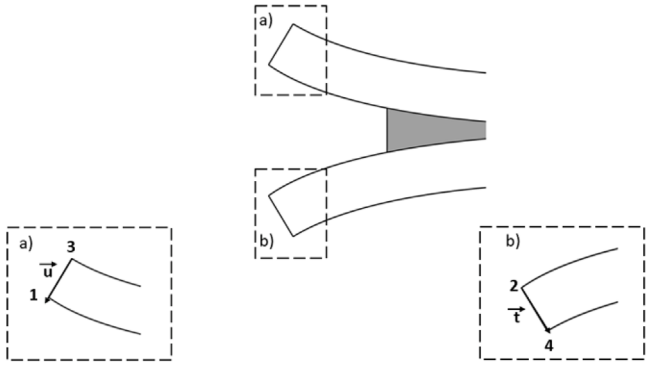


Fig. 7. Vector representation of θ_P determination: top substrate vector u (a), and lower substrate vector, t (b).

$$\vec{t} = (p_{4x} - p_{2x}, p_{4y} - p_{2y}) \tag{9}$$

Fig. 7, shows a vectorial representation of θ_P.

In addiction, in order to relate both vectors, the vector product between the vectors u and t results in the vector$t$:

$$\vec{s} = \vec{u} \wedge \vec{t} \tag{10}$$

and

$$|\vec{s}| = \sqrt{s_X^2 + s_Y^2} = |\vec{u}| \cdot |\vec{t}| \cdot \sin\theta_p \tag{11}$$

So, we can rewrite Eq. (11) in order to θ_p as:

$$\theta_p = \arcsin \frac{|\vec{s}|}{|\vec{u}| \cdot |\vec{t}|} \tag{12}$$

In Fig. 8 is shown a progressive crack growth process in the silicone adhesive.

Calberger et al. studied the effects of temperature and strain rate on the cohesive parameters for an engineering epoxy adhesive and concluded that the fracture energy is shown to be relatively insensitive to the variation in temperature [40]. Gustafson et al. stated that for low values of cohesive strength the model shows to be insensitive to variations of the G_{IC} and, in fact, it is particularly sensitive to the cohesive strength [41]. Therefore, in the numerical models, the G_{IC} of 3.3 N/mm, calculated with high strength steel substrates, was used for all temperatures and conditions, since it can be considered similar in all of them.

3. Numerical model

3.1. Water uptake of the joints

The water uptake of the joints at the moments the joints were removed from water were analyzed, with the main purpose of guaranteeing that, in the aged condition, the same water uptake in the adhesive and substrate was found for all the temperatures.

The water uptake was simulated using *Abaqus 2017*, through a heat transfer analogy. The water uptake is, analogously, temperature and the coefficient of diffusion is the thermal diffusivity. A heat transfer analogy was used instead of the usual mass diffusion simulation because this heat simulation is simpler and more versatile, for instance if the coefficient of expansion with temperature would be of interest to explain how the material swells with water, which does not happen in the case of these materials. It was considered that, when the material was placed under water, the nodes in direct contact with fluid immediately saturate. Therefore, in these nodes, a boundary condition of temperature equal to the maximum water uptake was defined and, the remaining temperature has temperature equal to zero.

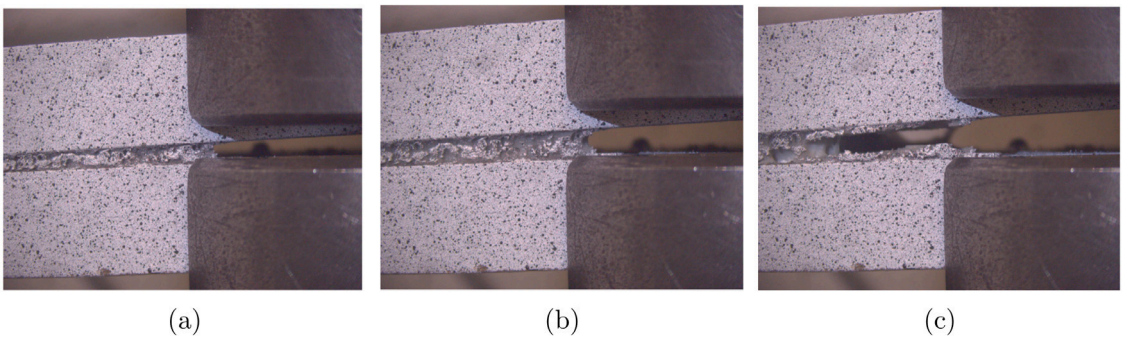


Fig. 8. Crack growth process: initial configuration (a), before the crack progresses (b) and crack propagation (c).

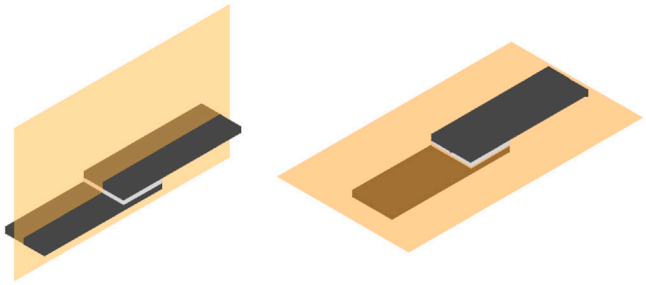


Fig. 9. Schematic representation of the symmetries used to simulate the water uptake of the joint, through the example of SLJs.

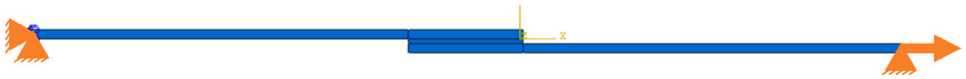


Fig. 10. Schematic representation of the boundary conditions imposed to the SLJ model.

For both joints, only one quarter of the joint was considered, taking advantage of symmetry, as shown in Fig. 9 for SLJs.

After a brief convergence study, the mesh used has cubic elements with a constant side length of 0.5 mm. The elements used are 8-node linear heat transfer bricks (DC3D8). The heat transfer through the adhesive/substrate interface was also considered.

3.2. Double cantilever beam and single lap joints

The FEM analysis was also performed using the software*Abaqus* with the main propose of simulating numerically the joint considering the effect of humidity on the mechanical properties of the bulk adhesive and substrate and understanding if they are similar to those obtained for the experimentally tested joint. The model employed cohesive elements with a triangular (bilinear) traction-separation law, based on the mechanical and cohesive properties of the silicone adhesive and considering the lack of any defect in the interface or within the adhesive layer. The adhesive layer, such as the experimental layer, was model with 1 mm thick cohesive elements.

The strength properties of the substrate and adhesive were set to those obtained from the bulk tensile tests performed for the correspondent tensing condition (dried, aged, dried after aging) and immersion temperature (70, 90 and 130 °C), presented in Table 1 for the adhesive and in the *Experimental Results* for the substrate. Since there is plastic deformation of the substrates, the plastic properties of the PBT-GF30 were also taken into consideration. The fracture toughness in pure mode I (G_{IC}) used was of 3.3 N/mm obtain with the high strength steel DCB. Regarding boundary conditions, in the SLJ FEM model, one of the ends was clamped, restrained in the two directions, while a longitudinal displacement was applied in the other end of the model, restrained in the transverse direction as well, Fig. 10.

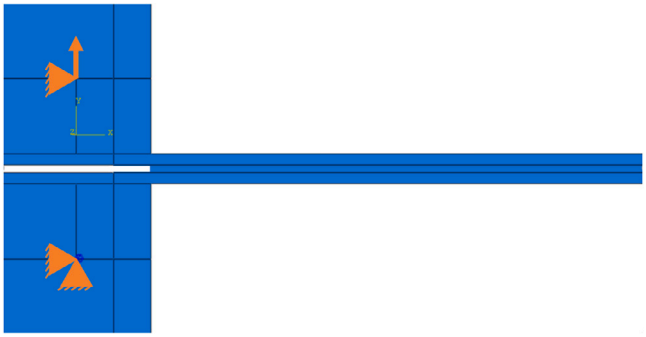


Fig. 11. Schematic representation of the boundary conditions imposed to the DCB model.

As for the DCB model, the node in the middle of the lower steel cube was restrained in the plane, and the node in the middle of the upper cube was held horizontally and pulled vertically, Fig. 11.

For the SLJ model, the size of the mesh was increased in areas away from the ends of the overlap, as the stress gradients are less severe, this technique allows a good compromise between accuracy and computational time. Regarding the elements type, for both models, a 4-node-two-dimensional cohesive elements (COH2D4) were used to define the bondline area, and a 4-node bilinear plane strain quadrilateral, reduced integration, hourglass control element (CPEAR) for the substrates and stainless steel cube. The mesh size of elements in the areas with severe stress was of 0.08 mm, while the cohesive elements were squares with 1 mm of side length. Both meshes are shown in Fig. 12.

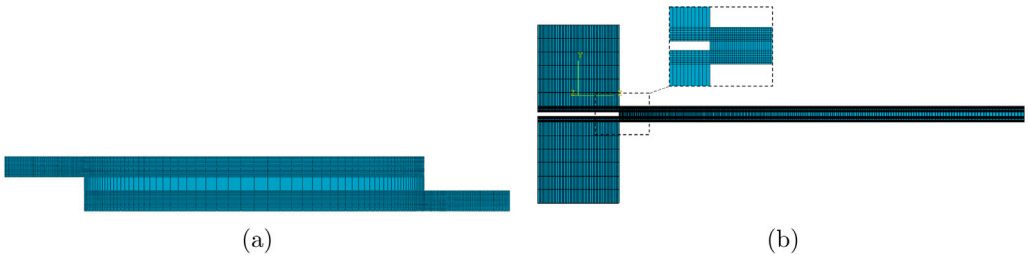


Fig. 12. Mesh used in the numerical models of the SLJs (a) and DCBs (b).

Table 3
Water uptake properties of the PBT-GF30 at 90 °C.

Material	T [°C]	D [m²/s]	M_∞ [%]
PBT-GF30	90	9.50×10^{-12}	0.49

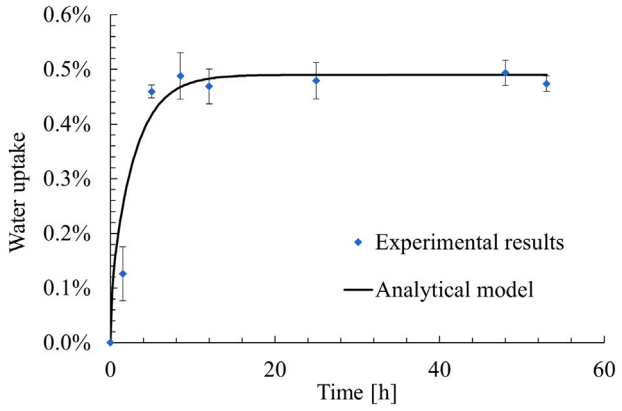


Fig. 13. Experimental results and analytical model of the gravimetric tests of the PBT-GF30 at 90 °C.

4. Experimental results

4.1. Gravimetric analysis

As previously said, the gravimetric study of the PBT-GF30 at 70 °C and 130 °C and of the silicone for all the temperatures under analysis were already done by Borges et al. [20,28]. However, it was still necessary to understand the water uptake behavior or the PBT-GF30 at 90 °C.

After the water uptake was defined for several time increments, to analyze the experimental results, the Fick's law of diffusion was used [10]:

$$M_t = \left[1 - \frac{8}{\pi^2}\prod_{n=0}^{N} exp\left(\frac{-D(2n+1)^2\pi^2 t}{4h^2}\right)\right] M_\infty \tag{13}$$

where t is the time, starting from immersion, and h the thickness of the specimen. Table 3 presents the values for the coefficient of diffusion, D, and the infinite water uptake, M_∞, obtained. The number of terms (N) used in the series expansion of M_t was 50.

The experimental results and analytical curves with the D and M_∞ is shown in Fig. 13.

4.2. Bulk tensile test

The results of the Young's modulus and strength of the different temperatures of the PBT-GF30 bulk tensile tests are showed in the following section.

4.2.1. 70 °C

Fig. 14 shows the strength and Young's modulus of the PBT-GF30 dried, aged, and dried after aging at 70 °C.

For 70 °C it is noticeable that there was a decrease of 26% in strength when aged, in comparison with the dried specimens. However, the PBT-GF30 was capable to recover after re-drying, which indicates that, after immersion at 70 °C, the degradation caused by water intake to the PBT-G30 is reversible. Regarding the Young's modulus, the decrease in the aged state is not as pronounced in relation to the dried state. With these results, we can infer that degradation of the properties occurred due to water absorption, however the material was able to recover the tensile properties. This result is in agreement with a study by Ishak et al. [21] that inferred that PBT-GF30 in a 100% RH environment at 80 °C is able to recover tensile properties. Since the temperature is higher than the one under analysis and chemical bonds and irreversible changes due to the water uptake increase with increasing temperature, at 70 °C the changes must also be recoverable.

4.2.2. 90 °C

Fig. 15 shows the strength and Young's modulus of the PBT-GF30 dried, aged, and dried after aging at 90 °C.

When analyzing the results at 90 °C, three distinct situations were evident for the three conditions. First, in the dried condition, when comparing to the same state at 70 °C, there was not a significant difference, which leads to the conclusion that the effect of the temperature from 70 °C to 90 °C was not significant, both for the Young's modulus and the strength. Secondly, the difference in the drop in properties between the dry and aged states does not change significantly between temperatures, Borges et al. [20] has analyzed the mechanical properties of PBT-GF30 and PBT across different immersion temperatures and stated that there was no clear trend in any temperature for the evolution of the strength and Young's modulus as function of water uptake, for the specimens with water, over the immersion time. However, Ishak et al. [21], Rosato et al. [42] and Gardner et al. [43] report that PBT is very sensitive to longer immersion times, showing higher strength drops. The immersion times used in this work were defined using the same criteria set by Borges et al. [20], which is lower than the ones used by the other authors. Therefore, the strength and stiffness decreases reported in this work are lower. Finally, and most importantly, at 90 °C the PBT-GF30 was not capable to recover its mechanical properties when dried after aging what leads to the conclusion that between 70 °C-90 °C there is mechanical degradation due to water intake. This result is in line with an experiment by Borges et al. [19] that stated that the PBT-GF30 starts to suffer chemical interaction with water at immersion temperatures between 80 ° and 85 °C.

4.2.3. 130 °C

Fig. 16 shows the strength and Young's modulus of the PBT-GF30 dried, aged, and dried after aging at 130 °C.

At 130 °C, the PBT-GF30 showed the same behavior as for 90 °C. Again, there was not a significant difference due to the influence of the temperatures and after the water intake the material was not capable of completely restore the previous properties, which leads to concluding more strongly that the PBT-GF30 undergoes degradation of its polymer matrix.

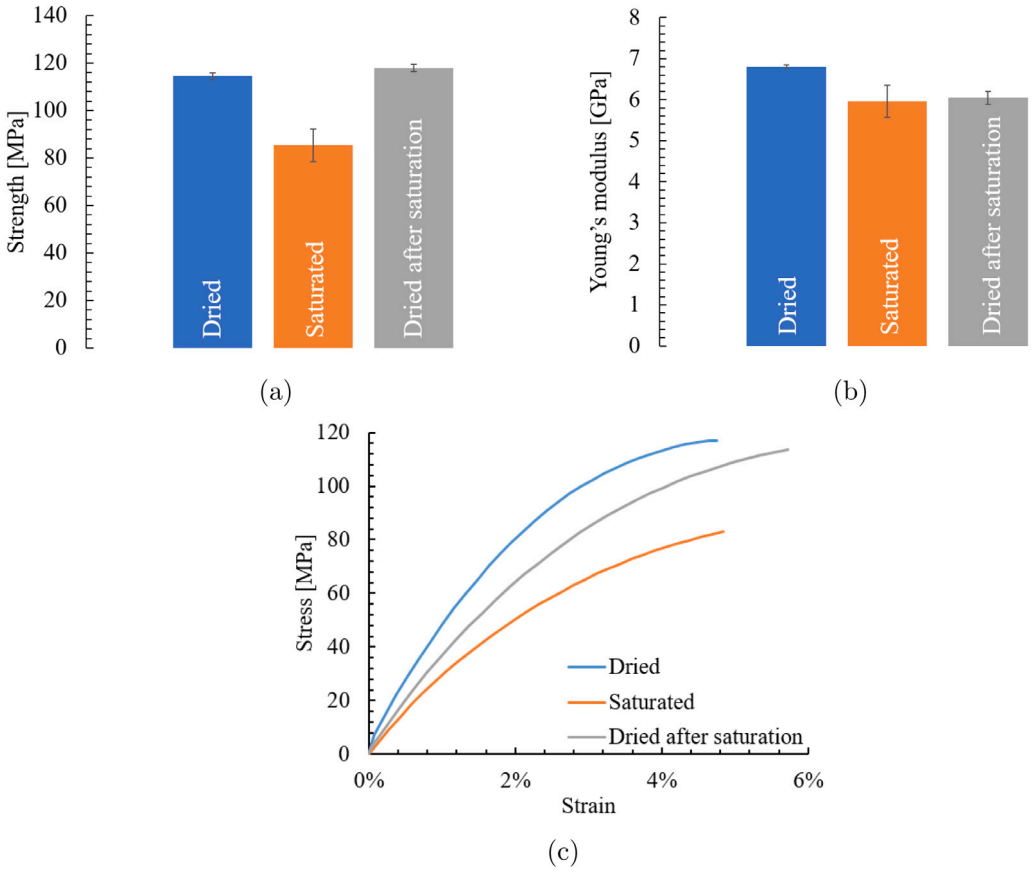


Fig. 14. Mechanical properties of the PBT-GF30 for the different conditions at 70 °C: strength (a), Young's modulus (b) and stress–strain curves (c).

4.3. Single lap joint (SLJ)

4.3.1. 70 °C

Figs. 17a and 17b show $P-\delta$ curves of the most representative curve for each state and the failure load, respectively.

For 70 °C, there was not a considerable difference between the three states. While the substrate material, PBT-GF30, decrease its strength and stiffness, the mechanical properties of the silicone adhesive slightly improve with water intake at 70 °C, as discussed by Borges et al. [28]. Therefore, as a result, the SLJ did not show a significant difference between the three conditions. As for the failure mode, Fig. 18, failure was cohesive for all of the conditions. However, for the aged specimen, failure was closer to the middle of the adhesive. This happens because, with increasing water uptake, the adhesive becomes stronger and, since the region of the adhesive closer to the interface absorbs more water, it is stronger, moving failure to the middle of the adhesive.

4.3.2. 90 °C

Figs. 19a and 19b show representative $P-\delta$ curves of the most representative curve for each state and the failure load, respectively.

For the dried state at 90 °C there was a decrease of 27% on the failure load when compared with the same state at 70 °C, since the strength of the adhesive reduces with drying temperature [28]. The aged condition presented higher failure load, due to the also higher strength of the silicone adhesive. Although the mechanical properties of the PBT-GF30 decrease with the water intake, the determining properties to the failure of the joint are those of the adhesive, since in these SLJ tests the loading of the substrates is not very severe.

Regarding failure mode, Fig. 20, failure moves from cohesive, in the dried condition, to mixed failure, with adhesive failure regions in the aged condition and a similar failure mode after re-drying. Although for 70 °C failure was closer to the middle of the adhesive as the adhesive aged, after water immersion at 90 °C [20] there is already chemical degradation of the substrate, which can lead to release of chemical agents to the interface, degrading the bond strength by remaining at the interface of the chemical properties of the adhesive closer to the substrate, if it absorbs these components.

4.3.3. 130 °C

Figs. 21a and 21b show representative $P-\delta$ curves of the most representative curve for each state and the failure load, respectively. The SLJs presented similar behavior as the two previous temperatures, the aged state was the one with higher strength, while the dried and dried after aging were very similar, due to the reversibility of the change in mechanical properties of the silicone.

In comparison to the dried state at 70 °C there was a decrease of 31% in failure load, as in comparison with 90 °C there was 5% decrease.

At 130 °C the failure is cohesive in the adhesive but near the substrate in all states. However in the dried after aging condition, the failure starts to become adhesive. The motive for this is the same presented for 90 °C, with temperature degradation playing an even higher role, that is why failure is always closer to the interface, and it increases from dried to aged, to dried after aging and, therefore, with increasing exposure time at 130 °C (see Fig. 22).

4.4. Double cantilever beam (DCB)

4.4.1. Adhesive characterization

From the results obtained from the DCBs with high strength steel substrates, a representative curve of the variation of the J-Integral with the normal end-opening displacement (δ_n) is shown in Fig. 23a. This curve represents G_I in the interval [0, δ_{nc}], where δ_{nc} is defined by the point when G_I is at its maximum value, G_{IC}. After reaching this

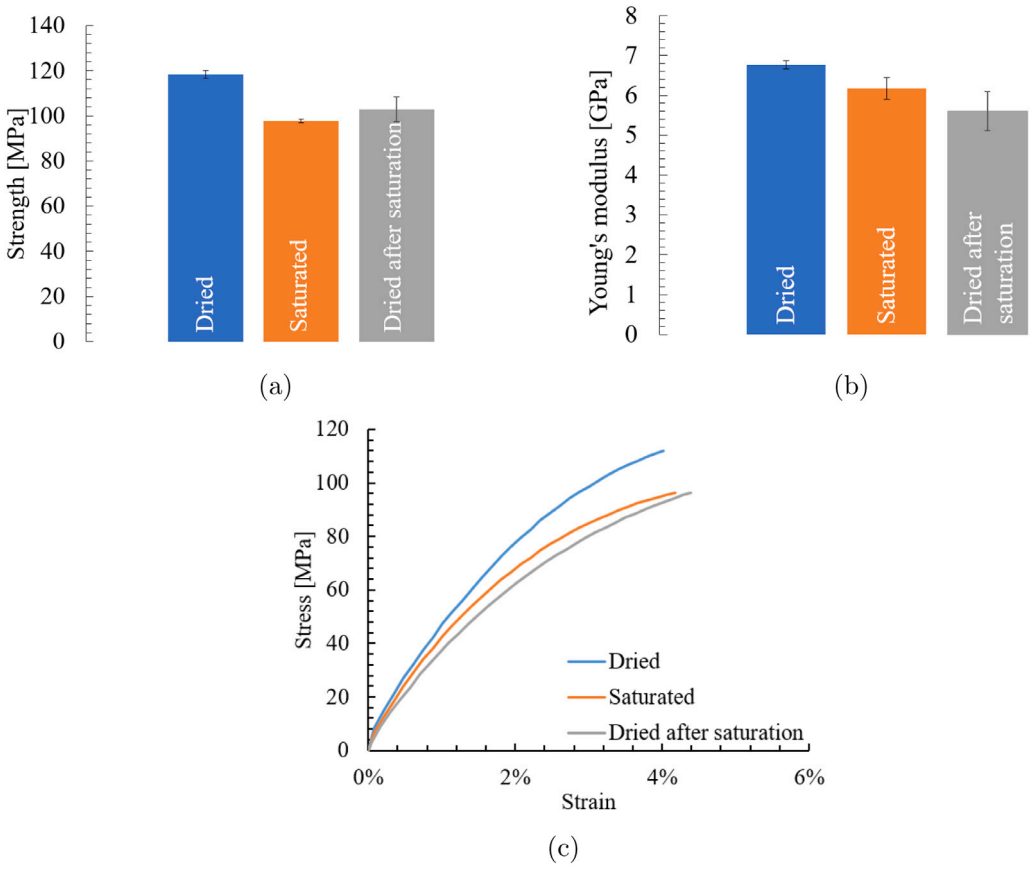


Fig. 15. Mechanical properties of the PBT-GF30 for the different conditions at 90 °C: strength (a) and Young's modulus (b) and stress–strain curves (c).

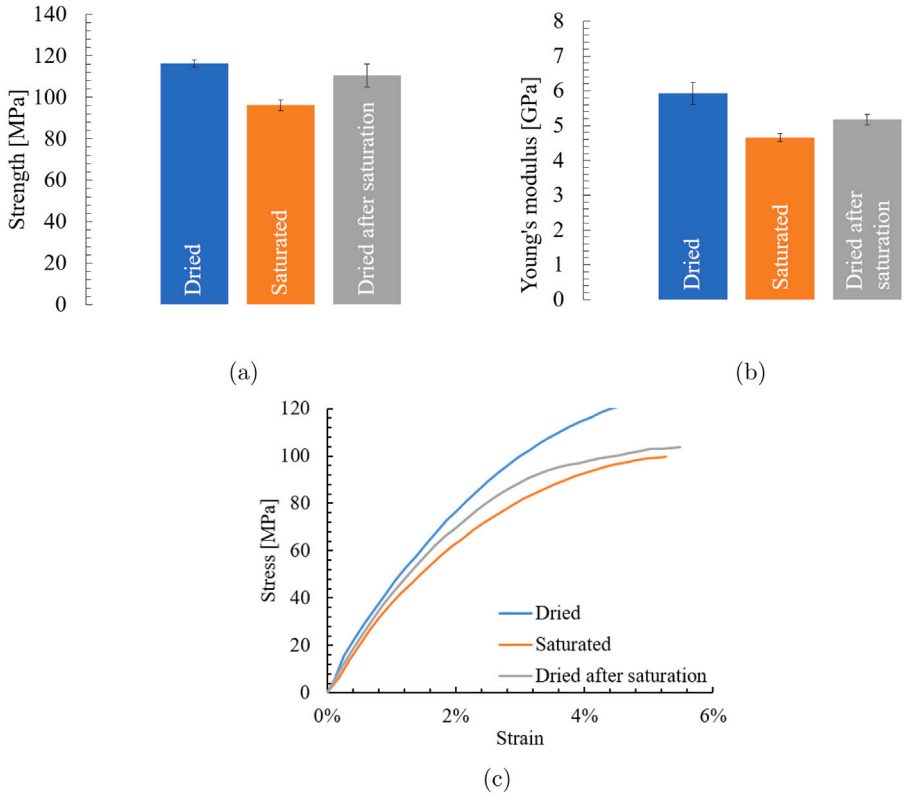


Fig. 16. Mechanical properties of the PBT-GF30 for the different conditions at 130 °C: strength (a) and Young's modulus (b) and stress–strain curves (c).

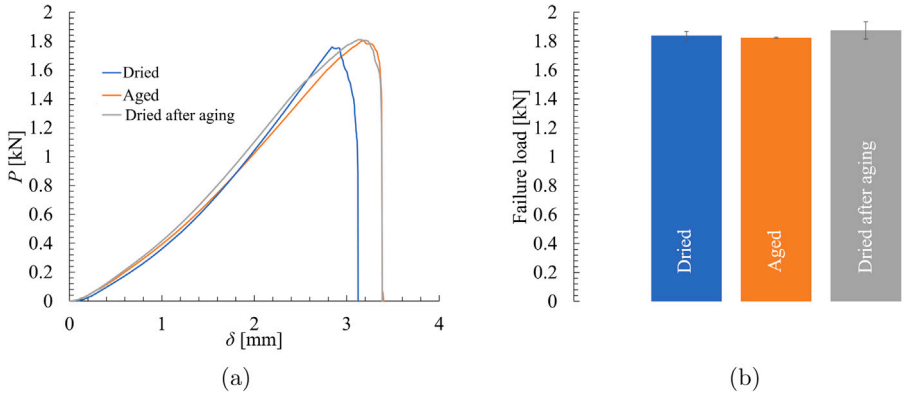


Fig. 17. SLJ results for the dried, aged and dried after aging conditions at 70 °C: load–displacement, $P-\delta$, curves (a) and failure load (b).

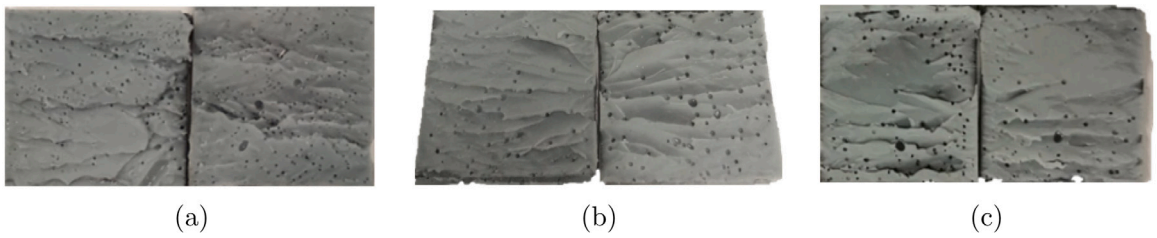


Fig. 18. Failure surfaces of the SLJs for the different conditions tested at 70 °C: dried (a), aged (b) and dried after aging (c).

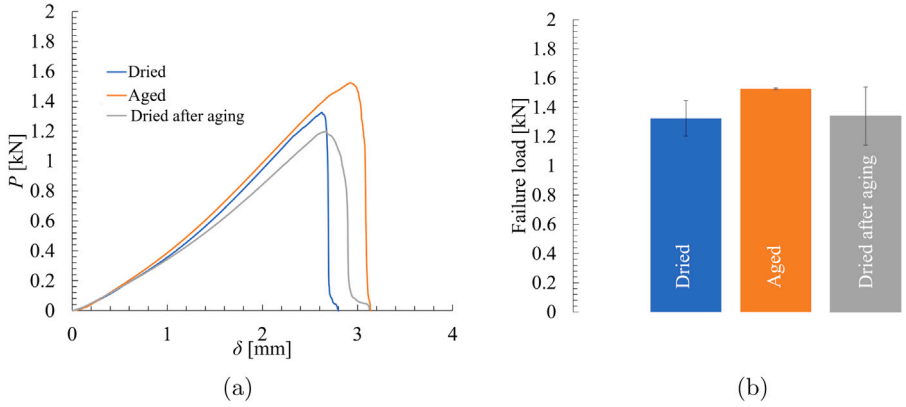


Fig. 19. SLJ results for the dried, aged and dried after aging conditions at 90 °C: load–displacement, $P-\delta$, curves (a) and failure load (b).

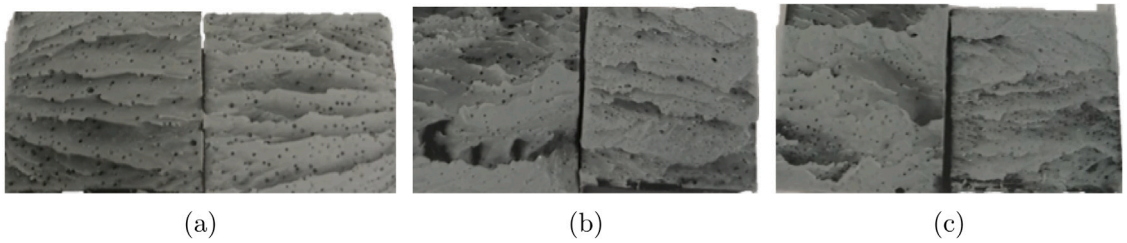


Fig. 20. Failure surfaces of the SLJs for the different conditions tested at 90 °C: dried (a), aged (b) and dried after aging (c).

point, testing always continue although only the region until this point is represented, since this fully defined the cohesive law [44]. The value of the G_{IC} was 3.3 ± 0.38 N/mm. The cohesive law of the adhesive in mode I was obtained by differentiation of the G_I with respect to (δ_n). From the most representative cohesive law in Fig. 23b, we infer that the adhesive has a very little ductile behavior, being practically nonexistent. This shows that the adhesive has a brittle behavior.

4.4.2. 70 °C

In the DCB test, Fig. 24, the substrates are under a more severe loading, and even plastic deformation, which means the effect of temperature and humidity is going to have a higher impact on the properties of the joint than what was found for the SLJ.

Even though the properties of the PBT-GF30 decrease in the aged states, it is clear that the DCB at 70 °C, increases its peak load and

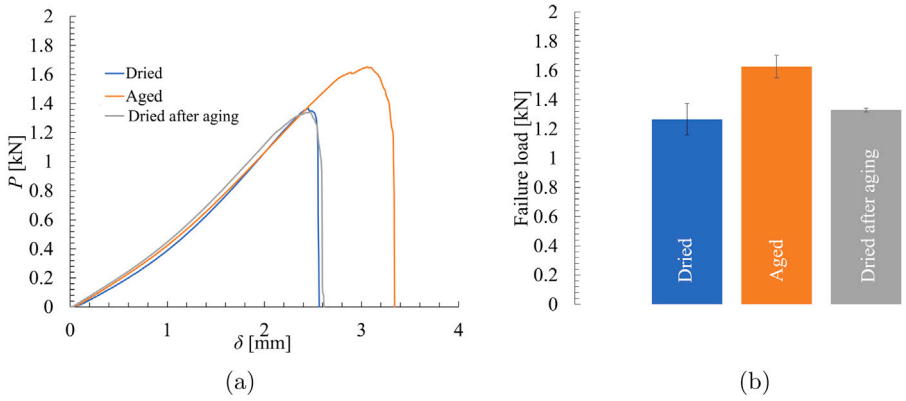


Fig. 21. SLJ results for the dried, aged and dried after aging conditions at 130 °C: load–displacement, $P-\delta$, curves (a) and failure load (b).

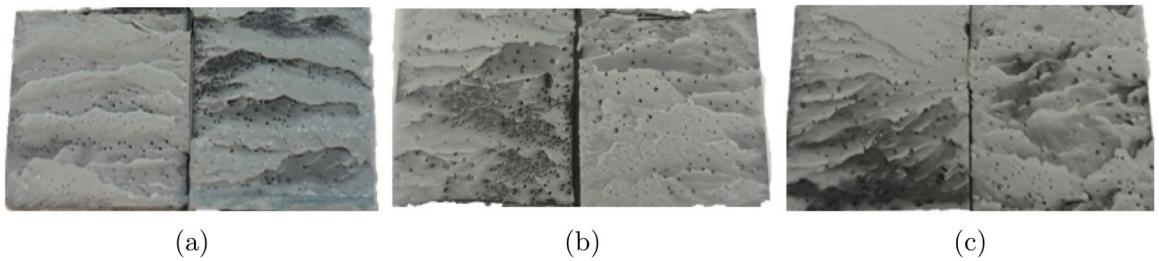


Fig. 22. Failure surfaces of the SLJs for the different conditions tested at 130 °C: dried (a), aged (b) and dried after aging (c).

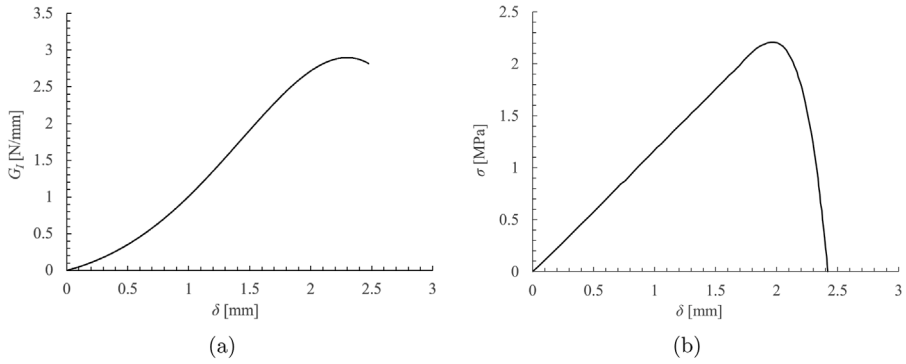


Fig. 23. Representative curves obtained from the J-integral: representative curve of the G_I (a) and cohesive law of the adhesive (b).

maximum displacement in the aged state, since the adhesive has better properties in this condition.

The failure mode, Fig. 25, did not change significantly for state to state, being always cohesive.

4.4.3. 90 °C

At 90 °C, Fig. 26, the impact of the hydrolysis of the PBT-GF30 with the water intake was noticeable. Comparing with the previous results, there was not an improvement in behavior in the aged state when comparing with the dried state.

This was due to the properties of the substrate in this test, the substrate was under a significant plastic deformation. In fact, during the aged test, the failure was at the PBT-GF30. As seen previously, the strength of the substrate decreases when aged at 90 °C with the aggravating factor of the chemical changes in the material, which led to failure of the substrate.

When comparing the failure modes, Fig. 27, the failure changed from cohesive near the substrate in the dried state to substrate failure in the aged condition. When re-dried, the substrate recovered some of its properties, and failure returned to the adhesive.

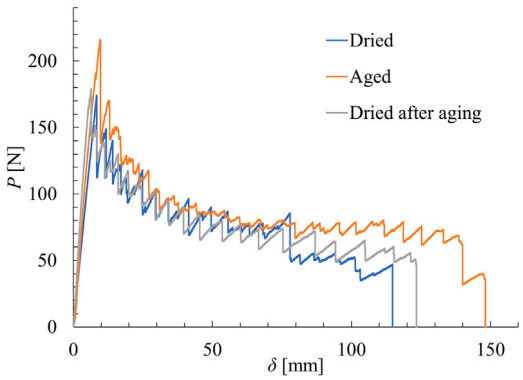


Fig. 24. DCB results for the dried, aged and dried after aging conditions at 70 °C: load–displacement, $P-\delta$, curves.



Fig. 25. Failure surfaces of the DCBs for the different conditions tested at 70 °C: dried (a), aged (b) and dried after aging (c).

4.4.4. 130 °C

Regarding the results obtained at 130 °C, Fig. 28, it can be inferred that, as for 90 °C, there was a degradation of the polymeric matrix of PBT-GF30 in the aged condition due to water ingress that led to a substrate rupture (Fig. 29), which explains the very significant decrease, to about 20% of the value, in maximum displacement for the aged and dried after aging conditions.

However, the substrate, did not recover its mechanical properties after re-drying, as it happened for 90 °C, which is agreement to that was found for the bulk tensile tests, the increasing temperature leads to more significant and irreversible damage on the PBT-GF30. However, both the DCB and bulk tensile tests, the specimens were kept in water until saturation is reached and, the joint takes a longer time to saturate, which means the DCB was kept in water for a longer period of time, explaining the more extensive damage.

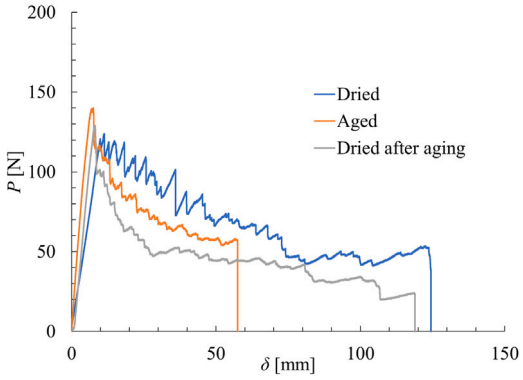


Fig. 26. DCB results for the dried, aged and dried after aging conditions at 90 °C: load–displacement, $P-\delta$, curves.

5. Numerical results

In this section, the water uptake level at the adhesive and substrate for the immersion times analyzed is defined. Additionally, for SLJ and DCB data from the numerical analysis is compared with the experimental data obtain in Section *Experimental results*. As explain in Section *Numerical model*, a SLJ and DCB model was created with the same geometry as the experimental geometry. The mechanical properties used in the simulations were obtained from the bulk tensile test of the adhesive [28] and the PBT-GF30. The results are divided into joint geometry and temperature.

5.1. Water uptake of the joints

The water uptake as a function of time, as well as the time at which the joints were removed from water at the three temperatures, are presented in Fig. 30. It should be noticed that, for SLJs, the respective immersion times of 30 days for 70 °C, 15 days for 90 °C and 1 day for 130 °C lead to the same water uptake in the adhesive and substrate.

The same immersion times were considered for DCBs, for the time exposed to high temperatures humid environments to be similar. However, in these joints the water uptake, particularly at the substrates at higher temperatures, was smaller, since the substrate area exposed to water also decreased, Fig. 31.

5.2. Single lap joints (SLJ)

5.2.1. 70 °C

Fig. 32, shows a comparison of the numerical and experimental failure load of the SLJs when dried, aged and dried after aging at 70 °C. For this temperature, both the experimental and numerical failure loads are fairly similar in all of the conditions. However, it can be seen that this numerical approach is valid to simulate the experimental result obtained at 70 °C.

The results being so accurately simulated from the bulk properties of the PBT-GF30 and silicone for each condition under analysis show that, although there is some water being absorbed by the adhesive/substrate interface, it does not have a significant effect on the water uptake or failure of the adhesive joints, since the behavior of the joint can be simulated by the adhesive and substrate property variation.

5.2.2. 90 °C

The numerical results obtained for the three different conditions at 90 °C are presented in Fig. 33. The results showed a good agreement with the experimental results, although the failure load obtained numerically was slightly higher for this temperature. This may have happened because the mechanical properties of the materials are affected not only by the immersion temperature but also by the immersion time and, since the immersion time required to saturate the bulk material is smaller than the immersion time required to saturate the joint, in the joint, and particularly at higher temperatures, the mechanical properties of the material may be slightly lower than expected.

5.2.3. 130 °C

For 130 °C, Fig. 34, the numerical model also proved to be capable of simulating the experimental results obtained. Again, the failure load in the numerical model was slightly higher.

5.3. Double cantilever beam (DCB)

5.3.1. 70 °C

In Fig. 35 a comparison between the numerical model $P-\delta$ curve with the mechanical properties obtain in the bulk tensile test of the

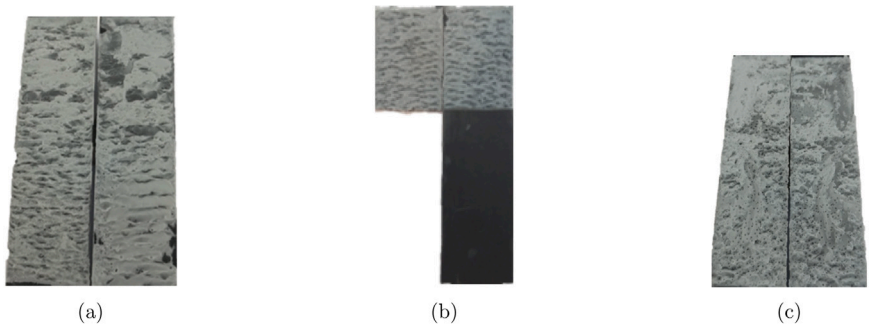


Fig. 27. Failure surfaces of the DCBs for the different conditions tested at 90 °C: dried (a), aged (b) and dried after aging (c).

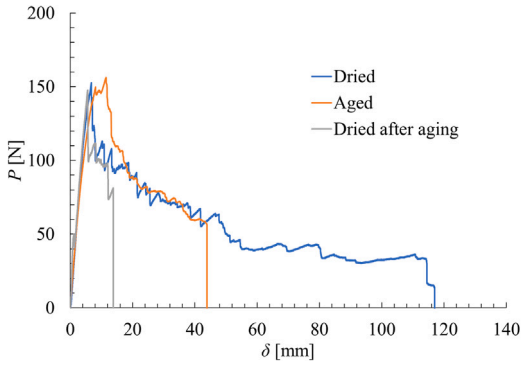


Fig. 28. DCB results for the dried, aged and dried after aging conditions at 130 °C: load–displacement, $P - \delta$, curves.

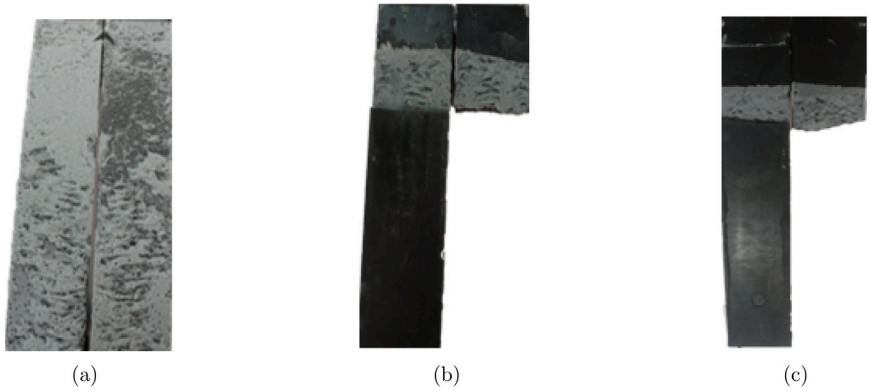


Fig. 29. Failure surfaces of the DCBs for the different conditions tested at 130 °C: dried (a), aged (b) and dried after aging (c).

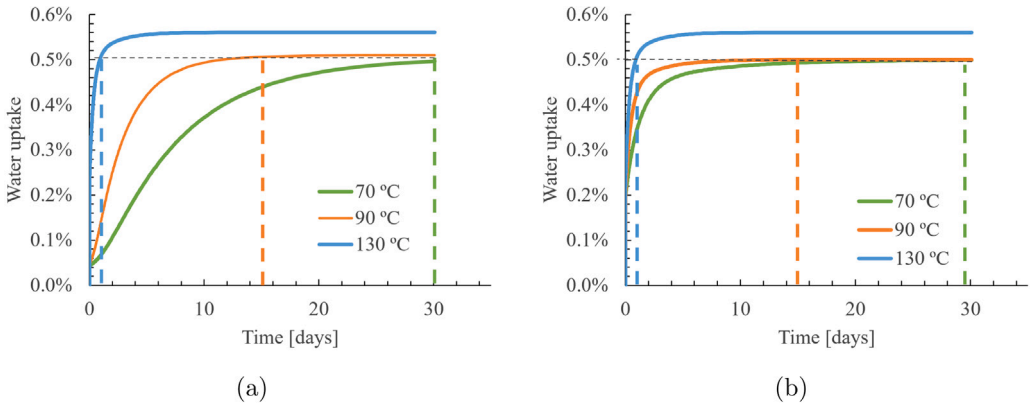


Fig. 30. Numerical simulation of the water uptake in the SLJs at the three temperatures considered: adhesive (a) and substrate (b).

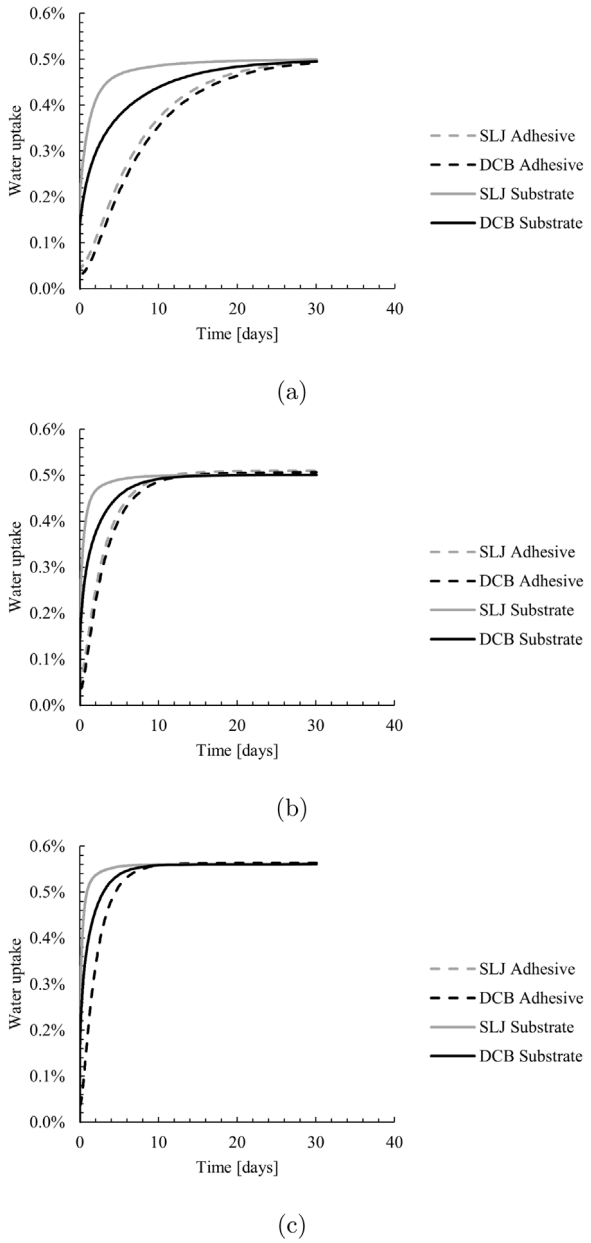


Fig. 31. Numerical simulation of the water uptake in the substrates and adhesive of the SLJs and DCBs for the three temperatures considered: 70 °C (a), 90 °C (b) and 130 °C (c).

substrate and adhesive, and the experimental $P-\delta$ curve are showed. The stiffness of the numerical model was almost equal to the experimental one and the failure progression after the peak load has a good approximation. The slightly higher error for the aged condition can be related to the change in properties of the silicone with increasing immersion time, since the time required to saturate the joint is higher than the necessary to saturate the bulk specimen. Particularly in the adhesive, it is possible that, although the mechanical behavior is not significantly different after aging, it might be affected when combined with longer immersion times.

5.3.2. 90 °C

At 90 °C the results were similarly to the ones at 70 °C, with basically the same stiffness as the experimental results and a good approximation of the peak load and crack progression. Since the substrate broke in the aged state, using the von Mises stress criterion, it was considered that, when the substrate reached its strength value (obtained in the bulk tensile test), it would fail, and the simulation ended. This approach showed a good approximation to the experimental $P-\delta$, as shown in Fig. 36.

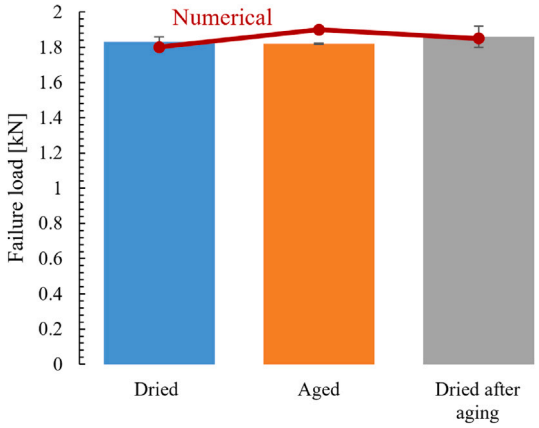


Fig. 32. Comparison of the numerical and experimental failure load of the SLJs for 70 °C.

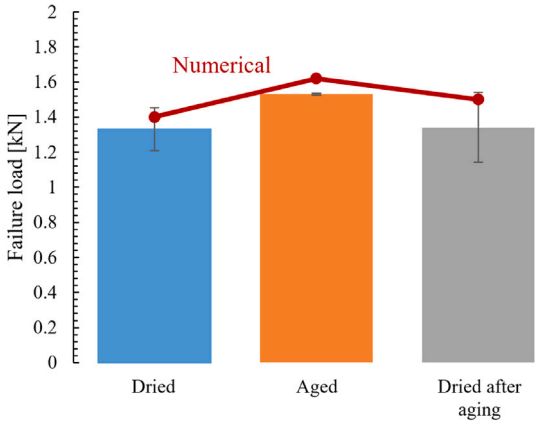


Fig. 33. Comparison of the numerical and experimental failure load of the SLJs for 90 °C.

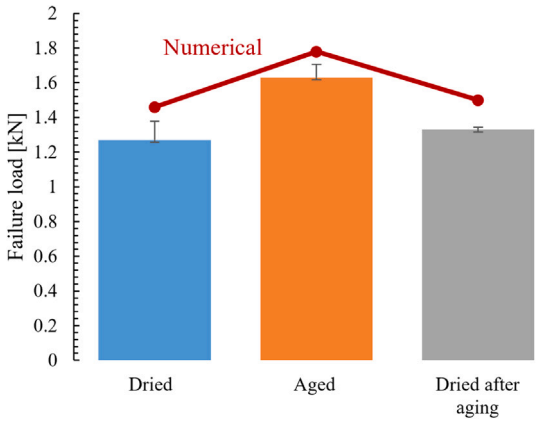


Fig. 34. Comparison of the numerical and experimental failure load of the SLJs for 130 °C.

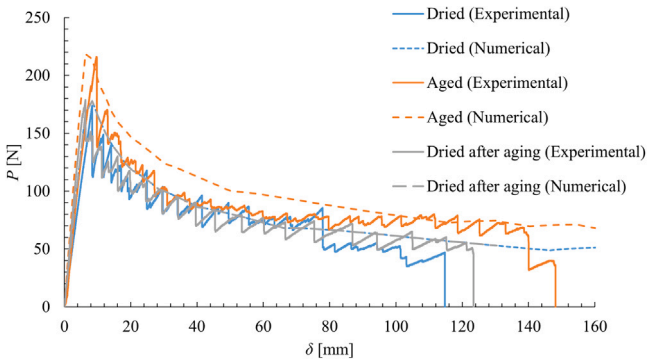


Fig. 35. Comparison of the numerical and experimental load–displacement, P-δ, curves of DCBs for 70 °C.

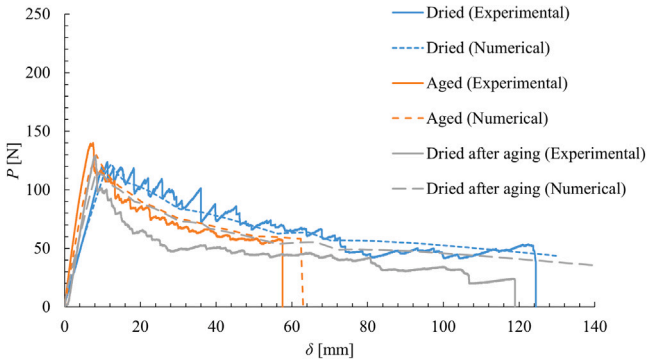


Fig. 36. Comparison of the numerical and experimental load–displacement, P-δ, curves of DCBs for 90 °C.

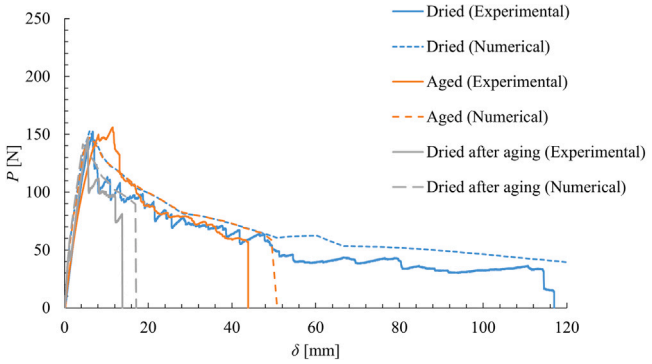


Fig. 37. Comparison of the numerical and experimental load–displacement, P-δ, curves of DCBs for 130 °C.

5.3.3. 130 °C

Regarding the simulation for the aged and dried after aging conditions at 130 °C, the same approach was taken. Again, it was considered that when the strength value of the PBT-GF30 was reached in the numerical simulation, the substrate would fail and, therefore, the simulation ended. The numerical results also showed an excellent approximation to the experimental results, which validates these and numerical approach, Fig. 37.

6. Conclusions

In this study, the effects of humidity and immersion temperatures of the properties and failure mode of PBT-GF30/silicone bonded joints were analyzed. Three different temperatures and three different states were applied to dogbone specimens of PBT-GF30, SLJ and DCB with PBT-GF30/silicone. Afterwards, a numerical model was created with the experimental values of the substrate from this work and the silicone values from [28]. It is possible to conclude the following:

- The PBT-GF30 decreases its strength and Young's modulus with temperature and water intake.
- Almost all of the joints analyzed exhibited a better mechanical behavior when aged, since the strength of the adhesive increases with humidity.
- The exceptions were, for the DCBs, the aged joint at 90 °C and the aged and dried after aging joints at 130 °C, which failed on the substrate. This happens due to chemical changes in the PBT-GF30 after water immersion at temperatures above 85 °C. Additionally, it was seen on the DCB and not on the SLJ because the loading of the substrate was more severe, with the substrate experiencing plastic deformation.
- With increasing temperature, there was a decrease in the mechanical behavior of the joints, regarding all humidity conditions, due to the decrease of strength of the adhesive with immersion temperature and the chemical changes and degradation of the substrate.
- With the experimental results of the tensile bulk tests of the PBT-GF30 and silicone from [28], it was possible to simulate the joint behavior (for SLJ and DCB), achieving good agreement with the experimental results. This shows that the interface does not have a dominant role in these phenomena.

CRediT authorship contribution statement

R. Brandão: Conceptualization, Methodology, Software, Investigation, Writing – original draft. **C.S.P. Borges:** Conceptualization, Methodology, Software, Investigation, Writing – original draft. **E.A.S. Marques:** Conceptualization, Investigation. **R.J.C. Carbas:** Methodology, Investigation. **A. Akhavan-Safar:** Methodology, Software. **F. Schmid:** Software, Writing – review & editing, Funding acquisition. **C. Ueffing:** Conceptualization, Writing – review & editing, Funding acquisition. **P. Weißgraeber:** Methodology, Writing – review & editing, Funding acquisition. **L.F.M. da Silva:** Writing – review & editing, Supervision, Project administration.

Declaration of competing interest

The authors declare that they have no known competing financial interests or personal relationships that could have appeared to influence the work reported in this paper.

Acknowledgments

The author(s) disclosed receipt of the following financial support for the research, authorship, and/or publication of this article: The authors wish to acknowledge and thank the funding and support provided by Robert Bosch GmbH, Corporate Research and Advance Engineering, Renningen. The authors also gratefully acknowledge the funding provided by Fundação para a Ciência e Tecnologia (FCT), Portugal for the Ph.D. Grant 2020.06055.BD through FSE.

References

[1] da Silva Lucas FM, Ochsner Andreas, Adams Robert D. Handbook of adhesion technology. Springer Science & Business Media; 2018.
[2] White Christopher, Tan Kar, Andreas wolf, Carbary Larry. Advances in silicone adhesives. Advances in Structural Adhesive Bonding, Woodhead Publishing Limited, Cambridge, -1; 2009.
[3] Ito Eiko, Kobayashi Yasuji. Effects of absorbed water on physical properties of polyesters. J Appl Polym Sci 1980;25(10):2145–57.
[4] Stein RS, Misra A. Morphological studies on polybutylene terephthalate. J Polym Sci: Polym Phys Ed 1980;18(2):327–42.

[5] Ishak ZA Mohd, Lim NC. Effect of moisture absorption on the tensile properties of short glass fiber reinforced poly(butylene terephthalate). Polym Eng Sci 1994;34(22):1645–55.
[6] Comyn J. Durability of structural adhesives. Appl Sci Lond 1983.
[7] Popineau Sylvain, Rondeau-Mouro Corinne, Sulpice-Gaillet Christine, Shanahan Martin ER. Free/bound water absorption in an epoxy adhesive. Polymer 2005;46(24):10733–40.
[8] Barbosa AQ, Da Silva LFM, Öchsner A. Hygrothermal aging of an adhesive reinforced with microparticles of cork. J Adhes Sci Technol 2015;29(16):1714–32.
[9] Viana GMSO, Costa M, Banea MD, Da Silva LFM. A review on the temperature and moisture degradation of adhesive joints. Proc Inst Mech Eng L: J Mater: Des Appl 2017;231(5):488–501.
[10] Fick Adolph. On liquid diffusion. J Membr Sci 1995;100(1):33–8.
[11] Pethrick Richard A. Design and ageing of adhesives for structural adhesive bonding–a review. Proc Inst Mech Eng L: J Mater: Des Appl 2015;229(5):349–79.
[12] Eftekhari Mohammadreza, Fatemi Ali. Tensile behavior of thermoplastic composites including temperature, moisture, and hygrothermal effects. Polym Test 2016;51:151–64.
[13] Loh WK, Crocombe AD, Abdel Wahab MM, Ashcroft IA. Modelling anomalous moisture uptake, swelling and thermal characteristics of a rubber toughened epoxy adhesive. Int J Adhes Adhes 2005;25(1):1–12.
[14] Errajhi OAZ, Osborne JRF, Richardson MOW, Dhakal HN. Water absorption characteristics of aluminised E-glass fibre reinforced unsaturated polyester composites. Compos Struct 2005;71(3):333–6.
[15] Li Yanmei, Miranda John, Sue Hung-Jue. Hygrothermal diffusion behavior in bismaleimide resin. Polymer 2001;42(18):7791–9.
[16] Carter HG, Kibler KG, Reynolds JD. Fundamental and operational glass transition temperatures of composite resins and adhesives. In: Advanced composite materials—environmental effects. ASTM International; 1978.
[17] Gurtin Morton E, Yatomi Chikayoshi. On a model for two phase diffusion in composite materials. J Compos Mater 1979;13(2):126–30.
[18] Mubashar Aamir, Ashcroft Ian A, Critchlow Gary W, Crocombe AD. Moisture absorption–desorption effects in adhesive joints. Int J Adhes Adhes 2009;29(8):751–60.
[19] Borges CSP, Marques EAS, Carbas RJC, Ueffing C, Weißgraeber P, da Silva LFM. Review on the effect of moisture and contamination on the interfacial properties of adhesive joints. Proc Inst Mech Eng C: J Mech Eng Sci 2021;235(3):527–49.
[20] Borges Catarina SP, Akhavan-Safar Alireza, Marques Eduardo AS, Carbas Ricardo JC, Ueffing Christoph, Weissgraeber Philipp, da Silva Lucas FM. Effect of water ingress on the mechanical and chemical properties of polybutylene terephthalate reinforced with glass fibers. Materials 2021;14(5):1261.
[21] Mohd Ishak ZA, Ishiaku US, Karger-Kocsis J. Hygrothermal aging and fracture behavior of short-glass-fiber-reinforced rubber-toughened poly(butylene terephthalate) composites. Compos Sci Technol 2000;60(6):803–15.
[22] Bergeret Anne, Ferry Laurent, Ienny Patrick. Influence of the fibre/matrix interface on ageing mechanisms of glass fibre reinforced thermoplastic composites (pa-6, 6, pet, pbt) in a hygrothermal environment. Polym Degrad Stab 2009;94(9):1315–24.
[23] Viana G, Costa M, Banea MD, da Silva LFM. Behaviour of environmentally degraded epoxy adhesives as a function of temperature. J Adhes 2017;93(1–2):95–112.
[24] Oldfield D, Symes T. Long term natural ageing of silicone elastomers. Polym Test 1996;15(2):115–28.
[25] Fan J, Wang Z, Zhang X, Deng Z, Fan X, Zhang G. High moisture accelerated mechanical behavior degradation of phosphor/silicone composites used in white light-emitting diodes. Polymers 2019;11(8).
[26] Wu Jian, Dong Jiyi, Wang Youshan, Gond Bipin Kumar. Thermal oxidation ageing effects on silicone rubber sealing performance. Polym Degrad Stab 2017;135:43–53.
[27] Bowditch MR. The durability of adhesive joints in the presence of water. Int J Adhes Adhes 1996;16(2):73–9.
[28] Borges Catarina SP, Brandão Ricardo, Akhavan-Safar Alireza, Marques Eduardo AS, Carbas Ricardo JC, Ueffing Christoph, Weissgraeber Philipp, da Silva Lucas FM. Influence of water and surfactant contamination on the properties of a silicone adhesive, before and after curing. 2021.
[29] ISO294-3. Plastics-injection moulding os test specimens of thermoplastic materials, part 3: Small plates.. 2002.
[30] ASTMD1002-99. Standard test method for apparent shear strength of SingleLap-joint adhesively bonded metal specimens by tension loading (metal-to-metal).. 2005.
[31] ISO 4587. Determination of tensile lap-shear strength of rigid-to-rigid bonded assemblies.. 1995.
[32] Banea Mariana D, da Silva Lucas FM, Campilho Raul DSG. Moulds design for adhesive bulk and joint specimens manufacturing. Assem Autom 2012.
[33] ISO B, 15024. Fibre-reinforced plastic composites. Determination of mode I interlaminar fracture toughness, GIC, for unidirectional reinforced materials. 2001.
[34] Rice JR. A path independent integral and the approximate analysis of strain concentration by notches and cracks. J Appl Mech 1968;35(2):379–86.
[35] Buschow KH Jürgen, Cahn Robert W, Flemings Merton C, Ilschner Bernhard, Kramer Edward J, Mahajan Subhash, Veyssière Patrick. Fracture toughness testing of metallic materials. 2001, p. 3336–40.
[36] Kurtz Steven M. 29 - Characterization of physical, chemical, and mechanical properties of UHMWPE. 2016, p. 531–52.
[37] Zhu Yong, Liechti Kenneth M, Ravi-Chandar K. Direct extraction of rate-dependent traction–separation laws for polyurea/steel interfaces. Int J Solids Struct 2009;46(1):31–51.
[38] Campilho RDSG, Moura DC, Banea MD, da Silva LFM. Adherend thickness effect on the tensile fracture toughness of a structural adhesive using an optical data acquisition method. Int J Adhes Adhes 2014;53:15–22, Joint Design.
[39] Loureiro F, Rocha RCampilho & R. J-integral analysis of the mixed-mode fracture behaviour of composite bonded joints. J Adhes 2020;96(1–4):321–44.
[40] Carlberger Thomas, Biel Anders, Stigh Ulf. Influence of temperature and strain rate on cohesive properties of a structural epoxy adhesive. Int J Fract 2009;155:155–66.
[41] Gustafson Peter A, Waas Anthony M. The influence of adhesive constitutive parameters in cohesive zone finite element models of adhesively bonded joints. Int J Solids Struct 2009;46(10):2201–15.
[42] Rosato Dominick V, Rosato Donald V, v Rosato Matthew. Plastic product material and process selection handbook. Elsevier; 2004.
[43] Gardner RJ, Martin JR. Effect of relative humidity on the mechanical properties of poly (1, 4-butylene terephthalate). J Appl Polym Sci 1980;25(10):2353–61.
[44] Högberg JL, Srensen BF, Stigh U. Constitutive behaviour of mixed mode loaded adhesive layer. Int J Solids Struct 2007;44(25):8335–54.

Appendix E

Paper E

Effect of the interface/interphase on the water ingress properties of joints with PBT-GF30 and aluminum substrates using silicone adhesive

Effect of the interface/interphase on the water ingress properties of joints with PBT-GF30 and aluminum substrates using silicone adhesive

C.S.P. Borges[1], E.A.S. Marques[1], R.J.C. Carbas[1], A. Akhavan-Safar[1], C. Ueffing[2], P. Weißgraeber[3], L.F.M. da Silva[4]

1 Instituto de Ciência e Inovação em Engenharia Mecânica e Engenharia Industrial (INEGI), Portugal
2 Robert Bosch GmbH, Corporate Research and Advance Engineering, Renningen, Germany
3 Chair of Lightweight Design, University of Rostock, Germany
4 Departamento de Engenharia Mecânica, Faculdade de Engenharia (FEUP), Universidade do Porto, Portugal

Abstract: One of the main setbacks of adhesive joints is their sensitivity to humid environments, particularly at high temperature. Although the adhesive and substrate (if polymeric in its matrix) can absorb water, failure of water aged joints has been seen to be ultimately interfacial. The aim of this work is to analyze the difference between adhesive/composite and adhesive/metal interphases, both in terms of water diffusion and failure of the aged joints, understanding if there is a difference in the failure of the adhesive joint, depending on the substrate material. For that, silicone joints with two different substrates were prepared. The substrates were polybutylene terephthalate with 30% of short glass fiber (PBT-GF30) and 6082-T6 aluminum. To study the water diffusion behavior, rectangular joints were prepared. The water immersion was conducted at 70 °C. These joints were prepared with three different adhesive thicknesses (0.5, 1 and 2 mm) so that the effect of the interphase could be isolated. It was concluded that the aluminum/silicone joints absorbed more water through the interphase region than the PBT-GF30/silicone joints, since the difference between the expected water uptake and the experimentally measured mass gain is significantly higher, causing adhesive failure of the joint. The same was not observed in the PBT-GF30/silicone, with a more stable interphase, that does not absorb measurable quantities of water and always exhibits cohesive failure.
Keywords: Adhesive joints, water uptake, interface, interphase, composite substrates, metallic substrates

1 Introduction

Two components can be joined using different methods, such as riveting, bolting or welding. However, on one hand, riveting and bolting rely on the opening of holes, creating stress concentration sites, which is particularly concerning when joining composite substrates. On the other hand, welding heavily depends on the substrate material and requires the local heating of the components, which can introduce a region of degraded properties. Therefore, adhesive bonding in an interesting solution, allowing to bond both metals and composites, and even enabling the assembly of dissimilar materials [1–4].

One of the main setbacks of adhesive joints is their sensitivity to humid environments. Since, due to their polymeric matrix, they generally absorb water and it can highly influence their mechanical properties. Additionally, some adhesives, such as silicones, are often used to not only bond assemblies but also to seal them. Therefore, it is important to understand the water uptake behavior or silicone adhesive joints to ensure they are following their sealing purpose. In adhesive joints, water may follow different paths, either through polymeric materials (such as the adhesive or the matrix of the substrate, if it is a composite material), through the pores and cracks of the adhesive or through the adhesive/substrate interface [5].

Considering the moisture absorbed by the bulk materials, it can be absorbed as free water or bound water. Free water fills the free spaces left in the polymeric chain of the material. Bound water creates chemical bonds [6, 7]. The water ingress behavior of materials is not described by a single universal rule. However, in the majority of the cases, the Fick's law can be used to fit the empirical results [8–12]. This law is defined by the coefficient of diffusion, D, which is related to the diffusion rate, and the water uptake at saturation, M_∞. In the case of the family of adhesive used in this study, silicones, the Fick's law of diffusion has been used by several authors. Dai et al. [13], for instance, used Fick's diffusion law to fit the water uptake behavior of silicone exposed to deionized water at temperatures between 20 and 60 °C. As temperature increases, the coefficient of diffusion also increases, but the water uptake at saturation was described as fairly insensitive to temperature. Khalilullah et al. [14] also studied silicone rubbers and concluded that not only does the material follow a Fickian law of diffusion, but also that the Arrhenius law can be used to describe the influence of temperature and relative humidity on the increase of the diffusion coefficient of the material. The same conclusions were reached by Borges et al. [15], that studied the same silicone adhesive used in this work. However, there are authors that use different diffusion laws, such as Lutz et al. [16], that used the Langmuir model to describe the water diffusion on high temperature vulcanized silicone (HTV-SR), and Fang et al. [17]. Ali and Hackman [18] studying high temperature vulcanized (HTV) silicone rubber, understood that, at high temperature (98 °C), as immersion time increases, the silicone becomes increasingly less hydrophobic.

Adhesives exposed to water, typically present a decrease in their mechanical properties, such as the elastic modulus [19–21]. The ductility is known to increase, leading to an increase in strain-to-failure and creep strain [20–22]. Regarding the toughness of the material, typically, decreases are reported [23–25]. However, silicones present a different behavior. Fan et al. [26] exposed silicone to an environment of 55 °C and 85% of relative humidity (RH) for 42 days. The silicone was periodically removed from immersion and tested. Over the tested time period, the material increased its strength and stiffness. Borges et al. [15], studying the same material used in this work, concluded that water

immersion does not significantly change the properties of the adhesive for immersions in a water container placed in a climatic chamber at temperatures between 70 and 130 °C.

Regarding the substrate, if they are metallic, they can oxidize or corrode. However, they are not expected to absorb water. Nonetheless, if working with composite substrates with polymeric matrices, the same effect recorded for bulk adhesives is expected. Borges et al. [27] studied the effect of moisture on the mechanical properties of one of the particular substrates used in the present study, polybutylene terephthalate with 30% of short glass fiber (PBT-GF30). This material also follows the Fick's law of diffusion, increasing its water ingress rate with temperature, according to the Arrhenius law. Additionally, it was seen that, for immersion temperatures between 80 °C and 85 °C, chemical changes start occurring in the material. Brandão et al. [28] studied the effect of immersion temperature on single lap joints (SLJ) and double cantilever beam (DCB) joints manufactured from the same adhesive and substrate material used in this work. Immersion in water inside a climatic chamber in which the temperatures were set to 70, 90 and 130 °C were studied and the specimens were analyzed dried at the considered temperature, after water aging and redried. It was concluded that the aged samples had a higher failure load, due to the slight increase in strength of the silicone when aged. However, the DCB joints aged at 90 °C and both aged and redried in the climatic chamber at 130 °C exhibited failure in the substrate due to the chemical changes in the PBT-GF30 material.

Until this point, the effect of water on the bulk materials, adhesive and substrates, was discussed. However, as said, there are two additional paths of water diffusion, through the pores and cracks of the adhesive and through the interface. The latter is referred to, by several authors, as the main cause of degradation of the joint [29].

When two or more substrates are joined using an adhesive, there is the creation of a layer, between the adhesive and each substrate, that is the interphase. This zone is a layered region, which has properties different from those of the adhesive and substrate, and this makes the interphase a region of heterogeneity, with a gradient of mechanical, chemical and thermal properties, among others [1,30]. Within the interphase, there is the plane of contact between adhesive and substrate, which is the interface [1]. In the case of metallic substrates, the oxides that can be found on the surface of the substrate may be dissolved in the adhesive layer close to the substrate. Considering one of the most commonly used adhesive systems, epoxy-amine, it has been seen that, on one hand, the amine is chemically adsorbed by the oxide on the substrate and, on the other hand, the amine component, which is basic, dissolves the oxide layer [30,31]. Ultimately, it has been observed a preferential adsorption of the curing agent, amine, by the substrate during the curing process of the adhesive, which can change inhibit chemical reactions between epoxy and curing agent, due to excess of epoxy, paired with an overcuring of the epoxy near the substrate, due to the excess of amino groups [4, 5, 32]. The study of silicone adhesive joints is less common, and is one of the motives behind the relevance of this research.

When exposed to water, joints commonly show a higher water uptake than what would be expected if water was only absorbed through the adhesive. Zanni-Deffarges and Shanahan [23] analyzed the coefficient of diffusion of an epoxy adhesive in bulk and in an adhesive joint. It was reported that, in the adhesive joint, the coefficient of diffusion is almost one order of magnitude higher, validating that there are alternative paths of water diffusion. The path of water diffusion suggested was the interface between the adhesive and substrate where, due to capillarity diffusion, the water flows quicker than in the bulk adhesive. Cognard et al. [33] suggests that, when water is absorbed by materials with pores, it will condensate when its chemical potential is equal to that of the liquid.

Therefore, if an adhesive joint there are pores close to the interface, the water condensates and agglomerates close to the interface, creating a debonding pressure. Combining these findings with the conclusions of Zanni-Deffarges and Shanahan [23], it can be inferred that, in adhesive joints, water flows quicker through the interface than through the bulk adhesive and promotes debonding. It is important to point out that these conclusions were drawn from adhesive joints with metallic substrates.

Drain et al. [34] analyzed polycarbonate (PC) and steel joints, bonded with a cyanoacrylate adhesive. It was concluded that, when bonding PC substrates, the interface could not be identified due to the dissolution of the composite in the adhesive, particularly in the ethylcyano monomer. However, for steel substrates, the interface was identifiable. This translates into a higher water resistance of the interface of the PC joint, when compared to that of the steel joint, because the water diffusion through the interface is negligible.

As seen, there are studies analyzing the effect of interfaces on the water diffusion of adhesive joints with epoxy adhesives and metallic substrates, and some first approaches trying to compare metallic and composite substrates. At this point, a remark must be done between interfaces and interphases. Generally, when studying this problematic, the water uptake between the adhesive and substrate is attributed to the interface. However, in most cases, there is no clear micro or nanoscale research performed to ensure the path of water diffusion and failure occurs exactly between adhesive and substrate (interface), and not in the interphase region. Therefore, since the interphase comprehends the interface, these results can be generally attributed to the interphase without harming the main conclusions drawn.

In many applications where the adhesive is subjected to high temperature and humid environments, silicones are used, and not epoxies, since this material is usually used as sealant for its elastic properties and for its coefficient of thermal expansion, which allows to accommodate different thermal expansions of the materials being bonded. This work arises from the study of a housing for electronic components manufactured from PBT-GF30 and bonded using a silicone adhesive, to seal the assembly. The silicone adhesive is also used to bond the housing to a heat sink, manufactured from aluminum. As said, the bulk materials, adhesive and substrate, were already studied in terms of water diffusion behavior and its effect on the mechanical properties [15, 27]. Additionally, the effect of moisture on SLJs and DCBs with PBT-GF30 substrates and the same silicone adhesive was analyzed. However, in this case, the effect of the interphase was not isolated [28].

The main aim of this work is analyzing the effect of interfaces and, more generally, interphases, on the water diffusion behavior of joints with silicone adhesive and both aluminum and PBT-GF30 substrates, along with the influence of water absorption on the mechanical properties of the joints. The water diffusion analysis was fully performed at 70 °C. To isolate the water diffusion behavior of the interphase, for both substrate materials, rectangular joints (RJ) with 0.5, 1 and 2 mm of adhesive thickness were prepared. A gravimetric study was performed and, knowing the water diffusion behavior of the bulk materials at this temperature, determined in previous studies [15, 27], the diffusion at the interphase was isolated. Afterwads, SLJs with the same adhesive thicknesses were prepared, and tested before water aging. The joints were immersed in water for the time needed to reach a constant mass and tested again, to analyze the effect of the water on the mechanical properties and fracture surface of the joints.

2 Methodology

This work aims to isolate the effect of the interface on silicone/aluminum and silicone PBT-GF30 adhesive joints. Therefore, first, joints with three different adhesive thicknesses were prepared, since, knowing the adhesive and substrate behavior and assuming the thickness of the interphase insensitive to the thickness of the adhesive, its behavior can be isolated, Figure 1.

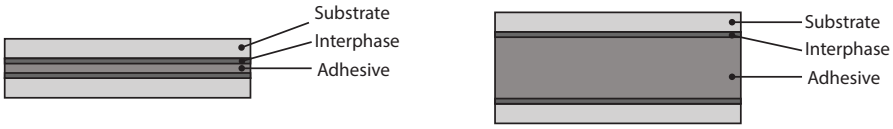


Figure 1: Different adhesive thicknesses to isolate the effect of the interphase.

The same is valid if the water uptake is not globally through the interphase but specifically through the interface, if the chemical affinity of the adhesive and substrate is lower, since the contact plane is also the same regardless of adhesive thickness.

The joints were immersed in water and their water uptake recorded. Generally, for all joints, it can be said that:

$$\Delta m_j = \Delta m_s + \Delta m_a + \Delta m_i \tag{1}$$

where Δm_x refers to the mass gain and j refers to the joint, s to the substrate, a to the adhesive and i to the interphase.

In the case of PBT-GF30 joints, the mass gains of adhesive and substrate are due to water uptake, and are, therefore, volumetric phenomena, Figure 2a. For joints with aluminum substrates, the mass gain of the adhesive is due to water uptake, however, the mass gain of the substrate is due to the oxidized layer that is created at the surface, Figure 2b. Therefore, since the phenomena that have a role in this process are different, the joints are going to be analyzed slightly differently.

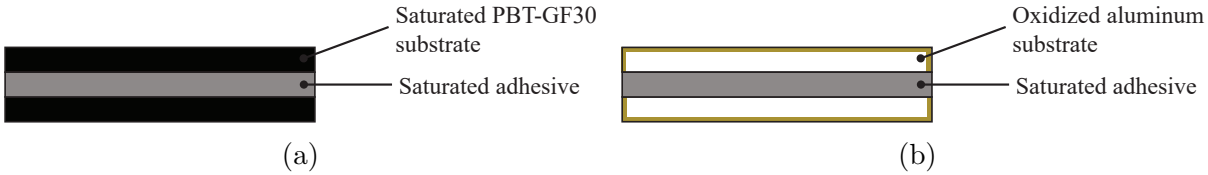


Figure 2: Effect of water on PBT-GF30 b) and aluminum joints b).

In the experimental gravimetric test, the mass of the joint is measured as a whole. However, the objective is to isolate the effect of the interphase. Therefore, it is necessary to eliminate the contribution of the adhesive and substrate from the equation. Considering that the real mass gain is the measured mass gain given by the combination of the factors described in equation (1) and that the theoretical mass gain would be the mass gain in the case where only adhesive and substrate absorb water:

$$\Delta m_i = \Delta m_j^R - \Delta m_{a+s}^T \tag{2}$$

where R and T refer to real and theoretical, respectively. Therefore, the concern now is calculating the theoretical mass gain of the joint.

Joints with PBT-GF30 substrates

The water uptake behaviors of PBT-GF30 and silicone have already been determined in other works by the same authors [15,27]. Therefore, it is possible to conduct a numerical simulation that is going to predict the mass gain of the adhesive and substrate and, finally:

$$\Delta m_{a+s}^{T} = \Delta m_{a}^{N} + \Delta m_{s}^{N} \tag{3}$$

where N refers to numerically defined.

Joints with aluminum substrates

In the joints with aluminum substrates, the mass gain of the adhesive can also be numerically simulated. However, the mass gain of the aluminum needs to be determined. For that, bulk aluminum plates were immersed in water and their mass gain as a function of the exposed area was established. Then, for each joint:

$$\Delta m_{s} = \frac{\Delta m_{p}}{A_{p}} \cdot A_{j} \tag{4}$$

where Δm_p is the mass gain of the aluminum plate and A_p and A_j are the exposed area of aluminum in a plate and joint, respectively. And, therefore:

$$\Delta m_{a+s}^{T} = \Delta m_{a}^{N} + \frac{\Delta m_{p}}{A_{p}} \cdot A_{j} \tag{5}$$

3 Experimental details

3.1 Materials

In this study, one adhesive and two different substrates were used. The adhesive was a two-component commercially available silicone. The adhesive/catalyst ratio used was 1:1 and the mixture was cured at 125 °C for 25 minutes. The substrates were PBT-GF30 and 6082-T6 aluminum.

3.2 Specimen manufacturing

Rectangular joints (RJ)

Joints with an overlap of 25x20 mm were used for the gravimetric study, Figure 3. PBT-GF30/silicone and aluminum/silicone joints were prepared and the substrate thickness was always 2 mm. To ensure the adhesive thickness, calibrated tape with the desired size was used. The joints were positioned in a mold to ensure the placement of the substrates and calibrated tape and the mold was introduced in the hot-plate press at 120 °C and 20 bar for 25 minutes. After curing, the excess substrate, used to place the calibrated tape, was cut, to ensure in all sides of the joint the adhesive are directly exposed to water and there is no water between substrates, without adhesive, Figure 4 .

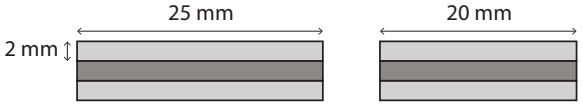


Figure 3: Rectangular joints manufactured.



Figure 4: Trim RJs to ensure the adhesive is in the same plane of the end of the substrate for every side.

Single lap joints (SLJ)

Two groups or SLJs were prepared: PBT-GF30/silicone and aluminum/silicone. For both groups, joints with 0.5, 1 and 2 mm of thickness were used. For all of the joints, the overlap was kept at 25 mm and the substrate thickness was 2 mm. The joints were placed in a mold [35] and the adhesive thickness was ensured using packing shims. The adhesive was then carefully applied to the substrates and the final joints were placed in the hot-plate press at 120 °C and 20 bar for 25 minutes.

The geometry of the joints used is based in ASTM D1002 [36] and ISO 4587:1995 [37] standards, Figure 5.

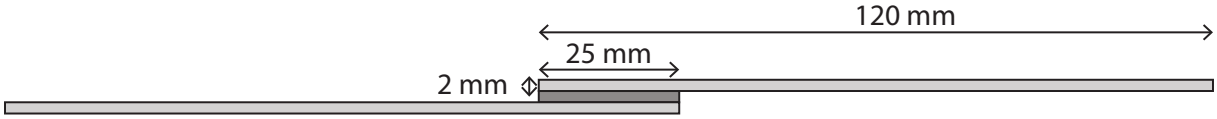


Figure 5: Single lap joints manufactured.

3.3 Testing procedures

Gravimetric study

The gravimetric study was performed using the RJs. The joints were fully dried in silica at 70 °C for two weeks. After drying, the joints were measured, in terms of geometry and mass and placed in a container with distilled water at 70 °C. When in water, it was confirmed none of the joint surfaces was in contact with the container walls or other joints. The temperature of immersion is controlled by placing the container in a climatic chamber (Memmert GmbH, Büchenbach, Germany). Periodically, the joints were removed from the immersion conditions and their mass was measured. All mass measurements were performed with a microbalance with 0.1 mg of accuracy (KernToledo, Balingen, Germany). For each substrate material and each adhesive thickness at least three specimens were used.

The water uptake recorded from these joints refers to the total mass of water that ingresses the joint during immersion, either through the adhesive, through the interphase or through the pores and cracks of the adhesive. However, superficial changes of the aluminum were observed during water immersion. To understand if that phenomenon had an effect on the mass gain of the joint, three plates of aluminum were also immersed in water and their mass periodically recorded. The dimension of the aluminum samples were measured prior to water immersion.

Single lap joint (SLJ) testing

The SLJ were tested after manufacturing and after being immersed in water at 70 ∘C for enough time for the overlap to reach a constant mass value, determined from the known behavior of the RJs. The joints were secured vertically using two grips prior to testing. To create pressure in the grips, four M6 bolts were used, with a torque of 20 Nm. To compensate for the opposing substrate and the adhesive thickness, metal tabs are positioned. Additionally, two center pins are used during testing to ensure proper positioning of the substrate, minimizing or preventing the specimens from slipping. The joint was tested at 2 mm/min and the load-displacement curves were recorded. The specimens tested after aging in water at 70 ∘C, were kept in the climatic chamber, immersed in water until testing. For each substrate material, each condition and each adhesive thickness at least three specimens were tested.

4 Numerical models

Numerical models were used to simulate the water uptake behavior of joints with aluminum and PBT-GF30 substrates. For these models, a heat transfer analogy was used, where the conductivity corresponds to the coefficient of diffusion and the temperature of the nodes exposed to water corresponds to the water uptake at saturation, the other nodal temperatures are set to zero in the beginning of the model.

4.1 Joints with aluminum substrates

This numerical model considers the ideal situation, where no water ingresses through the interphase. Therefore, each slice of adhesive parallel to the substrates has the same length exposed to water. For that reason, a 2D model, considering one of these slices, can be used to simulate the water uptake of the material, Figure 6. Since the model is symmetric in two axis, only one quarter of the slice of adhesive has to be simulated. A square mesh with a size length of 0.5 mm was used, with 4-node linear heat transfer DC2D4 elements.

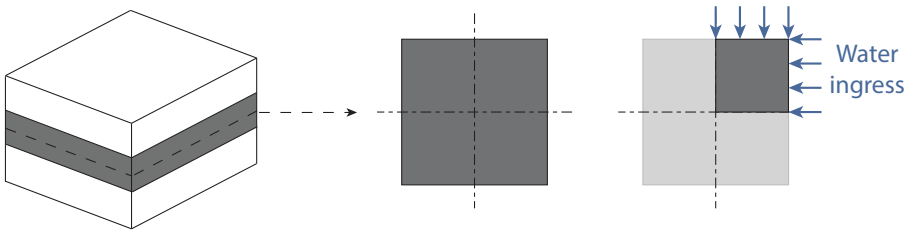


Figure 6: Numerical model developed for the gravimetric study of RJs with aluminum substrates, considering only water uptake through the adhesive.

The side length of the simulation was first set to the exact measurements of each specimen manufactured, to understand if the differences in water uptake were significant. Afterwards, seeing the difference was negligible, the average size was used.

4.2 Joints with PBT-GF30 substrates

The numerical simulation of the RJs with PBT-GF30 substrates has two be a 3D model, since it is important to consider the water ingressing through the substrates and through the adhesive. It is also important to consider the contact between substrate and adhesive. Taking advantage of symmetry, only one eighth of the joint has to be simulated, Figure 7. For the model, a brick mesh with a size length of 0.5 mm was used, with 8-node linear hear transfer DC3D8 elements.

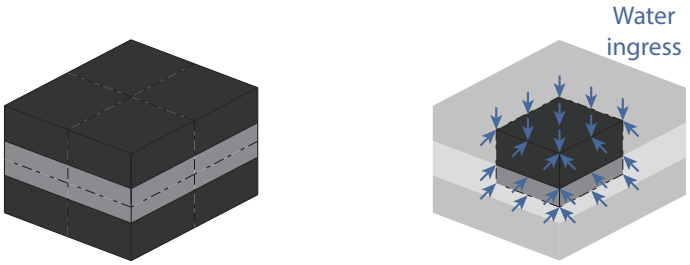


Figure 7: Numerical model developed for the gravimetric study of RJs with PBT-GF30 substrates, considering water uptake through the adhesive and substrate.

4.3 Numerical results

The numerical results in terms of water uptake as a function of time for the joints with aluminum substrates are shown in Figure 8. It is noticeable that the behavior is very similar, regardless of adhesive thickness, since it describes a hypothetical scenario where water only ingresses through the adhesive. In that scenario, the mass of water is proportional to the mass of adhesive, which is proportional to the adhesive thickness. Therefore, the adimensional water uptake at a given time t is independent of the thickness, since it is determined from:

$$M_t = \frac{m_t}{m_0} \tag{6}$$

where m_t is the mass at time t and m_0 is the initial mass.

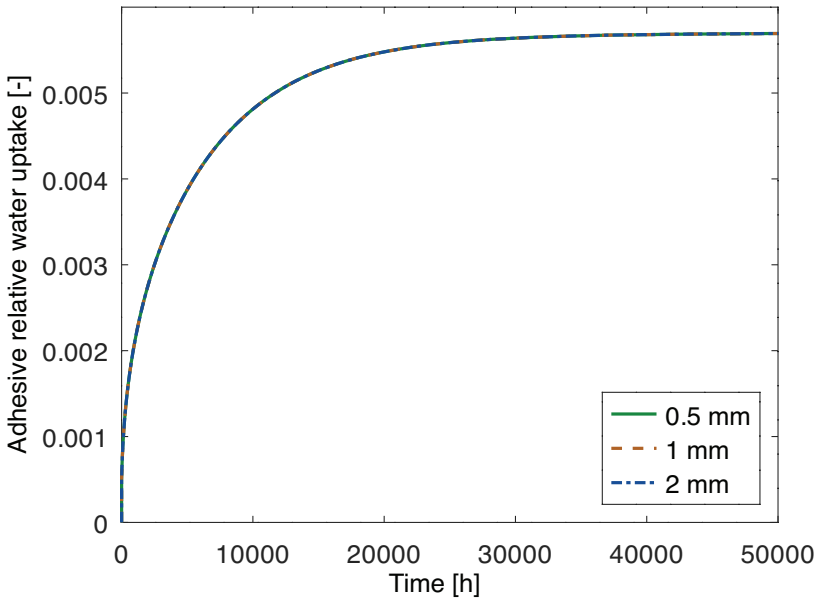


Figure 8: Numerical water uptake only through the adhesive layer of joints with 2 mm thick aluminum substrates and 0.5 mm, 1 mm, and 2 mm thick adhesive.

The joints with PBT-GF30 substrates have to be analyzed using a different approach since, in this case, water flows through the substrate and the adhesive. Therefore, in Figures 9a, 9b and 9c, the water uptake of the substrates and adhesive for joints with adhesive thickness of 0.5 mm, 1 mm and 2 mm, respectively, are presented.

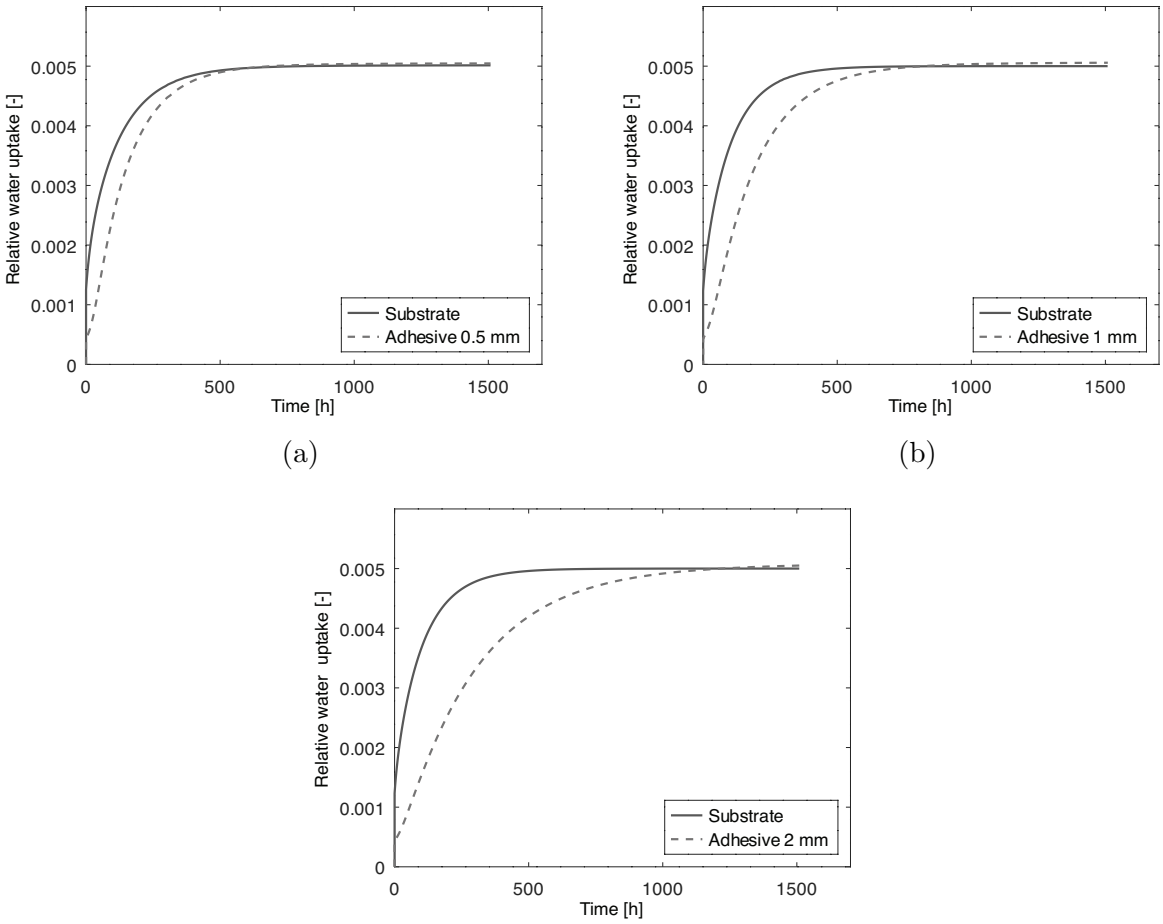


Figure 9: Numerical water uptake of adhesive and substrate of joints with 2 mm thick PBT-GF30 substrates and 0.5 mm a), 1 mm b) and 2 mm c) thick adhesive.

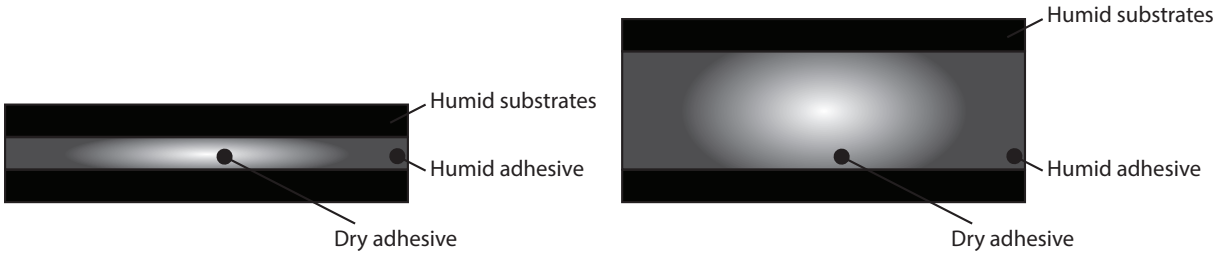
The chemical and geometrical properties of the PBT-GF30 substrate are the same for all the models, i.e., the area exposed to water, substrate thickness and water uptake behavior are constant. Therefore, as expected, the water uptake behavior of the substrates is the same for all of the joints. The main difference is concerning the adhesive. As seen in the aluminum joints, Figure 10a if water ingresses only through the adhesive, the water uptake is independent of the adhesive thickness. However, in this case, the substrate can also absorb water and, since the smaller water diffusion path is perpendicular to the adhesive/substrate interface, the substrate has a preponderant role in the water uptake of the adhesive, Figure 10b. Additionally, for this motive the theoretical water uptake of the joint with PBT-GF30 substrates is going to be significantly quicker, when compared to the water uptake of the adhesive in the joint with aluminum substrates, as it can be confirmed by the time scales in Figures 8 and 9.



(a) (b)

Figure 10: Water uptake of RJs with aluminum a), and PBT-GF30 b) substrates as expected from the numerical model.

That is also the motive behind the adhesive in the 0.5 mm joint having a higher water uptake, for the same time, than the 1 mm or 2 mm joints. Since water is also absorbed through the substrate, thicker joints have a lower portion of humid adhesive at a given time, Figure 11. However, the value at saturation is the same, since the materials used are the same and water uptake is given by equation (6).



(a) (b)

Figure 11: Water uptake of RJs with a thin layer of adhesive a), and a thick layer of adhesive b) as expected from the numerical model.

5 Experimental results

5.1 Gravimetric tests

Aluminum rectangular joints

The mass gain of the aluminum substrates was determined and divided, for each time increment, by the surface area of the aluminum exposed to water. Therefore, the mass gain per mm^2 was determined, Figure 12.

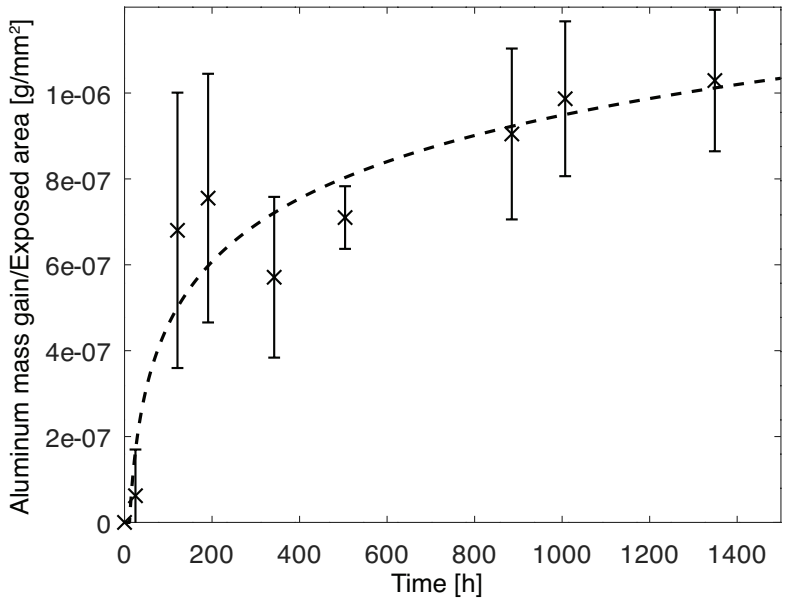


Figure 12: Mass gain of aluminum substrates immersed in water.

With the data collected, it is clear that a trend can be established in the time period considered, a logarithmic relation was used:

$$\Delta m/A_p[\mathrm{g/mm^2}] = 2.12 \cdot 10^{-7} \ln t - 5.16 \cdot 10^{-7} \tag{7}$$

The area of aluminum exposed to water was known for each joint. Therefore, the mass increase attributed to the oxidized layer was determined and subtracted from the mass gain of the joint. Finally, it was possible to determine the absolute water mass gain of the adhesive and interphase, Figure 13.

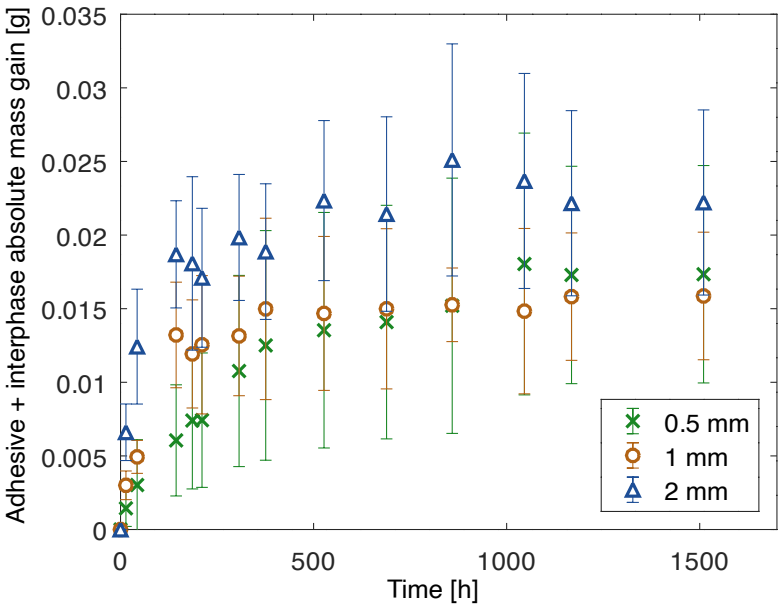


Figure 13: Mass gain due to water uptake of adhesive and interphase of joints with aluminum substrates and 0.5 mm, 1 mm, and 2 mm thick adhesive.

PBT-GF30 rectangular joints

The mass gain, through the water uptake, of the PBT-GF30/silicone joints for all of the adhesive thicknesses analyzed are shown in Figure 14.

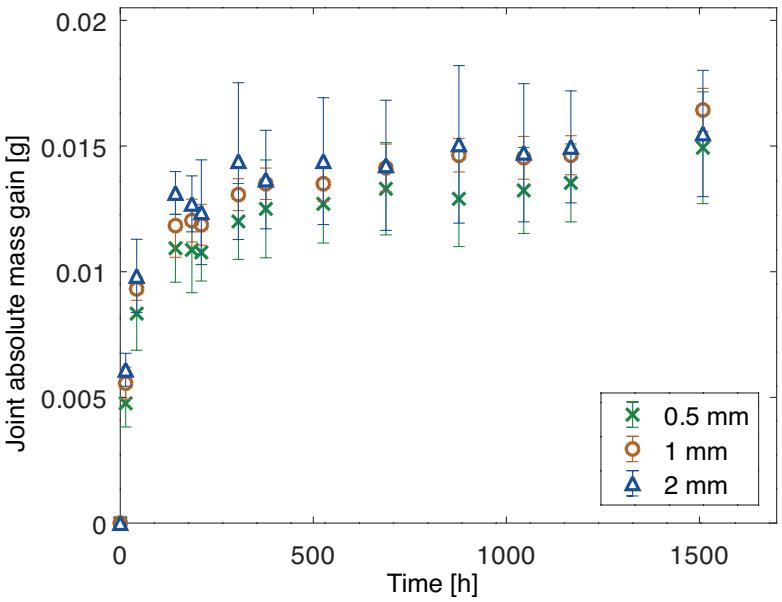


Figure 14: Mass gain due to water uptake of joints (adhesive, substrate and interphase) with PBT-GF30 substrates and 0.5 mm, 1 mm, and 2 mm thick adhesive.

It can be noticed that, when subjected to the same immersion conditions, the mass gain of the joints with PBT-GF30 (considering adhesive, substrate and interphase) is similar to that of the joints with aluminum (considering adhesive and interphase). Therefore, the interphase of the aluminum joints must be absorbing an amount of water similar to that of the substrate and interphase of the PBT-GF30 joints. Additionally, at this point, the time of water absorption until a constant mass gain value was reached is approximately the same and, for the theoretical model it was significantly higher for the joints with aluminum substrates. Therefore, the water uptake of the adhesive and interphase for the joints with aluminum substrates was higher and quicker than predicted.

5.2 Single lap joint tests

Aluminum single lap joints

The maximum load of joints with aluminum substrates before and after aging is shown in Figure 15. In the dry condition, it can be seen that, between 0.5 and 1 mm of adhesive thickness the maximum load is similar. However, for 2 mm of thickness the strength decreases. It has been seen that there is an optimum adhesive thickness to obtain maximum strength, and the joint with 2 mm is further away from that value [38].

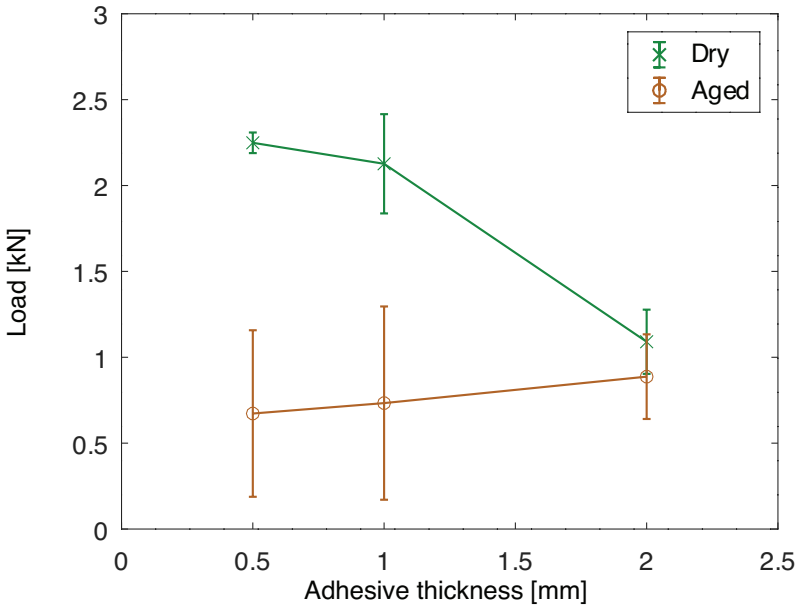


Figure 15: Maximum load for single lap joint tests for joints with aluminum substrates as a function of the adhesive thickness, dry and after aging at 70 °C for two months.

Comparing the dry and aged conditions, it is clear that the joint strength significantly decreases for 0.5 and 1 mm of adhesive thickness. However, for 2 mm the strength is similar, which can be correlated to the fracture surfaces. The fracture surfaces of the joints when dry are presented in Figure 16 and when aged in Figure 17. The joint with 0.5 mm of adhesive thickness changes from a saw-like cohesive fracture surface, typical of silicones (Figure 16a), to a failure surface with some areas of adhesive failure (Figure 17a). The same can be seen for the 1 mm thick adhesive joints when dry and aged, Figures 16b and 17b, respectively. For the 2 mm thick joints the failure remains cohesive from the dry to the aged condition, Figures 16c and 17c, respectively, which is going to be discussed in further detail in the *Discussion* section.



(a) (b) (c)

Figure 16: Fracture surfaces of dry joints with aluminum substrates with 0.5 mm a), 1 mm b) and 2 mm c) of adhesive thickness.



(a) (b) (c)

Figure 17: Fracture surfaces of aged joints with aluminum substrates with 0.5 mm a), 1 mm b) and 2 mm c) of adhesive thickness.

PBT-GF30 single lap joints

The maximum loads recorded for the SLJs with PBT-GF30 substrates when dry and aged are presented in Figure 18. The same trend described for the dry joints with aluminum substrates is found here. However, there is not a significant change between the dry and aged condition for these joints, with decrease of mechanical properties of the materials due to water immersion at high temperature.

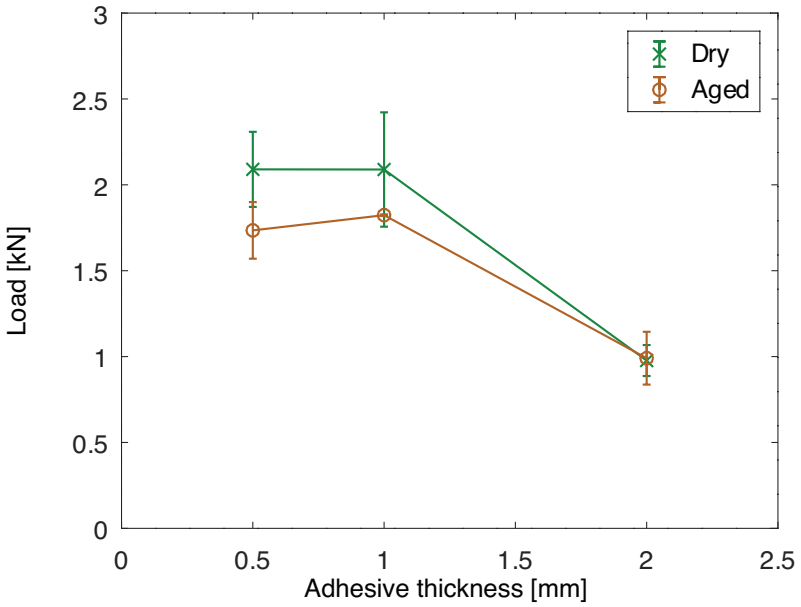


Figure 18: Maximum load for single lap joint tests for joints with PBT-GF30 substrates as a function of the adhesive thickness, dry and after aging at 70 °C for two months.

The same similarity between the failure load for the dry and aged condition is also shown in the fracture surfaces. Both in the dry and aged conditions (Figures 19 and 20, respectively), failure of the joints is cohesive through the adhesive.



(a) (b) (c)

Figure 19: Fracture surfaces of dry joints with PBT-GF30 substrates with 0.5 mm a), 1 mm b) and 2 mm c) of adhesive thickness.



(a) (b) (c)

Figure 20: Fracture surfaces of aged joints with PBT-GF30 substrates with 0.5 mm a), 1 mm b) and 2 mm c) of adhesive thickness.

6 Discussion

Joints with aluminum substrates, as seen, absorb water through the adhesive but the presence of additional diffusion paths at the interphase has been suggested. To isolate the effect of the interphase, the mass gain of the substrate was eliminated and the effect of the adhesive layer must also be disregarded.

The theoretical water uptake behavior of the adhesive is known from the numerical model, however, this water uptake was determined as a function of the mass of the adhesive from equation (6). Therefore, for each joint analyzed, the water uptake of the adhesive must be multiplied by its initial mass to obtain the mass gain the adhesive theoretically experiences. The initial mass of adhesive can be determined from the initial mass of the joint, eliminating the initial mass of the aluminum:

$$m_{a0} = m_{j0} - m_{s0} = m_{j0} - \rho_{s0} \cdot V_{s0} \tag{8}$$

where m_{x0}, ρ_{x0} and V_{x0} refers to the initial mass, density and volume of x, respectively, and a, j and s to the adhesive, joint and substrate.

Therefore, knowing the volume of aluminum in each joint, its density needs to be determined. This was achieved, from the initial dimensions and mass of the bulk aluminum plates, prior to water immersion, and a value of 2564±26 kg/m^3 was obtained. With this, the initial mass of adhesive was determined for each joint and its theoretical mass gain, numerically determined, was established, Figure 21.

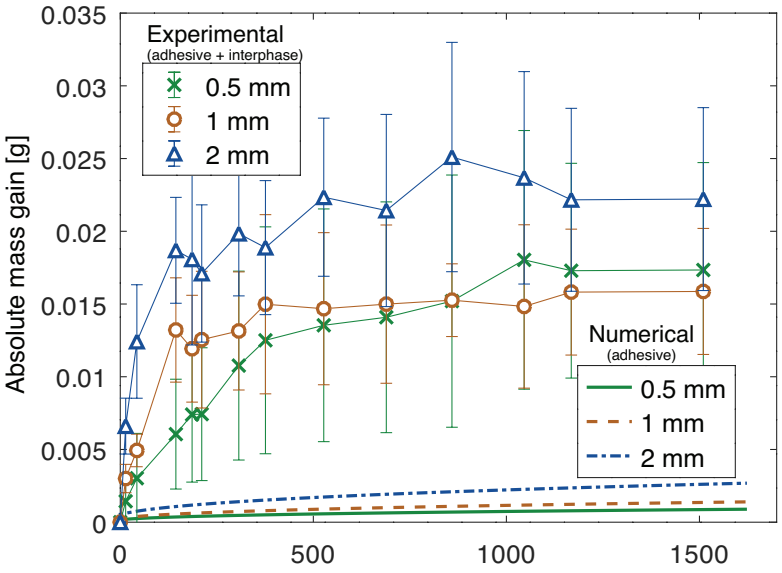


Figure 21: Mass gain due to water uptake of joints with aluminum substrates and 0.5 mm, 1 mm, and 2 mm thick adhesive: numerical (considering only water uptake in the adhesive) and experimental (considering adhesive and interphase).

The theoretical mass gain of water through the adhesive was then eliminated from the experimental results that considered the adhesive and interphase, Figure 21, obtaining the water mass gain of the interphase, Figure 22.

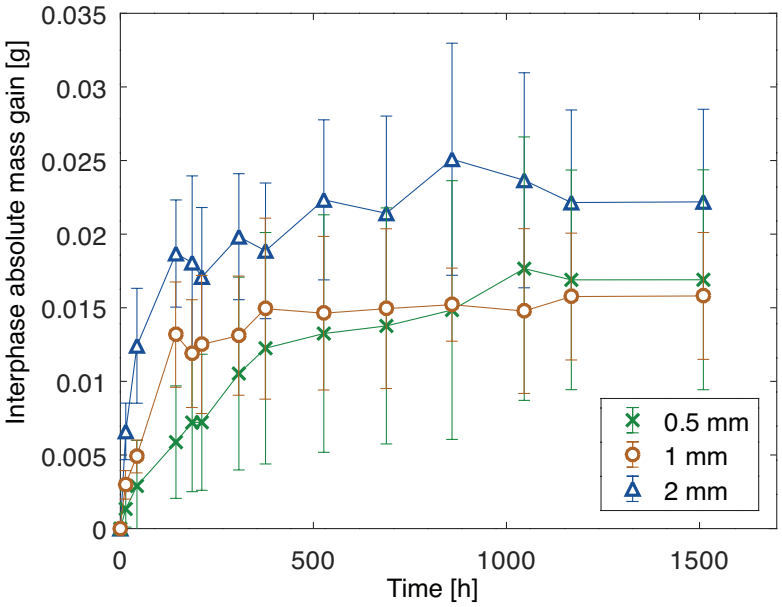


Figure 22: Mass gain due to water uptake of the interphase of joints with aluminum substrates and 0.5 mm, 1 mm, and 2 mm thick adhesive.

It could be argued that additional voids in the adhesive in the joint, when compared to the bulk plate of material, can also contribute to additional water uptake. However, this effect is negligible, as it can be confirmed from the matching results between the

theoretical numerical model of the adhesive and substrate of the joints with PBT-GF30 substrate and its experimental results, Figure 23. The adhesive layer, except interphase, is expected to have the same behavior in both groups of joints, and, therefore, if the difference was due to the voids in the adhesive, that would also be clear in the joints with PBT-GF30 substrates.

Therefore, the difference in mass gain can be attributed to the differences in the interphase, which contributes to the joints with aluminum absorbing water through this region and the joints with PBT-GF30 only significantly absorbing water through the bulk materials.

The agreement between experimental (adhesive, substrate and interphase) and numerical (adhesive and substrate) results of the joints with PBT-GF30 substrates shows that water is only significantly absorbed by the adhesive and substrate. It can not be excluded that the interphase of the PBT-GF30/silicone joints can also absorb a smaller amount of water. However, that effect is not clear in our tests. This is also confirmed from the fracture surfaces. The joints with aluminum substrates exhibit adhesive failure when aged, due to the water that ingresses between the adhesive and substrate and contributes to debonding. However, the joints with PBT-GF30 substrates consistently exhibit cohesive failure through the adhesive.

It has been mentioned that water uptake can occur non negligibly through the interface or interphase for aluminum/silicone joints. The failure path, which appears to be exactly between adhesive and substrate, exhibiting adhesive failure, points to a water ingress exactly through the interface plane. However, since in a micro or nanoscale, it is very complex to affirm that the failure path is exactly between adhesive and substrate or if it is globally within the interphase, both possibilities must be considered. And, since, the water uptake can be attributed more generally to the interphase. Nonetheless, these results prove that the region between adhesive and substrate must not be neglected.

These results corroborate the conclusion of Drain et al. [34], showing that, generally, the identification of the interface between composite materials with polymeric matrices and adhesive is more challenging, when compared to metal/adhesive interfaces, since the polymer of the adhesive dissolves in the polymer of the substrate and vice versa. This dissolution can be behind the apparently stronger, and more resistant to the humid environment, interphase between PBT-GF30 and silicone, when compared with the aluminum/silicone interphase.

Comparing the mass gain of the joints with PBT-GF30 substrates, Figure 23, it can be seen that, from the numerical model, the joints are expected to absorb water slower as the adhesive thickness increases. However, because the joint with 2 mm has more voids that with 0.5 mm or 1 mm, it is seen that the water uptake at saturation is slightly higher.

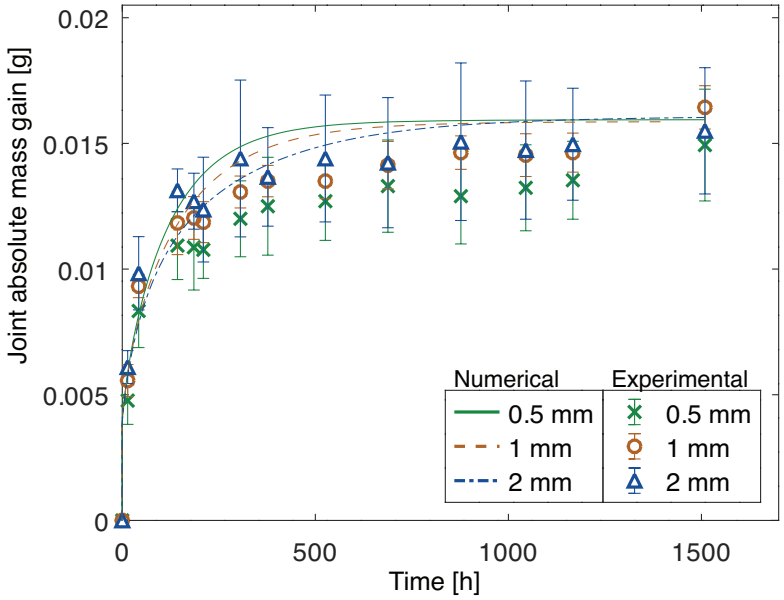


Figure 23: Mass gain due to water uptake of joints with PBT-GF30 substrates and 0.5 mm, 1 mm, and 2 mm thick adhesive: numerical (considering only water uptake through the adhesive and substrate) and experimental (considering adhesive, substrate and interphase)

When comparing between joints with aluminum substrates and different adhesive thicknesses, since the water uptake of the adhesive and the mass gain of the substrate were eliminated, the excess mass gain, which is attributed to the interphase, should be the same regardless of the adhesive thickness. However, this is not the case, which can be attributed to the slightly higher void content of the joints with 2 mm, which contributes to a higher mass gain of water. It must also be pointed out that this difference may contribute to the fact that, for SLJs with 2 mm of bondline thickness, failure is cohesive before and after water aging.

7 Conclusions

The main conclusions drawn from this work are that:

- The water uptake of joints with PBT-GF30 substrates and silicone adhesive can be approximated by the numerical model that considers only the water uptake though the bulk adhesive and substrate, since the effect of the interphase is negligible;
- For the determination of the water gain of joints with aluminum substrates and silicone adhesive, the effect of the interphase must be considered, since it contributes to a significantly higher mass gain;
- PBT-GF30/silicone adhesive SLJs exhibit cohesive failure before and after aging;
- Joints with aluminum substrates exhibit adhesive failure after aging because of the water uptake through the interphase;

- The environmental resistance of the PBT-GF30/silicone interphase appears to be higher than that of the aluminum/silicone interphase since the water absorbed through the interphase can not be identified in the gravimetric tests and after aging at 70 °C for two months failure is still cohesive in the adhesive, and for the aluminum/silicone joints adhesive failure is recorded.

Acknowledgments

The author(s) disclosed receipt of the following financial support for the research, authorship, and/or publication of this article: The authors wish to acknowledge and thank the funding and support provided by Robert Bosch GmbH, Corporate Research and Advance Engineering, Renningen. The authors also gratefully acknowledge the funding provided by Fundação para a Ciência e Tecnologia (FCT), Portugal for the Ph.D. Grant 2020.06055.BD.

References

[1] L. F. M. da Silva, A. Öchsner, and R. D. Adams. *Handbook of adhesion technology*, volume 1. Springer, 2018.

[2] R. D. Adams, J. Comyn, and W. C. Wake. *Structural adhesive joints in engineering*. Springer Science & Business Media, 1997.

[3] L. F. M. da Silva, A. Pirondi, and A. Öchsner. *Hybrid adhesive joints*, volume 6. Springer Science & Business Media, 2011.

[4] C. S. P. Borges, E. A. S. Marques, R. J. C. Carbas, C. Ueffing, P. Weißgraeber, and L. F. M. da Silva. Review on the effect of moisture and contamination on the interfacial properties of adhesive joints. *Proceedings of the Institution of Mechanical Engineers, Part C: Journal of Mechanical Engineering Science*, 235(3):527–549, 2021.

[5] J. Comyn. Durability of structural adhesives. *Applied Science, London*, 1983.

[6] A. Q. Barbosa, L. F. M. da Silva, and A. Öchsner. Hygrothermal aging of an adhesive reinforced with microparticles of cork. *Journal of Adhesion Science and Technology*, 29(16):1714–1732, 2015.

[7] G. M. S. O. Viana, M. Costa, M. D. Banea, and L. F. M. da Silva. A review on the temperature and moisture degradation of adhesive joints. *Proceedings of the Institution of Mechanical Engineers, Part L: Journal of Materials: Design and Applications*, 231(5):488–501, 2017.

[8] R. A. Pethrick. Design and ageing of adhesives for structural adhesive bonding–a review. *Proceedings of the Institution of Mechanical Engineers, Part L: Journal of Materials: design and applications*, 229(5):349–379, 2015.

[9] J. Crank. *The mathematics of diffusion*. Oxford university press, 1979.

[10] A. Malpot, F. Touchard, and S. Bergamo. Effect of relative humidity on mechanical properties of a woven thermoplastic composite for automotive application. *Polymer Testing*, 48:160–168, 2015.

[11] Z. A. Mohd Ishak, T. S. A. Tengku Mansor, B. N. Yow, U. S. Ishiaku, and J. Karger-Kocsis. Short glass fibre reinforcedpoly (butylene terephthalate) Part 1–Microstructural characterisation and kinetics of moisture absorption. *Plastics, rubber and composites*, 29(6):263–270, 2000.

[12] A. Boubakri, N. Haddar, K. Elleuch, and Y. Bienvenu. Impact of aging conditions on mechanical properties of thermoplastic polyurethane. *Materials & Design*, 31(9):4194–4201, 2010.

[13] J. Dai, X. Yao, H. Y. Yeh, and X. Liang. Moisture absorption of filled silicone rubber under electrolyte. *Journal of applied polymer science*, 99(5):2253–2257, 2006.

[14] I. Khalilullah, T. Reza, L. Chen, A. K. M. M. H. Mazumder, J. Fan, C. Qian, G. Zhang, and X. Fan. In-situ characterization of moisture absorption and hygroscopic swelling of silicone/phosphor composite film and epoxy mold compound in LED packaging. In *2017 18th International Conference on Thermal, Mechanical and Multi-Physics Simulation and Experiments in Microelectronics and Microsystems (EuroSimE)*, pages 1–9. IEEE, 2017.

[15] C. S. P. Borges, R. Brandão, A. Akhavan-Safar, E. A. S. Marques, R. J. C. Carbas, C. Ueffing, P. Weißgraeber, F. Schmid, and L. F. M. da Silva. Influence of water and surfactant contamination on the mechanical and chemical properties of a silicone adhesive before and after curing. *The Journal of Adhesion*, -(-):–, 2022.

[16] B. Lutz, Z. Guan, L. Wang, F. Zhang, and Z. Lü. Water absorption and water vapor permeation characteristics of HTV silicone rubber material. In *2012 IEEE International Symposium on Electrical Insulation*, pages 478–482. IEEE, 2012.

[17] S. Fang, Z. Jia, H. Gao, and Z. Guan. Influence of fillers on silicone rubber for outdoor insulation. In *2007 Annual Report-Conference on Electrical Insulation and Dielectric Phenomena*, pages 300–303. IEEE, 2007.

[18] M. Ali and R. Hackam. Effects of saline water and temperature on surface properties of HTV silicone rubber. *IEEE Transactions on Dielectrics and Electrical Insulation*, 15(5):1368–1378, 2008.

[19] G. Viana, M. Costa, M. D. Banea, and L. F. M. da Silva. Behaviour of environmentally degraded epoxy adhesives as a function of temperature. *The Journal of Adhesion*, 93(1-2):95–112, 2017.

[20] S. Sugiman, A. D. Crocombe, and I. A. Aschroft. Experimental and numerical investigation of the static response of environmentally aged adhesively bonded joints. *International Journal of Adhesion and Adhesives*, 40:224–237, 2013.

[21] Y. Hua, A. D. Crocombe, M. A. Wahab, and I. A. Ashcroft. Modelling environmental degradation in EA9321-bonded joints using a progressive damage failure model. *The Journal of Adhesion*, 82(2):135–160, 2006.

[22] R. S. Ashofteh and H. Khoramishad. The influence of hygrothermal ageing on creep behavior of nanocomposite adhesive joints containing multi-walled carbon nanotubes and graphene oxide nanoplatelets. *International Journal of Adhesion and Adhesives*, 94:1–12, 2019.

[23] M. P. Zanni-Deffarges and M. E. R. Shanahan. Diffusion of water into an epoxy adhesive: comparison between bulk behaviour and adhesive joints. *International Journal of Adhesion and Adhesives*, 15(3):137–142, 1995.

[24] M. Costa, G. Viana, L. F. M. da Silva, and R. D. S. G. Campilho. Environmental effect on the fatigue degradation of adhesive joints: a review. *The Journal of Adhesion*, 93(1-2):127–146, 2017.

[25] M. Costa, G. Viana, L. F. M. da Silva, and R. D. S. G. Campilho. Effect of humidity on the fatigue behaviour of adhesively bonded aluminium joints. *Latin American Journal of Solids and Structures*, 14:174–187, 2017.

[26] J. Fan, Z. Wang, X. Zhang, Z. Deng, X. Fan, and G. Zhang. High moisture accelerated mechanical behavior degradation of phosphor/silicone composites used in white light-emitting diodes. *Polymers*, 11(8):1277, 2019.

[27] C. S. P. Borges, A. Akhavan-Safar, E. A. S. Marques, R. J. C. Carbas, C. Ueffing, P. Weißgraeber, and L. F. M. da Silva. Effect of Water Ingress on the Mechanical and Chemical Properties of Polybutylene Terephthalate Reinforced with Glass Fibers. *Materials*, 14(5):1261, 2021.

[28] R. Brandão, C. S. P. Borges, E. A. S. Marques, R. J. C. Carbas, A. Akhavan-Safar, F. Schmid, C. Ueffing, P. Weißgraeber, and L. F. M. da Silva. The influence of humidity and immersion temperature on the properties and failure mode of PBT-GF30/silicone bonded joints. *Composite Structures*, page 115421, 2022.

[29] R. A. Gledhill and A. J. Kinloch. Environmental failure of structural adhesive joints. *The journal of adhesion*, 6(4):315–330, 1974.

[30] M.-G. Barthés-Labrousse. Mechanisms of formation of the interphase in epoxy-amine/aluminium joints. *The Journal of Adhesion*, 88(8):699–719, 2012.

[31] J. Delozanne. *Durabilité des époxys; application au collage structural aéronautique*. PhD thesis, Paris, ENSAM, 2018.

[32] S. G. Hong, N. G. Cave, and F. J. Boerio. The modification of epoxy/metal interphases by adsorbed contaminants. *The Journal of Adhesion*, 36(4):265–279, 1992.

[33] P. Cognard. *Collage des Composites: Construction Aerospatiale, Automobile et Ferroviaire*. Ed. Techniques Ingénieur, 2004.

[34] K. F. Drain, J. Guthrie, C. L. Leung, F. R. Martin, and M. S. Otterburn. The effect of moisture on the strength of polycarbonate-cyanoacrylate adhesive bonds. *International journal of adhesion and adhesives*, 5(3):133–136, 1985.

[35] M. D. Banea, L. F. M. da Silva, and R. D. S. G. Campilho. Moulds design for adhesive bulk and joint specimens manufacturing. *Assembly Automation*, 2012.

[36] ASTM D1002-99. Standard Test Method for Apparent Shear Strength of Single-Lap-Joint Adhesively Bonded Metal Specimens by Tension Loading (Metal-to-Metal). Standard, ASTM International, Pennsylvania, United States, October 2001.

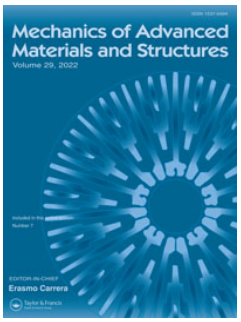
[37] ISO 4587. Adhesives — Determination of tensile lap-shear strength of rigid-to-rigid bonded assemblies. Standard, International Organization for Standardization, Geneva, CH, March 2003.

[38] M. D. Banea, L. F. M. da Silva, and R. D. S. G. Campilho. The effect of adhesive thickness on the mechanical behavior of a structural polyurethane adhesive. *The Journal of Adhesion*, 91(5):331–346, 2015.

Appendix F

Paper F

Effect of surfactant contamination on the properties of aluminum/silicone adhesive joints



Mechanics of Advanced Materials and Structures

ISSN: (Print) (Online) Journal homepage: https://www.tandfonline.com/loi/umcm20

Effect of surfactant contamination on the properties of aluminum/silicone adhesive joints

R. Brandão, C. S. P. Borges, E. A. S. Marques, R. J. C. Carbas, A. Akhavan-Safar, P. D. P. Nunes, C. Ueffing, P. Weißgraeber, F. Schmid & L. F. M. da Silva

To cite this article: R. Brandão, C. S. P. Borges, E. A. S. Marques, R. J. C. Carbas, A. Akhavan-Safar, P. D. P. Nunes, C. Ueffing, P. Weißgraeber, F. Schmid & L. F. M. da Silva (2022): Effect of surfactant contamination on the properties of aluminum/silicone adhesive joints, Mechanics of Advanced Materials and Structures, DOI: 10.1080/15376494.2022.2046217

To link to this article: https://doi.org/10.1080/15376494.2022.2046217

Published online: 09 Mar 2022.

Submit your article to this journal

View related articles

View Crossmark data

Full Terms & Conditions of access and use can be found at
https://www.tandfonline.com/action/journalInformation?journalCode=umcm20

MECHANICS OF ADVANCED MATERIALS AND STRUCTURES
https://doi.org/10.1080/15376494.2022.2046217

Taylor & Francis
Taylor & Francis Group

ORIGINAL ARTICLE

Check for updates

Effect of surfactant contamination on the properties of aluminum/silicone adhesive joints

R. Brandão[a], C. S. P. Borges[b], E. A. S. Marques[b], R. J. C. Carbas[b], A. Akhavan-Safar[b], P. D. P. Nunes[b], C. Ueffing[c], P. Weißgraeber[d], F. Schmid[c], and L. F. M. da Silva[a]

[a]Departamento de Engenharia Mecânica, Faculdade de Engenharia (FEUP), Universidade do Porto, Porto, Portugal; [b]Instituto de Ciência e Inovação em Engenharia Mecânica e Engenharia Industrial (INEGI), Porto, Portugal; [c]Corporate Research and Advance Engineering, Robert Bosch GmbH, Renningen, Germany; [d]Chair of Lightweight Design and Materials, University of Rostock, Rostock, Germany

ABSTRACT

Adhesives are used to join and seal electronic packaging. In these application, they are often used to bond aluminum components and, during the process of machining aluminum, oils and lubricants are used to facilitate the process. To remove these fluids, detergents such as surfactants are often used. However, if the surfactant itself is not removed completely and remains on the aluminum part, it can affect the bond properties of the joint, leading to abrupt joint failure. In this work, adhesive joint properties as a function of the amount of surfactant at the surface were studied. The joint substrates are Al6082-T6 aluminum, the adhesive a two-part silicone and the surfactant a cocosalkylaminethoxylate. For this, double cantilever beam (DCB) and single lap joints (SLJ) were used. An additional scanning electron microscopy (SEM) analysis was conducted to clarify the results. It was found that the adhesive bond strength continuously decreases with increasing amount of contaminant. Similarly, with increasing amounts of contaminant applied to the surface, the failure mode progressively changed from cohesive to adhesive, which was attributed to the adhesive at the interphase absorbing the contaminant during curing, moving the failure to this region, until the absorption limit of the adhesive is surpassed and the surfactant remains at the interface, leading to interfacial failure. A numerical model was created to simulate the behavior of the experimental joints and obtain the properties of the interphase by applying the inverse method, and a numerical study was done on the sensitivity of the model to variations in cohesive peel properties for the DCB and shear properties for the SLJ.

ARTICLE HISTORY
Received 6 August 2021
Accepted 21 February 2022

KEYWORDS
Adhesives; silicone; contamination; surfactant; double cantilever beam; single lap joint

1. Introduction

Adhesives are used in several applications due to their high strength to weight ratio, as well as not needing the introduction of holes or local heating of the components to join two materials [1]. As a result, they are a better option in a wide range of scenarios, particularly when bonding notch sensitive composite materials, for instance the polybutylene terephthalate with 30% of glass fiber (PBT-GF30) housings for electronic components to the aluminum heat sinks found in vehicles. The components of this housing are often bonded using silicone, since high strength and stiffness are not a requirement in these applications, and thermal insulation and sealing are crucial. Prior to bonding, the aluminum is processed to obtain the final component desired and oils are used in the procedure. These oils are then cleaned using a detergent, containing surfactants, which, if it is not carefully rinsed, can remain at the substrate surface and act as a contaminant.

When two substrates are joined using an adhesive, an interphase is formed between the adhesive and the substrate [2–4]. This interphase layer, created upon adhesive bonding due to the adhesive/substrate interations, has specific chemical, physical and mechanical properties, different from those of the adhesive and of the substrate [5, 6]. Possart et al. [7] stated that, in adhesive joints with metallic substrates, this interphase is created due to a segregation of components at the metal interface or at the air, leading to heterogeneities in the liquid stage. Thus, a specific layer, containing all those heterogeneities was formed between the adhesive and substrate and, since it has a gradient in chemical composition, chemical reactions during the curing of the adhesive also happen at different rates in this layer, thus leading to the conclusion that the cured interphase properties become field variables. The exact size of this layer has not been determined, but it was said that it extended over a long range of some hundred micrometers in a three-dimensional structure. A work carried out by Roche et al. [8] affirmed that in metal/epoxy adhesive joints, the glass transition temperature (T_g), the extent of the curing reaction between amine and epoxy, the interphase thickness, the residual stresses within the interphase and Young's modulus of the interphase all depend heavily on the amine nature, since it is the one that

CONTACT E. A. S. Marques emarques@fe.up.pt Instituto de Ciência e Inovação em Engenharia Mecânica e Engenharia Industrial (INEGI), Porto 4200-465, Portugal.

© 2022 Taylor & Francis Group, LLC

bonds with the metallic oxides on the surface of the substrate, creating organometallic complexes [9]. Voyutskii et al. [10] explained adhesion as the result of inter diffusion of the macromolecules of the two material being bonded at the interphase. This interphase arises from a chemical bond created between the metallic oxide at the substrate surface and the amine monomer from the adhesive. The reaction with the amine groups, that can be from an isophorone diamine (IPDA) monomers, form orgono-metallic complexes. If this concentration is higher than the solubility product, the complexes can crystallize as sharp needles [10]. These crystals perform as short fibers in an organic matrix which leads to improvements of the stiffness, although the practical adhesion decreases since there is a growth of the residual stress when the interphase is formed.

In the case of a contaminated substrate surface, the contaminant can either be displaced and absorbed by the adhesive or remain at the adhesive/substrate interface. In both scenarios, the contaminants may affect the mechanical, chemical and thermal properties of the joint. If the contaminant is absorbed by the adhesive, it can affect the mechanical properties, particularly of the interphase layer, since it is the one in close proximity to the contaminated substrate. If the contaminant remain at the adhesive/substrate interface, it forms a thin segregation layer, in a manometric scale, that can severely weaken the adhesive bond due to the physical separation between adhesive and substrate, not allowing mechanical interlocking and also making it difficult to establish chemical bonds. This can promote interfacial defects such as weak bonds or debonding of the adhesive. These interfacial defects are thought to arise either from surface contamination prior to the application of the adhesive, incorrect curing of the adhesive, adhesive chemistry, or due to the environment surrounding the components during its service life or any combination of these causes [11]. Weak bonds are very difficult to detect, often being only noticed when they cause premature failure of adhesive joints. Additionally, they are very challenging to reproduce experimentally so that detection mechanisms are developed. Brotherhood et al. [12] and Marty at al. [13] produced weak bonds by contaminating the joint with a very thin layer of several contaminants. In their research, contaminants such as release agents and silicone-based oil, showed promising results as candidates for creating constant zero volume debonds.

In addition to manufacturing weak bonds by surface contamination, Drewry et al. [14] created weak joints using a consistent amount of bearing grease (wet lubrication) in single lap joints. These joints showed a reproducible decrease in shear and tensile strength. In general, as seen, contamination studies are challenging since to characterize the effect of the contaminant joints with a constant amount of contaminant, distributed evenly along the overlap must be produced.

To avoid the weak bonds or zero volume debonds and create a strong bond between adhesive and an oil-contaminated metal surface, regardless of surfacial contamination, the adhesive needs to be able to perform two separate jobs. First, the adhesive must be able to move the oil from the metal surface directly. Second, the adhesive must be able to absorb most of the oil [15]. Greiveldinger et al. studied the diffusion of an industrial mineral oil into an epoxy resin in an adhesive joint. The contaminant was initially placed on the substrate. Once the adhesive begins to cure, the oil diffuses into the bulk adhesive. This process occurs quickly at the beginning of the curing cycle. Ahead of the adhesive curing, the Fourier-transform infrared spectroscopy (FTIR) profile at the interface is quite similar to that of the oil, showing that the oil is still at the adhesive/substrate interface [16]. However, at the end of the curing process, it resembles the uncontaminated adhesive. After a certain period of time in the curing cycle, it is noticeable that some oil leaves the adhesive, which is related to the crosslinking of the adhesive, since the adhesive shrinks just slightly on crosslinking, and this compression then result in the expelling of some contaminant from the adhesive. Crosslinking of the adhesive is very similar with and without the initial presence of oil at the interface, as far as the contaminant has been mostly absorbed by the adhesive [2, 16].

Contamination can have an impact on several stages of adhesion, the wettability of the surface, the curing process and the mechanical properties of the final joint such as strength [17] or in the curing process. The process of contamination can happen in different stages of the process; it can occur during manufacturing of the substrate which leads to a change in the surface energy. Hoffmann et al. studied different types of contamination such as release agents, moisture, fingerprint, thermal degradation and deicing fluid before being bonded on the metallic stamp. For all types, the different levels of contamination were evaluated and it was noticed a decrease of the adhesion strength for each scenario, especially with the increase of the level of contamination [18]. Rider et al. showed the surface energy changed during pretreatments of an aluminum substrate and with contaminant post pretreatments. During the pretreatments steps, the surfacial levels of hydrocarbon decrease which leads to an increase in surface hydrophicility, which means, an increase of the surface energy what enables the adhesive to wet the substrate and provides a better formation of adhesive bonds [19].

For a better contact between the substrate and the adhesive, the contaminant should be displaced from the substrate at adhesive application. However, some contaminant can be physically stuck due to the roughness of the substrate. This remaining contaminant must be absorbed by the adhesive to avoid a physical separation between the adhesive and substrate. Nonetheless, as discussed above, when the adhesive absorbs contamination, its properties might be affected. Debski et al. studied this effect, working on the T_g of resins as a function of the oil content. The results stated that T_g during cross-linking was heavily reduced by the oil content, the more contaminant is present the more the effect was noticeable [20]. Thus, there is an undeniable change in cross-linking kinetics due to the presence of contaminant.

Akiyama et al. examined the effect of various types of contaminants in the properties of two adhesive joints, one using an epoxy adhesive and the other an second generation acrylic (SGA) adhesive. Two of the contaminants were

Table 1. General properties of the silicone adhesive used.

Type of adhesive	Supplied as	Cure cycle
Silicone elastomer	Two-part	120°C/25 min

Table 2. Mechanical properties of the silicone adhesive used.

Tensile strength [MPa]	3.4 ± 0.1
Young's modulus [MPa]	1.3 ± 0.1
Elongation at break	200%

surfactants, stearic acid and dodium dodecyl sulfate (SDS). The authors found that the stearic acid decreased the bond strength of both joints even with a small amount of contaminant, while using SDS only after 5 layers of contaminant there was a breakdown in the properties of the joints [17].

Valoroso et al. [21] prepared DCBs with aluminum substrates and an epoxy with an aluminum powder filler adhesive to evaluate the mode I fracture energy and interphase strength. A new method for said measurement was developed, with good results, and, it was concluded that the extension and movement of the fracture process zone along the interphase was dependent on the thickness of the interphase and cohesive strength.

As discussed to this point, in the studies found in literature, the adhesives analyzed are usually epoxies. This study strives to enrich the knowledge developed up to this point by analyzing the effect on silicone adhesives.

Due to the low Young's modulus of silicone adhesives, which is generally below 10 MPa, they are usually applied in nonstructural and semi-structural applications that require flexible bonding, resistance to severe environmental and high service life [1]. One of the advantages of silicone adhesives is the wettability, silicons wet most substrates, even under disadvantageous conditions due to their low surface tension (ca. 21–22 mN m^{-1}). Another advantage is that cured silicone adhesives display good elastomeric properties like movement capability, elastic recovery (85–98%) and low creep when compared to others organic adhesives, they are much less temperature dependent. Their good fatigue resistance allows them to withstand cyclic loading in the adhesive joint caused by flexible flanges, equipment or component vibration, as well as temperature cycling of joints with high differential thermal expansion of substrates [22].

Regarding the effect of adhesive thickness, Han et al. [23] observed that, using aluminum substrates and a two-component, toughened epoxy adhesive the mode I fracture energy of the adhesive increases with the thickness of the adhesive layer up to a maximum value from which it starts decreasing. Therefore, this means that there is an optimum adhesive thickness that leads to the maximum fracture energy. Zarei et al. [24] prepared peel tests using different surface roughnesses of the substrate, adhesive thicknesses and loading rates. The substrates used were PBT-GF30 and the adhesive was silicone-based. It was concluded that the variation of adhesion strength of the silicone adhesive with adhesive thickness was dependent on the surface roughness, showing that a higher adhesive thickness contributes to a higher adhesion energy for smoother surfaces. It was also defined that the surface roughness of the substrate has an impact on adhesion strength for a ratio between adhesive thickness and root mean square roughness below 246.

In this study, the effects of the surfacial application of surfactant on the properties of joints with aluminum substrates and silicone adhesive were studied. For this, different contamination levels, imposed by the amount of contaminant applied, were analyzed. To fully study the effect on the joint, strength tests, such as single lap joints (SLJ) and facture tests, such as double cantilever beam (DCB) were performed. The contaminant used is a surfactant, used in the industry to clean oils or lubricants used during the manufacturing process of aluminum components. To validate the experimental results, a numerical simulation using *Abaqus 2017* through the inverse method was created. The numerical simulation showed a good approximation to the experimental study. The influence of the cohesive properties of the interface layer on the numerical model was also studied in detail.

2. Experimental details

2.1. Materials

The adhesive studied in this work is a two-part silicone elastomer adhesive cured by addition and commercially available. This adhesive is used both to join and seal the parts of the housing of electronic components used in the automotive industry. The general properties of the adhesive can be seen in Table 1.

The mechanical properties of the adhesive were determined by Borges et al. [25] using bulk tensile tests, Table 2. The elongation at break presented is given by the adhesive manufacturer.

The substrate used was aluminum 6082-T6. This material has an Young's modulus of 70 GPa and a Poisson's ration of 0.33.

The contaminant considered is a surfactant used to clean oil from aluminum surfaces, Cocosalkylaminethoxylate, supplied by SysKem Chemie GmbH (Wuppertal, Germany). The general specification are shown in Table 3.

2.2. Specimen manufacturing

2.2.1. Surface treatment and contamination

The aluminum substrates were treated using two different methods: sand paper and sulfuric acid anodizing. The sand paper is an intermediate cleaning, removing contaminated layers from the surface. As for the sulfuric acid anodizing, it is employed since it improves porosity, increasing the bond strength and giving the substrates better corrosion resistance. The aluminum substrates are immersed in an aqueous phosphoric acid solution with a concentration of 9% (m/m) during 25 min according to the ASTM D3933 standard [27]. Afterwards, they are cleaned with distilled water and acetone. For the uncontaminated specimens, the surface preparation ended at this point. For the contaminated specimens, after the pretreatments, the contaminant was applied through spraying an aqueous solution of contaminant with a concentration of 10 g/L. Four different levels of contamination were considered, governed by the number of sprays

applied, ranging from no contamination to 1, 4 and finally 10 sprays. When applying the contaminant, the spray nozzle was kept vertically aligned to the middle of the overlap and at a constant distance of 300 mm to ensure a homogeneous contaminant distribution across the surface area and repeatability of the process. To understand if this was the case, several 0.2 mm thick specimens with the same area as the specimens were prepared and the contaminant application process was conducted on them. Afterwards, the specimens were cut, to understand if half of the specimen had half of the amount of contaminant.

Finally, the substrates were placed in a climatic chamber at 70°C for 12 h to evaporate the water in the solution and ensure that, at the time of adhesive application, only contaminant would be present at the overlap.

2.2.2. Double cantilever beam (DCB)

Aluminum substrates were used for the DCB specimens. The bondline thickness was 1 mm, and it was controlled by the introduction of calibrated tape between the substrates before the application of adhesive, which was removed after curing of the adhesive. The pre-crack was guaranteed through the introduction of a 0.1 mm thick sharp razor blade mid-thickness of the adhesive layer. The thickness of 1 mm was used since it is representative of the joint used in the industrial application of the joint. The geometry of the joint is shown in the Figure 1.

2.2.3. Single lap joint (SLJ)

Aluminum substrates with 2 mm of thickness and 25 mm of width were used for SLJs for all levels of contamination. The overlap length was 25 mm and the bondline thickness of adhesive was 1 mm. In order to achieve that, packing shims were used to provide the necessary spacing between the two substrates. The geometry of the joint is represented in Figure 2.

2.2.4. Scanning electron microscopy (SEM)

Scanning electron microscope (SEM) was employed to analyze the contaminant influence on the substrate, in a joint with contaminant and in bulk adhesive. It was studied if the adhesive had absorbed contaminant particles or if it would only stay in the interface. Clean and contaminated substrates, neat adhesive and joints with contaminant were compared. To make the effect of contaminant clearly stand out, the higher contamination level (10 sprays) was used.

Borges et al. [25] investigated this effect on the adhesive, analyzing both neat adhesive and with multiple contamination levels, the substrate (without contaminant and contaminated) and a fracture surface of a SLJ were analyzed.

2.3. Experimental procedures

2.3.1. Double cantilever beam (DCB)

All tests were performed using an INSTRON® 3367 universal test machine (Norwood, MA, USA), with a load cell of 30 kN, at room temperature and constant displacement rate of 2 mm/min. The load–displacement (P–δ) curves for all tests were registered by the universal testing machine and were compared for all contamination levels. At least three specimens were tested for each contamination level.

The fracture toughness of the neat adhesive in mode I, G_{IC}, was determined in a previous work by the same authors using a standard DCB with high strength steel substrates [28].

Table 3. Product specification, given by the supplier [27].

Cocosalkylaminethoxylate	
Chemical name	*Amines, coco alkyl, ethoxylated*
Appearance	*Brown*
pH	9-11
Moisture	*max* 1.0%
Density	0.95

2.3.2. Single lap joints (SLJ)

The SLJ were vertically placed and fastened using two grips prior to testing (pressure was produced using four M6 bolts, with a thread pitch of 1 mm and exerting 20 Nm of torque to each bolt). Metal tabs were placed beneath one side of each substrate of the SLJs to keep the specimens horizontal when handled. During testing, two center pins were also used to control appropriate placement of the SLJ.

Load–displacement (P–δ) curves were obtained for all SLJs tested. At least three specimens were tested for each contamination level.

2.3.3. Scanning electron microscopy (SEM)

Two distinct SEM microscopes were used for the analysis: JEOL JSM 6301 F/Oxford INCA Energy 350/Gatan Alto 2500 (Tokyo, Japan) and FEI Quanta 400FEG ESEM/EDAX Genesis X4M (Tokyo, Japan) (Hillsboro, Oregon, United States). The research was carried out at CEMUP (University of Porto, Portugal). Using the SPI Module Sputter Coater, the samples were sputtered with an Au/Pd thin film for 120 seconds at a current of 15 mA.

3. Numerical model

In this study, four numerical models were implemented using the Finite Element Method (FEM) in *Abaqus* (Dassault Systèmes Simulia Corp. Providence, USA). Two different models were created for SLJ and DCB: one for the uncontaminated joints and other for the contaminated joints

The aim of the numerical model is obtaining the properties of the interphase, through reverse engineering, since the properties of the substrate and adhesive are known. For each level of contamination, with the load displacement curve from the DCB test, the tensile strength and mode I fracture toughness of the contaminant is tuned. Afterwards, with the load displacement curve of the SLJ, the shear strength and mode II fracture toughness of the contaminated layer are imposed.

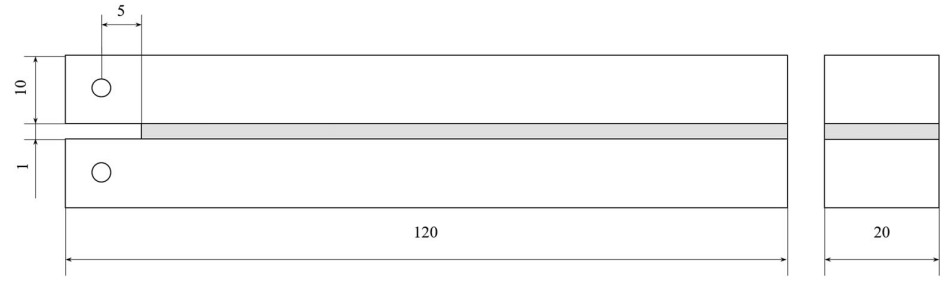


Figure 1. Schematic representation of the DCB specimens, dimensions in mm.

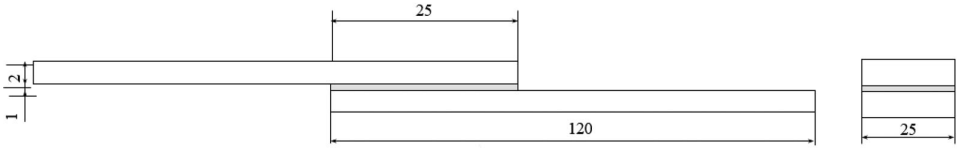


Figure 2. Schematic representation of the SLJ specimens, dimensions in mm.

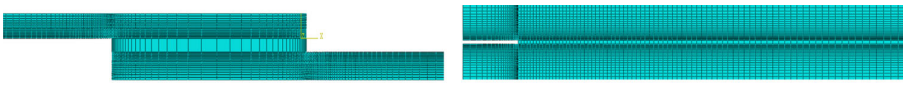


Figure 3. Mesh used in the numerical models of SLJs a) and DCBs b) for the models of the uncontaminated condition.

3.1. Models for uncontaminated joints

The substrate and the adhesive were modeled as elastic and cohesive elements, respectively. The model has the same geometry as the experimental specimens. The two-dimensional (2 D) mesh applied to the models was constructed with plain strain four-node quadrilateral solid finite elements (CPE4) for the aluminum substrates, and four-node cohesive elements (COH2D4) for the silicone adhesive. The mesh was refined to reduce element size in regions with large stress gradients. After a brief convergence study, the mesh size of the cohesive elements was 0.08 mm, with one element across the interphase thickness. The triangular CZM was chosen since the material does not present plastic deformation.

Regarding the SLJ model, the boundary conditions were set as indicated in Figure 4. At one end of the specimen, a clamp condition was added to simulate the static grip of the tensile machine while at the other end a longitudinal displacement was applied, retained in the perpendicular direction of displacement, thus simulating the grip that applies the force during the test.

As for the DCB model, a node on the edge of the lower substrate was restrained in the plane, and a node on the edge of the upper substrate was held horizontally and pulled vertically. Figure 5 shows the boundary conditions of the DCB numerical model.

3.2. Models for contaminated joints

The substrate and adhesive were modeled as elastic elements, while the contaminant layer was modeled as cohesive elements, Figure 6. In the model for uncontaminated adhesive joints the cohesive elements were placed in the adhesive since the failure was cohesive through the adhesive, however, the contaminated joints fail through the interphase. Therefore, the cohesive elements are placed in this section. The sum of the heights of the contaminant layer and adhesive layer must be equal to 1 mm, since it is the distance between the substrates imposed in the experimental work. Although various authors state that the interphase has a size between 1 and 100 μm [29]. The size of 0.1 mm was applied in *Abaqus*, however, it is important to emphasize that cohesive zone models are not especially affected by the size of the elements [30, 31].

A two-dimensional (2 D) mesh was used, with plain strain four-node quadrilateral solid finite elements (CPE4) for the substrate and adhesive, and four-node cohesive elements (COH2D4) for the contaminant layer. As in the uncontaminated model, the mesh was refined to reduce element size in regions with large stress gradients. The mesh size of the cohesive elements was 0.08 mm, with one element across the overlap thickness. The meshes of both SLJ and DCB are shown in Figure 7.

4. Experimental results and discussion

4.1. Double cantilever beam (DCB)

The load-displacement, P-δ curves of the DCB tests are shown in Figure 8, through a representative curve. The results show that, as the amount of surfactant contamination raises, the failure load decreases. It would appear that the stiffness of the joint would slightly increase from no contaminant to the DCB with 1 spray, however the trend is not followed for the other levels of contamination. It can be



Figure 4. Boundary conditions imposed in the numerical models of the SLJs of the uncontaminated condition.



Figure 5. Boundary conditions imposed in the numerical models of the DCBs of the uncontaminated condition.

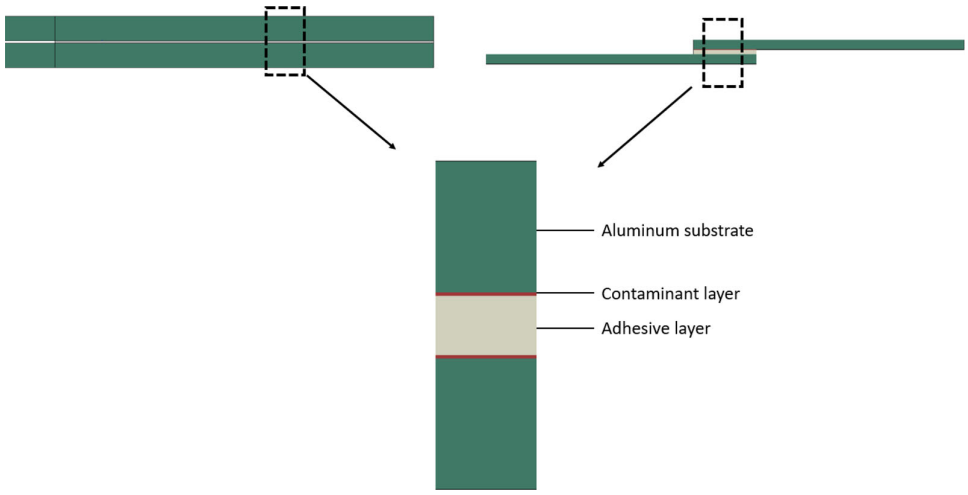


Figure 6. Scheme of the model developed to simulate the contaminated conditions, for DCBs and SLJs.

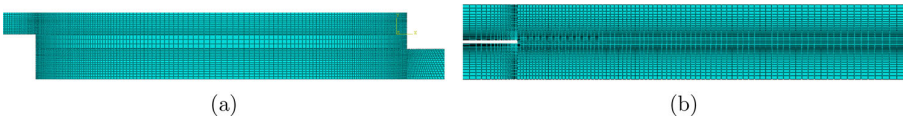


Figure 7. Mesh used in the numerical models of SLJs a) and DCBs b) for the models of the contaminated conditions.

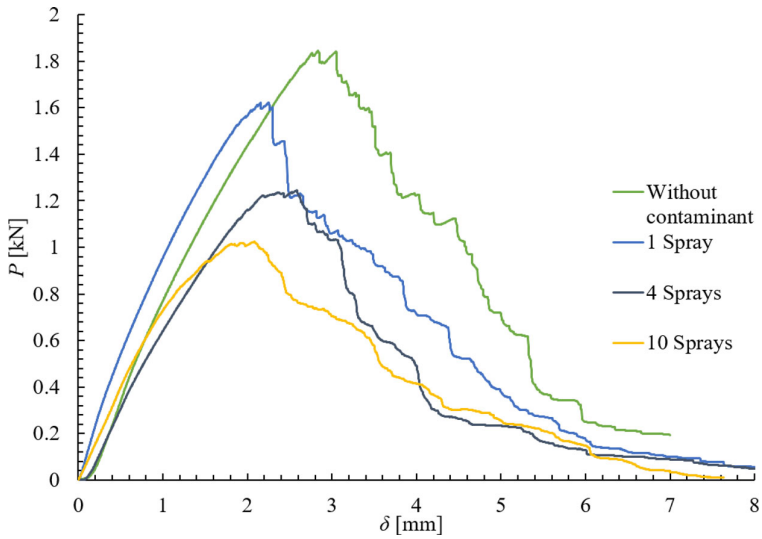


Figure 8. Representative load-displacement, *P*-δ, curves for the DCBs, uncontaminated and contaminated.

seen that there is unstable crack propagation. Therefore, the G_{Ic} obtained from these curves could only be from the initiation and not propagation, as it happened when the G_{Ic} of the adhesive was determined [25]. However, from these experimental results G_{Ic} was not established, since failure moves from the adhesive to the interface and would not

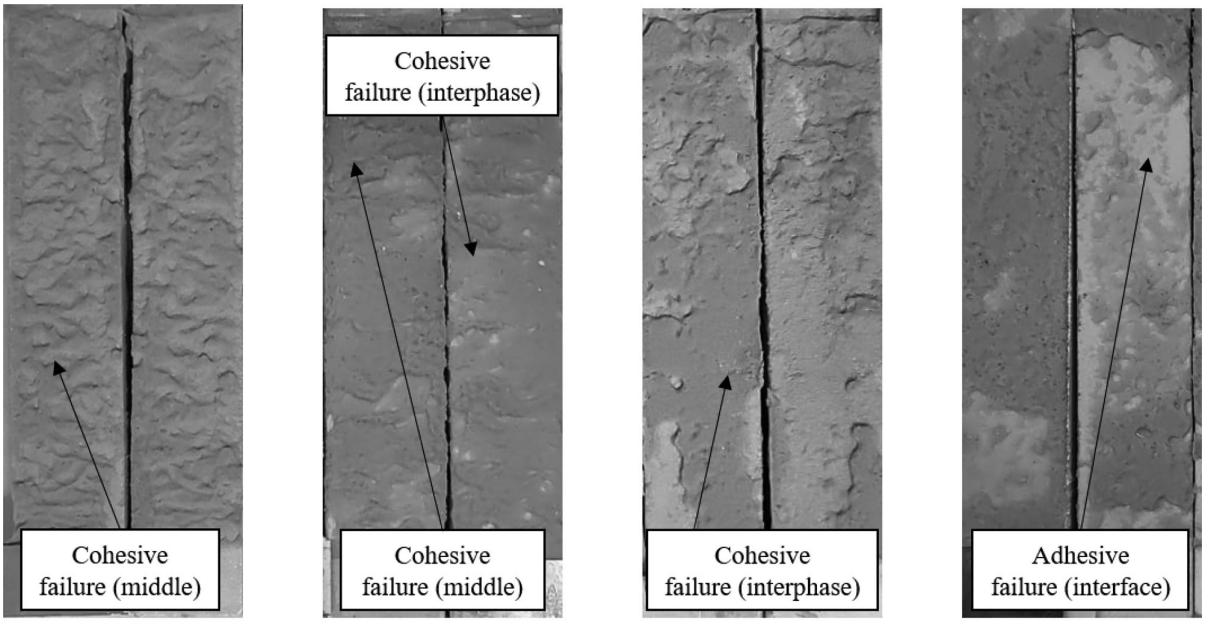


Figure 9. Failure surface of the DCBs for the uncontaminated condition a) and with 1 b), 4 c) and 10 d) sprays of contaminant.

give significant results. This is due to the fact that, with this silicone material, the direct method must be used to determine crack initiation and when the failure is interphasial or interfacial the measurement is not straightforward.

Figure 9, shows representative images of the failure surface of the DCB joints with different levels of contamination. When analyzing the failure surfaces it is noticeable that, as the amount of contaminant increases, the failure moves increasingly toward the interface. The joint without contamination exhibits cohesive failure through the middle of the adhesive. With 1 spray, the failure is still cohesive through the adhesive however, it is closer to the interface, at the interphase. With 4 sprays failure is adhesive in most of the overlap, with some areas of cohesive failure near the substrate. Finally, with 10 sprays, failure is predominantly adhesive. As observed by Borges et al. [25], the adhesive strength and stiffness decreases with increasing amount of contaminant included in the adhesive prior to curing. In this case, between the uncontaminated joint and the joint with 1 spray, it is thought that the adhesive at the interphase absorbs the contaminant placed in the substrate prior to bonding therefore, its strength decreases, leading failure to move closer to the interface. Increasing the contamination level, and reaching 10 sprays, the adhesive at the interphase absorbs as much contaminant as possible, however, there is still contaminant at the interface. At this point, because there is contaminant that remains at the interface, acting as a physical separation, the failure is adhesive.

4.2. Single lap joint (SLJ)

Representative load-displacement P-δ curves for the SLJ tested are shown in Figure 10(a). The results for the SLJ failure load for all levels of contamination are presented in Figure 10(b). The results show that there is a big decrease in the failure load from the uncontaminated SLJ to the SLJ with one spray and then a steady decrease between sprays. Likewise, the displacement did suffer a decrease in relation to the SLJ without contamination, however between the different levels of contamination there was not a significant difference.

Representative images of the fracture surface of each condition tested are shown in Figure 11. The failure clearly shifts to the interface as the contamination level increases, changing from cohesive failure through the middle of the adhesive for the uncontaminated joint, to cohesive failure near the interface for 1 spray of contaminant, mixed failure (with areas of adhesive failure and mainly cohesive failure in the adhesive near the interface) for 4 sprays and adhesive failure for 10 sprays. The reasoning behind these failure modes are the same presented for DCB tests.

From the results presented, it is clear that the existence of a layer of contaminant in the interface prior to adhesion has an impact in the bonding properties in SLJs. With the increase of the amount of contaminant, the average shear strength of the SLJ suffer a steady decrease and the failure path moved from cohesive to adhesive.

4.3. SEM analysis

Figure 12, shows a SEM image of the adhesive and the EDS profile obtained. As expected, discussing a silicone adhesive, it is clear that it has carbon, silicon and oxygen (Figure 12(b)).

Two substrates were also analyzed. One without contaminant (Figure 13) and one with the highest amount of contaminant, 10 sprays (Figure 14). It was clear that there is a considerable difference in the roughness of the substrate, the substrate became smoother and the quantity of carbon

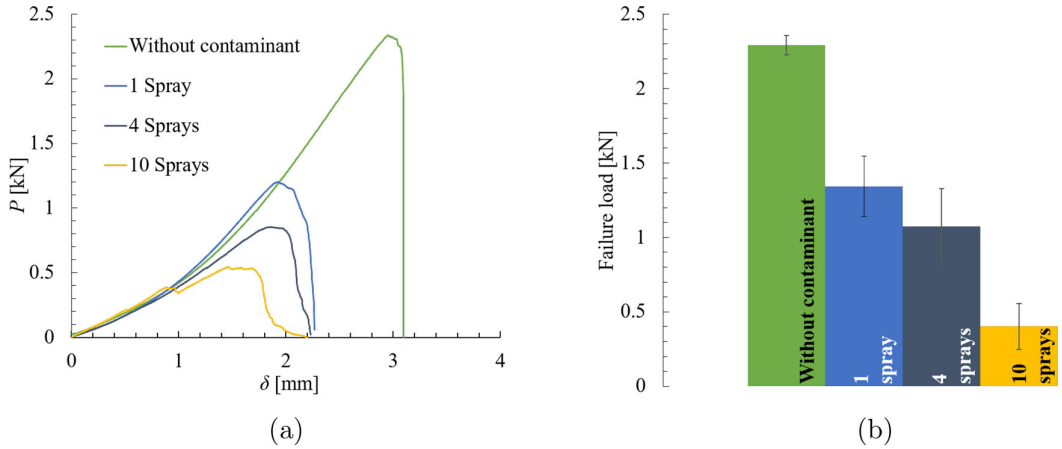


Figure 10. Representative load-displacement, *P*-δ, curves for the SLJ, contaminated and uncontaminated a), and failure loads b).

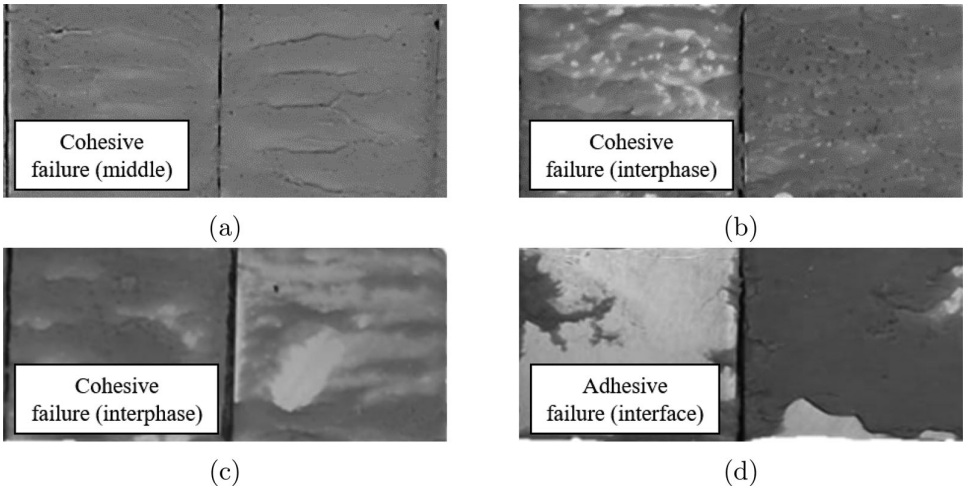


Figure 11. Failure surface of the SLJs for the uncontaminated condition a) and with 1 b), 4 c) and 10 d) sprays of contaminant.

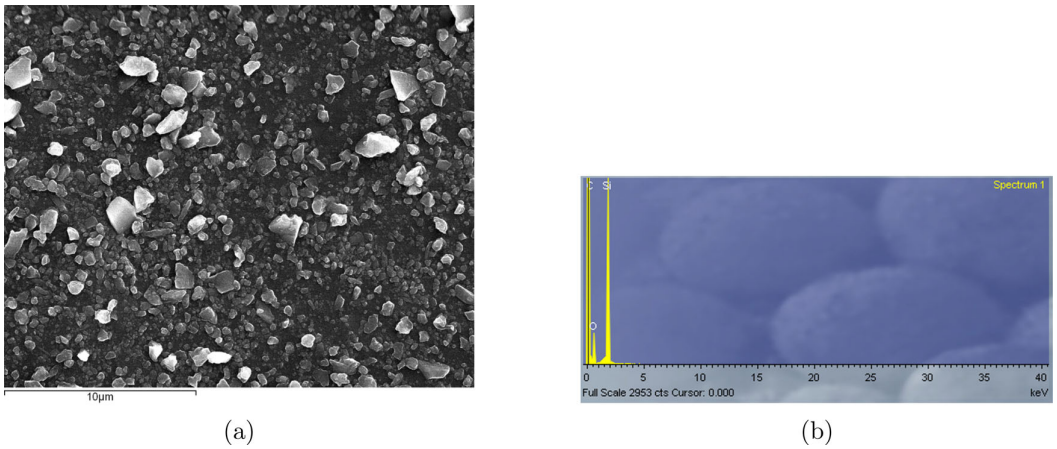
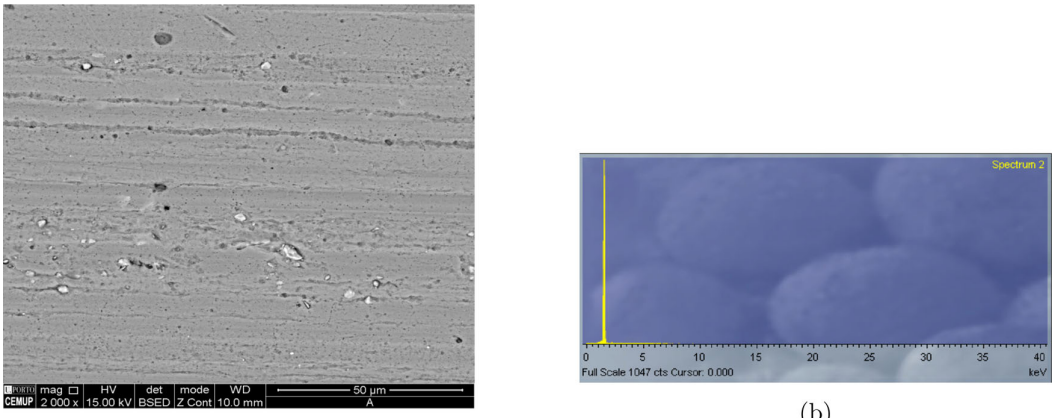


Figure 12. SEM images of neat silicone adhesive a) and energy-dispersive x-ray spectroscopy b).

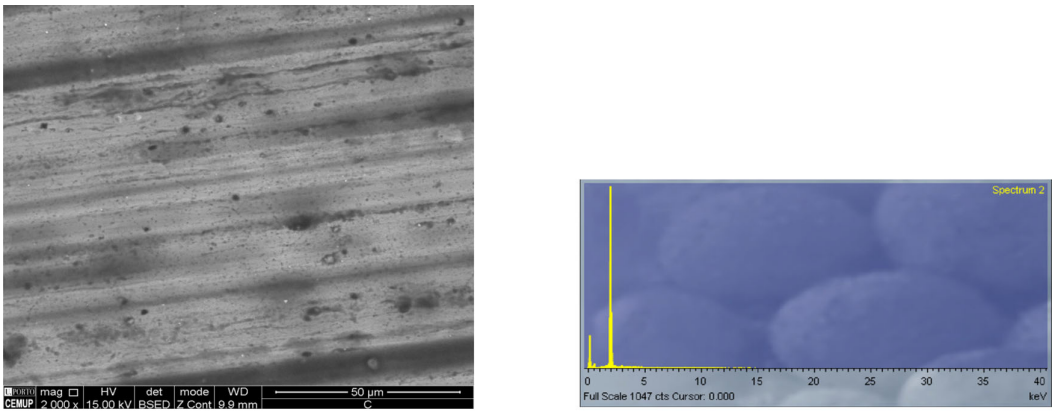
detected in the substrate with contaminant was higher, showing there was a second carbon rich component, which in this case is the contaminant.

This explains the difficulty silicone has in the mechanical interlocking to the aluminum, which causes a decrease in bondability between them. At this point, when the substrates are bonded, the adhesive has two main alternatives: absorbing the contaminant, decreasing the strength of the adhesive close to the substrate and exhibiting cohesive failure in the adhesive but at the interphase (as seen for 1 and 4 sprays of contaminant), or if the adhesive reaches a point where it cannot absorb more contaminant, it is going to remain at



(a) (b)

Figure 13. SEM images of the substrate without contaminant a) and energy-dispersive x-ray spectroscopy b).



(a) (b)

Figure 14. SEM images of the contaminated substrate a) and energy-dispersive x-ray spectroscopy b).

the adhesive/substrate interphase during curing, creating a physical separation between them (as seen for 10 sprays). Since in the SEM analysis the 10 sprays condition is being analyzed, the second behavior is expected.

Therefore, in order to fully understand if in fact that was the explication, the failure surface of an adhesive joint with 10 sprays of contaminant after test was also analyzed (Figure 15).

Although failure in these joints is mainly adhesive, it is clear that there is some adhesive that remains in small areas at the substrate, being detected in the EDS analysis. In this image, the remaining of contaminant at the substrate is not clear since the composition of the surfactant, in terms of chemical elements, is close to that of the adhesive. However, it is clear that the adhesive remains on small areas of substrate, but the failure is mostly interfacial, supporting the idea that the surfactant contamination is higher than what the adhesive can absorb.

5. Numerical results

5.1. Models for uncontaminated joints

All cohesive parameters were previously determined experimentally in other works. Brandão et al. [28] determined the G_{IC} for an uncontaminated DCB, while Borges et al. [25] produced a detailed study on silicone adhesive used in this work, showing the values of the stiffness and strength as a function of the amount of contaminant added to the adhesive prior to curing. These values are presented in Table 4.

Figure 16 presents P-δ curves of the uncontaminated DCB, both representative experimental results and the curves numerically obtained. As on the Figure 17, the experimental and numerical results for the SLJ are compared through the P-δ curves and the failure load. From these results, it is clear that the CZM and numerical model developed is capable of simulating the behavior of the silicone adhesive on the joints under analysis, though the properties previously determined using standard tests.

5.2. Models for contaminated joints

In this model, the cohesive parameters of the contaminant layer were obtain with an inverse method, fitting the numerical P-δ curves to the experimental ones and enabling a full characterization of the properties of the contaminant layer as a function of the quantity of contaminant applied in the substrate prior to adhesive bonding. This method consisted

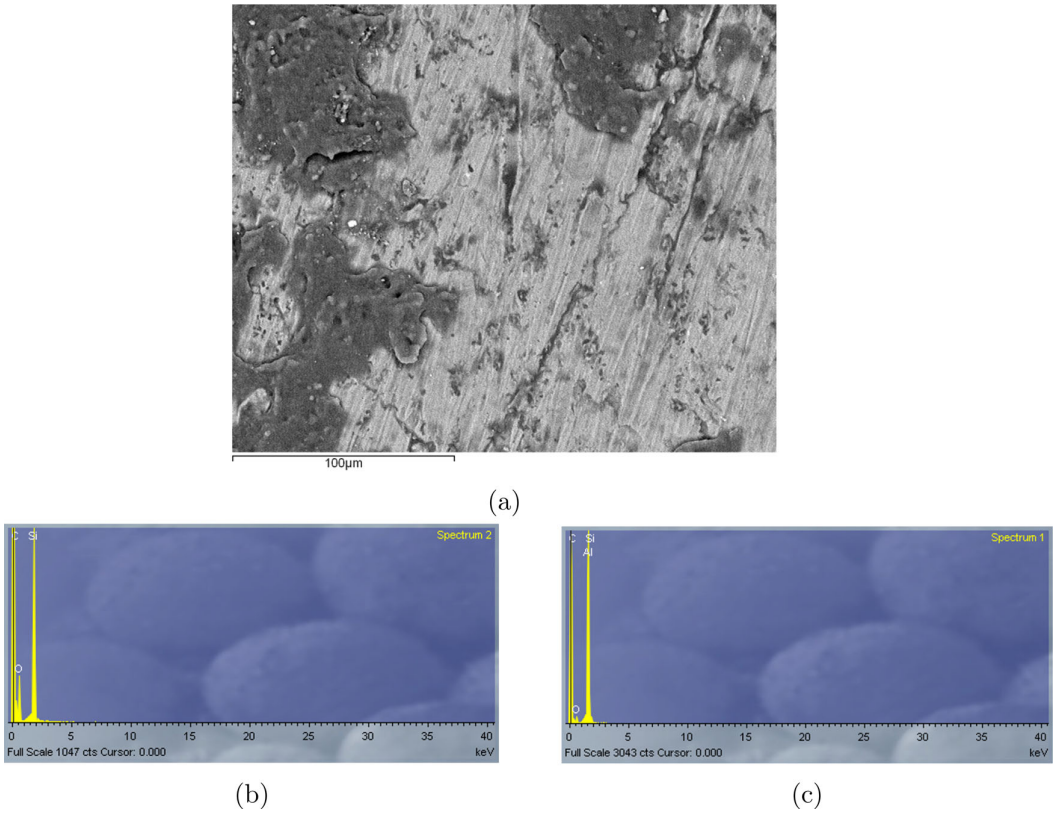


Figure 15. SEM images of the failure surface of a contaminated joint a) and energy-dispersive x-ray spectroscopy of the adhesive b) and exposed substrate c).

Table 4. Cohesive properties of the adhesive imposed in the numerical model.

G_{IC} [N/mm]	3.3
G_{IIC} [N/mm]	5
Tensile strength [MPa]	3.4
Shear strength [MPa]	2.5
Young's modulus [MPa]	1.3

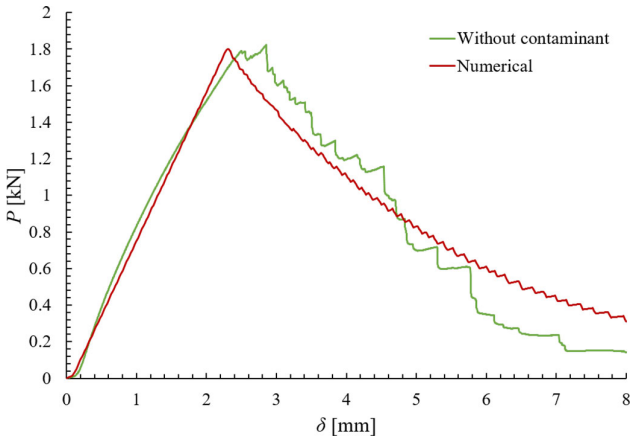


Figure 16. Numerical results of the DCB without contaminant through the load-displacement, *P*-δ curve.

in inputting the Young's modulus (E), the tensile stress (σ) and the G_{IC} in the respective DCB model, as a function of the quantity of contaminant. As for the elastic elements of the neat adhesive layer, the same Young's modulus as the one in the numerical model without contaminant was considered.

In Figure 18(a)–(c), experimental and numerical *P*-δ of the DCB specimens with 1, 4 and 10 sprays, respectively, are shown.

While for DCB models, the G_{IC} is the predominant parameter, it has been observed that, for small G_{IC}, [32], the model showed to be mostly insensitive to the variation. Regarding strength, it was very sensitive to small variations in the range of values for the σ [2.3–3.5 MPa]. This result is in line with a study done by Banea et al. who stated that to low values of the cohesive strength (under 7 MPa) this type of numerical model is very sensitive to cohesive strength while, for high values of cohesive strength, G_{IC} is the predominant parameter [33].

In order to confirm these results, a sensitivity study to mode I parameters was performed in the model for 1 spray DCB, since it was the model with higher strength (2.9 MPa). First, it was compared how the *P*-δ curve changed with the G_{IC}, the value applied in our numerical model for 1 spray was 0.08 N/mm, so a comparison was made either for a value well above and below. It was increased until 1 N/mm which (125% higher) and decreased until 0.05 N/mm. The results are shown in 19(a). Secondly, the same analysis was done for σ and the results are presented in 19(b).

In Figure 20(a) schematic representation is showed how the cohesive strength in mode I varied for the models used. There is a decrease of the property as the number of sprays increase.

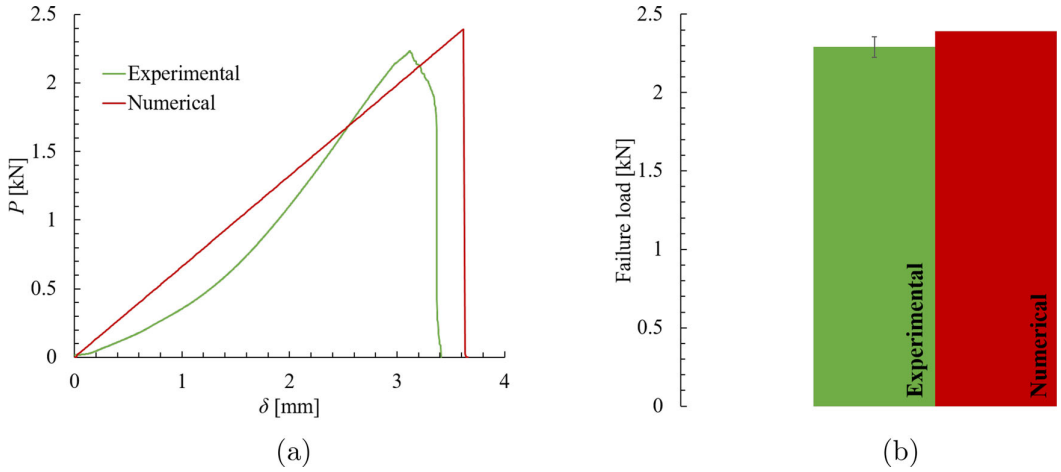


Figure 17. Numerical results of the SLJ without contaminated through the load-displacement, *P*-*δ*, curve a) and failure load b).

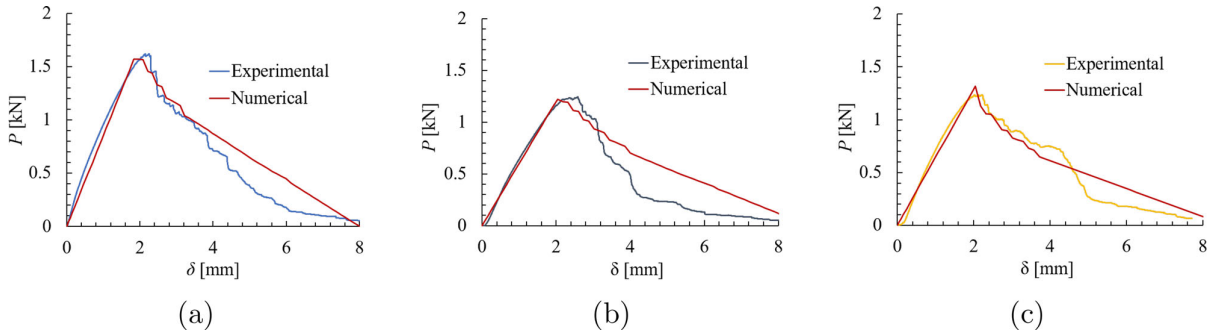


Figure 18. Numerical results of the DCB with 1 a), 4 b) and 10 c) sprays of contaminant though the load-displacement, *P*-*δ*, curve.

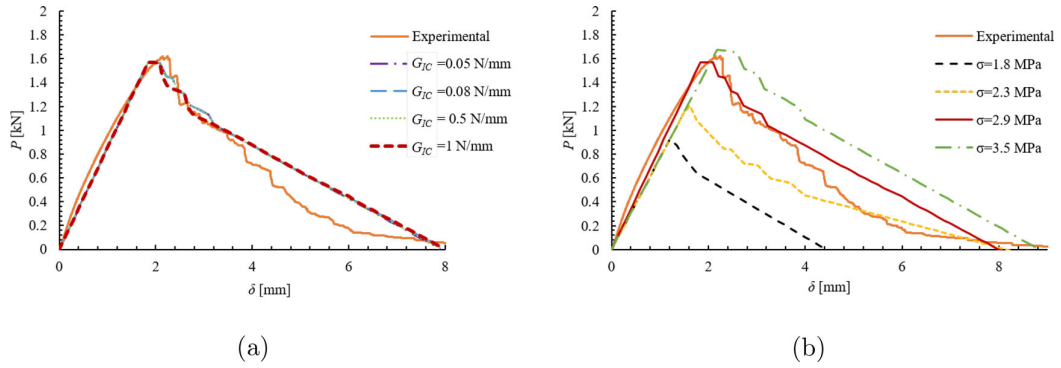


Figure 19. Sensitivity of the numerical models to the properties of the interface for peel. Strain energy release rate in mode I, G_{IC} a) and tensile strength, σ b).

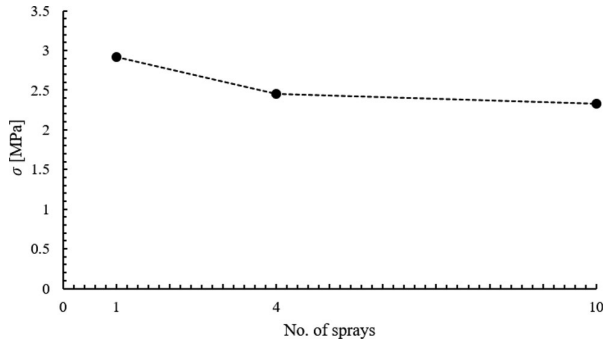


Figure 20. Tensile strength, σ, of the interphase for the contaminated conditions.

Considering the strength determined by Borges et al. [25], when mixing contaminant into the adhesive prior to curing, it can be said that, with 1 spray, the adhesive at the interphase has 0.2% of contaminant and, with 4 sprays 0.9%. For 10 sprays this analysis cannot be directly done, since failure is not through the adhesive at the interphase, but adhesive failure.

Afterwards, to further validate this method and to obtain a more complete characterization of the cohesive values of the contaminated layer, we repeated the process in a SLJ. This time, the values previously obtain in mode I (E, σ, G_{IC}) were used and found the remaining mode II parameters using the inverse method, fitting the numerical *P*-*δ* curves to the experimental ones.

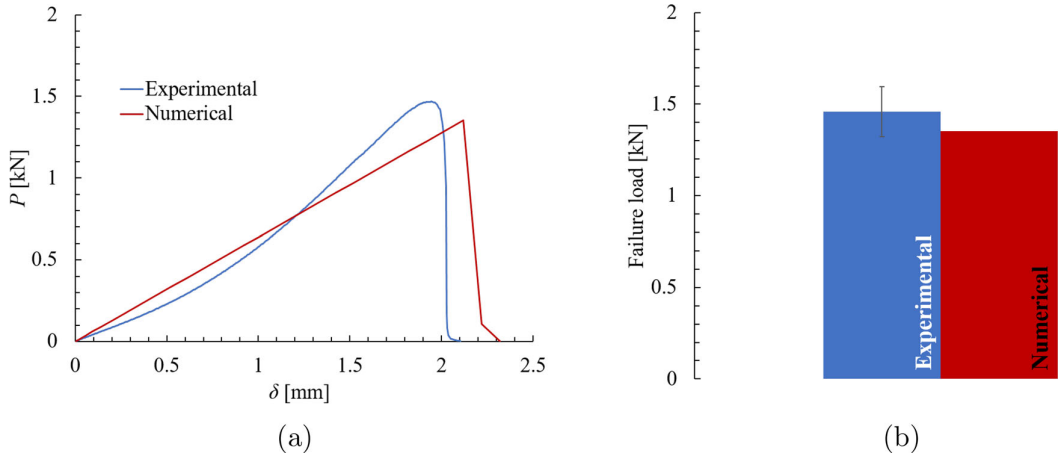


Figure 21. Numerical results of the SLJ with 1 spray of contamination through the load-displacement, *P*-*δ*, curve a) and failure load b).

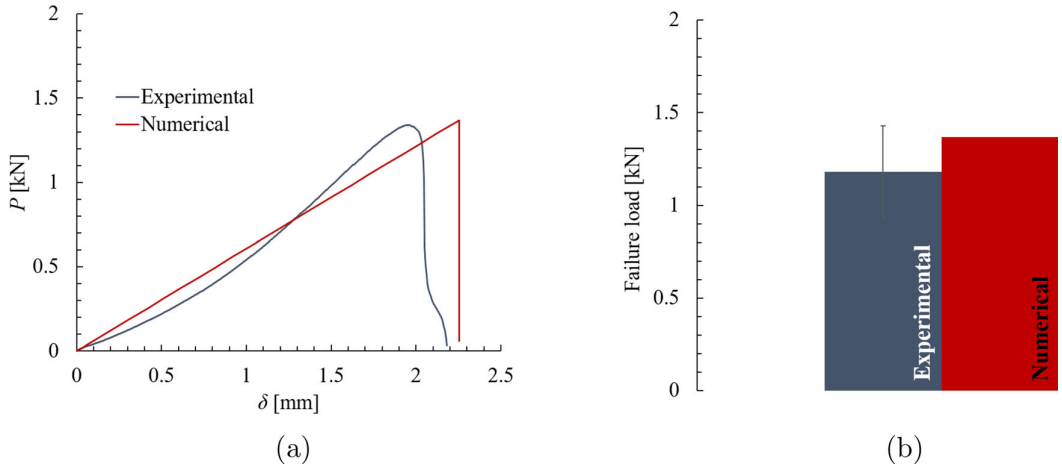


Figure 22. Numerical results of the SLJ with 4 sprays of contamination through the load-displacement, *P*-*δ*, curve a) and failure load b).

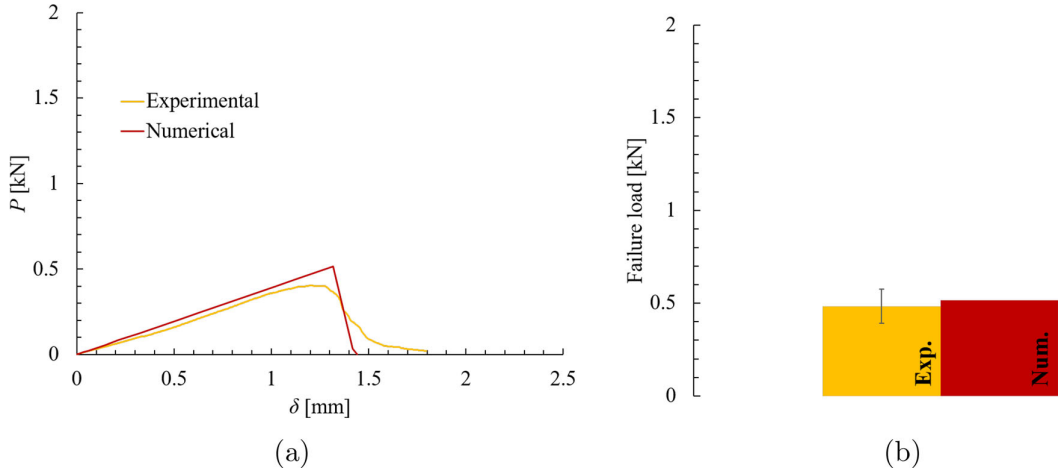


Figure 23. Numerical results of the SLJ with 10 sprays of contamination through the load-displacement, *P*-*δ*, curve a) and failure load b).

In Figures 21–23, experimental and numerical *P*-*δ* as well the failure load graphic to represent the difference of the failure load of the SLJ with 1, 4 and 10 sprays, respectively, are shown.

For all levels of contamination, by applying this method it was possible to reach a good prevision of the real properties of the contaminated layer, since the numerical curves of the SLJ model is very similar to the experimental one, reaching a good result.

Regarding the model sensibility to the cohesive parameters in mode II, the SLJ model was not very affected by the G_{IIC} values, and the parameter that had the most influence

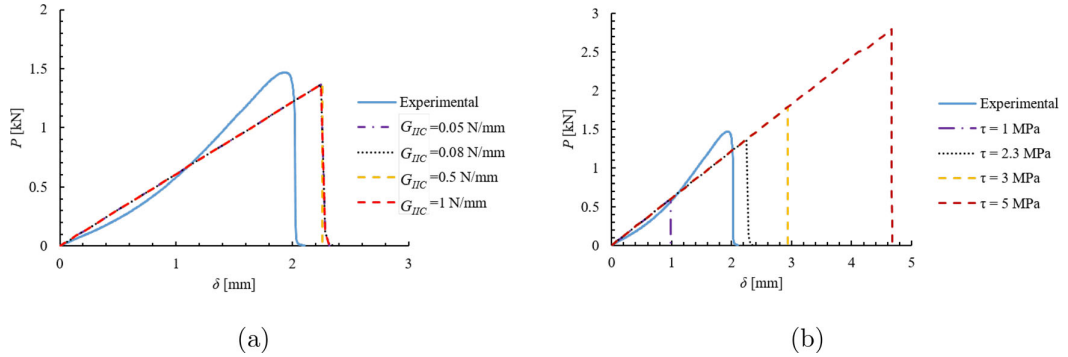


Figure 24. Sensitivity of the numerical models to the properties of the interphase for shear. Strain energy release rate in mode II, G_{IIC} a) and shear strength, τ b).

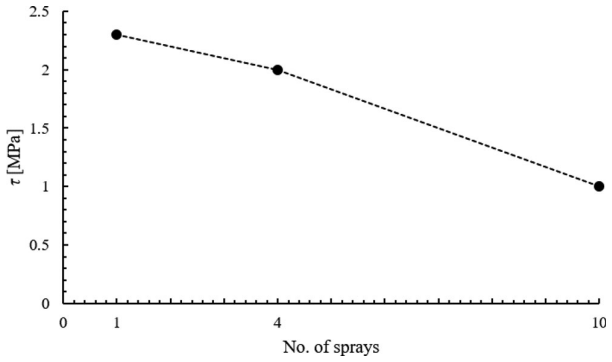


Figure 25. Shear strength, τ, of the interphase for the contaminated conditions.

was the critical shear stress (τ). These results are in agreement with Gustafson et al. who stated that for low G_{IIC}, the maximum load is primarily dependent. on τ [32].

To prove these results, a sensitivity study to mode II parameters was performed in the model for the SLJ with 1 spray of contaminant, as it was done for the DCB test. To analyze the sensitivity of G_{IIC}, a range of [0.05–1] N/mm was utilized and, for all the values input, there was not a considerable difference, which leads to the conclusion that, in this range of critical shear stress, the G_{IIC} does not significantly influence the model, Figure 24(a). To study the influence of the τ in the SLJ model, a range of values was applied and, for all the values inputted, the results significantly changed, Figure 24(b).

In Figure 25 shows how the critical shear stress varied for the models used. As the number of sprays increases, the property value decreases.

6. Conclusions

In this study, the effects of the surfacial application of surfactant on the properties of joints with aluminum substrates and silicone adhesive were studied. Different levels of contamination were applied in aluminum substrates before adhesive bonding. SLJ and DCB were used. Afterwards, a numerical model was created to verify the experimental results. The main conclusion are as follows:

- The application of a surfactant before bonding decreases the joint strength of DCB and SLJ. The deterioration of the properties varied directly with the amount of surfactant applied.
- In both SLJs and DCBs, the failure surface became increasingly interfacial as the amount of contaminant increased, changing from cohesive failure for the joints without surfactant application to adhesive failure for the maximum level of contamination. For the medium levels of contamination, the failure was cohesive near the substrate.
- The adhesive at the interphase absorbs the contaminant (decreasing its strength and stiffness), changing the failure from cohesive through the middle of the adhesive to cohesive at the interphase. As the contamination level increases, the adhesive reaches a limit of contaminant it can absorb, and the remaining contaminant is left at the interface, acting as a physical separation turning the failure adhesive.
- It was possible to simulate this behavior with *Abaqus*, using a model with a contaminated layer as cohesive elements. With the indirect method, good approximations of the $P-\delta$ curves of both SLJ and DCB were obtained.
- In addition, a cohesive properties' sensibility study was made. The results stated that, for this type of simulation with low tensile stress (under 5.5 MPa), the G_{IC} does not have an impact on the behavior of the model, for mode I the model was most sensitive to tensile stress variations. As for the mode II properties, the one that have the bigger impact was the shear stress.

Acknowledgments

The author(s) disclosed receipt of the following financial support for the research, authorship, and/or publication of this article: The authors wish to acknowledge and thank the funding and support provided by Robert Bosch GmbH, Corporate Research and Advance Engineering, Renningen.

Funding

The authors also gratefully acknowledge the funding provided by Fundação para a Ciência e Tecnologia (FCT), Portugal for the Ph.D. Grant 2020.06055.BD through FSE.

ORCID

C. S. P. Borges http://orcid.org/0000-0001-7721-7118
E. A. S. Marques http://orcid.org/0000-0002-2750-8184

R. J. C. Carbas http://orcid.org/0000-0002-1933-0865
A. Akhavan-Safar http://orcid.org/0000-0002-7168-7079
P. D. P. Nunes http://orcid.org/0000-0003-2382-4654
P. Weißgraeber http://orcid.org/0000-0001-8320-8672
L. F. M. da Silva http://orcid.org/0000-0003-3272-4591

References

[1] Lucas FM. da Silva, Andreas Ochsner, and Robert D. Adams, Handbook of Adhesion Technology, Springer Science & Business Media, Heidelberg, 2018.
[2] C.S.P. Borges, E.A.S. Marques, R.J.C. Carbas, C. Ueffing, P. Weißgraeber, and L.F.M. da Silva, Review on the effect of moisture and contamination on the interfacial properties of adhesive joints, Proc. Inst. Mech. Eng. C J. Mech. Eng. Sci., vol. 235, no. 3, pp. 527–549, 2021.
[3] Sergei Sergeevich Voiutskii, Autohesion and Adhesion of High Polymers, Wiley, USA, 1963.
[4] W.C. Wake Adhesion and the formulation of adhesives (2nd ed.), Applied Science Publishers Ltd., Essex (1982).
[5] Patrick Montois, Valérie Nassiet, Jacques Alain Petit, and Yves Baziard, Viscosity effect on epoxy–diamine/metal interphases: Part I: Thermal and thermomechanical behaviour, Int. J. Adhes. Adhes., vol. 26, no. 6, pp. 391–399, 2006. DOI: 10.1016/j.ijadhadh.2005.06.003.
[6] J.S. Crompton, Interfacial properties and stability in bonded aluminium, J. Mater. Sci., vol. 24, no. 5, pp. 1575–1581, 1989. DOI: 10.1007/BF01105673.
[7] Wulff Possart, et al., Formation and structure of epoxy network interphases at the contact to native metal surfaces, CR. Chim., vol. 9, no. 1, pp. 60–79, 2006. DOI: 10.1016/j.crci.2005.04.009.
[8] A.A. Roche, J. Bouchet, and S. Bentadjine, Formation of epoxy-diamine/metal interphases, Int. J. Adhes. Adhes., vol. 22, no. 6, pp. 431–441, 2002. DOI: 10.1016/S0143-7496(02)00021-0.
[9] Romain Grangeat, *Durabilité des assemblages collés en environnement humide: instrumentation par capteurs à fibre optique*, PhD thesis, Nantes, 2019.
[10] Maëlenn Aufray, and AlainAndré Roche, Residual stresses and practical adhesion: effect of organo-metallic complex formation and crystallization, J. Adhes. Sci. Technol., vol. 20, no. 16, pp. 1889–1903, 2006. DOI: 10.1163/156856106779116650.
[11] Choothum Jeenjitkaew, Zofia Luklinska, and Felicity Guild, Morphology and surface chemistry of kissing bonds in adhesive joints produced by surface contamination, Int. J. Adhes. Adhes., vol. 30, no. 7, pp. 643–653, 2010. DOI: 10.1016/j.ijadhadh.2010.06.005.
[12] C.J. Brotherhood, B.W. Drinkwater, and F.J. Guild, The effect of compressive loading on the ultrasonic detectability of kissing bonds in adhesive joints, J. Nondestruct. Eval., vol. 21, no. 3, pp. 95–104, 2002. DOI: 10.1023/A:1022584822730.
[13] Marty, P. N., Desai, N., & Andersson, J. (2004). NDT of kissing bond in aeronautical structures. In 16th world conference on NDT.
[14] MelodyA. Drewry, RobertA. Smith, AlbertP. Phang, Dawei Yan, Paul Wilcox, and DennisP. Roach, Ultrasonic techniques for detection of weak adhesion, Mater. Eval., vol. 67, no. 9, pp. 1048–1058, 2009.
[15] A. Pramanik, et al., Joining of carbon fibre reinforced polymer (CFRP) composites and aluminium alloys – a review, Compos Part A: Appl. Sci. Manuf., vol. 101, pp. 1–29, 2017. DOI: 10.1016/j.compositesa.2017.06.007.
[16] Marc Greiveldinger, MartinER. Shanahan, Denis Jacquet, and Didier Verchère, Oil-covered substrates: A model study of the evolution in the interphase during cure of an epoxy adhesive, J. Adhesion., vol. 73, no. 2-3, pp. 179–195, 2000. DOI: 10.1080/00218460008029305.
[17] H. Akiyama, T. Fukata, T. Sato, S. Horiuchi, and C. Sato, Influence of surface contaminants on the adhesion strength of structural adhesives with aluminium, J. Adhesion., vol. 96, no. 15, pp. 1311–1325, 2020. DOI: 10.1080/00218464.2019.1598393.
[18] M. Hoffmann, K. Tserpes, E. Moutsompegka, M. Schlag, and K. Brune, Determination of adhesion strength of pre-bond contaminated composite-to-metal bonded joints by centrifuge tests, Compos. Part B: Eng., vol. 147, pp. 114–121, 2018. DOI: 10.1016/j.compositesb.2018.04.014.
[19] D.R. Arnott, A.N. Rider, and C.L. Olsson-Jacques, Influence of adherend surface preparation on bond durability, Surf. Interf. Anal., vol. 27, pp. 1027–1118, 1999.
[20] M. Debski, M.E.R. Shanahan, and J. Schultz, Mechanisms of contaminant elimination by oil-accommodating adhesives Part 1: Displacement and absorption, Int. J. Adhes. Adhes., vol. 6, no. 3, pp. 145–149, 1986. DOI: 10.1016/0143-7496(86)90017-5.
[21] Nunziante Valoroso, Salvatore Sessa, Marcello Lepore, and Gabriele Cricri, Identification of mode-I cohesive parameters for bonded interfaces based on DCB test, Eng. Fract. Mech., vol. 104, pp. 56–79, 2013. DOI: 10.1016/j.engfracmech.2013.02.008.
[22] Christopher White, Kar Tan, Andreas Wolf, and Larry Carbary, Advances in Structural Adhesive Bonding, Woodhead Publishing Limited, Cambridge, 2009.
[23] Xiao Han, Yong Jin, F.M.da. Lucas, Marcelo Silva, and Chengwei Wu Costa, On the effect of adhesive thickness on mode i fracture energy-an experimental and modelling study using a trapezoidal cohesive zone model, J. Adhesion., vol. 96, no. 5, pp. 490–514, 2020. DOI: 10.1080/00218464.2019.1601087.
[24] Hamed Zarei, MariaRosaria Marulli, Marco Paggi, Riccardo Pietrogrande, Christoph Üffing, and Philipp Weißgraeber, Adherend surface roughness effect on the mechanical response of silicone-based adhesive joints, Eng. Fract. Mech., vol. 240, pp. 107353, 2020. DOI: 10.1016/j.engfracmech.2020.107353.
[25] CatarinaSP. Borges, et al., Influence of water and surfactant contamination on the properties of a silicone adhesive, before and after curing, 2021.
[26] Cocosalkylaminethoxylate. Syskem chemie gmbh. Accessed June 3, 2021, https://www.syskem.de/indexe.html, 2020.
[27] ASTM International. ASTM d3933-98, Standard Guide for preparation of aluminum surfaces for structural adhesives bonding (phosphoric acid anodizing), 2017.
[28] Ricardo Brandão, et al., The influence of humidity and immersion temperature on the properties and failure mode of pbt-gf30/silicone bonded joints, 2021.
[29] Shang-Lin Gao, and Edith Mäder, Characterisation of interphase nanoscale property variations in glass fibre reinforced polypropylene and epoxy resin composites, Composites Part A: Applied Science and Manufacturing., vol. 33, no. 4, pp. 559–576, 2002. DOI: 10.1016/S1359-835X(01)00134-8.
[30] R. Avendaño, R.J.C. Carbas, E.A.S. Marques, L.F.M. da Silva, and A.A. Fernandes, Effect of temperature and strain rate on single lap joints with dissimilar lightweight adherends bonded with an acrylic adhesive, Compos. Struct., vol. 152, pp. 34–44, 2016. DOI: 10.1016/j.compstruct.2016.05.034.
[31] M. Araújo, J. Machado, E. Marques, and L. da Silva, Dynamic behaviour of composite adhesive joints for the automotive industry, Compos. Struct., vol. 171, pp. 549–561, 2017. DOI: 10.1016/j.compstruct.2017.03.071.
[32] PeterA. Gustafson, and AnthonyM. Waas, The influence of adhesive constitutive parameters in cohesive zone finite element models of adhesively bonded joints, Int. J. Solids Struct., vol. 46, no. 10, pp. 2201–2215, 2009. DOI: 10.1016/j.ijsolstr.2008.11.016.
[33] M.D. Banea, L.F.M. da Silva, and R. D. S. G. Campilho, Mode i fracture toughness of adhesively bonded joints as a function of temperature: Experimental and numerical study, Int. J. Adhes. Adhes., vol. 31, no. 5, pp. 273–279, 2011. DOI: 10.1016/j.ijadhadh.2010.09.005.

Appendix G

Patent G

Test specimen, test device and method for the inspection of material connections and use of the test specimen

Prüfkörper, Prüfvorrichtung und Verfahren zur Überprüfung von stoffschlüssigen Verbindungen sowie Verwendung des Prüfkörpers

- Patent application translated into English

- Patent drawings

Description

Test specimen, test device and method for the inspection of material connections and use of the test specimen

Technical field

The invention is related to a test specimen and a testing device for testing material connections, in particular adhesive joints, with which different stress characteristics of the bonded joint can be recorded by means of the test specimen during a single test cycle. The invention is also related to a method for testing material connections and the use of test specimens according to the invention.

State of the art

From DE 10 2004 011 099 B3 of the applicant it is known in connection with a test device to use a test body consisting of two components with the features of the generic term of Claim 1. The known test body has a contact surface on each of its two facing end faces of the components, which is used to form the material connection. The testing device is also the two components of the test specimen in different directions or about different directions or about different axes.

Disclosure of the invention

The test specimen according to the invention for testing material connections with the features of Claim 1 has the advantage that it is suitable for generating at least two different load inputs into the bonded joint when performing a load test of the connection. This makes it possible to determine different characteristic stress values of the material connection, which are relevant for assessing the connection, individually or in combination. Different stress characteristics of a

bonded joint are understood to be characteristic values that are recorded, for example, when performing peel tests or tensile tests.

The invention is based on the idea of designing the test specimen, which consists of one or more interconnected elements, by means of sections with different stiffnesses or strengths in such a way that, when the test specimen is subjected to a load in order to release the bonded connection between the different sections, different types of stress occur in succession over time, to which different characteristic stress values are assigned.

Against the background of the above explanations, it is therefore provided in a test specimen according to the invention for testing material connections with the features of Claim 1 that the test specimen, viewed in a longitudinal direction, has at least two sections having different bending stiffnesses perpendicular to the longitudinal direction, which, on the side facing the inspected object, form the at least one contact surface, and in that the different bending stiffnesses are selected in such a way that, when the materially bonded connection is released, different load introductions into the material connection can be achieved in order to determine different characteristic stress values of the material connection.

Advantageous further embodiments of the test specimen according to the invention for testing material connections are listed in the dependent claims.

In a preferred constructive implementation of the test specimen, it is provided that it has a flat, in particular strip-shaped, flexible element running in a direction perpendicular to the longitudinal direction and preferably essentially rigid in the longitudinal direction, or alternatively a flat element, in particular strip-shaped, flexible in the direction perpendicular to the longitudinal direction and preferably essentially rigid in the longitudinal direction as the first element and a second element operating with the strip and rigid at least in some areas.

In a further preferred embodiment for achieving the different bending stiffnesses at the at least two sections, in particular in the case of a test specimen formed in

one piece, it is provided that the at least two sections, viewed perpendicularly to the longitudinal direction of the test specimen, have a different thickness or height and/or consist of layers of materials having different strength values. In particular in the case that the different bending stiffnesses are formed by the fact that the test body has a different thickness or height in the sections, such a test specimen can be produced relatively easily, for example by providing recesses or similar on the surface in the region of the sections which are to have the lower bending stiffness, or by achieving the sections with higher bending stiffness by several layers or doublings.

Another structurally preferred design, which enables homogeneous load introduction into the test specimen without load interruptions, provides that the at least two sections each form a contact surface, wherein the contact surfaces, viewed in the longitudinal direction of the element, adjoin or connected to one another without gaps. This makes it possible to avoid impulse peaks on the connections during the transition to the different sections and simplifies the manufacture of the test specimen.

Alternatively, it is also conceivable that the at least two sections each form a contact surface, and that at least one joining interruption to the object to be tested is formed between the contact surfaces as viewed in the longitudinal direction of the element. Such a design makes it possible, for example, to recognize very quickly during the evaluation of the tests when a transition has occurred between the two sections having different bending stiffnesses.

In a preferred further development of the latter case, it may be provided that at least one joint interruption is formed by a non-stick coating on the side of the test specimen facing the object to be inspected. Such a non-stick coating can, for example, consist of Teflon or similar and can be relatively easily produced or applied.

Alternatively, it can also be provided that the at least one joint interruption is formed by a recess or similar geometry on the side of the test piece facing the

object, so that a connection-free distance is formed between the test specimen and the object to be inspected.

A further preferred constructive design of the test specimen provides that the test specimen has an additional connection between the, at least two sections, which is connected to the section having the greater bending stiffness on its upper side, preferably in a central region of the upper side. Such a constructive design has the particular advantage that a tensile load acting on the test specimen perpendicularly to its longitudinal plane is transmitted centrally to the second section when checking the stress characteristic value in the area of the second section. This in turn has the effect that the stress between the object to be inspected and the second section takes place in the manner of a tensile test, perpendicular to the plane of the second section.

A preferred dimensioning of the test specimen is one in which the width is between 3mm and 10mm and the length of between 50mm and 200mm, as well as a thickness or height in the section with the lower bending stiffness of less than 1mm. However, depending on the surface or geometry of the object to be inspected, the preferred geometric dimensioning may also deviate from the above values. In particular, the width can also be significantly less than 3mm if, for example, material-fit connections formed in grooves are to be inspected.

The test specimen can basically be made of different materials or consist of different materials. In a first embodiment, it is provided that the test specimen consists of at least one layer of metal. Alternatively, or in combination with at least one metallic layer, it is also possible for the test body to consist of at least one layer of plastic. It is also conceivable that the test body is formed from a composite material or from different materials of a plastic film.

However, it is particularly preferred that in the case of a two-part test specimen, the element with the higher bending stiffness is made of plastic and is designed as a 3D printed part.

In particular, in order to enable the different stress characteristics to be detected or tested several times when performing a stress test, it is also of particular advantage if the test specimen has at least two first sections and at least two second sections, with either the first and second sections alternating with one another or the at least two first sections or the at least two second sections being followed by the at least two second sections or the at least two first sections. This allows, for example, an averaging of the of the characteristic stress values of the respective sections. In addition, a possible scattering of the characteristic values can be determined and statistically recorded in a single test.

Furthermore, the invention also comprises a test device for or with a test specimen according to the invention as far described, wherein the test device comprises means for exerting a tensile load on the coupling point of the test specimen, and wherein the means is adapted for the tensile load to act on the test specimen at an oblique or perpendicular angle between the material connection and the plane of the test specimen connected to the object.

In a preferred further development of such a test device, it is provided that the test device has measuring means for recording a load/time curve and/or a load/displacement curve when applying the tensile load to the test specimen. Such measuring means thus serve to record the tests for checking the material connection and are preferably designed in such a way that an automated recording of the corresponding measured values.

Furthermore, the invention also comprises a method for testing material connections, in particular by means of a test body according to the invention or by using a test device according to the invention, the method having at least the following steps: First, at least one material connection is formed in the region between a surface of an object to be tested and the at least two sections of the test body having different bending stiffnesses. Subsequently, a tensile load is exerted on the coupling point of the test body at an oblique or perpendicular angle to the plane of the test body connected to the inspected object, the tensile load being selected in such a way that the at least one material connection is released

in the region of the at least two sections. Furthermore, the recording of measured values, in particular of a load/time curve and/or a load/displacement curve takes place during the application of the tensile load. Preferably, the method is designed to determine a strength and/or a fracture toughness and/or a peel strength and/or a shear strength of the materially bonded joint from the recorded measured values for checking the material connection. The strength is a mechanical resistance that a material connection offers to separation. The fracture toughness in this context is the resistance of the material connection to unstable crack propagation. The test specimen and the method have the advantage that two fundamentally physically different characteristic values, in particular strength and fracture toughness, can be investigated in a single operation.

Lastly, the invention comprises the use of a test specimen according to the invention for testing adhesive bonds on object surfaces, in particular on surfaces of substrates.

Further advantages, features and details of the invention will be apparent from the following description of preferred embodiments of the invention and from the drawings.

Brief description of the drawings

Fig. 1 shows a longitudinal section of a test arrangement with a first, test specimen with stiffeners,

Fig. 2 a top view of the first test specimen according to Fig. 1,

Fig. 3 a longitudinal section in the area of a second test specimen,

Fig. 4 a top view of the second test specimen according to Fig. 3,

Fig. 5

and

Fig. 6 show modified test specimens in perspective,

Fig. 7

and

Fig. 8 illustrations to explain the tests using the first and second test specimens in a side view and

Fig. 9 a diagram explaining a measurement test when inspecting material connections using the test specimen.

Embodiments of the invention

Identical elements or elements with the same function are identified in the figures with the same the same reference numbers.

Figs. 1 and 2 show a first test specimen 10 for inspecting at least one material connection 1 between the test specimen 10 and a surface 2 facing the test specimen 10 of an object 3 to be inspected. The object 3 can, for example, be the surface of a substrate that must have a certain surface condition or surface quality, for example no impurities, in order to ensure a sufficiently strong adhesion between the object 3 and the substrate during the formation of the material connection 1 between the object 3 and elements to be connected to the object 3, for example electronic components. At the material connection 1 is, in particular, an adhesive bond, but the invention is not intended to be limited to adhesive connections. Furthermore, Fig. 1 shows a single, continuous adhesive joint or

material connection 1. This can, however, also comprise different or several areas separated from each other.

The test specimen 10 is designed as a one-piece, strip-shaped and flat element 12, which is connected to the object 3 by its underside facing the object 3, which forms a contact surface 4, via the material connection 1. Viewed in its longitudinal direction 17, the element 12 has at least one first section 14 and at least one second section 16. The two sections 14, 16 have different bending stiffnesses in a direction perpendicular to the longitudinal direction 17. This is achieved by the fact that the test specimen 10 or the element 12 has a greater thickness or height H in the region of the second sections 16, having the greater or higher bending stiffness than in the region of the first sections 14, in which the test specimen 10 or the element 12 has the height h. The height h in the region of the first sections 14 can be, for example, a maximum of 1mm, while the height H in the region of the second sections 16 is several millimeters. Since the bending stiffness changes with the third power of the height h, H, thus, for example, in the case where the height H is twice as great as the height h, an eightfold increase in bending stiffness is achievable in the second sections 16 compared to the first sections 14. Furthermore, the length L of the test specimen 10 is between 50mm and 200mm, and its width B between 3mm and 10mm.

The element 12 or the test specimen 10 consists either of at least one layer of plastic and/or of at least one layer of metal. For forming the second sections 16, separate elements can be arranged as stiffening elements 19 on a material web forming the first sections 14 or connected to it. Composite structures consisting of different materials are also conceivable.

It is further essential that the element 12 is flexible in a direction perpendicular to the longitudinal direction 17 of the element 12, while it is relatively stiff or has high strength values when viewed in the longitudinal direction 17, in particular to avoid tearing of the material of the element 12 in the longitudinal direction 17. According to the illustration of Figs. 1 and 2, the element 12 or the test specimen 10 is connected to the object 3 to be inspected over the major part of its length L by

means of the material connection 1. Only one end section 18 of the test specimen 10 is not connected to the object 3, but protrudes from it and forms a coupling point 20 there for coupling the test specimen 10 to a testing device not shown in Figs. 1 and 2. In the embodiment example shown in Figs. 1 and 2, the test specimen 10 or the element 12, with the area of the end section 18, is connected over its entire surface to the surface 2 of the connection 1 with the surface 2 of the object 3 to be inspected.

Figs. 3 and 4 show a test specimen 10a which differs from the first test specimen 10 in that third sections 22 are formed between the first sections 14a and the second sections 16a, in the regions of which the test specimen 10a is not connected to the object 3 via the material connection 1. The third sections 22 or joining interruptions are formed in that, in the region of the third sections 22, the test specimen 10a is provided with a coating 24, for example consisting of Teflon, on the contact surface 4 facing the material connection 1. The joint interruptions or coatings 24 are arranged directly in front of and behind the second sections 16a. Furthermore, it can be seen that the first sections 14a are joined to the second sections 16a, as viewed in the longitudinal direction 17, in each case starting in front of the third sections 22, are connected to the second sections 16a via additional, loop-shaped connections 26. The additional connections 26 serve to transmit forces from the first sections 14a to the second sections 16a. In particular, the additional connections 26 are connected to the second sections 16a in the region of the upper sides 28 of the second sections 16a, preferably in a central or central region of the second sections 16a.

Figs. 5 and 6 show modified test specimen 10b and 10c, each of two-part design. The two test specimens 10b and 10c each consist of a first element each consist of a first element 29, which is rigid at least in some areas, and a second, flexibly formed element 35 in the form of a strip 36, the two elements 29 and 35 being connected to one another in different ways, and the strip 36 forming a first section 14b, 14c in each of the areas connected to the object 3.

The first element 29 is formed, for example, as an injection-molded body consisting of plastic or, however, has preferably been produced in a 3D printing process. In particular, it can be seen that the first element 29 comprises, for of example, three rigid subsections 31a to 31c, between which V-shaped indentations 30 are formed on the underside facing the object 3, which indentations 30 serve as predetermined breaking points or separation points between the subsections 31a to 31c. Furthermore, the subsections 31a to 31c each form a second section 16b, 16c. As a result, the second sections 16b, 16c can be separated from each other by the user prior to performing the tests, or they can separate from each other when the tests are performed in the area of the indentations 30. This is to ensure that the detachment processes occur independently of each other. Alternatively, the mutual influence can also be tolerated or taken into account during a data evaluation.

In the area between the longitudinally arranged indentations 30, moreover, the material of the first element 29 is recessed in the form of apertures 33. In addition, centrally with respect to the longitudinal direction 17, the subsections 31a to 31c each have, on the upper side facing away from the object 3, a bracket 32 for guiding the strip 36.

In the arrangement shown in Fig. 5, the strip 36 is guided over the underside of the bracket 32 on the subsection 31a to the underside of the subsection 31a. There, like the subsection 31a itself, it is connected to the surface 2 of the object 3 via the material connection 1. It is then guided through the aperture 33 between the two subsections 31a and 31b to the upper side of the bracket 32 on the subsection 31b. Via the lower side of the bracket 32 at the subsection 31b, the strip 36 again enters the aperture 33 between the subsections 31a and 31b toward the subsection 31c. At the subsection 31c, the guidance of the strip 36 is repeated as described in connection with the subsection 31b. After the strip 36 has left the subsection 31c at its underside facing the object 3, it is (still) connected to the surface 2 of the object 3.

The connection or arrangement of the two elements 29 and 35 of the test specimen 10b described so far has the effect that, when a tensile load F is applied to the strip 36 in the region of a coupling point not shown, the strip 36 in the region of the subsections 31a to 31c can be used both for a tensile test and for a peeling test, i.e. it acts there in each case as the first section 14b. In the area in which it has left the subsections 31a to 31c and is connected to the object 3, it acts as the first section 14b exclusively for carrying out a peeling test.

The connection or arrangement of the two elements 29 and 35 of the test specimen 10b described so far has the effect, when a tensile load F is exerted on the strip 36 in the region of a coupling point not shown, that the strip 36 in the region of the subsections 31a to 31c can be used both for a tensile test and for a peel test, i.e. acts there in each case as first section 14b. In the area in which it has left the subsections 31a to 31c and is connected to the object 3, it acts as the first section 14b exclusively for carrying out a peel test.

In Fig. 7, a simplified test arrangement with a test device 100 is shown, which performs a detachment test of the test specimen 10 on the object 3 using the first test specimen 10. In particular, it can be seen that the test device 100 has a device 101 which is designed to grip the test specimen 10 in the region of the coupling point 20 and transmits a tensile load F to the first test specimen 10 there. It is essential here that the direction of the tensile load F is at an oblique angle α or preferably perpendicular, i.e. at an angle α of 90°, to the surface of the object 3. For this purpose, at least the device 101 is arranged to be horizontally movable in the direction of the Arrow 103. Furthermore, the testing device 100 has measuring means 102, which are shown only symbolically in the illustration of Fig. 7.

The measuring means 102 enable a load/time curve and/or a load/displacement curve to be recorded when the detachment test is performed. From the illustration of Fig. 7, it can be seen that when the tensile load F is applied to the first test specimen 10, the material of the first test specimen 10 in the region of the first sections 14 detaches from the surface 2 of the object 3 to be tested. Thereby, a

bending stress of the first section 14 takes place, which leads to a deformation of the first section 14. When the first section 14 detaches from the surface 2 of the object 3, releasing the material connection 1, peeling of the first section 14 takes place in the direction of the respective following second section 16. The values thereby revealed by means of the measuring means 102 thus enable the generation of a first stress characteristic value, which is typically determined as a characteristic value generated during corresponding peeling tests. On the other hand, when the second sections 16 are peeled off, releasing the material connection 1, a second stress characteristic value is generated, which corresponds, for example, to a tensile load F applied (depending on the angle α) to the material connection 1 almost perpendicularly to the surface 2 due to the increased bending stiffness of the sections 16, so that a tensile stress is simulated in order to detect a maximum strength of the material connection 1.

Fig. 8 shows the basic measurement setup as shown in Fig. 7 using the test specimen 10a. It is obvious that when the tensile load F is applied in the area of the second sections 16a, the tensile load F acts centrally on the second sections 16a, and in particular in perpendicular alignment to the surface 2 of the object 3.

Finally, Fig. 9 shows a curve of the tensile load F over a distance s or time t when a test is performed as shown in Fig. 7. One can see the force peaks S1, which always occur when a detachment of the test specimen 10a occurs in the area of the second sections 16a. The load level S2 occurring between the force peaks S1 corresponds to the tensile load F that occurs during the detachment in the area of the first sections 14a.

The test specimen 10, 10a to 10c described so far or the test device 100 can be modified in many ways without deviating from the idea of the invention.

In particular, it is also conceivable not only to provide identically formed first sections 14, 14a, 14b and 14c and/or second sections 16, 16a, 16b and 16c, but also to form them differently if necessary, in particular with different bending

stiffnesses or strength characteristics or different lengths in the longitudinal direction 17.

Claims

1. Test specimen (10; 10a; 10b; 10c) for testing material connections (1), in particular adhesive connections, having at least one contact surface (4) which can be connected via the material connection (1) to a surface (2) of an object (3) to be tested, and having at least one coupling point (20) for connecting the test specimen (10; 10a; 10b; 10c) to a device (101) which is designed to apply a load to the test specimen (10; 10a; 10b; 10c) which serves to release the material connection (1).
   characterized by,
   a test specimen (10; 10a; 10b; 10c), viewed in a longitudinal direction (17), that has at least two sections (14; 14a; 14b; 14c, 16; 16a; 16b; 16c) which form the at least one contact surface (4) on the side facing the object (3), and in what the different bending stiffnesses are selected in such a way that, when the material connection (1) is released, different load inputs into the material connection (1) can be achieved in order to determine different characteristic stress values of the material connection (1).

2. Test specimen according to Claim 1,
   characterized by,
   a flat, in particular strip-shaped element (12), which is flexible in a direction extending perpendicularly to the longitudinal direction (17) and preferably substantially rigid in the longitudinal direction (17), or alternatively a flat, in particular strip (36), which is flexible in a direction extending perpendicularly to the longitudinal direction (17) and preferably substantially rigid in the longitudinal direction (17), as a first element (35) and a second element (29), which cooperates with the strip (36) and is rigid at least in regions.

3. Test specimen according to Claim 1 or 2,

characterized by,

having at least two sections (14; 14a; 14b; 14c, 16; 16a; 16b; 16c), viewed perpendicular to the longitudinal direction (17), which have different thickness or height (h, H) and/or consist of layers of materials having different strength values.

4. Test specimen according to any one of Claims 1 to 3,
characterized by,
having at least two at least two sections (14; 14a; 14b; 14c, 16; 16a; 16b; 16c), which each form a contact surface (4), the contact surfaces (4) viewed in the longitudinal direction (17) of the element (12) without gaps adjoin one another or are connected to one another.

5. Test specimen according to any one of Claims 1 to 3,
characterized by,
having at least two sections (14a; 14b; 14c, 16a; 16b; 16c), which each form a contact surface (4), and in that, viewed in the longitudinal direction (17) of the element (12), at least one joining interruption (24; 30) is formed between the contact surfaces (4) and the object (3) to be checked is formed.

6. Test specimen according to Claim 5,
characterized by,
having at least one joining interruption (24), which is formed by a non-stick coating on the side of the element (12) facing the object (3).

7. Test specimen according to Claim 5,
characterized by,
having at least one joining interruption (30), which is formed by an indentation or similar geometry on the side of the element (29) facing the object (3).

8. Test specimen according to any one of Claims 1 to 7,
characterized by,

the test specimen (10a) having an additional connection (26) between the at least two sections (14a; 16a), which connection (26) is connected to the section (16a) having the greater bending stiffness on the upper side (28), preferably in a central region of the upper side (28).

9. Test specimen according to any one of Claims 1 to 8,
characterized by,
the test specimen (10; 10a; 10b; 10c) having a width (B) of between 3mm and 10mm and/or a length (L) of between 50mm and 200mm and/or a thickness or height (h) in the section (14; 14a; 14b; 14c) having the lower bending stiffness section (14; 14a; 14b; 14c) of less than 1mm.

10. Test specimen according to any one of Claims 1 to 9,
characterized by,
the test specimen (10b; 10c) being at least partly made of plastics material and the part consisting of plastic is formed as a 3D printed part.

11. Test specimen according to any one of Claims 1 to 10,
characterized by,
the test specimen (10; 10a; 10b; 10c) comprising at least two first sections (14; 14a; 14b; 14c) and at least two second sections (16; 16a; 16b; 16c), wherein either the first and second sections (14; 14a; 14b; 14c, 16; 16a; 16b; 16c) alternate with each other or at least two first sections (14; 14a; 14b; 14c) or at least two second sections (16; 16a; 16b; 16c) are followed by the at least two second sections (16; 16a; 16b; 16c) or the at least two second sections (16; 16a; 16b; 16c).

12. Test device (100) for or with a test specimen (10; 10a; 10b; 10c) formed according to one of Claims 1 to 11, and with a means (101) for exerting a tensile load (F) on the coupling point (20) of the test specimen (10; 10a; 10b; 10c), wherein the means (101) is designed so that the tensile load (F) is applied to the test specimen (10; 10a; 10b; 10c) at an oblique or

perpendicular angle (α) between the material connection (1) and the plane of the test specimen (10; 10a; 10b; 10c) connected to the object (3).

13. Test device according to Claim 12,
characterized by,
the test device (100) having measuring means (102) for recording a load/time curve and/or a load/displacement curve when the tensile load (F) is exerted on the test specimen (10; 10a; 10b; 10c).

14. Method for testing material connections (1), in particular by means of a test specimen (10; 10a; 10b; 10c) which is constructed according to one of the Claims 1 to 11 and/or by using a testing device (100) according to Claim 12 or 13,
comprising at least the following steps:
- Formation of at least one material connection (1) in the region between a surface (2) of an object (3) to be tested and at least two sections (14; 14a; 14b; 14c, 16; 16a; 16b; 16c) of a test specimen (10; 10a; 10b; 10c) having different bending stiffnesses
- exerting a tensile load (F) on the at least one coupling point (20) of the test specimen (10; 10a; 10b; 10c) at an oblique or perpendicular angle (α) to the plane of the test specimen (10; 10a; 10b; 10c) connected to the object (3), the tensile load (F) being selected in such a way that the at least one material connection (1) is released in the region of the at least two sections (14; 14a; 14b; 14c, 16; 16a; 16b; 16c)
- recording of measured values, in particular a load/time curve and/or of a load/displacement curve, during the exertion of the tensile load (F).

15. Method according to Claim 14,
characterized by,
the recorded measured values for inspecting the material connection (1) being used to determine a strength and/or a fracture toughness of the material connection (1).

16. Use of a test specimen (10; 10a; 10b; 10c), which is formed according to one of Claims 1 to 11, for inspecting adhesive bonds on surfaces (2) of objects (3), in particular on surfaces (2) of substrates.

Fig. 1

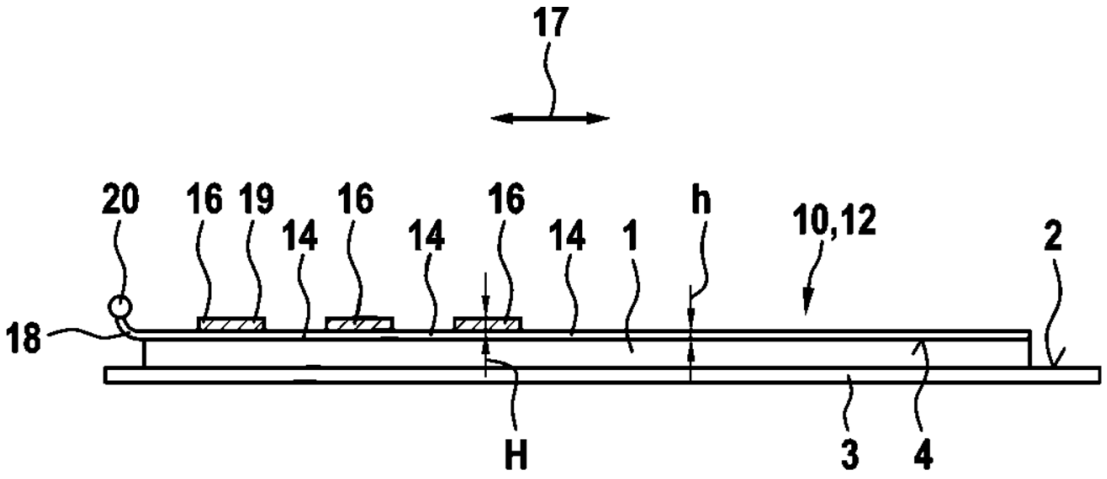

17
20
16
19
16
16
h
10,12
2
14
14
14
1
18
H
3
4

Fig. 2

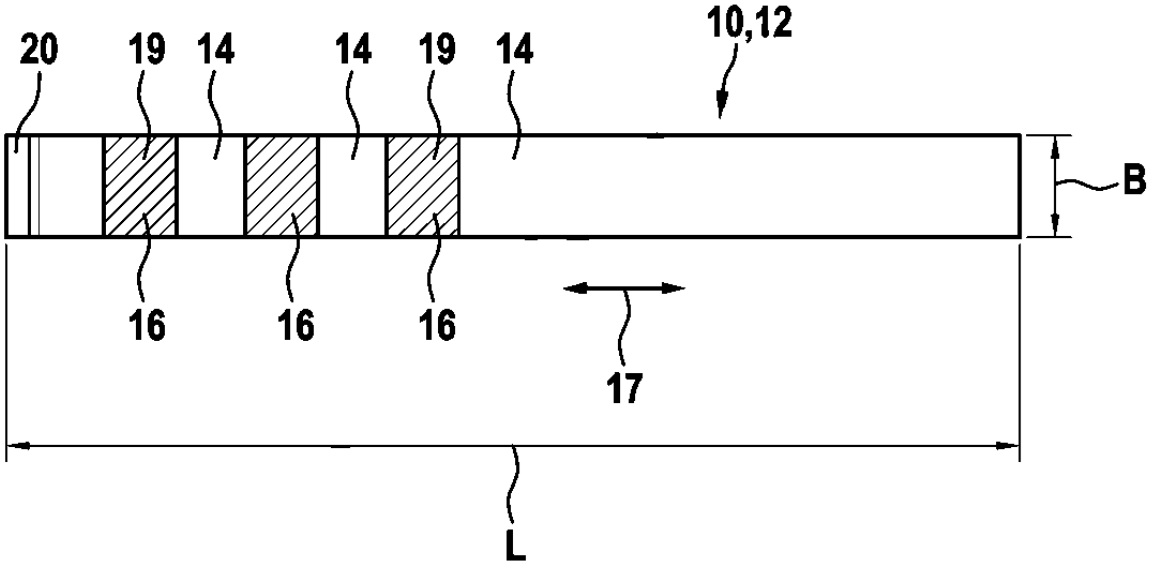

10,12
20
19
14
14
19
14
B
16
16
16
17
L

Fig. 3

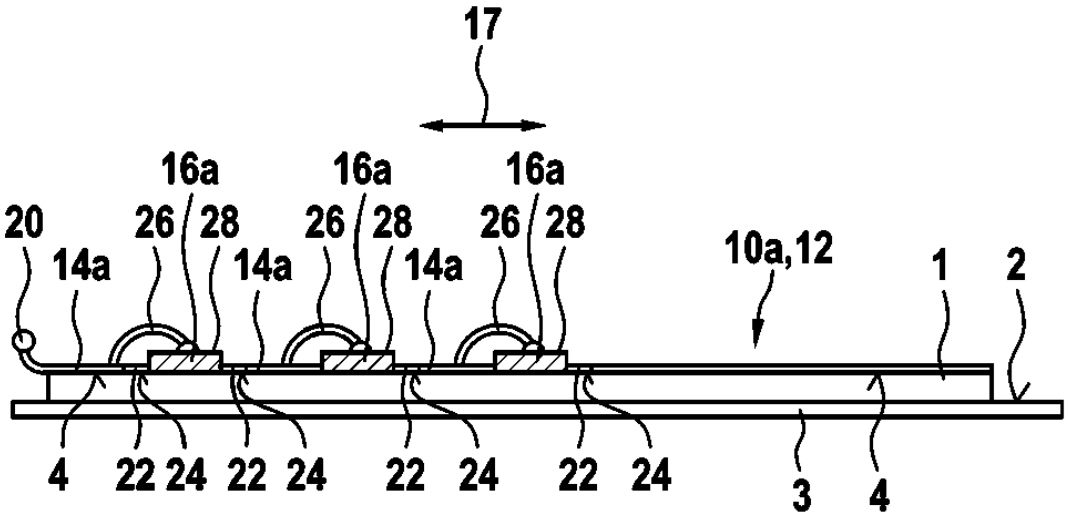

17
16a
16a
16a
20
26
28
26
28
26
28
14a
14a
14a
10a,12
1
2
4
22
24
22
24
22
24
22
24
3
4

Fig. 4

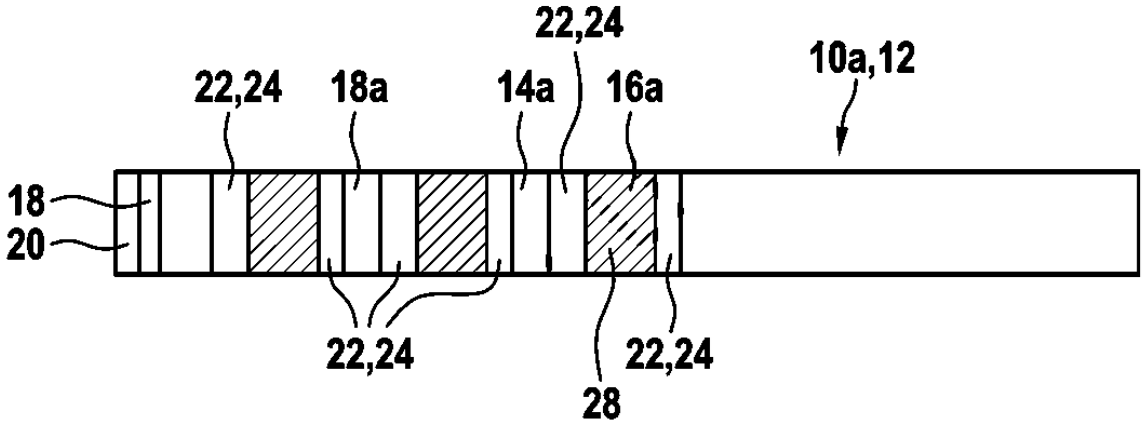

22,24
10a,12
22,24
18a
14a
16a
18
20
22,24
22,24
28

Fig. 5

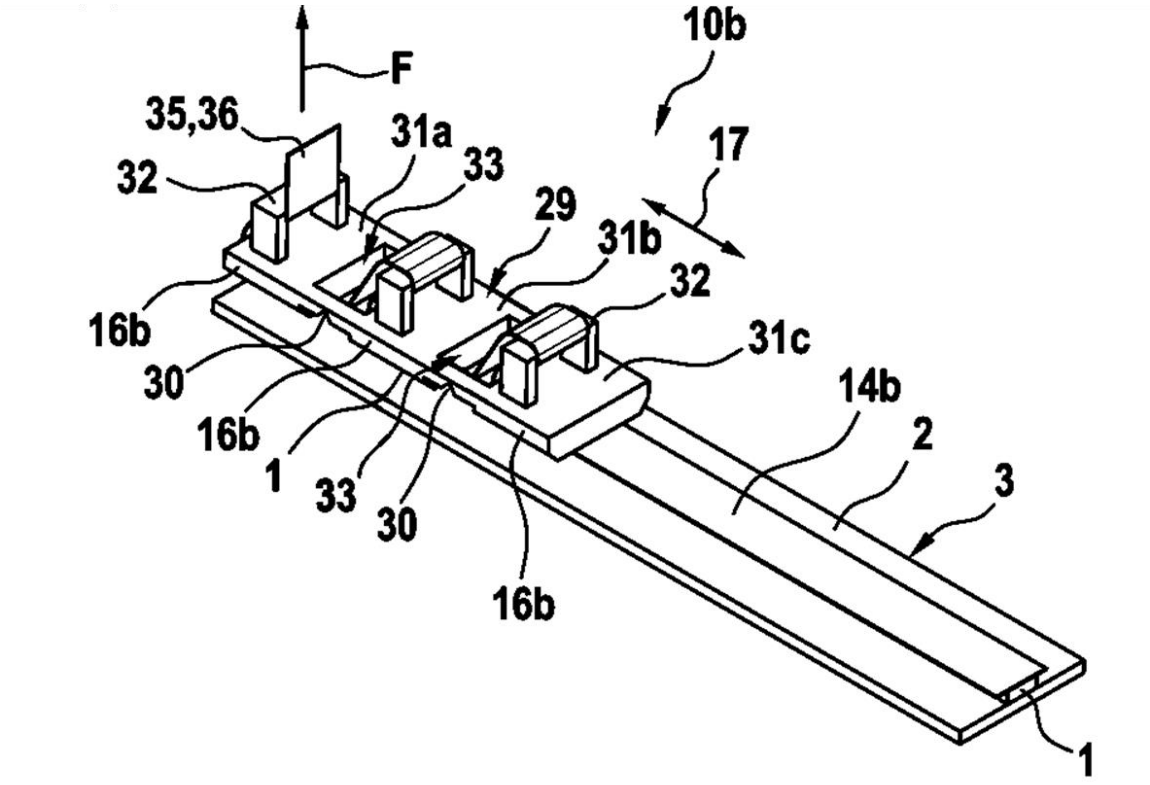

F
10b
35,36
31a
33
17
32
29
31b
32
16b
31c
30
14b
16b
2
1
33
3
30
16b
1

Fig. 6

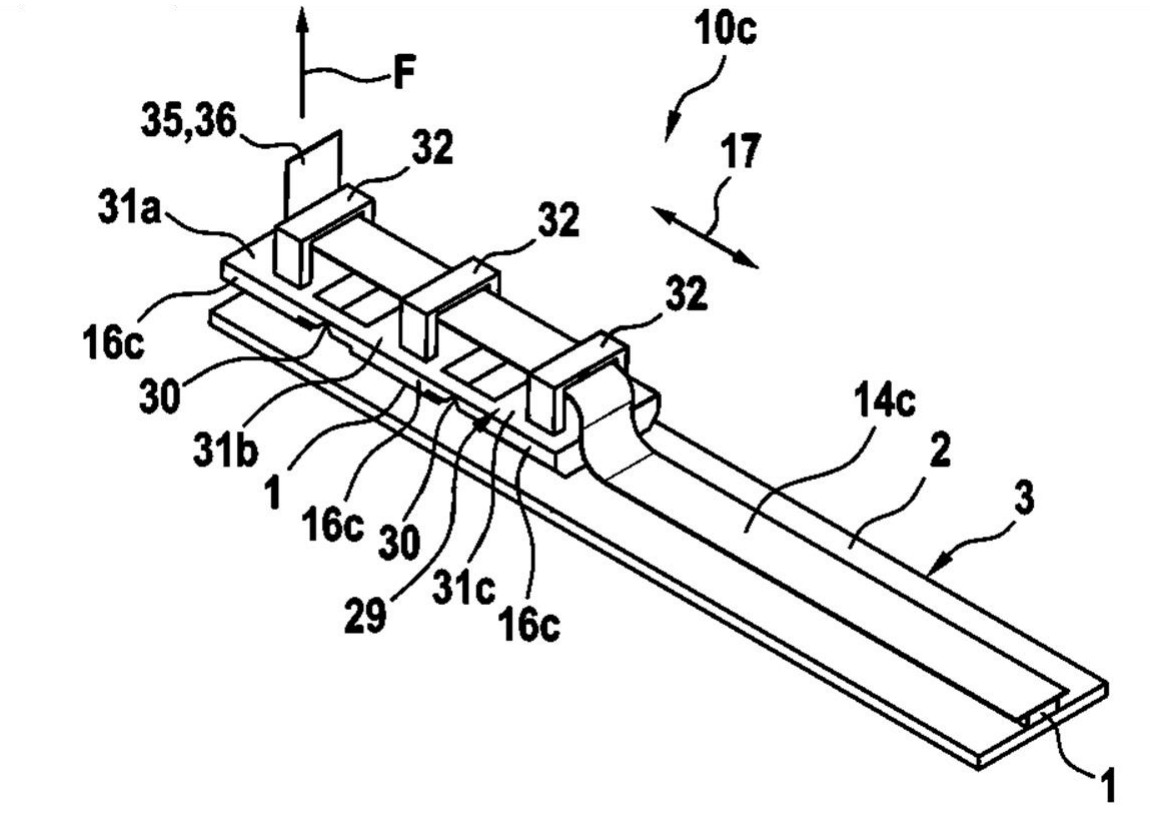

F
10c
35,36
32
17
31a
32
32
16c
30
14c
31b
2
1
3
16c
30
29
31c
16c
1

Fig. 7

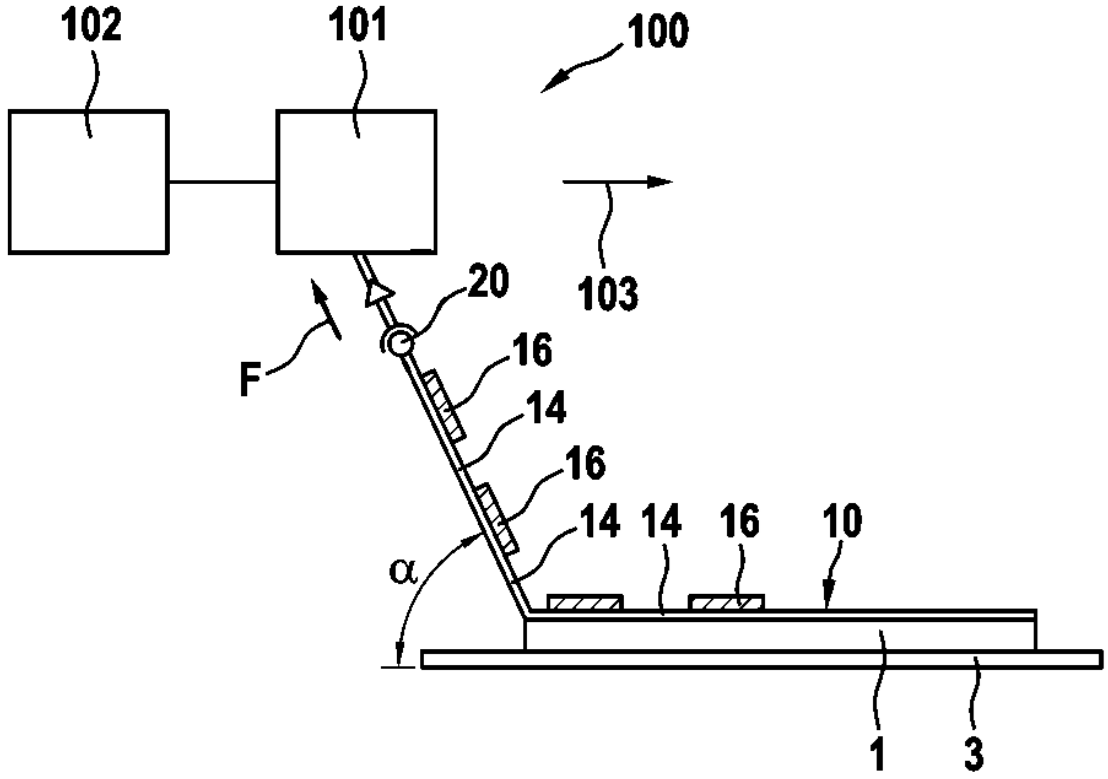

102
101
100
103
20
F
16
14
16
14 14 16 10
α
1
3

Fig. 8

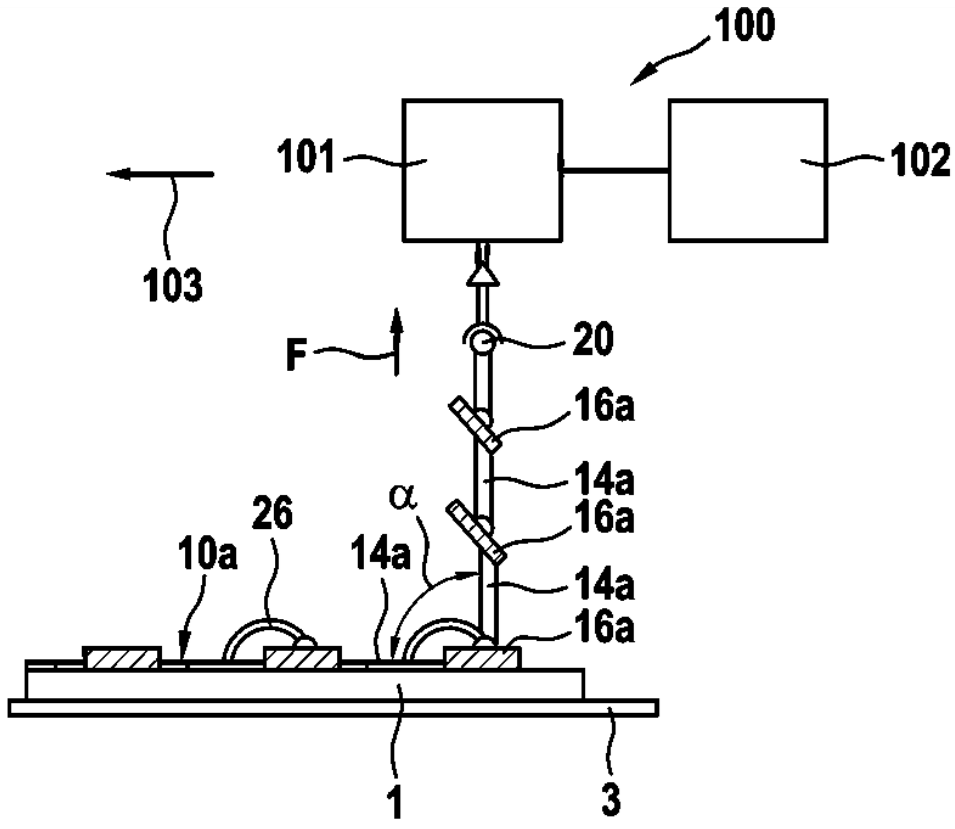
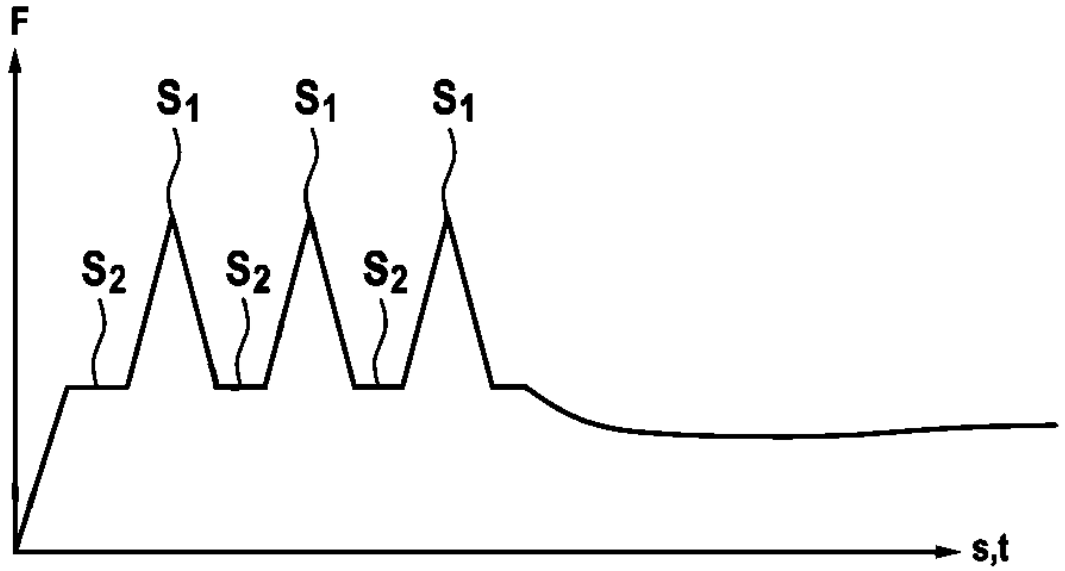

100
101
102
103
F
20
16a
14a
16a
14a
16a
α
26
10a
14a
1
3

Fig. 9



Appendix H

Paper H

Testing method to determine the strength and fracture energy of adhesives in a single continuous test

Testing method to determine the strength and fracture energy of adhesives in a single continuous test

C.S.P. Borges[1], E.A.S. Marques[1], R.J.C. Carbas[1], A. Akhavan-Safar[1], C. Ueffing[2], P. Weißgraeber[3], L.F.M. da Silva[4]

1 Instituto de Ciência e Inovação em Engenharia Mecânica e Engenharia Industrial (INEGI), Portugal
2 Robert Bosch GmbH, Corporate Research and Advance Engineering, Renningen, Germany
3 Chair of Lightweight Design, University of Rostock, Germany
4 Departamento de Engenharia Mecânica, Faculdade de Engenharia (FEUP), Universidade do Porto, Portugal

Abstract:
In this work, a new testing method for adhesive joints under tensile loading is presented. This method comprised three pull-off tests and one peel test in one single loading step, which enables the determination of the strength and fracture toughness of the material. The properties determined can be of the adhesive, if cohesive failure occurs, or of the interface, in the event of adhesive failure. To validate the testing method, the adhesive used was a commercially available silicone, for which strength and fracture toughness had already been determined using standard methods. It was concluded that this method accurately enables the determination of strength and toughness, using one single joint and loading.
Keywords: adhesive joints, pull-off, peel, strength, fracture toughness, combined testing method.

1 Introduction

In an adhesive joint, generally, failure can be cohesive, in the adhesive or substrate, or adhesive, between the two materials [1]. Usually, when testing an adhesive joint, adhesive or interfacial failure is associated to a contaminated condition, either due to surface contamination prior to bonding or due to contamination that comes into contact with the joint during its service life [2, 3]. Therefore, it is important to develop testing methods to inspect if a given adhesive/substrate combination, which can be in a given contaminated condition, have the suitable mechanical properties for the purpose they must fulfill during their service life.

To evaluate the mechanical performance of an adhesive joint, the most common joint configuration is the single lap joint (SLJ) [4]. These tests are defined by standards such as the ASTM D100 [5] or ISO 4587 [6]. These joints mainly withstand shear loading, but, due to the bending of the substrates during the test, they also experience peel loading, particularly close to the overlap ends. This loading can lead to the yielding or failure of the substrates prior to the failure of the adhesive or interface [7]. Therefore, they are adequate to establish joint properties but not specifically adhesive or interface properties.

Damage mechanics models are often used to characterize adhesive joints, such as cohesive zone models (CZM) or other coupled stress and energy criteria. These models stipulate that two criteria must be fulfilled for the failure of the adhesive, first, when a stress criterion is reached, a relaxation process that simulates the degradation of the material occurs, until a toughness criterion is met. Therefore, in adhesive characterization, there are two main parameters that must be evaluated: strength and fracture toughness [8, 9]. These parameters must be determined for tension and shear to fully describe the joint's behavior. Damage models are, therefore, able to predict the formation of finite cracks in the material when its strength is reached and the energy released is higher that the energy required for crack formation [10].

There are two main objectives for this new testing method: (i) allowing the swift inspection of a given adhesive/substrate combination in a given contaminated environment; (ii) determining strength and fracture properties using one single loading step. To create a universal joint that can be used with a wide variety of substrates and geometries, mode I loading, or tension, is focused, so that the new testing specimen can be bonded to the inspected surface and pulled vertically using a simple testing machine or device. The two variables that must be determined are, therefore, tensile strength and fracture toughness in mode I.

To evaluate the tensile strength of an adhesive, the two tests most commonly adopted are bulk tensile tests and axially loaded butt joints [1]. Bulk tensile tests, described by ISO 527-1 [11], are usually performed using "dogbone" specimens, which are commonly described by the ISO 527-2 [12] or ASTM D638 [13] standards. However, these specimens do not enable the evaluation of an adhesive/substrate combination. Butt joints, on the other hand, allow this analysis. These joints consist on a layer of adhesive between two substrates. There are different standards for this test, being the most common ones ASTM D897 [14], which considers circular substrates manufactured from metal or wood and ASTM D2095 [15], which includes a wider variety of substrate geometries. In industrial environments, a variation of the butt joint, the nail test described by DIN 50002-1 [16], is commonly used to evaluate the quality of the bond between a given substrate and adhesive. This test consists simply on applying tensile load to a nail bonded to a flat substrate.

As stated, knowing only the strength of the adhesive is insufficient and, therefore, the fracture toughness must also be determined. To evaluate the mode I fracture toughness, the most common tests are double cantilever beam (DCB) and peel tests [1]. DCBs consist on an adhesive joint between two similar stiff rectangular substrates. During the test, these substrates are separated, loading one of the ends of the overlap and propagating a pre-existing crack [17]. There are also peel tests, in which adhesive is peeled using flexible substrates. These tests can be described by ISO 8510-1 [18] or ISO 8501-2 [19] depending on if the peel is performed at 90 or 180°, respectively. There are several different arrangements for this test, being one of the most popular the fixed-arm peel, in which one substrate is fixed to a rigid base and other is peeled using a testing device, which applies a predetermined peel angle. The angle typically can change between 45 and 180° [1]. Peel tests enable the determination of the fracture toughness of the adhesive, even if there is plastic deformation of the flexible substrates, as long as there are mechanisms to take that deformation into consideration [20, 21]. This test is more flexible than the DCB, in terms of design, since it can be performed on a wider variety of substrates, as long as the fixed substrate is a flat surface.

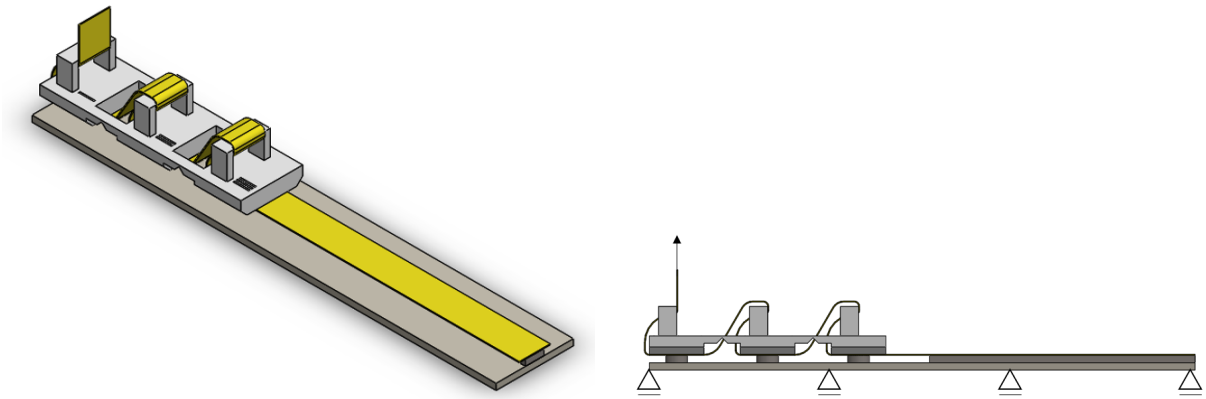
To this point, it was seen that there is no simple test to use in both laboratory and industrial environments that can swiftly allow the combined determination of strength and fracture toughness of an adhesive joint, as well as inspect if the failure of the joint is cohesive or adhesive. However, the two tests that have a higher adaptability are, for strength, the variation of the butt joint test, the nail test, which consists of a pull-off test and, for fracture toughness, the peel test.

This work aims to validate an in-house developed apparatus and method [22], which can be used to inspect a wide variety of adhesive bonds. This testing method aims to analyze both strength and fracture properties in one single loading step, through three pull-off tests and one peel test, respectively. In industrial applications, this can be used to analyze the failure path and, regardless of if the failure is cohesive or adhesive, make sure that the mechanical properties of the joint fall within a acceptable envelope of strength and toughness.

2 Experimental details

2.1 Testing method

The testing method used in this work [22] consisted of three pull-off tests followed by one peel test, Figure 1a. These four tests were performed in a single loading step, Figure 1b. The steel strip was used as the flexible substrate of the peel test, as well as to ensure that the loading of the pull-off tests is purely tensile.



(a) (b)

Figure 1: Schematic representation of the joint on which the test was based a) and of the testing method b).

The pull-off test overlaps are circular, with a diameter of 6 mm. The width of the peel test is also 6 mm.

The strength of the adhesive was considered, simply, as the load obtained divided by the area of the overlap.

For the peel test, the fracture energy release rate of the adhesive can be determined by [20]:

$$G_{adhesive} = G_{total} - G_{plastic} \tag{1}$$

where $G_{plastic}$ is the plastic energy associated with the peel arm and G_{total} is the total external input energy for the peeling process, determined by [20]:

$$G_{total} = \frac{P}{b}(1 - \cos\theta) \tag{2}$$

where P is the peel load, b the overlap width and θ the peeling angle. In this work, load was applied perpendicularly to the adhesive thickness, θ=90°. Therefore, equation (2), is simply:

$$G_{total} = \frac{P}{b} \tag{3}$$

2.2 Materials

The testing specimen used was composed of several materials, Figure 2. The part (1), correspondent to the pull-off tests was manufactured from polycarbonate (PC). The strip identified with the number (2) was 0.03 mm thick carbon steel with the material no. 1.1274. The adhesive overlaps identified by (3) were manufactured from a two-part silicone adhesive, commercially available, characterized by Borges et al. [23], that cures at 120 °C for 25 minutes. The substrate identified by (4) was 6086-T6 aluminum.

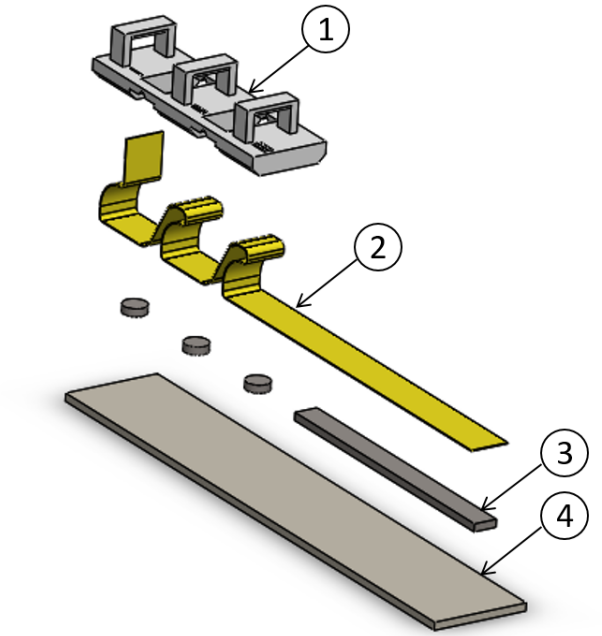
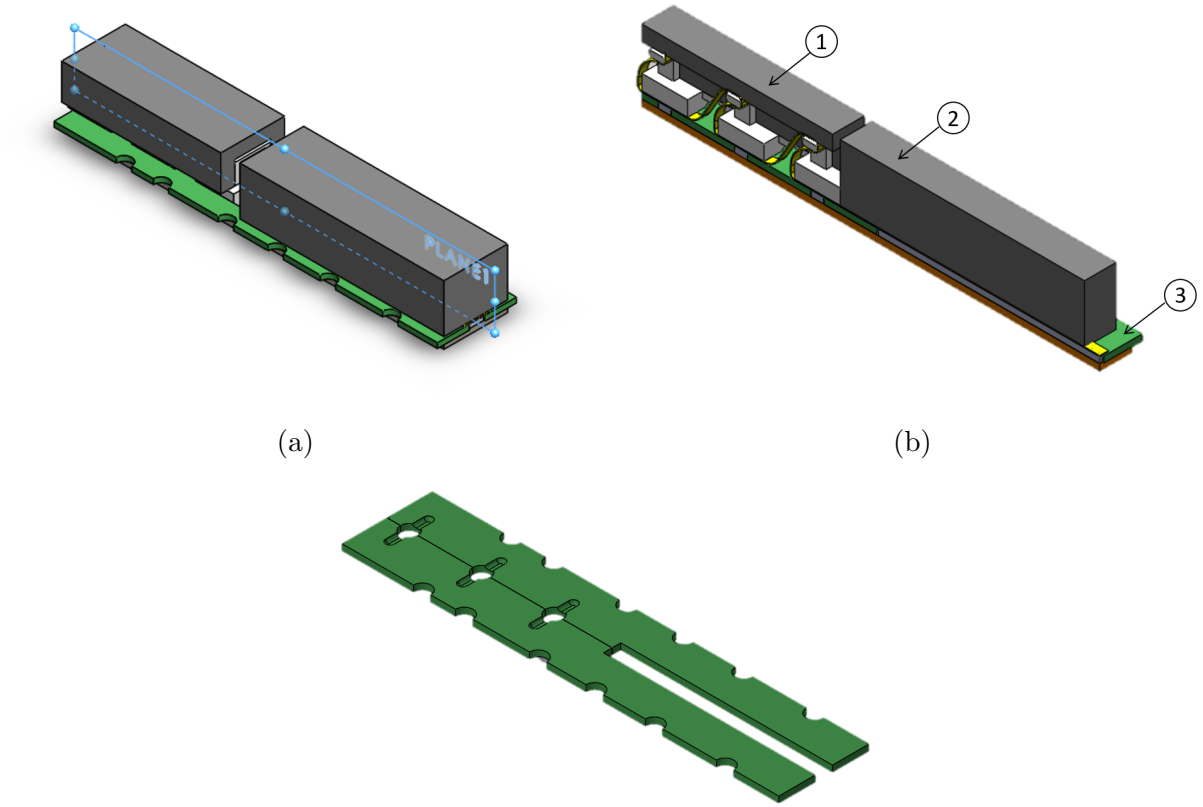


Figure 2: Schematic representation of the different parts of the joint used for the test. The part identified with (1) is the pull-off test part, PC (2) is the steel strip, (3) is the adhesive under analysis, silicone and (4) is the substrate, aluminum.

2.3 Specimen manufacturing

To manufacture the specimens, an assembly was produced, Figure 3. The parts represented by the numbers (1) and (2) are aluminum blocks used to apply pressure evenly, guarantee a good quality overlap and proper alignment. The polytetrafluoroethylene (PTFE) mask (3), Figure 3c, was used to ensure the adhesive overlap area and thickness.



(a) (b)

(c)

Figure 3: Assembly used to simplify joint manufacturing a), cut view, considering the cut by plane 1 b) and mask used to ensure the overlap area c).

For the manual manufacture of the joint, first, the substrate was treated with sandpaper and cleaned with acetone. Afterwards, the mask, cut in half (as shown in Figure 3c), was placed on top of the substrate, inside a mold, Figure 4. In the mold, pins were placed to guarantee the alignment of the assemblies. The pull-off test part was treated with low pressure oxygen plasma. The steel strip was primed, on the side that was in contact with silicone, using a silicone primer from the same manufacturer of the adhesive. Afterwards, it was looped around the pull-off test part as shown in Figure 1 and hold in place using an epoxy adhesive with a shore D hardness of 86, mode I fracture toughness of 8 N/mm and elongation at failure of 10%, given by the manufacturer. Then, the silicone adhesive was prepared. For that, adhesive and hardener were mixed at a 1:1 ratio and properly combined. The adhesive was placed in the designated cut-offs of the mask, Figure 3c. The pull-off test part was placed on top of the adhesive with the help of the pressure block identified by (1) in Figure 3b. The steel strip was placed on top of the adhesive for the peel test. Lastly, the pressure block for the peel test was placed, the mold, Figure 4, was closed and put in a hot-plate press at 120 °C for 25 minutes and a pressure of 7 bar.

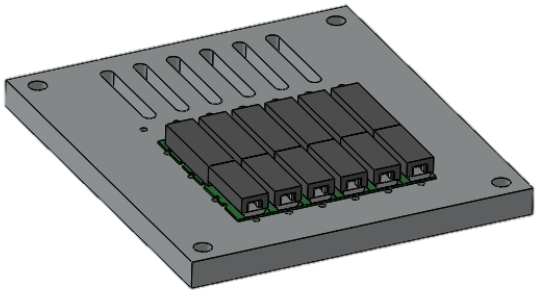


Figure 4: Schematic representation of the joints and assemblies used to assist joint manufacturing in a mold.

2.4 Testing procedure

To conduct the tests, a setup that restrains the specimen vertically but not horizontally was required. This setup, Figure 5, consists of two lateral supports (1), used to fix the bars (2) which are manufactured from polished steel, to decrease friction with the rollers of the part where the specimens are attached (3). The attachment of the specimens was performed using bolts in the six designated gaps, as shown by two bolts in Figure 5. Aftwerwards, the complete setup was attached to a universal testing machine.

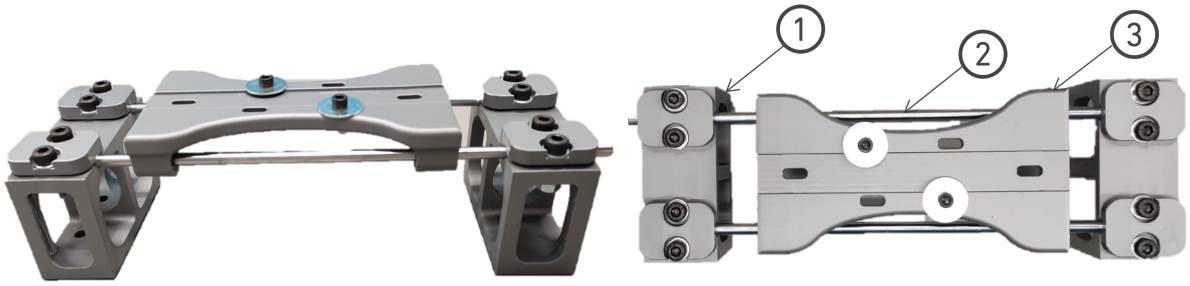


Figure 5: Test setup attached to the universal testing machine to test the specimens.

The tests were conducted at a loading rate of 10 mm/min, in an INSTRON® 3367 (Norwood, MA, USA) universal testing machine, with a load cell capacity of 30 kN. Six specimens were tested.

3 Numerical details

For the numerical simulation of the joint, the pull-off and peel tests were simulated separately, since a two-dimensional model is enough to simulate the peel test. But, for the pull-off test, a three-dimensional model is necessary.

The general elastic properties of the substrate materials used are shown in Table 1. The tensile strength and mode I fracture toughness used for the adhesive were the ones determined in this work. The plastic properties of the steel and aluminum were also considered. These properties were obtained from the stress-strain curves presented by Pavliuchenko et al. [24] and Farahani et al. [25] for steel and aluminum, respectively.

Table 1: Properties of the substrate materials used in the numerical simulation

Material	Young's modulus [GPa]	Poisson's ratio
Steel	210	0.30
Aluminum	70	0.33
PC	2.3	0.36

3.1 Pull-off test

The pull-off tests were simulated through a three-dimensional (3D) model, Figure 6. The substrate was simulated using a small block, just modeling the portion below the pull-off part. The substrate was restricted in all directions, except the direction in which the test setup allows movement. A simplification was made to the model, since the two models are equivalent when the test is perfectly aligned. The horizontal movement of the pull-off testing part was restricted where in contact with the strip and the base of the part is pulled as it would be by the strip.

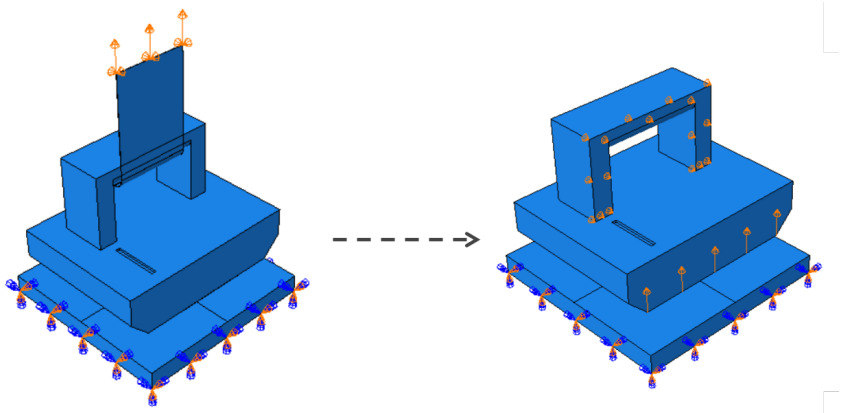


Figure 6: Numerical model used to simulate pull-off tests.

The mesh used for the model can be seen in Figure 7. The mesh of the adhesive has an element size of 0.25 mm at the base and 2 mm through the adhesive thickness, to ensure one element is considered. The mesh of the substrate is constant with a side length of 1 mm. The mesh of the pull-off test part changes from 1 mm at the arch to 0.25 mm at the overlap. The elements used in the adhesive were 8-node three-dimensional cohesive elements (COH3D8), in the pull-off part, 10-node quadratic tetrahedrons, 3D stress elements (C3D10) and, in the substrate, 8-node linear bricks, using reduced integration, hourglass control (C3D8R).

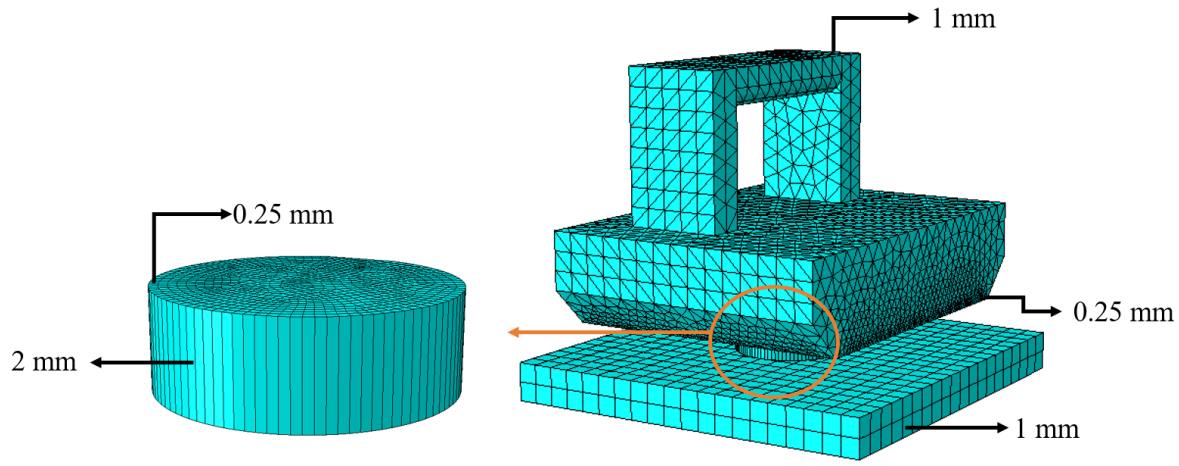


Figure 7: Mesh used in the numerical model of the pull-off tests.

3.2 Peel test

The peel tests can be simulated using a two-dimensional (2D) model, considering an out-of-plane dimension of 6 mm, which is the overlap width. The displacement is simulated in the left edge of the steel strip. The substrate is pinned in the vertical direction, Figure 8.



Figure 8: Numerical model used to simulate peel tests.

The adhesive employed a mesh size of 2 mm through the thickness, to ensure only one element was used. The steel strip has six elements through the thickness and the substrate has 3 elements. Regarding the horizontal meshing dimension, the mesh size was constant and equal to 0.33 mm, Figure 9.

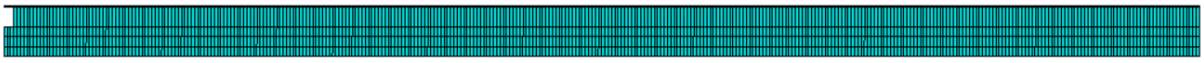


Figure 9: Mesh used in the numerical model of the peel test.

In the adhesive, 4-node two-dimensional cohesive elements (COH2D4) were used. In the steel strip and substrate the elements used were 4-node bilinear plane strain quadrilateral elements, with reduced integration, hourglass control (CPE4R).

4 Results and discussion

4.1 Experimental results

The tests performed in this work correspond to three pull-off test, which allow the determination of the strength of the adhesive, and one peel test, which allows the de-

termination of the fracture toughness of the adhesive. However, for both tests, first, the fracture surface of the joints was analyzed, exhibiting cohesive failure both in the pull-off and peel tests, Figure 10. Additionally, the assembly used to manufacture the joints guaranteed a good alignment and precision on the geometry of the adhesive overlap.



(a) (b)

Figure 10: Representative fracture surfaces of pull-off a) and peel tests b).

The curves obtained from these tests are similar to the one represented in Figure 11.

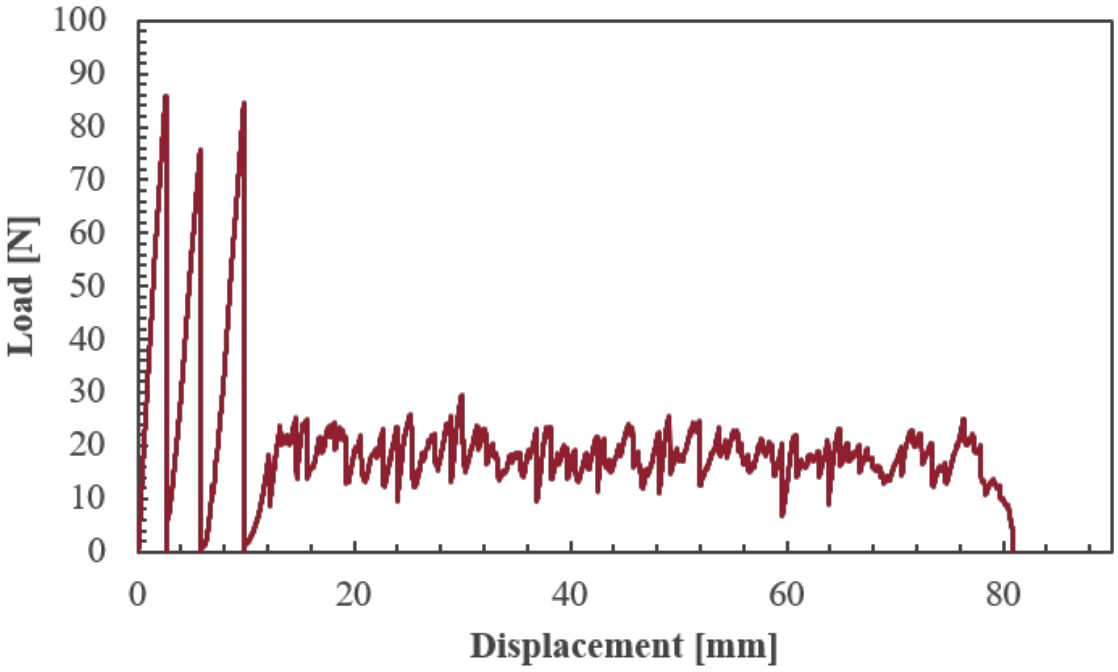


Figure 11: Representative curve of the experimental results for one test.

In Figure 11, the intervals between tests, that have a negligible load, were deleted. From the results obtained it was possible to determine that the strength of the adhesive is 2.7±0.2 MPa.

The peel test results, isolated, display a curve similar to the one shown in Figure 12.

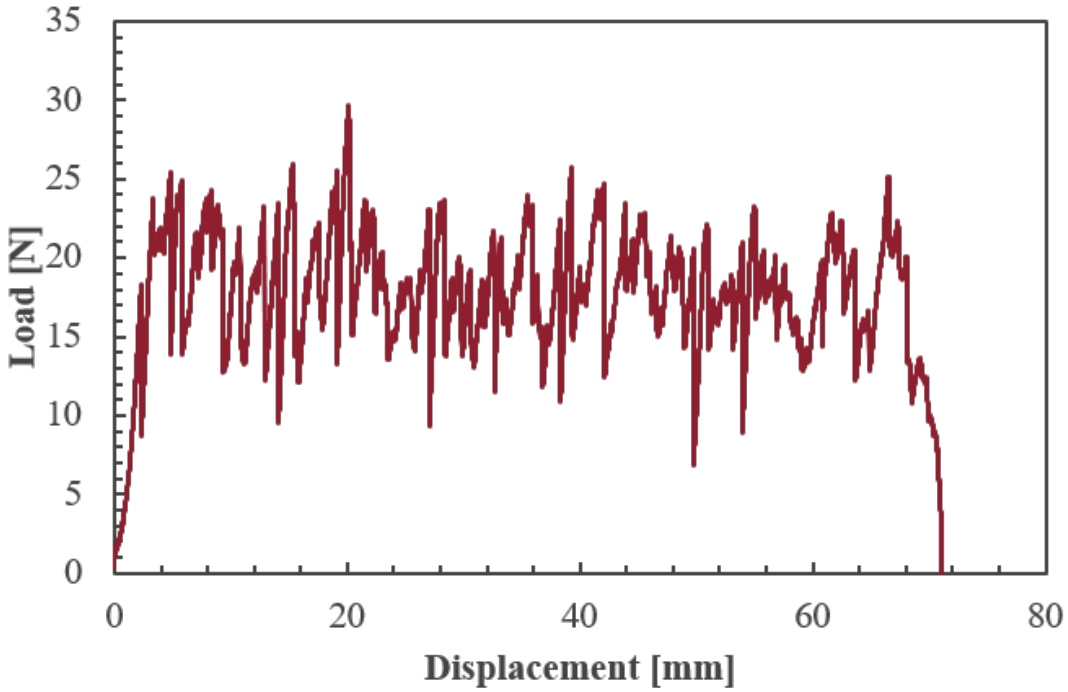


Figure 12: Representative curve of the results for the peel tests.

As it was stated, the fracture energy of the adhesive is equal to the total input energy minus the plastic bending energy of the substrates. Therefore, to determine the fracture energy of the adhesive, first it is important to understand if there was plastic deformation of the substrates. For that, the numerical model was used.

Considering that there was no plastic deformation, the fracture toughness of the adhesive would be given by:

$$G_{adhesive} = G_{total} = \frac{P}{b} \tag{4}$$

which would result in a curve similar to the one presented in Figure 13.

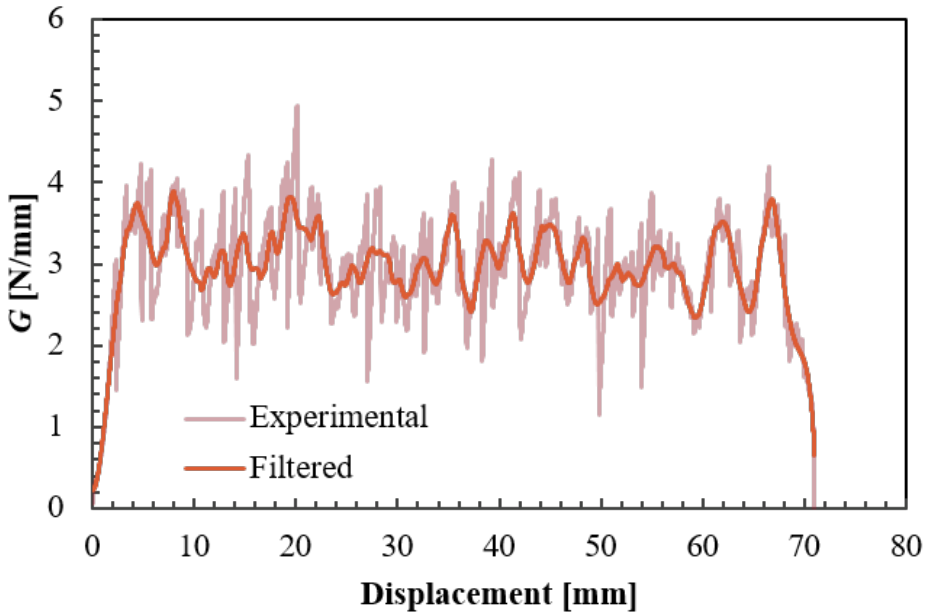


Figure 13: Representative curve of the results for the peel tests.

Performing the same data treatment to the different tests performed, the energy release rate obtained was 3.0±0.1 N/mm.

If there was plastic deformation of the substrate during the test, the fracture toughness of the adhesive would always be lower than this value. This occurs because, at this point it is being considered that $G_{total} = G_{adhesive}$ and, if the plastic energy is not negligible ($G_{plastic} > 0$), $G_{total} = G_{adhesive} - G_{plastic} \implies G_{total} > G_{adhesive}$. Therefore 3.0±0.1 N/mm represents the maximum possible fracture toughness of the adhesive.

The numerical model was run considering that the total energy can be attributed to the fracture of the adhesive, i.e., $G_{adhesive}$=3.0 N/mm. If in this numerical model no plastic deformation is identified, it can be considered that there was no plastic deformation of the adhesive during the test.

4.2 Numerical results

4.2.1 Pull-off test

The numerical results of the pull-off tests are presented in Figure 14.

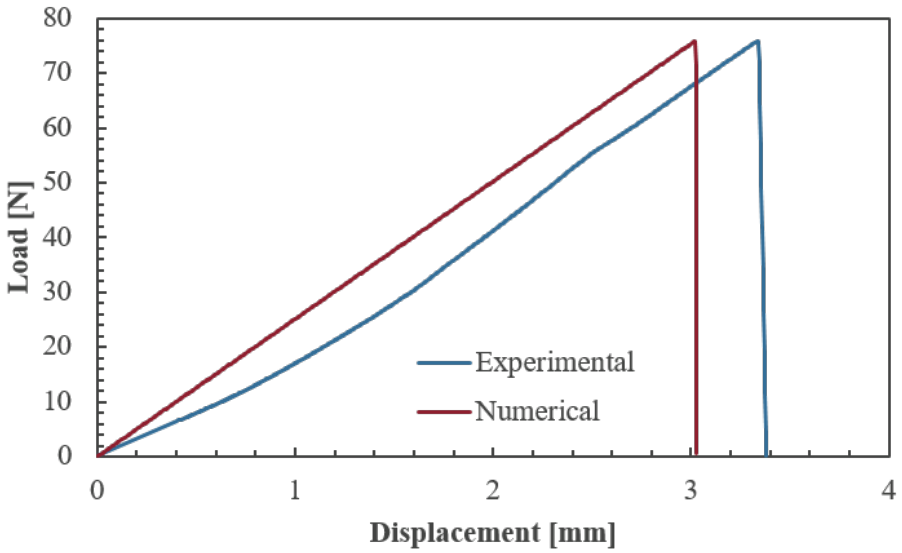


Figure 14: Comparison between experimental and numerical load-displacement curves of the pull-off tests.

It can be observed that the experimental results match the numerical simulation. There is a slight difference in the beginning of the curve compatible with the accommodation and start of the tension of the steel strip in the experimental results, which was, therefore, not accounted for in the numerical model.

Isolating the adhesive in the time increment prior to failure, Figure 15, it is clear that the load applied was purely tensile, showing a slight stress concentration at the edges of the overlap.

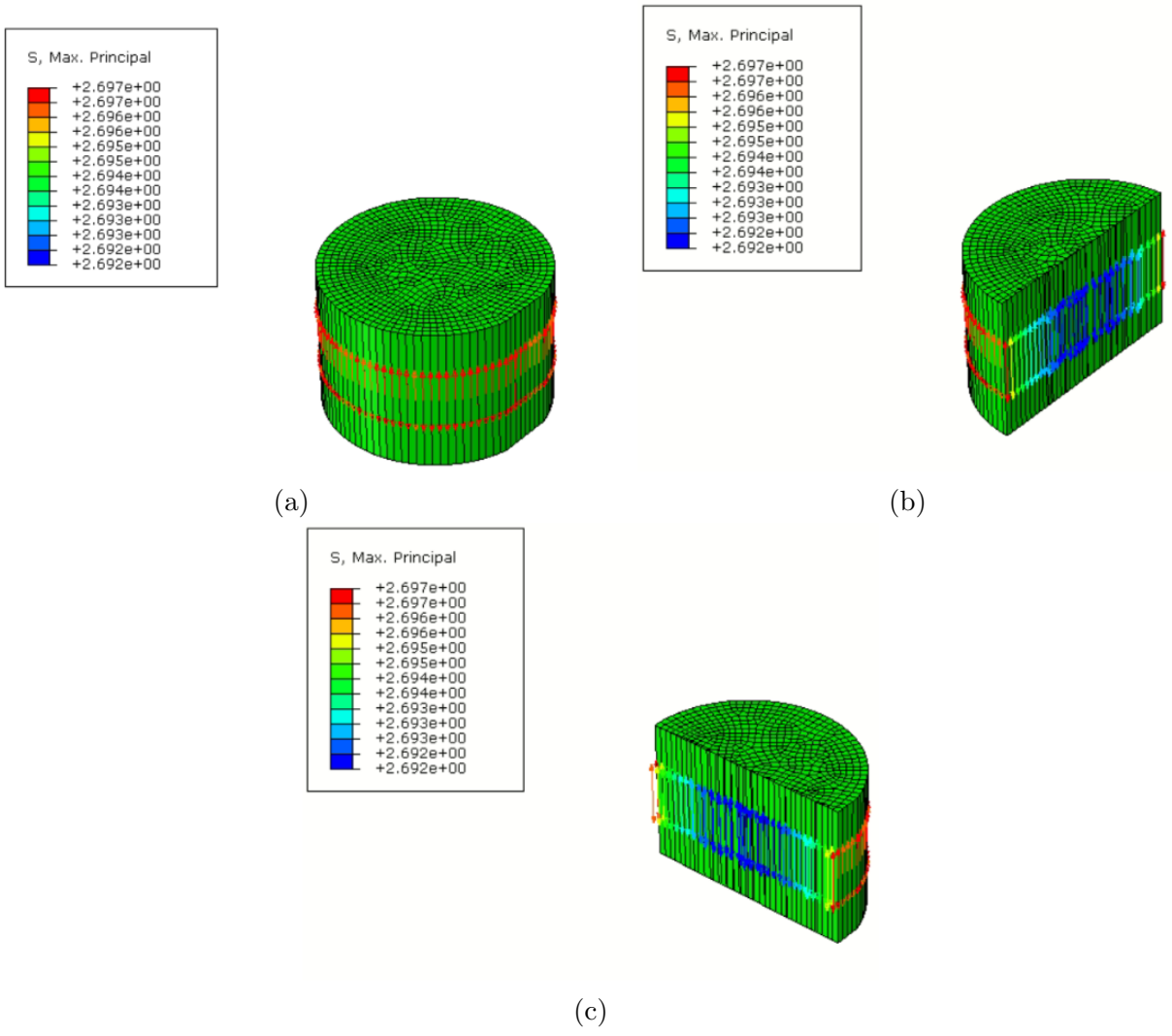


Figure 15: Maximum principal stress distribution, in MPa, in the adhesive a), cut view b) and perpendicular cut view c).

4.2.2 Peel test

The numerical results of the simulation of the peel test, compared with the experimental results are shown in Figure 16.

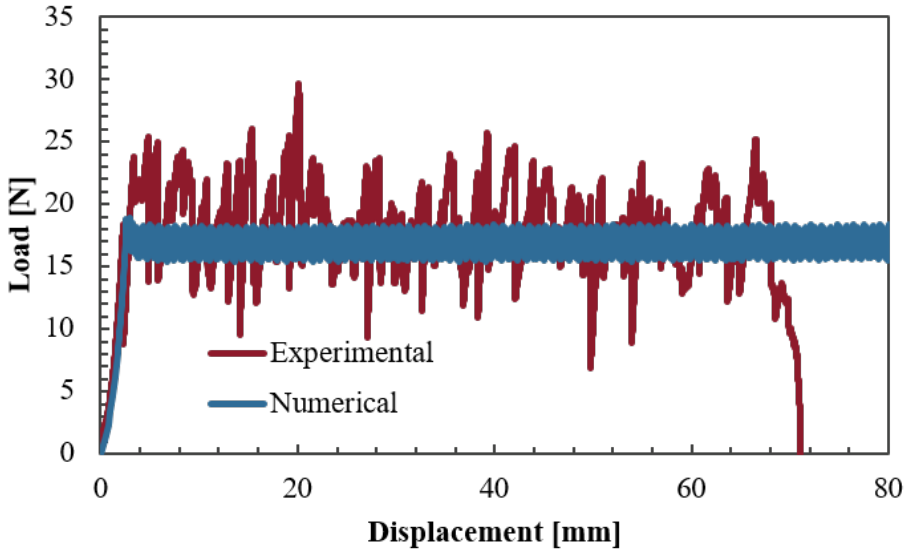


Figure 16: Comparison between experimental and numerical load-displacement curves of the peel tests.

Also in this numerical simulation, considering the yield stress of steel and aluminum, it was possible to identify if there was plastic deformation of the materials during the test. The *PEEQ* output value corresponds to the plastic deformation, therefore, if it is null throughout the test, there was no plastic deformation during the test, Figure 17.

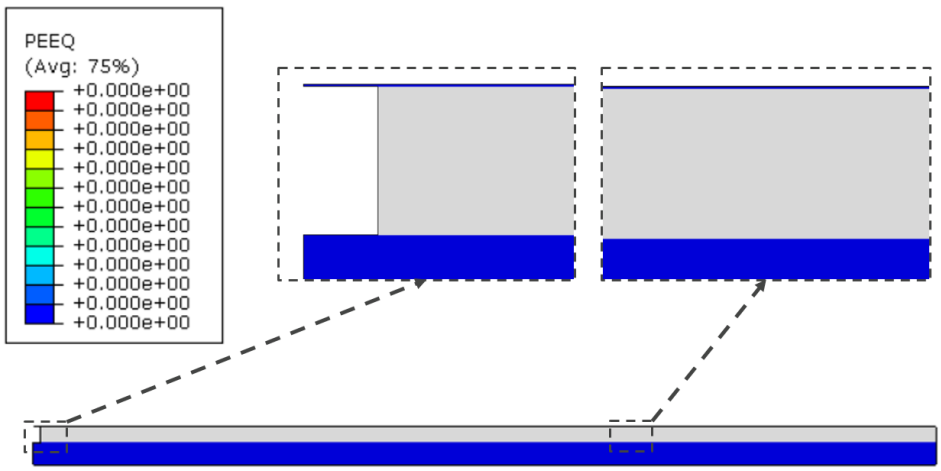


Figure 17: Numerical plastic deformation of the specimen in the end of the test, the undeformed joint is presented to improve readability.

4.3 Discussion

Regarding the pull-off tests, as presented, the strength of the adhesive determined was 2.7±0.2 MPa. In previous work by the same authors [23], the adhesive strength determined was 3.4 MPa. The difference may be attributed to the fact that, in the previous work, the adhesive strength was determined using bulk adhesive and, in this work, a joint was used.

Adams and Coppendale [26] compared tensile tests using butt joints and bulk specimens for a brittle and a ductile adhesive. The brittle material is of more importance to the analysis of the results obtained in the present work since the silicone adhesive used is very brittle, although it is very flexible. Adams and Coppendale [26] stated that if a bulk material has brittle failure, the butt joint of the same material is likely to fail at a lower stress because of the stress concentrations at the overlap edges, due to the constrain of the substrates. This occurs because the lateral contraction of the adhesive is not free, introducing radial and circumferential stresses at the edges of the joint [1]. The strength of the brittle adhesive studied by these authors, when using a butt joint, exhibited an error from 31 to 45%, depending on the strain rate applied, considering the value obtained using bulk tensile tests the reference strength. If the same analysis is done to the results obtained in the present work, that error is 20%.

Regarding the peel test, as it was seen in the numerical model, there is no plastic deformation of the steel strip, therefore, $G_{total} = G_{adhesive}$ and the fracture toughness of the adhesive is 3.0±0.1 N/mm. In previous work using the same material [27], the fracture toughness determined using standard DCB joints was 3.3±0.4 N/mm.

Regarding the numerical model, it was shown that the steel strip does not suffer plastic deformation during the test, which is executed at a 90° loading angle. The pull-off test loads the adhesive in pure tension and does not introduce significant loading to the pull-off test part, as long as the steel strip in the experiment is correctly aligned. Otherwise, it can introduce bending on the arches used to loop the steel strip, biasing the results obtained.

Therefore, the joint proposed can be used to determine strength and fracture toughness of an adhesive. Along with the advantage of the combined determination of the two properties, this joint has the several advantages when compared to standard specimens. The most clear of them is not needing a specific geometry of the bottom substrate, apart from the flat area, which allows its use to inspect the quality of wide variety of joints.

5 Conclusions

This work aimed to validate a new, expedite, testing method, that allows the determination of the strength and fracture toughness of an adhesive in the same loading step. The main conclusions produced in this work were:

- This method allowed the determination of the strength and fracture toughness of the adhesive. And, if the joint was damaged or contaminated and adhesive failure was observed, this method could be used to determine interfacial properties;

- The strength determined for the adhesive was 2.7±0.2 MPa and its fracture energy release rate 3.0±0.4 N/mm;

- The determined strength of the adhesive is lower than the one obtained using bulk tensile tests, which can be attributed to testing a joint instead of bulk material since, typically, in a joint, the constraint of the substrates leads to a lower determined strength of brittle adhesives;

- The fracture energy release rate determined using the peel test was similar to the one determined using standard DCB joints;

- The loading of the pull-off test was purely tensile and there was no plastic deformation of the substrates in the peel test.

Acknowledgments

The author(s) disclosed receipt of the following financial support for the research, authorship, and/or publication of this article: The authors wish to acknowledge and thank the funding and support provided by Robert Bosch GmbH, Corporate Research and Advance Engineering, Renningen. The authors also gratefully acknowledge the funding provided by Fundação para a Ciência e Tecnologia (FCT), Portugal for the Ph.D. Grant 2020.06055.BD.

References

[1] L. F. M. da Silva, A. Öchsisner, and R. D. Adams. *Handbook of adhesion technology*, volume 1. Springer, 2018.

[2] R. Brandão, C. S. P. Borges, E. A. S. Marques, R. J. C. Carbas, A. Akhavan-Safar, P. D. P. Nunes, C. Ueffing, P. Weißgraeber, F. Schmid, and L. F. M. da Silva. Effect of surfactant contamination on the properties of aluminum/silicone adhesive joints. *Mechanics of Advanced Materials and Structures*, pages 1–14, 2022.

[3] C. S. P. Borges, E. A. S. Marques, R. J. C. Carbas, C. Ueffing, P. Weißgraeber, and L. F. M. da Silva. Review on the effect of moisture and contamination on the interfacial properties of adhesive joints. *Proceedings of the Institution of Mechanical Engineers, Part C: Journal of Mechanical Engineering Science*, 235(3):527–549, 2021.

[4] Flake C. Campbell Jr. *Manufacturing processes for advanced composites*. Elsevier, 2003.

[5] ASTM D1002-99. Standard Test Method for Apparent Shear Strength of Single-Lap-Joint Adhesively Bonded Metal Specimens by Tension Loading (Metal-to-Metal). Standard, ASTM International, Pennsylvania, United States, October 2001.

[6] ISO 4587. Adhesives — Determination of tensile lap-shear strength of rigid-to-rigid bonded assemblies. Standard, International Organization for Standardization, Geneva, CH, March 2003.

[7] L. F. M. da Silva and R. D. S. G. Campilho. Design of adhesively-bonded composite joints. In *Fatigue and fracture of adhesively-bonded composite joints*, pages 43–71. Elsevier, 2015.

[8] R. D. S. G. Campilho, M. D. Banea, J. A. B. P. Neto, and L. F. M. da Silva. Modelling adhesive joints with cohesive zone models: effect of the cohesive law shape of the adhesive layer. *International journal of adhesion and adhesives*, 44:48–56, 2013.

[9] A. Hillerborg, M. Modéer, and P.-E. Petersson. Analysis of crack formation and crack growth in concrete by means of fracture mechanics and finite elements. *Cement and concrete research*, 6(6):773–781, 1976.

[10] P. Weißgraeber, J. Felger, A. Talmon l'Armée, and W. Becker. Crack initiation in single lap joints: effects of geometrical and material properties. *International Journal of Fracture*, 192(2):155–166, 2015.

[11] ISO 527-1. Plastics — Determination of tensile properties — Part 1: General principles. Standard, International Organization for Standardization, Geneva, CH, July 2019.

[12] ISO 527-2. Plastics — Determination of tensile properties — Part 2: Test conditions for moulding and extrusion plastics. Standard, International Organization for Standardization, Geneva, CH, February 2012.

[13] ASTM D638. Standard Test Method for Tensile Properties of Plastics. Standard, ASTM International, Pennsylvania, United States, February 2017.

[14] ASTM D897. Standard Test Method for Tensile Properties of Plastics. Standard, ASTM International, Pennsylvania, United States, October 2008.

[15] ASTM D2095. Standard Test Method for Tensile Strength of Adhesives by Means of Bar and Rod Specimens. Standard, ASTM International, Pennsylvania, United States, January 1996.

[16] DIN 50002-1. Adhesive bondings in electronic applications - Bonding strength on surfaces - Part 1: Tensile test. Standard, Deutsches Institut für Normung, Berlin, DE, March 2020.

[17] BS 7991. Determination of the mode I adhesive fracture energy, G_{Ic}, of structural adhesives using the double cantilever beam (DCB) and tapered double cantilever beam (TDCB) specimens. Standard, British Standard Institution, London, UK, October 2001.

[18] ISO 8510-1. Adhesives — Peel test for a flexible-bonded-to-rigid test specimen assembly — Part 1: 90° peel. Standard, International Organization for Standardization, Geneva, CH, December 1990.

[19] ISO 8510-2. Adhesives — Peel test for a flexible-bonded-to-rigid test specimen assembly — Part 2: 180° peel. Standard, International Organization for Standardization, Geneva, CH, December 2006.

[20] A. J. Kinloch, C. C. Lau, and J. G. Williams. The peeling of flexible laminates. *International Journal of Fracture*, 66(1):45–70, 1994.

[21] A. J. Kinloch and J. G. Williams. The mechanics of peel tests. *Adhesion Science and Engineering*, 1:273–301, 2002.

[22] C. S .P. Borges, E. A. S. Marques, C. Ueffing, P. Weißgraeber, and L. F. M. da Silva. Prüfkörper, Prüfvorrichtung und Verfahren zur Überprüfung von stoffschlüssigen Verbindungen sowie Verwendung des Prüfkörpers, German Patent and Trade Mark Office Patent Application No. 102022202551.2, March 2022.

[23] C. S. P. Borges, R. Brandão, A. Akhavan-Safar, E. A. S. Marques, R. J. C. Carbas, C. Ueffing, F. Weißgraeber, P .and Schmid, and L. F. M. da Silva. Influence of water and surfactant contamination on the mechanical and chemical properties of a silicone adhesive, before and after curing. *The Journal of Adhesion*.

[24] P. Pavliuchenko, G. Hirt, and M. Teller. Analysis and manufacturing of bistable metallic profiles. *Archive of Applied Mechanics*, 91(8):3501–3511, 2021.

[25] Mohammadreza Farahani, Iradj Sattari-Far, Davood Akbari, and Rene Alderliesten. Numerical and experimental investigations of effects of residual stresses on crack behavior in Aluminum 6082-T6. *Proceedings of the Institution of Mechanical Engineers, Part C: Journal of Mechanical Engineering Science*, 226(9):2178–2191, 2012.

[26] R. D. Adams and J. Coppendale. The stress-strain behaviour of axially-loaded butt joints. 1979.

[27] R. Brandão, C. S. P. Borges, E. A. S. Marques, R. J. C. Carbas, A. Akhavan-Safar, F. Schmid, C. Ueffing, P. Weißgraeber, and L. F. M. da Silva. The influence of humidity and immersion temperature on the properties and failure mode of PBT-GF30/silicone bonded joints. *Composite Structures*, page 115421, 2022.